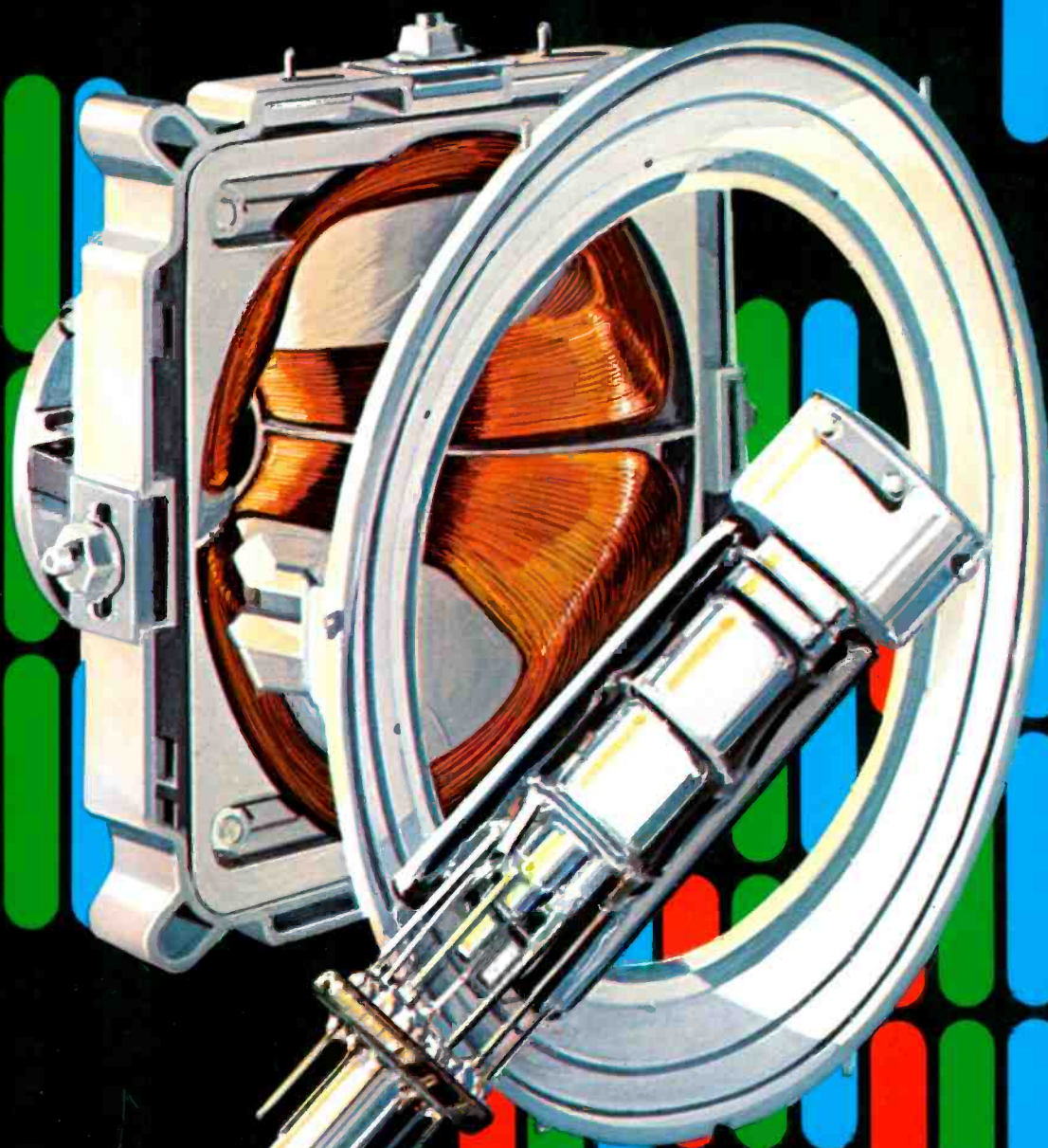


RCA Engineer

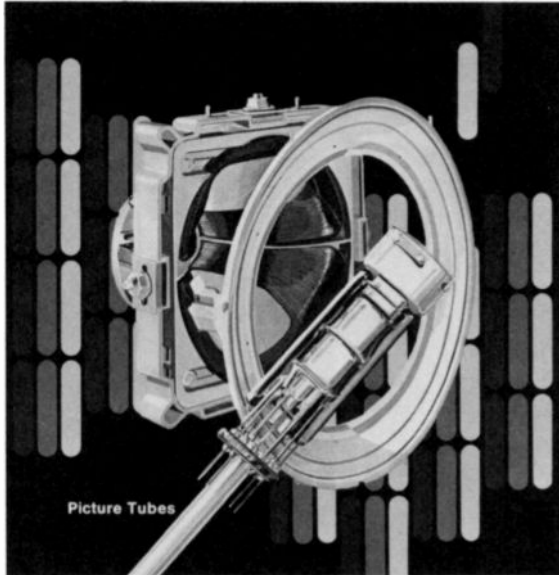
Vol. 25/No. 2 Aug./Sept. 1979



Picture Tubes

RCA Engineer

A technical journal published by
RCA Research and Engineering
Bldg. 204-2
Cherry Hill, N.J. 08358
Tel. 222-4254 (609-338-4254)



The elements depicted in the cover illustration represent significant advances in color picture tube design which have occurred within the last seven years. In 1972, RCA announced the precision in-line color picture tube system. It incorporated a screen structure consisting of continuous vertical phosphor stripes with 100% screen coverage. Line segments of the phosphor stripes are illuminated to form the image on the screen.

The in-line electron gun (in the foreground on the cover) permits extremely accurate beam alignment through the use of one-piece triple-aperture electrodes.

Yoke design is now even more intimately related to the tube. The 110° ST yoke shown on the cover is the product of computer-aided design and many innovations in yoke manufacturing techniques.

Read more about the development of new concepts in color picture tube technology in the article starting on page 4.

Vince Piecyk, from Missile and Surface Radar, Moorestown, N.J., prepared the cover illustration.

RCA Engineer Staff

Tom King	Editor
Betty Stotts	Assistant Editor
Louise Carr	Art Editor
Frank Strobl	Contributing Editor
Betty Gutchigian	Composition
Dottie Snyder	Editorial Secretary

Editorial Advisory Board

Pete Bingham	Div. VP, Engineering, Consumer Electronics Div.
Jay Brandinger	Div. VP, SelectaVision VideoDisc Operations
John Christopher	VP, Tech. Operations, RCA Americom
Bill Hartzell	Div. VP, Engineering, Picture Tube Division
Jim Hepburn	VP, Advanced Programs RCA Globcom
Hans Jenny	Manager, Engineering Information
Arch Luther	Chief Engineer, Commercial Communications Systems Div.
Howie Rosenthal	Staff VP, Engineering
Carl Turner	Div. VP, Product Assurance and Planning, Solid State Div.
Bill Underwood	Director, Engineering Professional Programs
Joe Volpe	Chief Engineer, Missile and Surface Radar
Bill Webster	VP, Laboratories

Consulting Editors

Ed Burke	Administrator, Marketing Information and Communications, Government Systems Div.
Walt Dennen	Director, Public Affairs, Solid State Division
Charlie Foster	Mgr., Scientific Publications, Laboratories
John Phillips	Mgr., Proposals and Publicity, Automated Systems

•To disseminate to RCA engineers technical information of professional value • To publish in an appropriate manner important technical developments at RCA, and the role of the engineer • To serve as a medium of interchange of technical information between various groups at RCA • To create a community of engineering interest within the company by stressing the interrelated nature of all technical contributions • To help publicize engineering achievements in a manner that will promote the interests and reputation of RCA in the engineering field • To provide a convenient means by which the RCA engineer may review his professional work before associates and engineering management • To announce outstanding and unusual achievements of RCA engineers in a manner most likely to enhance their prestige and professional status.

Picture tubes

A challenge to continue our success



Joseph H. Colgrove

No mass-produced high-technology product marketed today is subjected to greater critique of worldwide media than the color television receiver and its components. RCA, its engineers and technical personnel are strongly identified with that product. Our established position in color television is due to the joint endeavors of the Consumer Electronics, Picture Tube and Solid State Divisions with the RCA Laboratories and rests upon years of outstanding technical effort and cooperation at every organizational level.

Confronted with a highly competitive worldwide marketplace, the engineers and technical staffs of these organizations are continually called upon to design, develop, manufacture, and market systems improved for performance, styling, reliability, and safety. In addition, the product must meet today's stringent competitive pricing requirements. In an intensively competitive market, the color television receiver represents an outstanding customer value.

This edition of the *RCA Engineer* features color television picture tubes. It contains articles covering overviews and trends, materials and components, processes and methods. These provide an insight into the technical and management complexities of this portion of the television industry.

RCA engineers can be proud of their past contributions to color television. Our future success will be based on the continued technical excellence of the readers of this journal. I salute you for your accomplishments and challenge you anew.

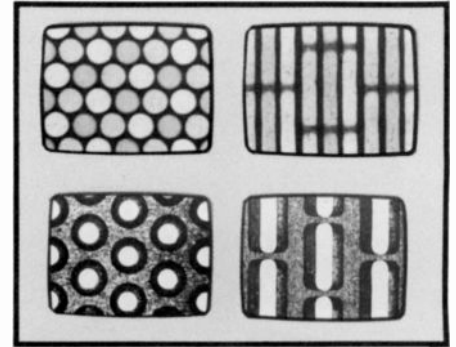
A handwritten signature in black ink, reading "JH Colgrove". The signature is written in a cursive, flowing style.

Joseph H. Colgrove
Vice President and
General Manager
Picture Tube Division

Highlights

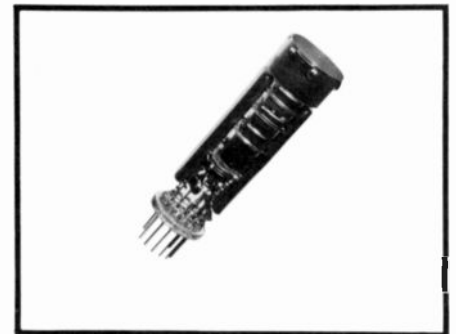
technology surveys —

the evolution of the picture tube art



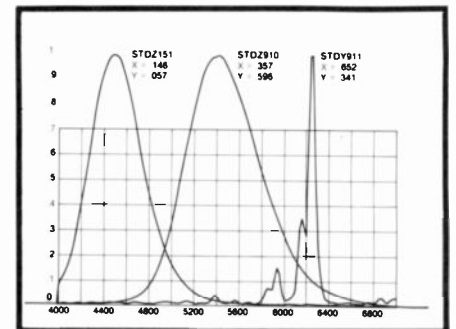
picture tube elements —

new elements, such as filter phosphors, bipotential focus guns and contoured-line screens are found in recent picture tubes



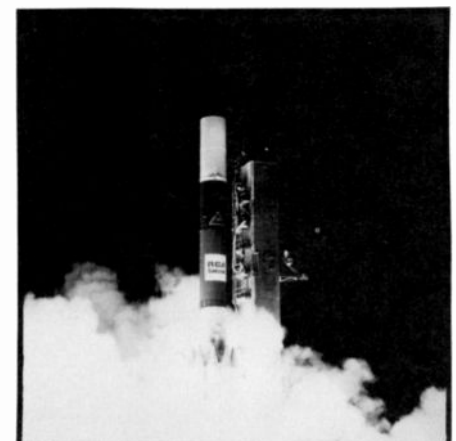
techniques —

several techniques used in picture tube development may be applicable to other fields



general interest —

several papers relative to communications satellites



In future issues

microprocessor applications, quality & reliability, RCA worldwide, color TV receivers, anniversary issue

- picture tube technology surveys**
- 4** Recent trends in color picture tube design
T.W. Branton|R.H. Godfrey|W.D. Masterton
A.M. Morrell|M.E. Trim|D.L. Weber
 - 12** Major developments in phosphors and screen application techniques for cathode ray tubes
A.E. Hardy
- picture tube elements**
- 19** Filter phosphors
S.S. Trond
 - 25** High-resolution bipotential focus gun for color picture tubes
R.H. Hughes|H.Y. Chen
 - 30** Process requirements for a new generation of precision in-line shadow masks
J.J. Moscony
 - 35** Contoured-line screens for new in-line color picture tubes
A.M. Morrell
- picture tube techniques**
- 40** Measurement of cathode temperatures using the retarding potential method
P.R. Liller
 - 45** Rapid scan determination of optical spectra
G.M. Ehemann, Jr.
 - 49** Statistical techniques for evaluation of test results from small groups of data
F.J. Hinnenkamp
 - 53** Picture tube x-radiation measurement and control
B.Z. Littlefield
- general interest**
- 58** A cure for FM modulation overshoot
R.F. Abt
 - 65** RCA Americom spacecraft reliability
P.W. DeBaylo
 - 73** NTSC color television performance measurements in communication systems
M. Shumila
 - 79** C-band FET power amplifier for TWTA replacement
H. Huang|B. Dornan|F. Drago|J. Hawley
- on the job/off the job**
- 83** An engineering approach to building bamboo fly rods
W.R. Fink
- departments**
- 87** Dates and Deadlines
 - 88** Pen and Podium
 - 90** Patents
 - 91** Engineering News and Highlights

Recent trends in color picture tube design

Recent trends in color picture tube designs have led to improved performance and cost savings for the receiver manufacturers.

Abstract: *The paper outlines the transition in color picture tube design in the past seven years — dot-trio screens have been superseded by line screens; delta guns have been replaced by in-line guns; and self-converging yoke systems have eliminated dynamic convergence circuits. Also, deflection angles have been increased. These new trends have affected many phases of tube construction. Changes in the screen structure have had an effect on*

screen tolerance and screen printing. Changes in the shadow mask and its assembly were also required. The new in-line gun designs are part of these new trends and even the bulb designs are affected by the new trends. Yoke design is even more intimately related to the tube in these new trends, and in some cases the yoke is attached to the tube and adjusted in the tube factory.

Over the last seven years there has been a major transition in the design of color picture tubes. This can be characterized by several significant changes from previous tubes as follows: dot-trio screens have been superseded by line screens, delta guns have been superseded by in-line guns, and self-converging yoke systems have eliminated dynamic convergence circuits.

In addition, the deflection angles have been increased from the previous standard of 90° to 110° for most tubes designed for the European market and 100° deflection is becoming common in the U.S. market. The neck diameter of most types has also been changed from 36 mm to 29 mm. This smaller neck has allowed increased yoke efficiencies but has also challenged the gun designer to achieve improved focus with smaller lenses. Gun developments within the last several years have resulted in the introduction of high-focus-voltage guns providing a substantial improvement in

resolution. Figure 1 shows pictorially what has happened to the color picture tube and its associated circuitry through a comparison between the latest RCA tube assembly and an earlier tube with all of the associated components and circuitry that have now been eliminated.

RCA pioneered and continues to lead in this new trend in color picture tubes, starting with the introduction of the 90° precision in-line family in the U.S. in 1972 and the 110° precision in-line family in Europe in 1975. These initial families used yokes incorporating precision-wound toroidal coils for both vertical and horizontal deflection. This precision-wound yoke was a key element in the success of self convergence. Recently, deflection yokes having saddle-shaped horizontal coils and toroidal vertical coils have become popular because of their higher efficiencies and circuit considerations. Improved yoke-winding technology has allowed these yokes to approach the accuracy of the original precision-wound toroidal yokes.

Coupled with the introduction of the

self-convergence feature was the concept of the tube having integral components — whereby the yoke and its neck components are assembled onto the tube, preadjusted at the factory, and sold as a combined package to the receiver manufacturer. This preadjusted tube assembly has been very successful in Europe and remains today as a standard in that market area. Recently, however, the trend in the U.S. has reversed to having the components assembled onto the tube and adjusted at the receiver plant.

The new trend toward in-line guns, line screens, and self convergence has raised many new design considerations which are described in this article.

Screen structure

For over 19 years the color picture tube industry was dominated by a dot-trio screen structure arranged in a hexagonal array as shown in Fig. 2a. In 1972, RCA announced the precision in-line color picture tube system, which incorporated a screen consisting of continuous vertical phosphor stripes with 100 percent screen coverage as shown in Fig. 2b. The apertures in the shadow mask are now vertically oriented slits with small cross ties (tie bars) which make it possible to form the mask into the basically spherical contour needed to match the glass/screen surface contour. This results in the illumination of rectangular segments of the phosphor with separations created by the tie-bar shadows, as seen in Fig. 3b.

In either system, the fundamental requirement for color fidelity is that each

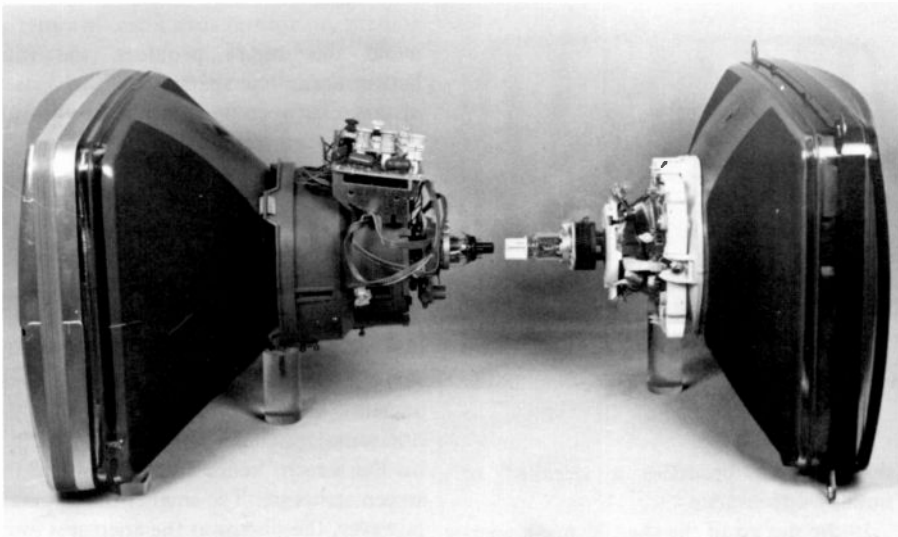


Fig. 1. Photograph showing the latest precision in-line tube (right) and a typical 1970 tube.

transmitted beam strikes only its own color phosphor and that the proper balance in light output be maintained between the three primary colors. Register between the electron beam and its phosphor element is subject to variations by phosphor printing errors, static and dynamic forces on the mask support assembly, thermal effects of mask support assembly, and varying ambient magnetic field conditions during operation of the finished tube. The desire for maximum light output would result in zero tolerance for misregister; however, this desire must be compromised in order to provide acceptable white uniformity and individual color purity.

For light output equivalent to that of the dot-trio screen, the line screen system has essentially the same tolerance at the screen center but somewhat more tolerance at the screen edge. This is particularly true with tubes incorporating the Super Arch mask which is discussed in a companion article in this issue.¹

Matrix and Sunshine screens

Today in the U.S. market, receiver manufacturers are almost exclusively using tubes having matrix screens. When first announced in 1969, the RCA matrix

system together with improved phosphors doubled the light output over the then existing RCA tubes. The matrix color screen system employs a black material around the phosphor dots or between the phosphor lines. This black matrix absorbs ambient light, which would normally be reflected by the screen of a non-matrix color picture tube, with minimum effect on the light output from the screen. This feature permits the use of a high-transmittance faceplate (typically 85 percent as compared to the previous typical value of 52 percent) to provide pictures with increased brightness. This increased brightness is obtained without sacrifice of picture contrast even under high ambient light conditions.

Because of the greater emphasis on white uniformity in the European market, RCA types produced for this market incorporate a non-matrix "Sunshine" screen, where comparable light output is achieved by increasing mask transmission and faceplate transmittance (from the previous typical value of 52 percent to a typical value of 72 percent). In order to maintain contrast and enhance the color in these non-matrix tubes with high faceplate transmittance, red and blue pigments are added to the red- and blue-emitting phosphors, respectively. This reduces the screen reflectivity and maintains the contrast. Pigmented phosphors are also incorporated in some matrix types to enhance the color and contrast even beyond that provided by the matrix alone. Pigmented phosphors are described more fully in a companion article in this issue entitled "Filter Phosphors."²

Screen printing

The phosphor screen is printed on the inside surface of the panel by a photodeposition technique on a lighthouse utilizing an ultraviolet light source and a lens system to refract the light in a manner simulating the deflection of the electron beams in the finished tube. In the dot-trio system it was determined that a continuous-surface glass lens could not be designed to simulate precisely both the vertical and horizontal deflection of the beam. To minimize this inherent misregister, extraordinary measures were employed including the use of "second-order" light source positions, or multi-element lenses which had to be oscillated during exposure. The advent of the line screen eliminated all vertical misregister and allowed the design of a continuous-

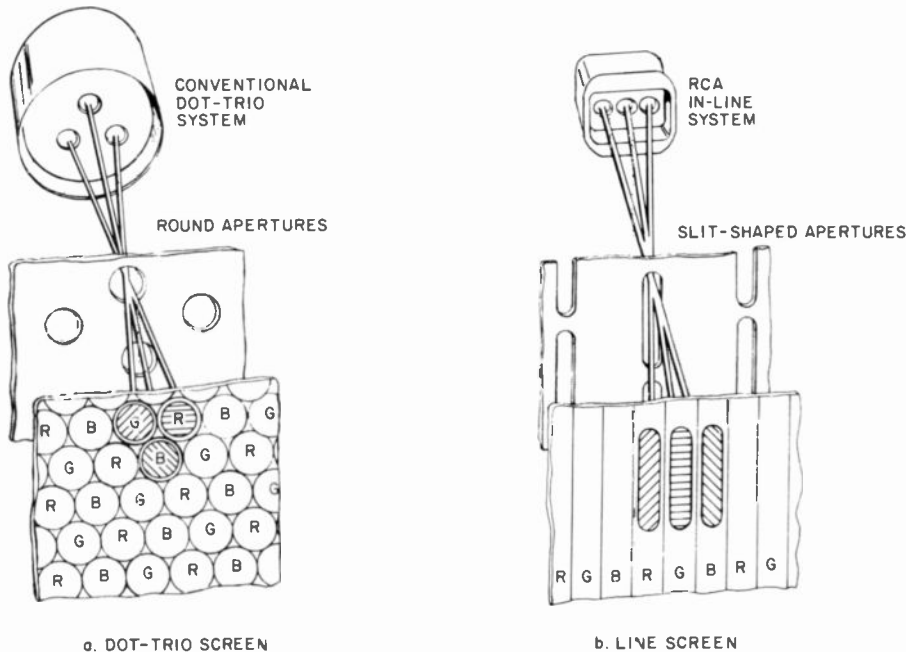


Fig. 2. Sketches of the dot-trio system compared with the in-line system showing the beam paths and the screen structures.

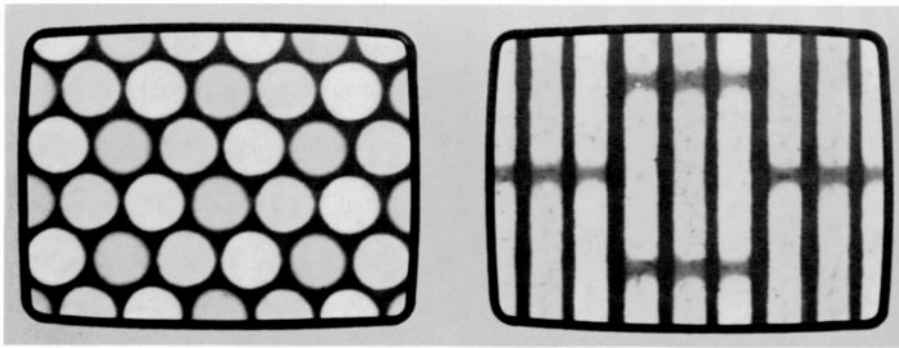


Fig. 3. Photomicrographs of an operating dot-trio screen and line screen showing tie-bar shadows.

surface glass lens that virtually eliminates horizontal register error.

In printing dot-trio screens, a circular light source was required. This was achieved by using a quartz collimator placed above an elongated mercury arc lamp. To improve the uniformity of the light across the screen, the collimator was frosted. The efficiency of this system was such that exposures were typically three to four minutes long.

In exposing line screens, an elongated source is desirable to connect the images from vertically-adjacent slits in the mask. This creates a continuous phosphor line which eliminates the need for beam register in the vertical direction. A mercury arc lamp is a line source; therefore, it can be used without the need for a collimator with its inefficiency. Exposure times are thereby reduced to a typical value of 30 seconds.

Printing with a line source instead of a circular source led to aberrations of the screen images as well as problems in printing smooth, constant-width lines. These distortion problems, referred to as "skew" and "necking", absorbed tolerance to misregister and had to be solved. A companion article in this issue¹ discusses alternate solutions to these problems and the reasons for RCA's choice of the curved mask aperture line approach.

Shadow mask

Etching elongated slits (Fig. 4b) involved a considerable development cycle to achieve in-line masks with quality comparable to that of dot-trio masks. Manufacturing processes had to be refined to achieve aperture crosssections that would avoid the production of stray electrons (which excite all three color phosphors with any particular beam on, and hence desaturate the intended color), while at the same time avoiding the variability in aperture size and

shape which produces a streaked or smudgy appearance.

In the design of the shadow mask aperture array, the basic parameters to be determined are the horizontal width of the aperture slits and the separation between them as well as the vertical height of the aperture slits (distance between the tie bars). The selections for these parameters involve a performance vs. manufacturability decision.

Vertical size and frequency of tie bars

The tie bars are made only as wide as necessary to avoid tearing during the forming process. The vertical separation between tie bars is made as large as possible to maximize the mask transmission hence light output. This parameter is subject to two constraints. First, it is chosen to be small enough to maintain the structural rigidity required to withstand handling during tube manufacture and to meet the extremely tight tolerance on mask replaceability during the screen printing operation. In addition, this choice must be restricted to certain "preferred" periodic values in order to avoid the production of a moiré or beat pattern caused by the interaction between the horizontal rows of tie bars

and the horizontal scan lines. In order to avoid this moiré problem, the ratio between scan-line spacing and the vertical distance between tie bars must be an odd multiple of one-eighth.

Horizontal slit width and frequency

In contrast to dot-trio screens, line screens permit a choice of horizontal dimensions that is completely independent of the vertical. The selection of the horizontal aperture separation determines the horizontal spacing between phosphor lines on the screen, hence the visibility of the screen structure. The smaller this spacing, however, the narrower the apertures must be to provide the necessary tolerance to mask motion and other sources of misalignment between the electron beam spot and its phosphor stripe array. The smaller the apertures, the more difficult it is to accurately etch them in such a way as to maintain a uniform mask transmission.

A more acceptable compromise between these conflicting demands has been achieved through the introduction of the variable horizontal spacing concept (inherent in the Super-Arch mask).¹ Selections are possible which not only accommodate the highest bandpass of most receivers but also are at a manufacturable level.

The remaining variable, the horizontal width of the slits, is made as high as possible to maximize transmission consistent with the tolerance needed to maintain field purity and white uniformity despite the misregister created by residual magnetic field, thermal, and mechanical effects.

Mask support assembly

The function of the mask support assembly (Fig. 5) is to maintain register between the

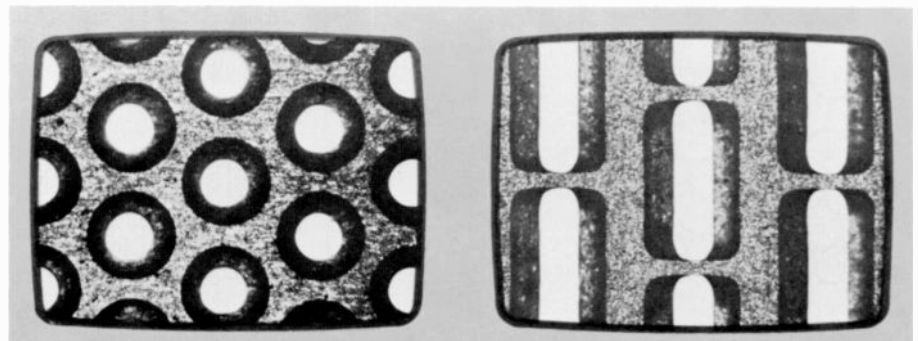


Fig. 4. Photomicrographs of small sections of a dot-trio aperture mask and of an aperture mask used in in-line tubes showing the slit-shaped apertures.

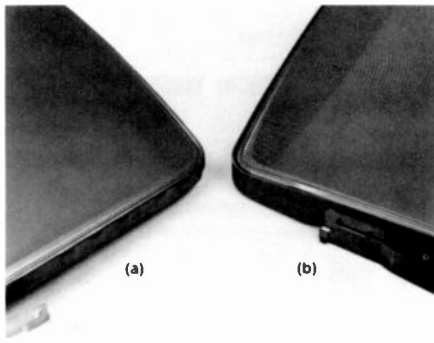


Fig. 5. A mask outside frame assembly (MOFA) (left) and a mask inside frame assembly (MIFA).

electron beams and the corresponding phosphor array within acceptable limits as the screen assembly and tube are subjected to thermal and mechanical stresses. Typically, this departure from register, i.e., misregister from all sources should be kept below $30\mu\text{m}$.

The q values (the spacing between the mask and the screen surface) of the assembly are critical since they determine the proper triad size needed to optimize both light output and register tolerance for either dot-trio or line screens. Values are determined by the geometric parameters associated with each tube type. The changes in q from the center to the edge of the screen in the dot-trio systems are dictated by the dynamic convergence requirements of the respective yoke designs, producing relatively low curvature surfaces of simple definition at higher deflection angles. However, the q requirements of the self-converging in-line systems, when tied in with Super Arch mask and contoured-line array configurations, have produced relatively high surface curvatures of a more complex nature. This increased curvature together with the increased q due to the smaller beam spacing have resulted in the mask being farther away from the screen in comparison to the older delta types. Since the panels are the same, this has presented a problem in maintaining the structure of the mask support assembly within the panel by a sufficient amount to allow proper handling in the factories. A solution to this problem was offered by the mask-inside-frame-assembly (MIFA) system as shown in Fig. 5b.

The virtues of the MIFA, as used for most new Super Arch mask tube types, lie in the fact that the mask is nested within the frame, allowing a shallower assembly to be located entirely within the panel. Doming misregister is reduced because the beam also heats a portion of the mask skirt formerly hidden by the frame structure of

the MOFA (mask-outside-frame-assembly). This results in less thermal gradient from the center to the edge of the mask; therefore, less doming misregister is developed. The frame also provides dent protection for the mask during normal tube fabrication.

Thermal compensation

Approximately 80 to 85 percent of the beam current is absorbed by the mask-frame assembly. Because of the differences in mass between the thin mask and the heavy frame, the mask temperature will rise faster than the frame temperature. Thus, the mask's shape will be distorted early in tube operation. This surface distortion, called doming, causes transient misregister. However, in-line tubes have one advantage over the dot-trio tubes in that all vertically-oriented beam motion resulting from this distortion is absorbed by the continuous line structure of the screen without misregister.

To minimize the peak doming misregister for in-line and delta types, maximizing thermal emissivity of the mask and decoupling of the mask to frame have been employed. The primary heat sink for the mask is the funnel; however, an obvious means for increasing the radiation from the mask is to use the panel as an additional heat sink. This has been done in certain wide-angle types by the use of a carbon-graphite coating applied to the back of the aluminized screen. To provide judicious decoupling of mask to frame, the number of mask-to-frame attachment points must be minimized; however, they must also be properly located to achieve structural rigidity of the assembly.

To provide additional accommodation for short-term doming misregister in certain areas of the screen, the phosphor lines are printed radially inward by a small amount (between 12 and $25\mu\text{m}$ from what they normally should be for best beam register). This process, which is called ADR (anti-doming radial), provides some absorption for the inward motion of the beam in the early stages of tube operation. Better white uniformity and field purity are maintained in the first five to ten minutes than would otherwise be possible. Sufficient tolerance must be designed into the system such that, as the beams move back out to their normal steady-state position, adequate register guard band is still preserved to maintain good purity and white uniformity.

Perma-Chrome,³ a system originally

developed for dot-trio tubes, compensates for misregister caused by long-term mask expansion and continues to be used in in-line tubes. Compensation in the Perma-Chrome system is achieved by moving the expanding mask assembly slightly towards the screen in such a way that the mask apertures follow the normal beam path and thus maintain good register between the beams and the phosphor dots or lines. This is accomplished by use of bi-metal mask support elements which expand in response to an increase in frame temperature.

The change from 90° to 110° tube deflection increases the misregister sensitivity of the screen-to-mask motion by up to 40 percent. Thus, the needs are greater in the higher deflection angle types not only for limiting doming but also for controlling the size and position of each screen element more precisely in order to absorb its effects.

Magnetic shields

Internal magnetic shields are standard in European tube types. Although they require more ampere-turns from the degaussing system employed to produce the same magnitude of register recovery for the earth's magnetic field, they potentially provide a more complete recovery for the axial component. To the set designer, internal magnetic shields make a neater, lower volume tube assembly for packaging considerations within the cabinet. To the tube designer, the internal shield represents a *known* register influence regardless of the differences in various receiver chassis designs. This permits the tube designer to design screen printing lenses and in-line tube assemblies more precisely for best performance in the field. In general, in-line tubes have presented easier solutions in the magnetic shielding area since the system need only minimize horizontal register changes.

In-line electron guns

There has been a dramatic revolution in electron gun design in recent years as shown in Fig. 6. The delta electron gun, designed to fit a 36 mm diameter neck, has been replaced by an in-line electron gun, designed to fit a 29 mm diameter neck. Extremely accurate beam alignment is obtained in the in-line gun through the use of one-piece, triple-aperture electrodes. The beam-to-beam spacing of this unitized

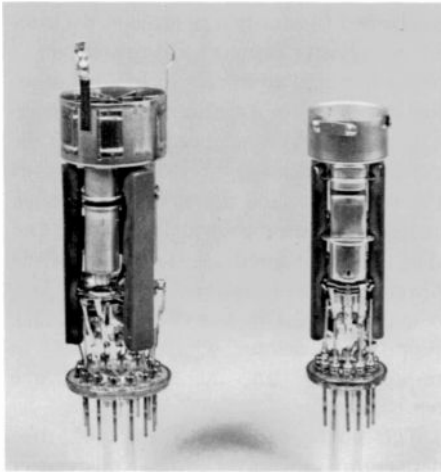


Fig. 6. A delta electron gun (left) and a high-voltage-focus precision in-line electron gun.

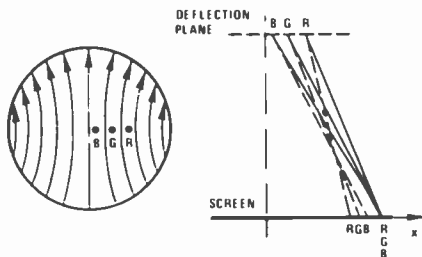


Fig. 7. Self-converging horizontal deflection field.

construction is a function of tool-and-die accuracy rather than mount-assembly techniques. This feature makes the inherent self-convergence feature of the precision in-line system practical.

Two new developments in the past two years have resulted in an improvement in the focus performance of RCA precision in-line tubes. The spacing between the electron beams was increased from 5.1 to 6.6 mm. This allowed the lens diameter to be increased resulting in the improved performance. The focus was further improved through the development of a high-focus-voltage bipotential precision in-line electron gun (see companion article in this issue).⁴

Bulb development

In the last seven years bulb developments from the viewing side of the tube have been rather insignificant. The last major change was the ultra-rectangular screen first introduced in 1969 with the 21V tube as the initial size. This family gradually increased until the latest addition of the 13V tube size in 1974 and now includes 13V, 15V, 17V, 19V, 21V and 25V sizes. The only other visible change in the exposed panel surface

has been the glass transmittance which was compromised between best light output and best contrast. Currently non-matrix tubes use 72 percent panel transmittance and the matrix tubes use 85 percent transmittance.

The change in screen structure from dot-trio to line-trio screens and the addition of matrix have placed more stringent requirements on glass blemishes. Thus, cords (very light line striations due to a non-homogeneous mixture) in the glass are less tolerable because they produce a beat interference pattern with the lines of the screen making them more visible as a blemish. New panel inspection techniques and equipment were developed to make these cord blemishes visible in the panel before screening. Inside panel-face surface blemishes also become more objectionable because matrix application is sensitive to surface blemishes.

The other half of the bulb, the funnel, has had many design changes due to innovations and developments in deflection angles, yokes, and electron guns. Such designs can be placed into three general funnel areas: the body, the yoke area, and the neck.

The funnel body length varies with changes in deflection angle and tube size. Other than size and deflection angle, the body contour is designed to meet strength requirements. During the latter half of the 1960s the 90° deflection angle was the industry standard. Early in the 1970s, RCA introduced the 110° narrow-neck delta system into Europe which permitted the TV cabinet to be about 12 cm smaller in depth than those for 90° tubes. The 110° development was offered only in the larger tube sizes (19V and up). More recently the 100° deflection angle tube which required a new funnel body design was introduced

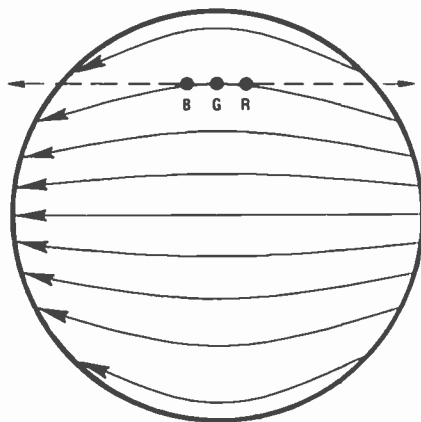


Fig. 8. Self-converging vertical deflection field.

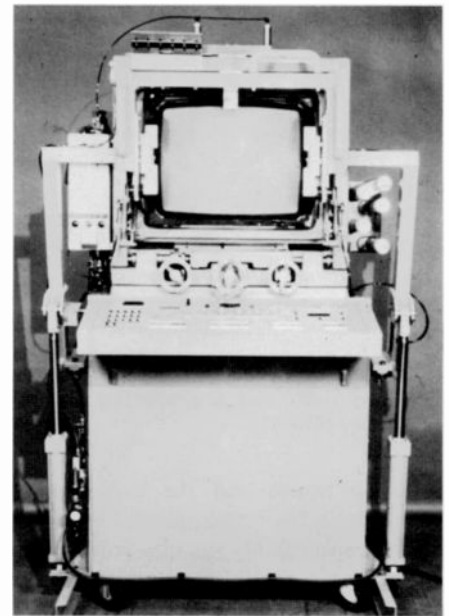


Fig. 9. One hundred and ten degree YAM (yoke adjusting machine) used in the picture tube factory for accomplishing the yoke adjustments on the tube.

into the U.S. market. Now the tube maker is faced with supplying three funnel body designs for any particular tube size: 90°, 100° and 110° deflection types.

The second funnel area which has undergone extensive changes is the contour in the yoke region. This was necessary to accommodate three general types of yokes. Until 1971 the color tube yokes were made with saddle-type coils for both horizontal and vertical deflection. The complementary yoke-area contour was long with a gentle taper down to a 36 mm diameter neck. The RCA European 110° narrow-neck delta system incorporated a yoke with toroidal-shaped deflection coils on a shorter core. The required funnel contour was shorter and more sharply flared than that required for the former saddle-type yoke.

This new yoke then set the pace and the same type was used in the 90° Precision In-Line tubes, the next later development for the U.S. market. The funnel yoke-area contour for this 90° in-line tube was similar to the 110° contour but with a slightly smaller yoke diameter. The latest yoke-area funnel contour was developed for in-line tubes using saddle-toroidal yokes. This construction employs a so-called "open-throat" (OT) funnel where the yoke-area contour lies between that required for saddle-type yokes and toroidal-type yokes. This development coincided with the advent of 100° deflection so the 100° funnel was designed for saddle-toroidal yokes from the outset; however, open throat

funnels had to be designed for 90° and 110° types in all of the current sizes.

Another development of the in-line construction was to permanently attach the yoke to the tube by means of a plastic ring cemented to the funnel. This construction required a larger diameter yoke-area contour control to assure fit between the yoke support ring and the glass.

The third major area of change in the funnel has been neck size and length. The 36 mm neck size which was standard for 90° delta types was changed to a 29 mm diameter for the 110° delta system and all RCA in-line types to improve convergence and reduce deflection power.

Neck length is a function of the electron gun length and its proximity to the yoke field and of other minor mechanical considerations such as having sufficient length for positioning the neck components. The several generations of in-line electron guns and associated yokes each have a unique seal length. A single funnel body design may have to be supplied with several different neck lengths.

Yokes and yoke-tube assemblies

RCA introduced the 90° Precision In-Line Color Picture Tube Assembly in 1972⁵ incorporating a line focus type PST (precision static toroid) deflection yoke attached and adjusted at the tube factory. This self-converging system was superior to the previous delta-gun configuration in that it eliminated dynamic convergence corrections and extra circuitry which significantly reduced the receiver costs. The resultant convergence is far superior to that achieved with delta tubes utilizing saddle type yokes and extra circuitry.

The delta-gun systems used yokes whose fields overconverged the deflected beams, and electromagnets driven by the dynamic convergence circuits reconverged them. The PST yoke was designed to have non-uniform fields to counteract this overconvergence by diverging the beams horizontally in the yoke field. This was accomplished by producing a pincushion-shaped field whose intensity increased with horizontal distance from the minor axis. Figure 7 shows the overconverged beams and the converged beams when deflected by the non-uniform field. The vertical coils generate a barrel-shaped field that diverges the offset beams horizontally in the yoke as shown in Fig. 8.

Yoke adjustments for ITC (integral tube

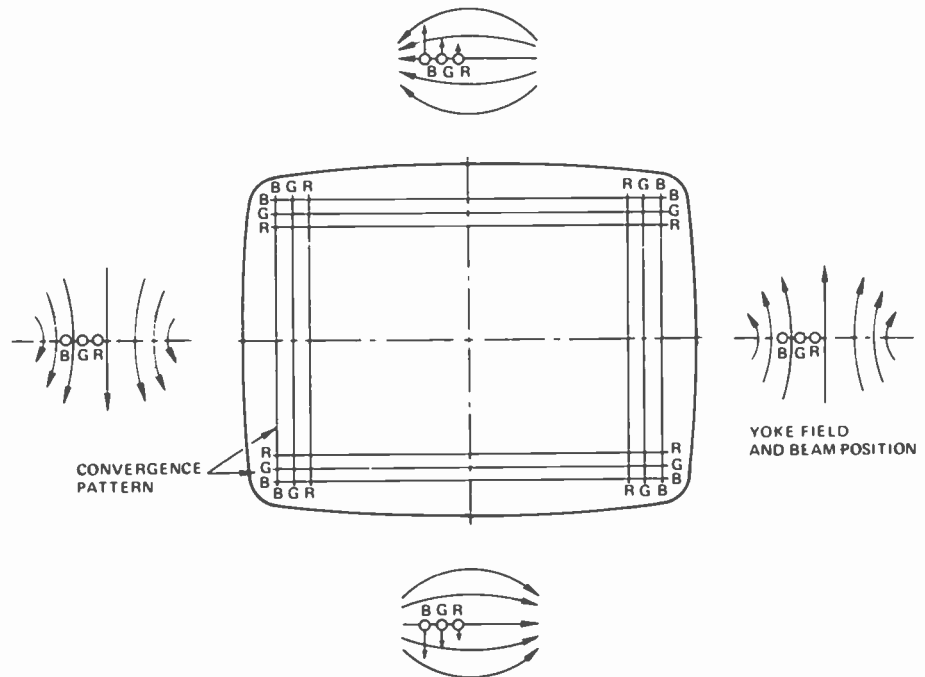


Fig. 10. Horizontal alignment errors and their correction.

component) tubes are accomplished at the tube factory in a YAM (yoke adjusting machine, see Fig. 9) that provides precise motions while an operator observes the tube's screen. Adjusting the yoke horizontally with respect to the electron beams increases the width and height of the raster generated by one of the outer beams while reducing the width and height of the other outer-beam raster as shown in Fig. 10. A vertical yoke motion will cause a raster

rotation of the outer beams; one will rotate clockwise and the other counterclockwise. This action is illustrated in Fig. 11. After adjustment, the yokes are held in position and locked to the tube using a hot-melt glue. Ninety-degree deflection tubes have molded plastic rings cemented to the tube before the YAM operation and the yoke is attached to this funnel ring (Fig. 12).

In 1975 a 110° precision in-line tube assembly was evolved through design

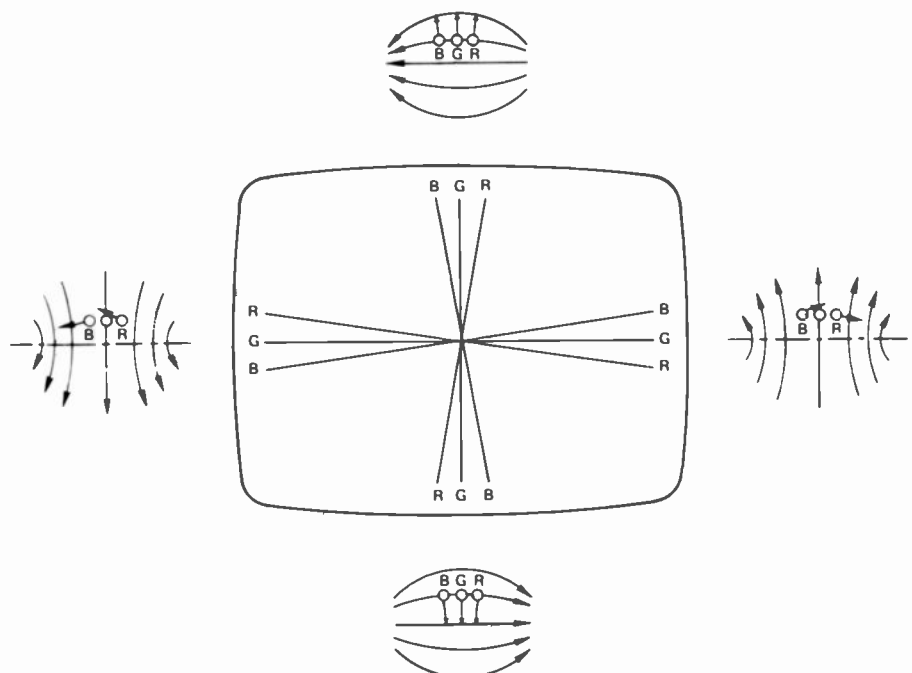


Fig. 11. Vertical alignment errors and their correction.

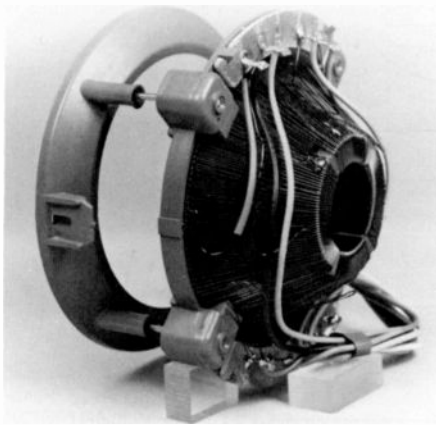


Fig. 12. Ninety-degree PST yoke and its associated funnel ring showing posts and sockets for hot-melt glue.

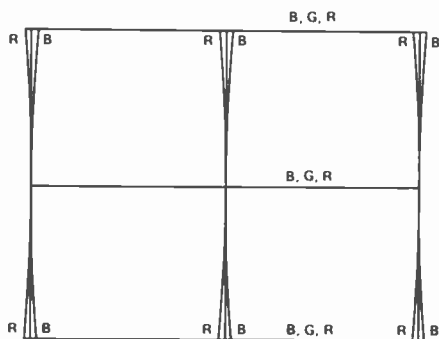


Fig. 13. Convergence errors of 110° in-line system without quad correction.

changes to the 90° PST-type deflection and introduced in Europe. The yoke incorporated in this system also has horizontal and vertical astigmatism caused by a barrel-shaped vertical deflection field and a pincushion-shaped horizontal deflection field. The systematic convergence errors

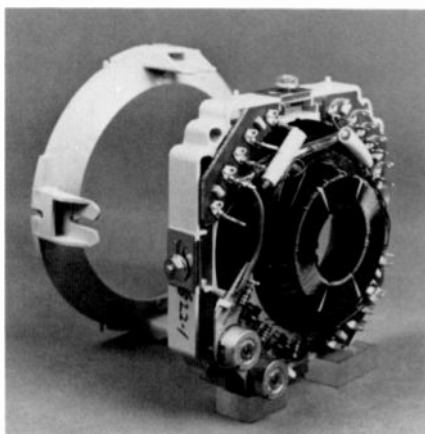


Fig. 14. One hundred and ten degree PST yoke and its associated funnel ring showing adjustment bolts and the set of quadrupole windings.

Table I. Comparison between the precision static toroid (PST) deflection yoke and the saddle-toroid (ST) yoke characteristics.

Parameter	90° deflection		110° deflection				Units
	ST yoke	PST yoke	ST yoke		PST yoke		
	Parallel	Series	Series	Parallel	Series	Parallel	
L_H	2.18	0.66	1.20	.30	—	0.28	mH
R_H	1.50	1.45	1.05	.26	—	0.36	Ω
I_{PP}	2.6	5.9	5.2	10.4	—	12.0	A
E	1.8	2.9	4.0	4.0	—	5.0	mJ
L_V	7.68	1.14	25.0	6.25	3.2	—	mH
R_V	3.15	1.87	9.6	2.4	3.9	—	Ω
I_{PP}	1.6	3.6	1.2	2.4	3.1	—	A
P_P	2.0	6.1	3.5	3.5	9.4	—	W

were reduced to a vertical line separation at the ends of the minor axis (Fig. 13).

These reduced errors were eliminated by driving a set of quadrupole windings, positioned on the yoke at the $\pm 45^\circ$ diagonals, with a vertical-frequency waveform. By wiring a simple circuit in series with the vertical windings, the vertical pulse drives the combination. The amount of correction varies tube-to-tube and is adjusted at the tube factory during the YAM operation.

This 110° yoke also uses a molded plastic mounting ring cemented to the bulb funnel. The mounting ring has four tabs with slots so that the yoke housing can be secured to the mounting ring by nuts and bolts (Fig. 14) and readjusted if necessary.

With the advent of higher impedance circuits, a yoke with matching characteristics was needed, and the saddle-toroidal (ST) yoke was chosen. The ST yoke uses a toroidal winding on a ferrite core for its vertical coils. In order to increase the horizontal impedance over the PST yoke, the saddle coil configuration was required (Fig. 15). Many innovations

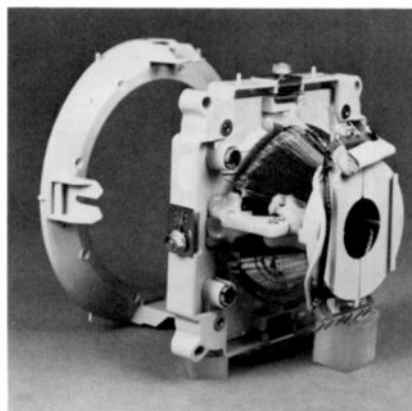


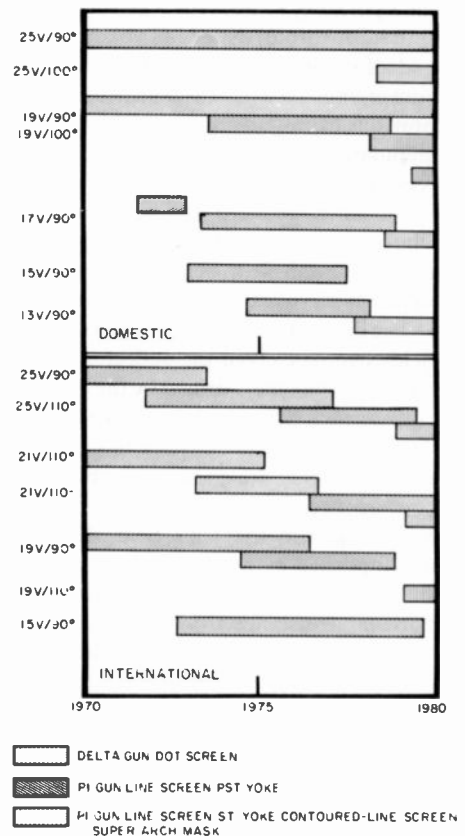
Fig. 15. One hundred and ten degree ST yoke with a toroidal winding for its vertical coil.

in yoke manufacturing techniques and the use of computer-aided design were required to achieve an ST yoke that provided the same quality performance as the earlier PST yokes.

The new ST yoke also offers the following advantages: no NS raster distortion and reduced EW raster distortion, lower horizontal energy storage, less vertical power dissipation, and reduced magnetic field leakage.

Computer-aided design concepts have helped to reduce the systematic errors apparent in the PST yokes. The saddle

Table II. Trends in major RCA color picture tubes since 1970.



coils permit more design flexibility than the toroidal coils, and the winding variations apparent in earlier saddle coils have been reduced by the use of precision high-speed coil winding machines.

In the latter part of 1978 an RCA 110° deflection yoke was demonstrated with initial production started in the first quarter of 1979. The goals set for the 90° ST yokes in 1978 were carried into the 110° system with several additional requirements not attainable in previous 110° deflection ST yokes. The efficiency of the 90° and 110° ST yokes has been significantly increased over that of the PST systems, as shown in Table I.

Summary

Recent trends in color picture tube designs have resulted in shorter and lighter tube-yoke systems with improved focus and convergence, lower energy requirements, and cost savings to the receiver manufacturers through eliminated circuitry. The

chronology of these trends in tube design for the U.S. and international markets is shown in Table II.

Acknowledgments

The development of the new concepts in color picture tubes and tube systems is the result of work by various engineering departments of the Picture Tube Division. The yoke developments were accomplished by the Consumer Electronics Division and the RCA Laboratories.

Bibliography

1. Masterton, W.D., Barbin, R.L.: "Designing Out the Problems of Wide-Angle Color TV Tubes," *Electronics* (Apr 26, 1971).
2. Thierfelder, C.W.: "RCA Large-Screen, Narrow-Neck 110° Color Television System," *IEEE Transactions on Broadcast and Television Receivers* (Aug 1971).
3. Barkow, W.H., Gross, J.: "The RCA Large Screen 110° Precision In-Line System," Second Annual Convention Fernseh-und Kinotechnische Gesellschaft, Munich, Germany (Oct 15, 1974).
4. Morrell, A.M.: "Design Principles of the RCA 110° Precision In-Line Picture Tube," Second Annual Convention Fernseh-und Kinotechnische Gesellschaft, Munich, Germany (Oct 15, 1974).
5. Morrell, A.M.: "Design Principles of the RCA Large-Screen 110° Precision In-Line Color Picture Tube," 1975 IEEE Chicago Fall Conference on Consumer Electronics.
6. Morrell, A.M., Law, H.B., Rambers, E.G., and Herold, F.W.: "Advances in Image Pickup and Display Supplement I, Color Television Picture Tubes," *Academic Press* (1974).

References

1. Morrell, A.M.: "Contoured-Line Screens for Color Picture Tubes," 1977 IEEE Chicago Fall Conference on Consumer Electronics and *RCA Engineer*, this issue.
2. Trond, S.S.: "Filter Phosphors," *RCA Engineer*, this issue.
3. Godfrey, R.H., Shrader, I.M., and Demmy, R.D.: "Development of the Perma-Chrome Color Picture Tube," *IEEE Transactions on Broadcast and TV Receiver* (Sep 1968).
4. Hughes, R.H., Chen, H.Y.: "A Novel High Voltage Bipotential CRT Gun Design," 1978 IEEE Chicago Fall Conference on Consumer Electronics and *RCA Engineer*, this issue.
5. Barbin, R.L., Hughes, R.H.: "New RCA Color Picture Tube System for Portable TV Receivers," IEEE Spring Conference, Chicago, Ill. (Jun 13, 1972).

Tom Branton joined the picture tube design staff at the Marion Plant in 1965. Currently he is an engineering leader in the Tube Development Department of the Picture Tube Division and is responsible for deflection yoke interface, mask artwork, prototype equipment, and competitor evaluations.

Contact him at:
Tube Development
Picture Tube Division
Lancaster, Pa.
Ext. 3483

Dick Godfrey has been associated with Picture Tube Design and Manufacturing since joining the Picture Tube Division in 1950. In his present position of engineering leader, Tube Development, he is responsible for the tube product design, development, testing, and specifications of all new color picture tube types.

Contact him at:
Tube Development
Picture Tube Division
Lancaster, Pa.
Ext. 3483

Walt Masterton joined the Picture Tube Division in 1965 and has been involved with tube and screen geometry. He is responsible for special problems in that area, as well as, all phases of lighthouse lens design.

Contact him at:
Tube Development
Picture Tube Division
Lancaster, Pa.
Ext. 3483



From the left, Walt Masterton, Marv Trim, Don Weber, Al Morrell, Dick Godfrey, and Tom Branton.

Al Morrell has been with the Picture Tube Division since 1950 and has specialized in color picture tube design and development. In his present capacity as Manager, Tube Development, he is responsible for all phases of tube development, yoke interface, testing, specifications, competitor evaluations, prototype equipment, and issuing engineering standards for new color picture tube designs. Mr. Morrell recently received the IEEE Vladimir K. Zworykin Award for contributions to shadow-mask color picture tube design and development.

Contact him at:
Tube Development
Picture Tube Division
Lancaster, Pa.
Ext. 2184

Marvin Trim has been with RCA since 1960, first in Commercial Engineering and since 1976 in Tube Development, Picture Tube

Division. In both departments he has been responsible for the publication of technical data sheets, application notes, and other promotional material covering color picture tubes.

Contact him at:
Tube Development
Picture Tube Division
Lancaster, Pa.
Ext. 3483

Don Weber has over thirty years experience in the electron tube industry. Since 1963, he has worked at the Picture Tube Division. His responsibilities include glass bulb development, implosion protection and mounting system design, and development of dimensions for finished tubes.

Contact him at:
Tube Development
Picture Tube Division
Lancaster, Pa.
Ext. 3483

Major developments in phosphors and screen application techniques for cathode ray tubes

The cathode ray tube, as a display device, is more than fifty years old. The applications for CRT displays continue to increase. The most promising of the flat panel TV systems still use phosphors to convert electron beam energy into light.

Abstract: *A review of commercial phosphors and screen application techniques are presented, beginning with the radar tubes of the 1943 period up to the materials and processes used in present-day color television picture tubes. The discussion includes phosphors for industrial and military tubes, voltage dependent multicolor emitting phosphors, and projection tube phosphors. The history of the screen deposition techniques of water setting, dusting, slurry and black matrix application is described briefly. A projection of the future of phosphor-cathode ray tube display is given.*

The first crystalline inorganic luminescent materials were prepared as early as 1603. For the next 283 years alchemists synthesized long phosphorescent alkaline earth sulfides but these phosphors were unstable and decomposed slowly in moist air producing hydrogen sulfide.

In 1886 copper activated zinc sulfides were synthesized which were relatively stable and were used as the first practical detectors of ultraviolet radiation, cathode rays and x-rays.

One of the earliest books on phosphors is Lenard *et al.*'s tome printed in 1928 (Fig. 1). About 1929, a cathode ray tube containing a phosphor viewing screen was used as a potential electronic television system. At this time only two phosphors were

available with enough efficiency for television use. These phosphors were blue-green-emitting zinc sulfide:copper, and green-emitting zinc silicate:manganese. Interestingly enough, these same two phosphors, in a highly developed state, are still used today in some color television tubes and various cathode ray tubes for military and industrial applications. For example, zinc cadmium sulfide:copper:aluminum is one of the commonly used green primary color phosphors used in direct view color picture tubes. The green-emitting zinc silicate:manganese is still

used in some color television projection tube systems since its light output as a function of beam current density is nearly linear over a wide range.

Work on radar and television screens

In 1943, the big challenge in CRT phosphors was to improve the performance characteristics of the cascade P7 radar screen. The critical characteristic of this screen was the so-called build-up ratio



Fig. 1. Early publications on the subject of fluorescent and phosphorescent materials.

Reprint RE-25-2-2
Final manuscript received May 24, 1979.

which permitted an operator to distinguish random noise signals from real targets. The electron beam was scanned in a radial mode, while being rotated continuously in synchronism with the radar antenna. Real target signal pulses would occur at the same spot on the phosphor screen with each revolution of the antenna. As a result of the repetitive pulsing, the spot brightness would increase. On the other hand, random noise pulses would not repeat and hence would disappear into the background.

A substantial increase was made in this build-up ratio and more importantly a high level of control was achieved in the reproducibility of production batches of phosphors.

At the end of World War II, the work on the black and white television phosphors was resumed. The first black and white screens in the United States used a physical mixture of blue-emitting zinc sulfide:silver, and yellow-emitting zinc beryllium silicate:manganese. By 1947, the zinc beryllium silicate had been replaced by zinc cadmium sulfide:silver, with a very substantial increase in picture brightness. Much effort went into further improving the all-sulfide (P4) black and white screen efficiency.

Today many P4 screens use a blue-emitting zinc sulfide:silver, and yellow-emitting zinc cadmium sulfide:copper:aluminum. Some Japanese manufacturers are using a yellow-emitting zinc sulfide:copper:aluminum:gold, plus a rare-earth red-emitting third component to avoid the need to use cadmium. The basic screen efficiency of P4 is in the range of 36-40 lumens per watt dissipated in the screen, depending on the shade of white that is specified.

Color television phosphors

Phosphors for color television screens (P22) have undergone a spectacular development since the first all electronic color receiver of 1951 and so has the test equipment for measuring phosphor optical characteristics. For example, in 1943, if anyone wanted a spectroradiometer he had to build it (Fig. 2).

The Tektronix digital processing oscilloscope (DPO) is a system in which oscilloscope displays can be digitized as 512 points and stored in a minicomputer for processing. The computer uses a modified form of the BASIC language which is optimized for processing arrays in which oscilloscope waveforms are stored.

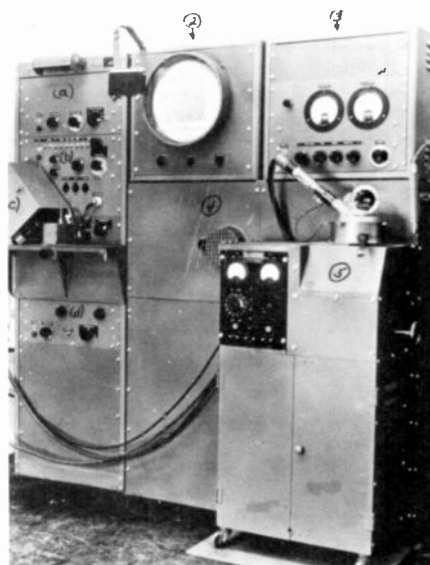


Fig. 2. Laboratory constructed spectroradiometer of the early forties compared with new Tektronix model.

The 7704A oscilloscope system accepts input from the 7J20 rapid scan spectrometer plug-in. At the other end of the 7J20 is the silicon vidicon 512 channel detector, whose readout beam scans the 400 nm spectrum at rates as fast as 20 ms. The computer is a DEC PDP-1135 with a hard disc drive. Tristimulus and calibration arrays are stored on a disc memory. Calculations performed in the 28 K memory are displayed in tabular and graphic form on the 4010 graphic terminal (Fig. 3).

More than 20 phosphors have been used commercially in color picture tubes for home viewing. This list includes at least 10 red emitters, 8 green emitters and 3 blue emitters. At the present time only two reds are used, three greens and basically one blue. The red emitters are either yttrium oxide:europium or yttrium oxysulfide:europium. The greens include zinc sulfide:copper:aluminum, zinc sulfide:copper:aluminum:gold and zinc cadmium sulfide:copper:aluminum.

The blue emitter is basically zinc sul-

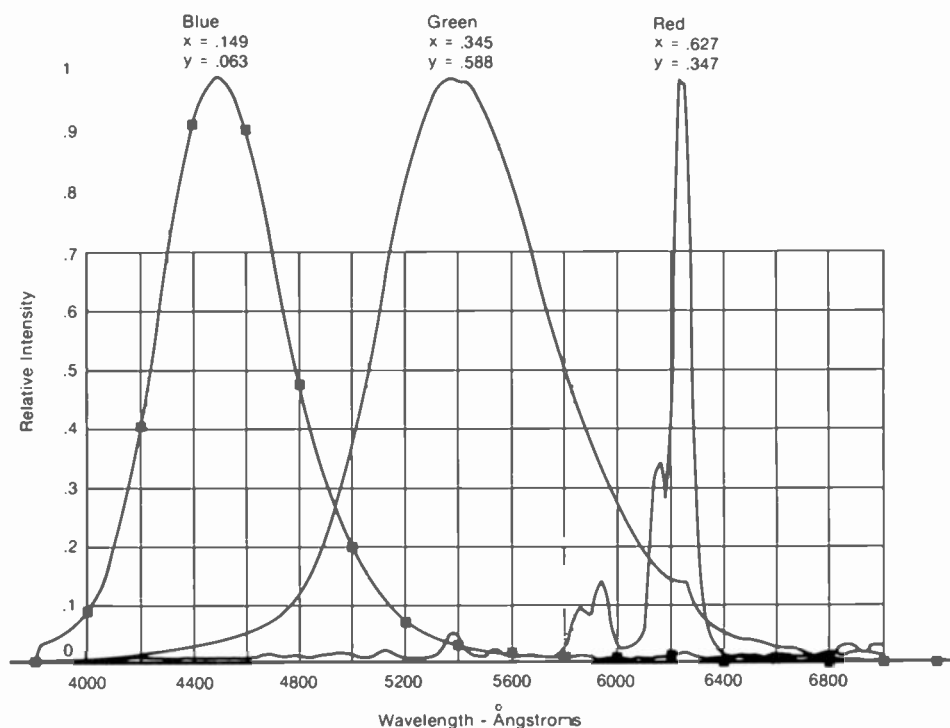


Fig. 3. Typical display from the 4010 graphic terminal

side:silver in cubic crystalline form with minor variations in preparation conditions which are tailored to specific screening methods.

White brightness improvement

As a result of this vigorous and sustained color television phosphor development for 25 years, the basic white light screen efficiency has been increased from 8 lumens per watt to 48 lumens per watt, a factor of 6 (Figs. 4, 5). It seems very likely that any further substantial improvements in basic phosphor efficiency will be realized in the foreseeable future only with great difficulty. The first step was the change from the blue sulfide, green silicate and red phosphate system to the all-sulfide system. There was a substantial increase in white brightness, with a trade-off in green and red saturation. The screen application of the all-sulfide was more difficult in respect to adherence and cross-contamination, but the increased brightness was badly needed.

The next significant advance was the use of the rare-earth red-emitting yttrium vanadate:europium by Sylvania. The introduction of yttrium vanadate as such did not greatly increase white brightness but it did open the door to a new phosphor system.

In a relatively short time RCA developed the rare-earth red yttrium oxysulfide:europium which did significantly increase white brightness. At this point, the vanadate became obsolete and was replaced by the straight yttrium oxide:europium or the yttrium oxysulfide:europium. Most companies today use the latter.

In the filming area another noteworthy brightness gain was obtained with RULP. This is a four-component filming emulsion consisting of Rhoplex (an acrylic polymer), Unisize (a mixture of polyvinyl alcohol and boric acid), Ludox (colloidal silica) and hydrogen peroxide. This improved emulsion gave results equivalent to spray filming.

The last big step was the use of larger particle size phosphors, increased screen weight, longer settling out time and gentle ball milling. The top step is TAP which is a "thick adherent precoat" on the glass prior to screening. This improvement is not in use at the present time. In Fig. 4, it can also be seen that the green chromaticity was shifted several times to increase white light output.

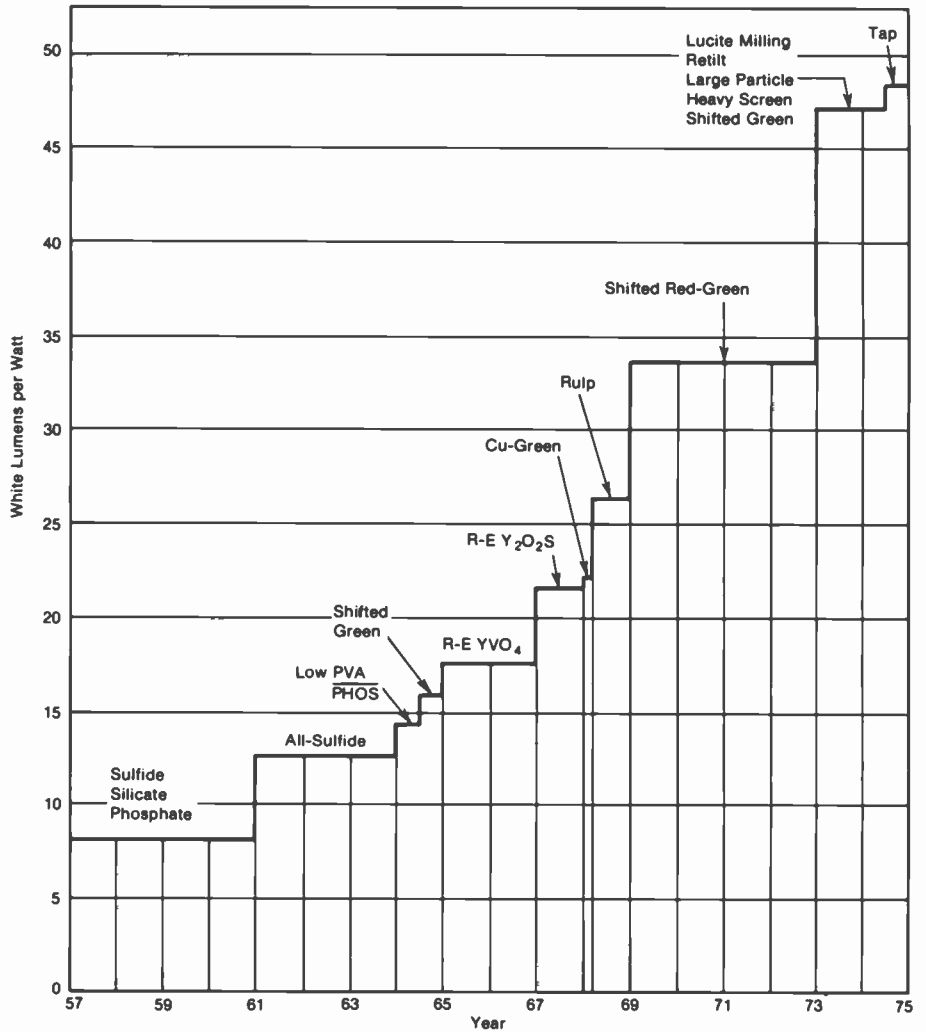


Fig. 4. Intrinsic phosphor screen efficiency, white lumens per watt.

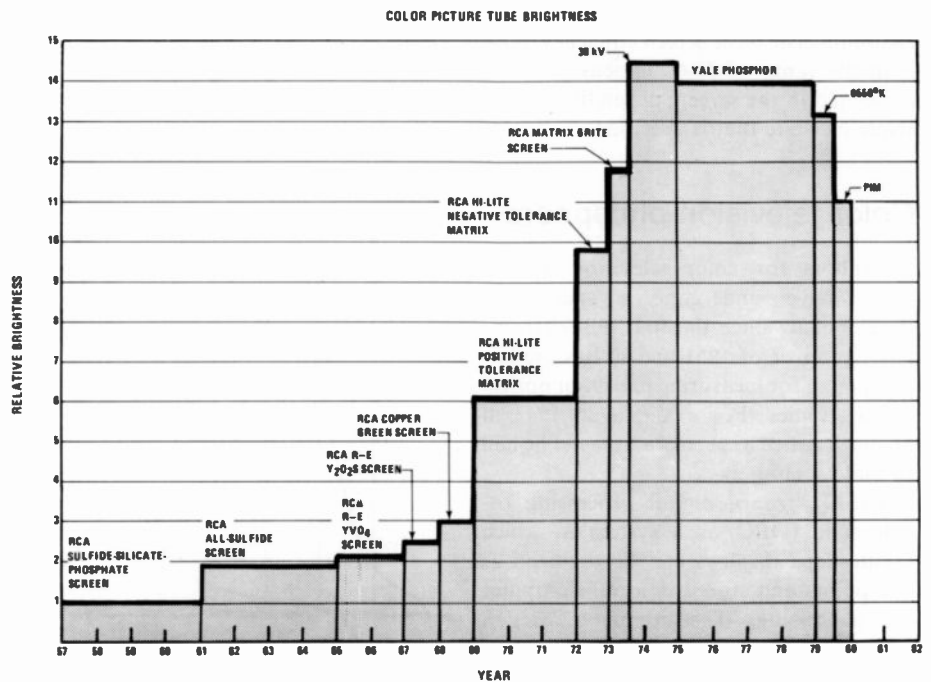


Fig. 5. The relative color picture-tube brightness increases over a seventeen-year period.

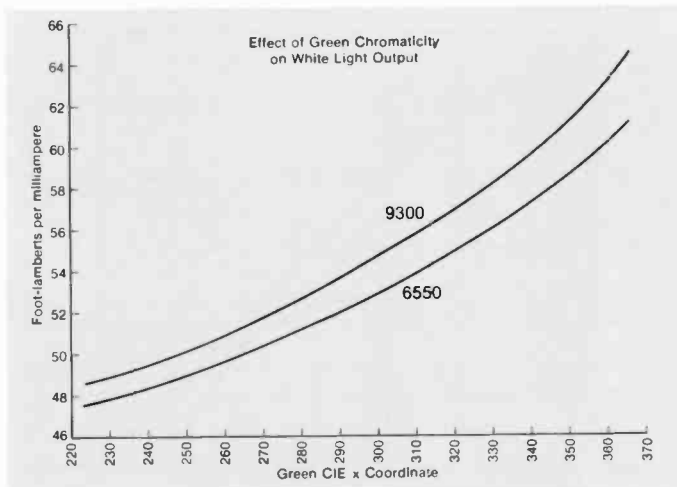


Fig. 6. Effect of green chromaticity on white light output.

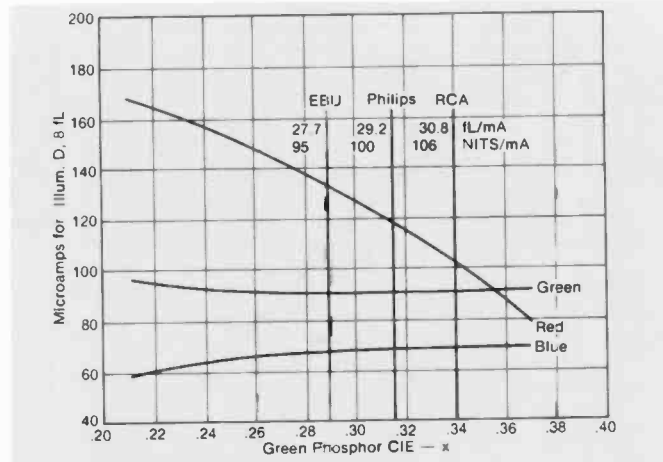


Fig. 7. Effect of green phosphor CIE-x on screen currents for tubes of three manufacturers.

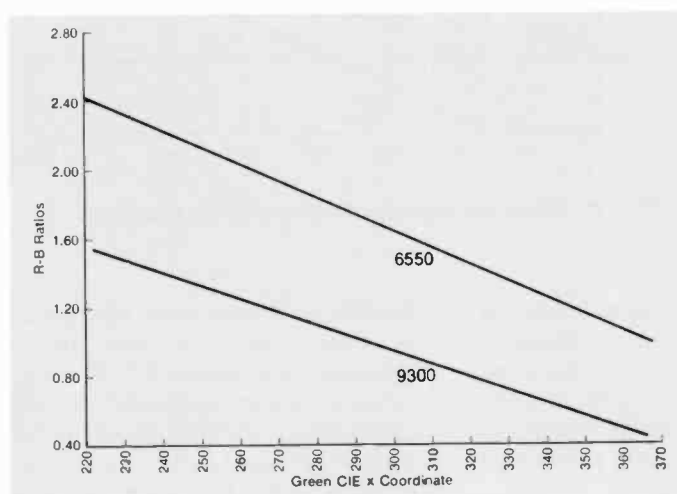


Fig. 8. Effect of green chromaticity on R-B current ratios.

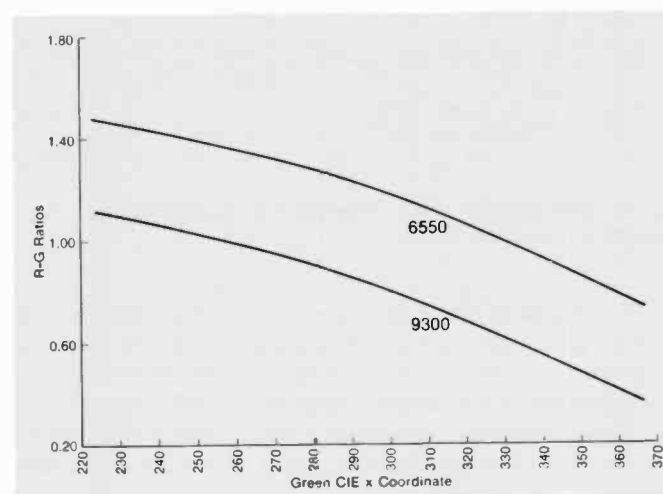


Fig. 9. Effect of green chromaticity on R-G current ratios.

The chromaticities of the primary phosphors as well as their basic efficiencies determine white brightness and white gun current ratios for a fixed amount of beam current into the phosphor screen. The white brightness is particularly sensitive to the green chromaticity (Fig. 6, 7, 8, and 9). The rule of thumb is that a change of 0.001 in the green CIE x causes a 0.20 percent change in white brightness.

Improving contrast

Another significant step on the brightness staircase is the matrix screen. In this system, a black graphite surround is provided for the phosphor mosaic. The black surround reduces ambient light reflection, thus permitting the use of a higher transmission faceplate glass. This combination permits a significant brightness increase while retaining picture contrast. The present day negative

tolerance matrix tube represents essentially the optimum trade-off of brightness and contrast. Increasing the matrix area or decreasing the faceplate glass transmission would further improve picture contrast but only with an unacceptable loss in picture brightness.

Pigmented phosphors

There is one avenue of approach for increasing contrast which may be considered as an extension of the matrix principle. This approach is to reduce the reflectivity of the phosphor elements directly. The general means for accomplishing this is to incorporate appropriate light absorbing pigments or filters with the light emitting phosphor elements. The particular technique that RCA has developed for accomplishing this is to apply a red-reflecting inorganic material to a preshifted red phosphor core

material. The red phosphor core is still the RCA rare-earth yttrium oxysulfide:europium and differs from the standard red only in chromaticity. This core is red when combined with red pigment and has the same chromaticity as standard red.

The pigmented blue is prepared in the same way using a pre-shifted blue core of zinc sulfide:silver.

The green is not pigmented since there are no suitable green pigments. However, the green already has a greenish body color.

One interesting aspect of the pigmented phosphor screen is the ambient appearance of the tube in the unlit condition. The red-emitting phosphor elements appear red, the blue appear blue and by contrast the green appears green.

Actual tube measurements confirm that the tube face reflectivity is reduced from 40 percent to 30 percent while the light output reduction is less than 5 percent.

The pigmented phosphor screen is one of

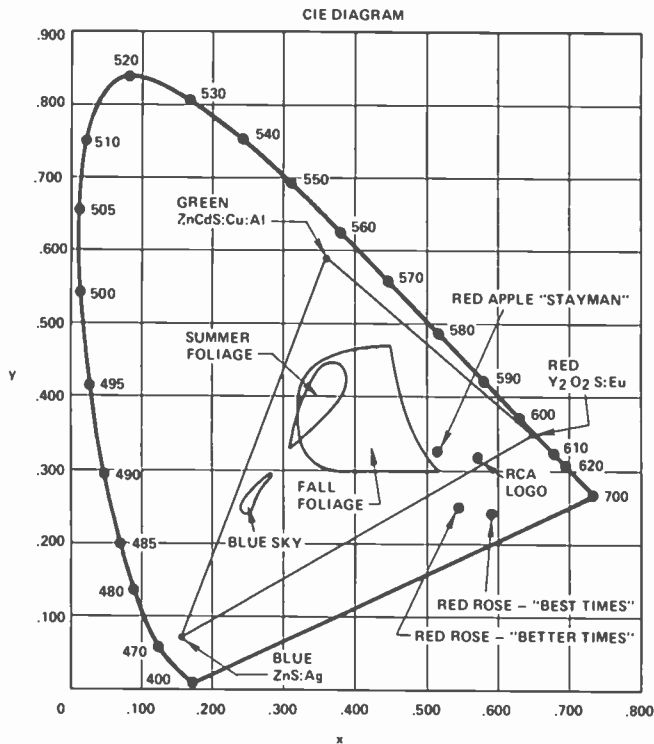


Fig. 10. Chromaticity chart showing x-y coordinate area for pigment, dye and ink colors.

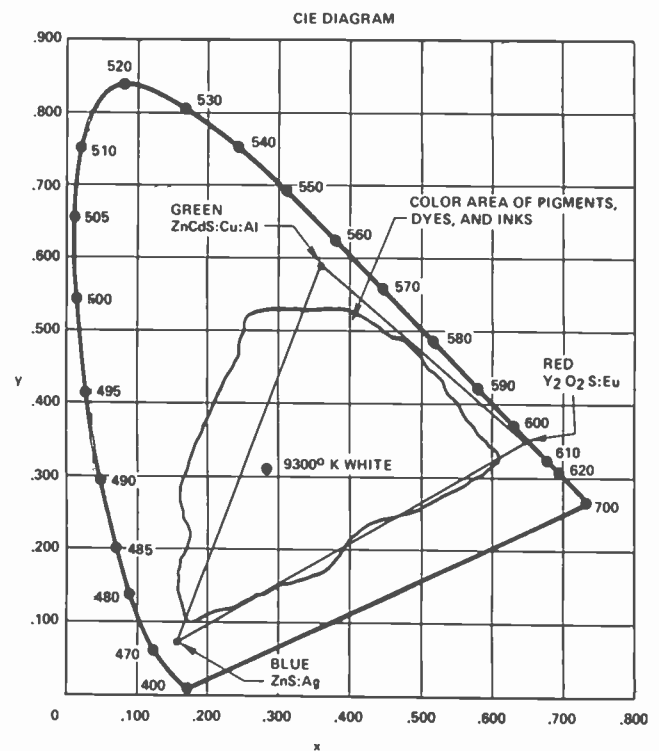


Fig. 11. Chromatic areas for summer and fall scenery.

the few remaining means known to improve the performance of the shadow mask picture tube. The improvement is small but measurable and can be demonstrated under proper viewing conditions. Improvements can be expected in light output linearity as a function of electron beam current density. Some improvement may also be realized in the green and red chromaticities which would enlarge the color gamut of the system. As shown in Fig. 10, 11 and 12, the U.S. domestic phosphors already provide a very satisfactory color gamut when compared to what can be achieved with color printing and color photography. The only real deficiency is in the cyan region which is relatively unimportant. Early color tubes using Willemite green and zinc phosphate:manganese red had a significantly larger color gamut. However, countless closed circuit demonstrations failed to show any significant difference in perceived color renditions. The visual phenomenon of color contrast tends to minimize the effect of a reduced gamut.

There is also a possibility that high-brightness non-rare-earth red emitters may be developed which would result in a significant material cost reduction.

In calculating phosphor efficiency, there are several subtleties that must be considered. For example, the transmission of the glass faceplate is obviously a factor in

light output. Glass transmission, as measured by the point source technique, is determined by Fresnel reflection losses and bulk absorption. However, when a broad light source, such as a phosphor screen, is used with the glass, most of the Fresnel losses are recovered (Fig. 13).

In the case of negative tolerance picture tubes, there is an interaction between the mask transmission and the matrix transmission. This interaction leads to the concept of a systems transmission which is lower than either the mask or matrix and is the proper number to use in calculating basic screen efficiency (Fig. 14).

Phosphor documentation

The Electronics Industry Association registers new cathode ray tubes at the request of its members. In connection with the tube type designation, a P-number for the phosphor screen is included. With this system, phosphor screens are not registered independently of a specific tube. The P-numbers are assigned in chronological order and give no information of the nature of the phosphor or its intended use. The only exceptions are P4 and P22 which are general designations for direct view black and white and color picture tube screens respectively.

By 1943, the P designations had reached P11. Today, 36 years later, the P designations have reached P53. However, this does not give an accurate picture of the actual number of different phosphors that have been developed or are in use. It has been estimated that there are at least 10 to 20 times as many unregistered specialty tube types without P number phosphors as there are registered types. (In some cases, it is known that these specialty tube phosphors represent only minor deviations from registered P number types.)

There is a worldwide tube type and phosphor designation system, called Pro Electron, which utilizes a letter code to describe the phosphor. Application to the full P-number list has not been completed.

Recently, there has been an upsurge in the use of multilayer phosphor particles which exhibit a color change as a function of the velocity of the electron beam. These materials are called penetration or "onionskin" phosphors. An early 3-color "onion" consisted of a 25- μ blue-emitting zinc sulfide:silver core. The core was surrounded by a thin, fine particle layer of green-emitting zinc silicate:manganese and another thin layer of red-emitting zinc magnesium cadmium silicate (Fig. 15). In the two-color version the core may be green-emitting zinc silicate:manganese and the outer layer a red-emitting rare-earth phosphor. Both in industrial CRTs and

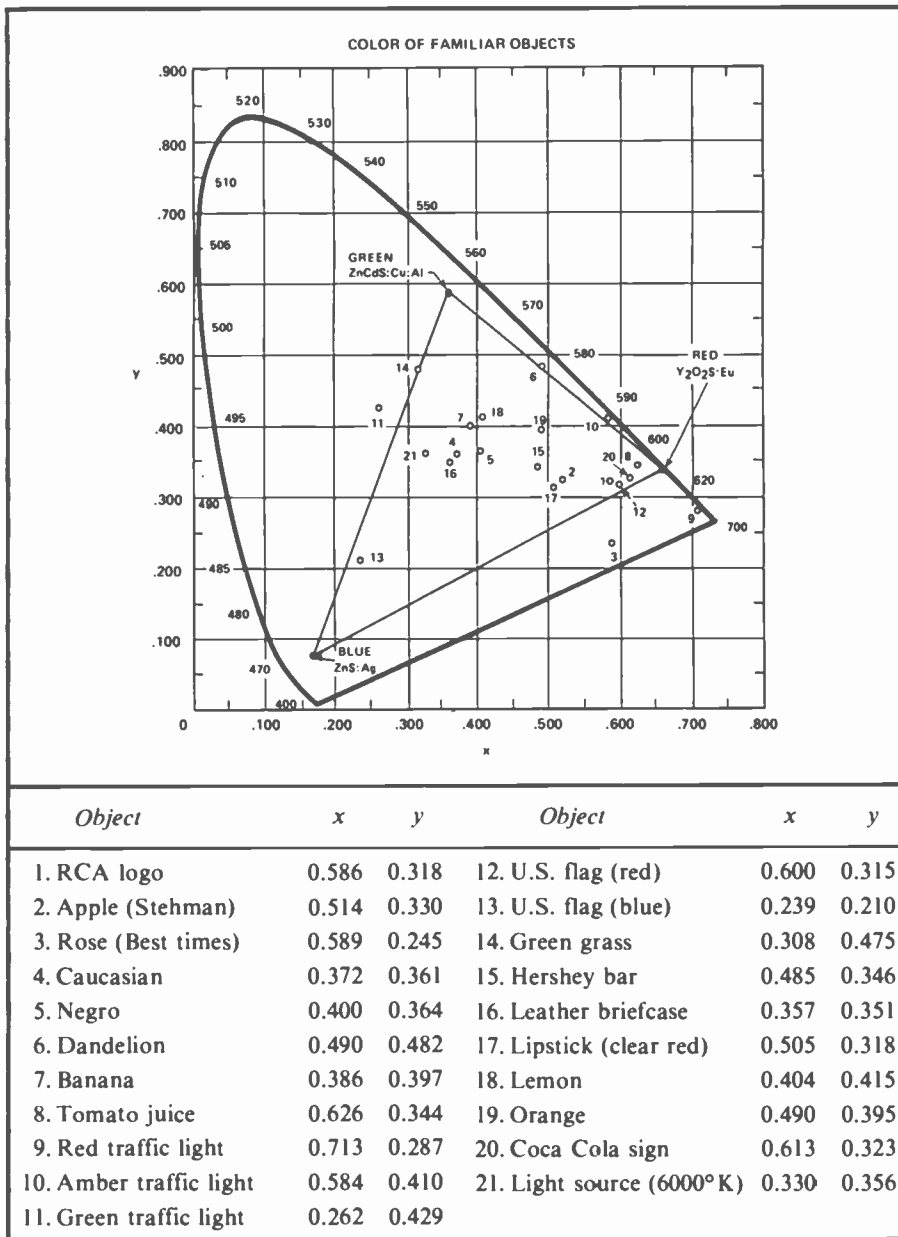


Fig. 12. C.I.E. coordinates for several familiar objects.

color TV pigments are being added to the phosphors to enhance contrast.

In summary, cathodoluminescent phosphors continue to find a large and varied commercial use in display devices. It is estimated that on a worldwide basis, approximately 1,000 tons of phosphors were used in new television picture tubes for home entertainment in 1977.

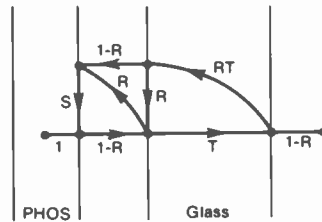
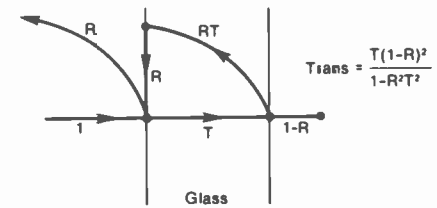
Screen deposition techniques

The techniques of depositing phosphors to form a viewing screen in a cathode ray tube have not undergone the proliferation that has occurred in phosphor development.

For many oscilloscope tubes and black and white picture tubes the water-settling technique is still used. In the case of color television picture tubes the slurry process is used by most companies (Table I). Two companies use a dusting process where the dusting is carried out prior to lighthouse exposure. At an earlier period one company dusted the phosphor after lighthouse exposure and still another company applied the phosphor slurry suspension by spraying.

The black matrix or grill application process is essentially the same at all color picture tube plants. The only difference that has been published, of which I am aware, is the use by Hitachi of a reciprocity failing resist. The future of the matrix

$$\text{Trans} = \frac{\text{"Direct Trans."}}{1 - \text{Summation of individual loops}}$$



$$\text{Trans} = \frac{(1-R)^2 T}{1 - (1-R)RS - (1-R)^2 RST^2 - RT^2}$$

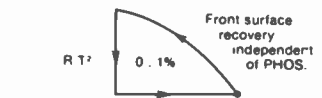
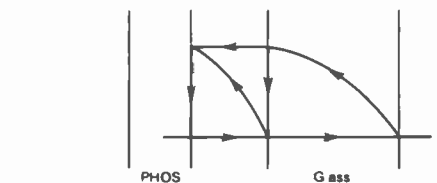


Fig. 13. Analysis of glass transmission from a broad area light source.

Table I. Commercial methods for phosphor screen deposition on color picture tubes.

Method	No. Companies
Water settling	(2)
Slurry — puddle	15 — 12
Slurry — spray	(1)
Dusting — before exposure	2
Dusting — tacky image	(1)

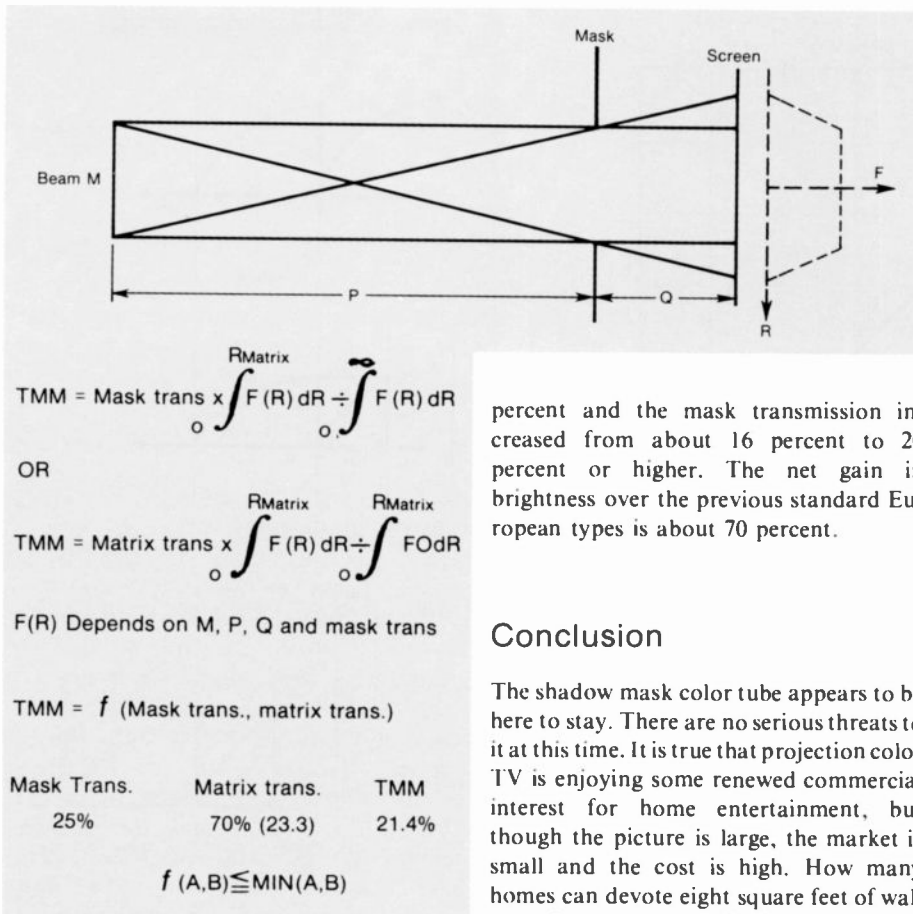


Fig. 14. Interactive transmissions of mask and matrix.

concept is uncertain. It is well entrenched in the U.S. and Japan but not in Europe. The Western European response to the matrix is the HiBrit/Helichrome or Sunshine tube. These tubes are non-matrix line screen tubes with the glass transmission increased from 52 percent to 70

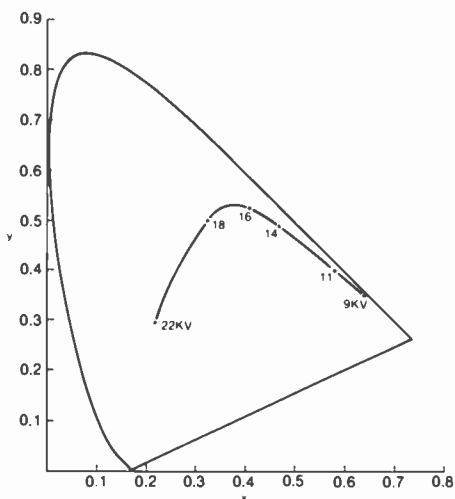


Fig. 15. Color gamut for 3-color penetration phosphor.

percent and the mask transmission increased from about 16 percent to 20 percent or higher. The net gain in brightness over the previous standard European types is about 70 percent.

Conclusion

The shadow mask color tube appears to be here to stay. There are no serious threats to it at this time. It is true that projection color TV is enjoying some renewed commercial interest for home entertainment, but though the picture is large, the market is small and the cost is high. How many homes can devote eight square feet of wall space for a permanent viewing screen plus a projection console critically positioned in respect to the screen?

A much more imaginative approach is the flat panel display. Three years ago, James Schwartz of Zenith presented a review of various light generating systems and addressing schemes. He outlined what he considered the basic performance conditions that would have to be met. He suggested an eight-square-foot display which could produce a brightness of 100-foot-lamberts with a power consumption of 200 watts.¹

At the spring meeting of SID held in San Francisco last year, John Endriz and other authors reviewed recent work done at the RCA Princeton Labs on a flat TV display using feedback multipliers which meet the performance requirements suggested by Schwartz.²

It is interesting to note that the feedback multiplier scheme uses tri-color phosphor elements deposited in a precision pattern.

It seems very probable that cathodoluminescent phosphors have a long and useful future. Any young person entering this field at this time can look forward to an interesting and exciting career. Perhaps the gains will not be as spectacular as in the last 30 years, but there is still much work to be done.

Acknowledgment

I wish to thank L.C. Riedlinger and G.M. Ehemann of Lancaster for their assistance in preparing this material, in particular, the sections on system transmission and broad source glass transmission.

References

- Schwartz, J.W., "Twenty-five Years Without Panel TV," *SID 76 Digest*.
- Endriz, J.R., Keneman, S.A., Catanese, C.A., and Johnson, L.B., "Flat TV Display Using Feedback Multipliers," *SID Symposium*, San Francisco (Apr 1978).
- Seats, P., "The Cathode Ray Tube—A Review of Current Technology and Future Trends," *IEEE Trans. on Electron Devices*, Vol. ED-18, No. 9 (Sep 1971).
- Penetration Phosphors, U.S. Patent 3,714,490.
- "Penetration Cathode Ray Tubes," *Thompson-CSF Application Note*, TEV 6036 (May 1974).
- Vogel, R.Q., "Color Television Brightness—Yesterday, Today and Tomorrow," *IEEE Trans. Broadcast & Television Receiver*, BTR-2, No. 1 (Feb 1974).



Austin Hardy joined the Chemical and Physical Laboratory at RCA, Lancaster, in May, 1943, as a phosphor chemist on the development of zinc sulfide and zinc cadmium sulfide phosphors for radar display tubes. He designed and constructed a recording spectroradiometer and other colorimetric and photometric equipment. Later he became active in phosphor screening and was intimately involved in the development of black-and-white and color television picture tubes. Mr. Hardy has served as chairman of the Electronics Division of the Electrochemical Society and was chairman of the JTC 6.3 subcommittee on phosphor-screen characteristics for ten years. He is currently Manager of the Panel Process Development and Laboratories, Color Picture Tube Development Engineering in Lancaster.

Contact him at:
**Color Picture Tube
 Development Engineering,
 Lancaster, Pa.
 Ext. 3637**

Filter phosphors

The use of prepigmented filter phosphors has enabled RCA to reach its goal of a 25 percent reduction in tube face reflectivity with a minimal loss of light output.

Abstract: *The development of filter phosphors has enabled RCA to reach its goal of a 25 percent reduction in tube face reflectivity in its matrix product. Tubes prepared with filter phosphors can be operated at high ambient light levels without degradation to the picture quality.*

The paper is a discussion on the properties and problems of incorporating filtered phosphors into cathode ray color

picture tubes. A filter phosphor is one made up of a combination of a phosphor core and a specific pigment. Chromaticity, brightness, and reflectivity comparisons are shown between tubes prepared with conventional phosphors and filter phosphors. Screening characteristics of filter phosphors, such as adherence and cross-contamination, are discussed for matrix and non-matrix types.

The light output race within the U.S. domestic color television industry appears to have run its course and currently the industry is concentrating on picture quality. Significant effort is being placed on brightness contrast performance (BCP):

$$BCP = LO/\sqrt{R}$$

where LO is the tube light output; and R is the tube face reflectivity.

The tube face reflectivity is the ratio of a sample surface reading to a standard surface reading times the absolute reflectivity of the standard. The standard surface used in the measurements for this discussion was a vitrolite tile with 88 percent reflectivity. The light source for these measurements was a warm-light fluorescent ring lamp, which was eight inches in diameter. The use of the square root of the tube face reflectivity in the formula cancels out the effect of the glass. The light output is given as foot

lamberts per milliampere (fL/mA) and is determined by the following formula:

$$LO = fL/mA = 8000/WCUR9$$

where WCUR9 is the red + green + blue gun currents at 8 foot lamberts and a color temperature of 9300°K + 27 MPCD white.

The introduction of the matrix tube in the late 1960s gave the industry a big improvement in brightness contrast performance while realizing a significant gain in light output. The industry consistently chose a tube that gave the maximum light output gain by using a higher transmission glass

and mask. A few years ago, RCA management set a goal for a 25 percent reduction in tube face reflectivity (TFR) of its matrix product.

Table I compares the nonmatrix and matrix products. Of course, the improvement in BCP of the matrix screen is due to the incorporation of graphite. The higher glass transmission (54.6 percent to 85 percent) results in a higher TFR. As measured by RCA, the contrast ratio of this nonmatrix tube is 6.9 when viewed under an ambient light level of 25 foot candles. The standard matrix tube has a contrast ratio of 7.6, which is a 10 percent improvement over the nonmatrix product. It can be seen that the proposed 25 percent reduction in reflectivity (TFR from 0.4 to 0.3) could result in an improvement of 15.5 percent in BCP if this reduction in reflectivity could be achieved without any losses in light output. This can be translated to a tube contrast ratio improvement of 27.6 percent relative to the standard matrix tube.

Tube contrast ratios under an ambient light level of 25 foot candles at 9300°K + 27

Table I. BCP of 25 V-90°-Δ product (matrix vs. nonmatrix).

	TMO* (%)	TFR	fL/mA	BCP	Tube contrast ratio
Nonmatrix	16	0.204	41.0	90.8	6.9
Standard matrix product (1974)	25	0.400	90.0	142	7.6
Proposed matrix product with 25 percent lower TFR	25	0.300	90.0	164 (15.5%)	9.7

* TMO = mask transmission

Table II. Red filter phosphor — pigment concentration series.

	Percent CdSSe pigment	Baked at 380° C		Baked at 425° C	
		x	y	x	y
Standard Y ₂ O ₂ S:Eu red	—	0.652	0.341	0.652	0.341
Desaturated Y ₂ O ₂ S:Eu red core	—	0.632	0.352	0.632	0.352
	0.6	0.652	0.341	0.648	0.344
	0.8	0.654	0.337	0.650	0.342
	1.0	0.656	0.336	0.651	0.340
	1.2	0.659	0.333	0.654	0.337

Note: Color measurements made on 2 x 2-in settled slides (TIC coated glass).

MPCD are determined from the following formula:

$$\text{Contrast ratio} = \left[0.02 + \frac{25 \times \text{TFR}}{\text{LO}} \right]^{-1}$$

This improvement in contrast was desired in order to allow the operation of kinescopes at high ambient light levels with reduced degradation in picture quality. With conventional tubes, the picture loses a degree of colorimetric saturation and black level as the ambient light level is increased (the picture becomes washed-out). It was found that improved contrast could be achieved by adding pigments to the blue and red fields. These phosphors are then referred to as filter phosphors.

A filter phosphor is made up of a combination of phosphor core and a specific pigment. The blue and red phosphor cores are synthesized with desaturated emission colors. When these desaturated phosphors are applied as a homogeneous mix of phosphor and pigment, the resultant tubes have blue and red field chromaticities that are equivalent to the respective fields in tubes prepared with standard phosphors. This is accomplished by the filtering action of the pigments. Early in our program we settled on cobalt aluminate as the blue pigment and cadmium sulfoselenide as the red pigment.

It was found that there is a direct relationship between the red pigment concentration and the chromaticity of the resultant red filter phosphor; on the other hand, the blue filter phosphor chromaticity is constant over a wide range of blue pigment concentrations. Therefore, it was decided to optimize the red filter phosphor for its desired chromaticity characteristics first and then vary the blue pigment concentration until the desired gain in tube face reflectivity was achieved.

The standard nonpigmented Y₂O₂S red phosphor and the desaturated, nonpigmented Y₂O₂S red phosphor core are listed at the top of Table II. It can be seen

that as the pigment concentration increases, the resultant red filter phosphor becomes more saturated in emission color. This table also shows that the CdSSe red pigment becomes less effective as a filter when baked above 400°C. The chromaticity data of unbaked and 380°C baked slides were identical. At tube process bake temperatures of 425°C, the pigment undergoes some oxidation and the filter phosphor emission color is desaturated; therefore, this color shift during tube processing must be compensated-for during the filter phosphor synthesis. At 1 percent red pigment, a saturated x coordinate of 0.656 is realized and the desired value of 0.651 is achieved after baking. Therefore, tubes prepared with the standard red phosphor from this table and tubes prepared with the 1 percent CdSSe filter phosphor from this table will have identical red field chromaticities.

Figure 1 shows the reflectivity curves of

the red phosphor core, the CdSSe red pigment, and the resultant filter phosphor (before and after a 425°C bake). These reflectivity curves are generated relative to a magnesium carbonate powder standard. The reflectivity of the magnesium carbonate is assumed to be 100 percent. Baking the filter phosphor at higher temperatures lowers the composite reflectivity curve as the temperature increases. Analytical testing has shown that the CdSSe becomes a two-component system when baked at 425°C or higher. One component is CdSSe of increasing CdSe content as the temperature increases and the second component is CdSO₄.

The standard RCA nonpigmented blue phosphor and the desaturated nonpigmented blue phosphor core are listed at the top of Table III. This table shows that the blue filter phosphor emission color is constant over a wide range of pigment concentrations. It can be seen from these data that the RCA blue filter phosphor is slightly desaturated relative to the standard RCA blue phosphor. By RCA measurements, the RCA blue phosphor has always been more saturated than competitive blue phosphors. Even at an x coordinate of 0.065, this sample is still more saturated than most competitive blue products. Of course, the emission color can be shifted by adjusting the core phosphor; however, it was decided that this was an acceptable emission color.

Empirically, it was found that a pigment

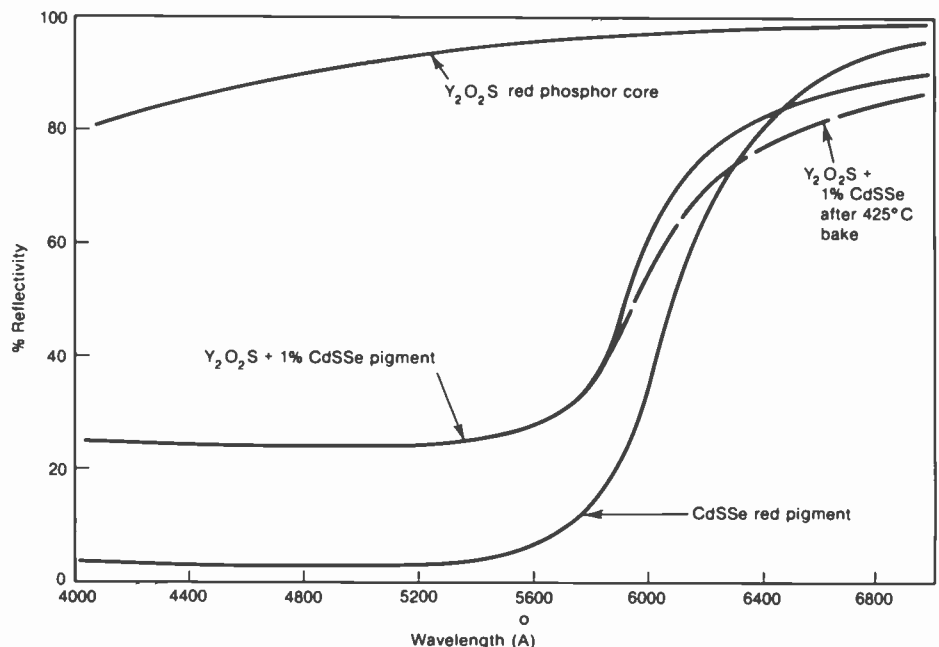


Fig. 1. Red reflectivity curves of red phosphor core, the CdSSe red pigment, and the resultant filter phosphor. The composite reflectivity curve is lowered as the temperature is increased when the filter phosphor is baked at higher temperatures.

Table III. Blue filter phosphor — pigment concentration series.

	Percent CoAl_2O_4 pigment	Baked at 425°C	
		x	y
Standard ZnS:Ag, Cl blue	—	0.146	0.057
Desaturated ZnS:Ag, Cl blue core ↓	—	0.146	0.074
	0.2	0.146	0.072
	0.6	0.146	0.069
	1.0	0.146	0.067
	1.4	0.146	0.066
	1.8	0.146	0.065
	2.2	0.146	0.065
	2.6	0.146	0.065

concentration of 2.4 percent on the blue filter phosphor and 1 percent on the red filter phosphor would result in the desired 25 percent reduction in tube face reflectivity.

Figure 2 shows the reflectivity curves of the blue phosphor core, the CoAl_2O_4 blue pigment, and the resultant filter phosphor. Baking has no effect on the blue filter phosphor with respect to chromaticity or reflectivity.

Screening — admix technique

Phosphor screens in color tubes are made up of an array of green, blue, and red phosphor dots or phosphor lines. Each phosphor is applied as a dichromated polyvinyl alcohol (PVA) slurry. The phosphor powder is ball-milled in water and a small amount of PVA. Some slurry mills contain surfactants for wetting or defoaming purposes. Following the milling, additional PVA and water are added to yield the desired slurry formulation. A typical slurry is 30 percent phosphor by weight with a PVA/phosphor ratio of approximately 0.08. The slurry is sensitized with 2 to 10 percent by weight of a dichromate salt.

This slurry is applied to the faceplate panel by a combination spinning and tilting cycle. Selected areas (dots or lines) of the dried layer are exposed to ultraviolet radiation. The ultraviolet exposed areas become insoluble, while the remaining unexposed areas are still water soluble and may be removed by washing them away. The phosphor in the washed-away (or developed-off) areas is known as salvage and will be discussed later.

Each of the three phosphor slurries is applied in this fashion. The normal sequence of application is green, blue, and red. One of the most common problems in

making the phosphor screen for a color picture tube is cross-contamination. Cross-contamination is the failure to remove all of the phosphor particles of a subsequent color from a preceding phosphor image. This problem is very evident in the filter phosphor system and must be controlled. Each stock slurry is stored in a holding pot and is dispensed onto the faceplate from a Mateer dispenser.

Initial high contrast tubes were prepared by an admix slurry technique. The phosphor core and the pigment were added to the slurry mill as separate components. The pigment was added as a well dispersed suspension. Adding the pigment to the slurry mill as a dry powder resulted in pigment aggregates, which were not very effective in filtering characteristics. It was found that during slurry milling, surfactant

slurry additives should be kept to a minimum. These surfactants could be added later during the final slurry adjustments. This precaution was needed to minimize pigment separation. During slurry milling, the pigment attaches itself to the phosphor surface; however, the abrasive action in holding pots and Mateer dispensers caused some pigment separation. This loose pigment could readily be detected in the leading edge of the slurry puddle during the coating application.

The application characteristics of admix blue and red filter phosphor slurries are very similar to standard slurries with respect to adherence, structure, and cross-contamination. Cross-contamination by filter phosphors is a unique problem because the pigment in the filter phosphor will absorb a portion of the available light output and will also alter the emission color of the phosphor that it contaminates. Pigment contamination can be a problem with admix filter phosphor slurries because the loose pigment, which becomes detached from the phosphor core, has a particle size of less than one micron and can lead to pigment cross-contamination.

Tubes prepared with admix filter phosphor slurries were down 7 percent in light output when compared to standard tubes. Essentially all of this loss in light output was in the green field due to pigment contamination. Some of the pigment contamination was in conjunction with blue and/or red phosphor contamina-

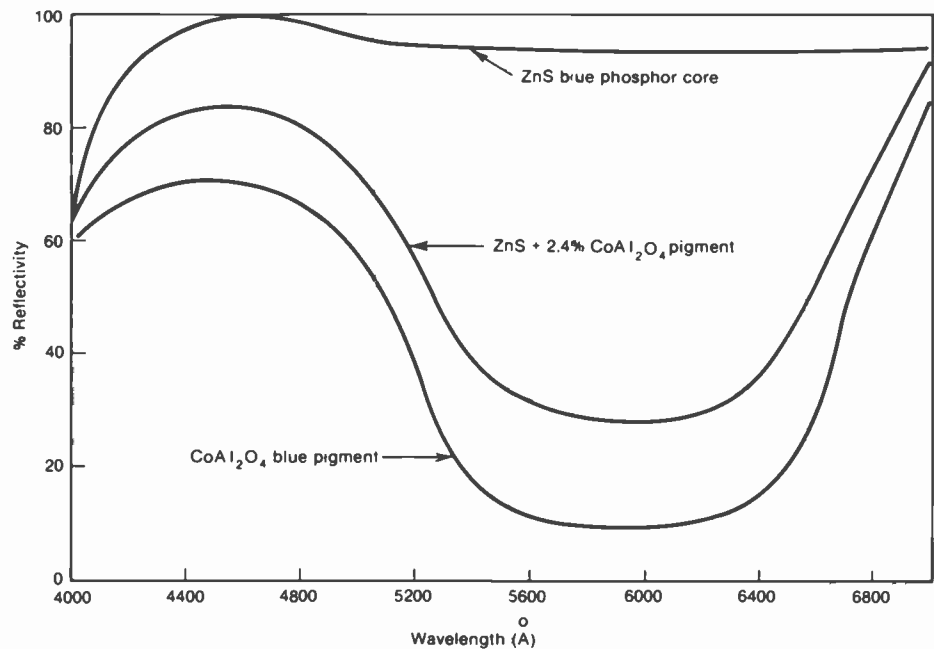


Fig. 2. Reflectivity curves of the blue phosphor core, the CoAl_2O_4 blue pigment, and the resultant filter phosphor. Baking has no effect on the blue filter phosphor with respect to chromaticity or reflectivity.

Table IV. Admix slurry results on 25V-90°-Δ matrix product.

	TMO(%)	TFR	fL/mA	BCP
Standard tube	25	.400	90.0	142.0
Filter phosphors (admix slurry technique)	25	.300	83.7	152.8 (+7.6 percent)

Table V. Pigment contamination of ZnCdS:Cu,Al green phosphor.

<i>CoAl₂O₄ blue pigment</i>				<i>CdSSe red pigment</i>			
PPM pigment contamination	Relative brightness	C.I.E. x	C.I.E. y	PPM pigment contamination	Relative brightness	C.I.E. x	C.I.E. y
0	100	0.357	0.596	0	100	0.357	0.596
25	100			25	95		
50	98	0.351	0.600	50	91	0.361	0.590
100	97			100	86		
250	93			250	80		
500	88			500	74		
1000	82	0.346	0.601	1000	66	0.376	0.580

tion, which of course contained some pigment; however, it was also due to loose pigment in the blue and red slurries.

Table IV shows that the gain in BCP of the initial tubes was only 7.6 percent because of the loss in light output due to pigment contamination.

Table V shows how the green field is affected by pigment contamination. The samples in Table V are mechanical mixes of the green phosphor, which is a zinc cadmium sulfide coactivated with copper and aluminum, and the pigments. The brightness and color measurements were taken before and after a 450°C air bake. Baking these samples did not alter the brightness or emission color; therefore, no chemical reaction is involved in the listed results. The red pigment contamination is significantly more detrimental than the blue pigment contamination. The blue pigment contamination shifts the emission color toward the blue, while the red pigment contamination shifts the emission color toward the red. Contamination with both pigments was found to have a cumulative effect on the green field brightness and the emission color shifts were cancelled out.

Red on blue phosphor contamination is always possible. Table VI shows the effect of red pigment contamination of the blue filter phosphor. At the higher levels of contamination, the blue emission color begins to shift toward the green.

Table VI. Red pigment contamination of the blue filter phosphor.

PPM pigment concentration	Relative brightness	C.I.E. x	C.I.E. y
0	100	0.144	0.065
25	99		
50	98	0.144	0.065
100	96		
250	93	0.145	0.068
500	88		
1000	80	0.145	0.070

and red phosphors are difficult to wet and have a tendency to foam. With the proper defoaming and wetting agents in the slurry mill, the resultant slurries have excellent screening characteristics. The adherence of these phosphors is actually superior to standard blue and red phosphors and their use has led to increased screen room yields at all RCA screening facilities. Of course, good adherence can also lead to cross-contamination, which was a problem in early production runs.

After some slurry modifications were made, it was found that phosphor cross-contamination of prepigmented phosphors was no more of a problem than cross-contamination of nonfilter phosphors. However, as pointed out earlier, contamination in this filter phosphor system is more detrimental than in a nonfilter phosphor system because of the presence of the pigments.

As shown earlier, tubes prepared with admix filter slurries were down 7 percent in light output when compared to standard tubes. Tubes prepared with prepigmented phosphor slurries were down approximately 3 percent in light output. The increase in light output is due to the elimination of the loose pigment contamination (especially in the green field).

Table VII shows how these prepigmented phosphors improved the BCP of RCA's 25V-90°-Δ matrix product. This table shows that the BCP has been increased by 12.3 percent with the incorporation of prepigmented filter phosphors compared to the 7.6 percent gain with the

Screening — prepigmented phosphors

The pigment separation problem was solved by developing blue and red prepigmented phosphors. The first approach was to use standard coatings (such as silicates or phosphates) to fix the pigments onto the surface of the respective phosphor cores. Many of the coatings evaluated worked very well with respect to pigment pickup during coating; however, there was significant pigment separation during slurry preparation with all of these samples.

An extensive study led to the use of latex coatings. The pigment is added as a well-dispersed suspension to the phosphor core and then the latex is added to encapsulate the phosphor and fix the pigment onto the phosphor surface. After thorough curing of the latex coating, the resultant prepigmented phosphor is stable to slurry milling and there is no pigment separation in holding pots or Mateer dispensers.

These latex-coated prepigmented blue

Table VII. Filter phosphors in the 25V-90°-Δ matrix product.

	TMO (%)	TFR	fL/mA	BCP	Percent increase in BCP
Standard tube	25	0.400	90.0	142.0	—
Filter phosphors (admix slurry)	25	0.300	83.7	152.8	7.6
Prepigmented filter phosphors	25	0.300	87.3	159.4	12.3

Table VIII. Filter phosphors in the 25V-90°-Δ nonmatrix product.

	TMO (%)	Glass		TFR fL/mA BCP	
		transmission (%)			
Standard tube	16	54.6	0.204	41.0	90.8
Standard phosphors with high glass transmission	16	70.9	0.418	56.3	87.1
Prepigmented phosphors with high glass transmission	16	70.9	0.280	52.9	100.0

Table IX. Red filter phosphor — pigment concentration series.

	Percent Fe ₂ O ₃ pigment	C.I.E.	
		x	y
Standard Y ₂ O ₂ S:Eu red	—	0.652	0.341
Desaturated Y ₂ O ₃ S:Eu red core	—	0.632	0.352
	0.3	0.645	0.346
	0.4	0.649	0.342
	0.5	0.652	0.339
	0.6	0.653	0.339

admix system. This product has a tube contrast ratio improvement of 24 percent relative to the standard matrix product. This 25V-90°-Δ matrix product has been used as an example vehicle. Similar results were attained with line screens and various sizes of delta and line screens.

Nonmatrix product

The examples used thus far have all been matrix products. The use of filter phosphors in nonmatrix color tubes will also offer a gain in contrast. However, because of the lower light output in this product, it is more advantageous to use pigmented phosphors in combination with a glass of higher transmission to realize a gain in light output.

Table VIII shows that if the glass transmission is increased with standard phosphors, there is a loss in BCP. With the incorporation of filter phosphors into this product, a 25 percent gain in light output and a 10 percent gain in BCP are realized. The tube contrast ratios of the standard tube and the filter phosphor tube are equivalent. In other words, there is a 25 percent gain in LO, at no sacrifice in tube contrast. RCA is actually using this system in a European product at present.

Phosphor reclaim

As pointed out earlier, that portion of the exposed phosphor screen that is washed off

during developing is collected as salvage. This salvaged phosphor is reclaimed to be reused in subsequent slurries.

When admix slurries of the filter phosphors are being used, the pigment is stripped off the salvage during each reclaim; therefore, virgin pigment is added to each subsequent slurry mill. This stripping is done because the concentration of the pigment varies from salvage batch to salvage batch due to the pigment separation in admix slurries.

For prepigmented phosphor salvage, the pigment is intact and both phosphor and pigment are reclaimed. A baking step, which strips the salvage of slurry organics, also removes the latex from the prepigmented phosphors; therefore, the reclaimed phosphors must be relaxed. This is easily accomplished during the washing steps after baking. The pigment remains uniformly dispersed on the phosphor surface. It was pointed out earlier that the CdSSe red pigment begins to oxidize at temperatures above 400°C, therefore, the salvage baking is carefully carried out at 375°C. All of the RCA screening facilities reclaim their own salvage quite successfully.

Alternate pigments

The only other blue pigment that was seriously considered was ultramarine blue.

In the admix slurry system, there was a large variation in the amount of ultramarine blue pigment separation from slurry lot to slurry lot. The amount of pigment separation was usually higher than with CoAl₂O₄. Therefore, the pigment cross-contamination was higher and the tube light output was lower.

The ultramarine blue pigment is not compatible with the present latex coatings in the prepigmented filter phosphor system. It is not completely picked up during coating and always has some separation in slurry. With more effort, the

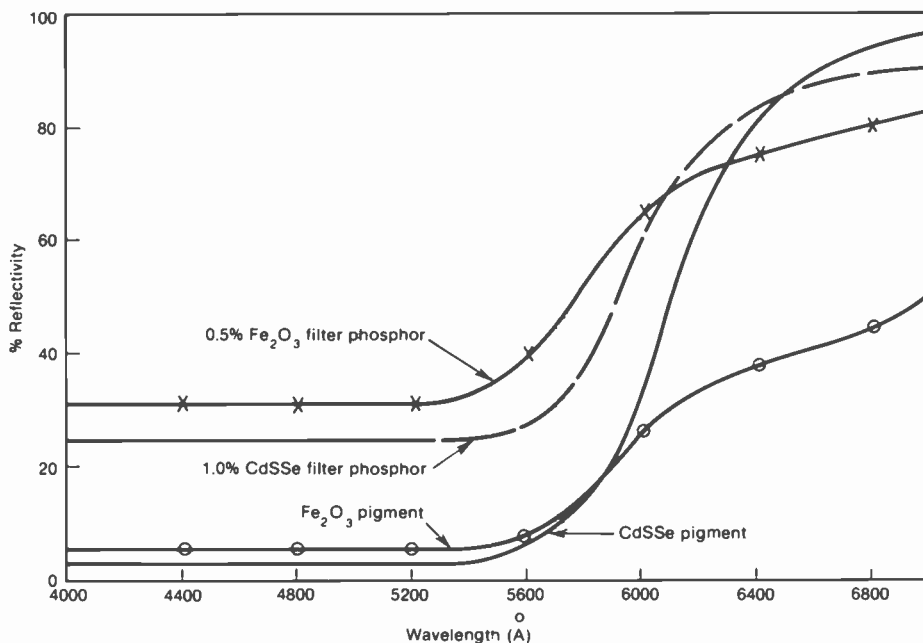


Fig. 3. Red reflectivity curves of CdSSe vs Fe₂O₃. The Fe₂O₃ prepigmented filter phosphor is totally stable to baking.

Table X. Fe₂O₃ red pigment contamination.

<i>ZnCdS: Cu, Al green</i>				<i>Prepigmented blue</i>			
<i>PPM pig- ment contam- ination</i>	<i>Relative brightness</i>	<i>C.I.E.</i>		<i>PPM pig- ment contam- ination</i>	<i>Relative brightness</i>	<i>C.I.E.</i>	
		<i>x</i>	<i>y</i>			<i>x</i>	<i>y</i>
0	100	0.357	0.596	0	100	0.144	0.065
25	96	0.360	0.593	25	99	0.144	0.065
50	91	0.363	0.591	50	96	0.144	0.066
100	89	0.366	0.589	100	93	0.144	0.066
250	79	0.372	0.584	250	87	0.144	0.068
500	71	0.379	0.579	500	77	0.145	0.070
1000	59	0.391	0.569	1000	68	0.145	0.073

latex problems associated with this material could be solved, however, it was decided not to pursue a solution at this time because of some additional instability problems. Test results were erratic, however, the ultramarine blue pigment has shown signs of instability at the tube process baking temperature. The cobalt aluminate blue pigment is definitely a superior material.

Recent tests with Fe₂O₃ red pigment have been very encouraging and RCA is considering a changeover to this material. This iron oxide is very compatible in the latex prepigmented filter phosphor system and Table IX shows the effect of pigment concentration on the red filter phosphor chromaticity. The same desaturated red phosphor core as used with the CdSSe pigment was used here. The desired chromaticity is attained with 0.5 percent iron oxide pigment.

The filter and reflectivity characteristics of the cadmium sulfoselenide red pigment and the iron oxide red pigment are quite different. Figure 3 compares the reflectivity characteristics of the two red pigments and the resultant prepigmented filter phosphors. As stated earlier, the CdSSe prepigmented filter phosphor desaturates with baking. The Fe₂O₃ prepigmented filter phosphor is totally stable to baking. Its reflectivity and chromaticity characteristics remain constant.

The two filter phosphors in Fig. 3 yield tubes with the same TFR, red field

chromaticity, and red field light output. In other words, from a finished tube standpoint, these two prepigmented phosphors are identical.

Advantages of the Fe₂O₃ red pigment are:

- *Cost saving*—CdSSe costs \$11.00/lb, while Fe₂O₃ costs \$0.50/lb.
- *Heat stability*—Not only is the Fe₂O₃ prepigmented filter phosphor stable to tube processing conditions, but it offers more latitude during reclaiming. Reclaim bake temperatures for CdSSe prepigmented filter phosphor salvage have to be closely monitored to prevent oxidation of the CdSSe pigment.
- *Chemical stability*—If the red phosphor salvage should become contaminated with blue and/or green phosphor, a hypochlorite process for removing these contaminants is used. If this reclaim process is used with a CdSSe pigmented phosphor, the pigment is stripped off and the phosphor has to be repigmented. The Fe₂O₃ pigmented phosphor is stable to this reclaim process without any pigment loss.

Table X shows the effect of Fe₂O₃ pigment contamination of the green and blue phosphors. These contamination results are quite similar to those obtained with CdSSe red pigment; however, the green emission color is shifted more with Fe₂O₃.

Summary

- The development of prepigmented blue and red filter phosphors has enabled RCA to reach its goal of a 25 percent reduction in tube face reflectivity in its matrix product at a minimal loss of light output. These kinescopes can now be operated at high ambient light levels without degradation in picture quality. These tubes are presently used in RCA's Color-Trak line of television sets.
- The use of prepigmented filter phosphors in nonmatrix European television tubes has resulted in a significant gain in light output and a 10 percent gain in brightness contrast performance.
- Control of cross-contamination is a key to tube quality throughout the television industry. Its importance is emphasized in the filter phosphor system.



Steve Trond joined RCA in 1959. He is a Senior Member of the Technical Staff in the Color Tube Materials and Process Laboratory. His primary efforts have been in developmental phosphor engineering, however, he has also been involved in developmental screening.

Contact him at:
Color Tube Division
Lancaster, Pa.
Ext. 2237

High-resolution bipotential focus gun for color picture tubes

A novel CRT gun design has been produced in response to the more stringent performance requirements of large-screen color television displays.

Introduction

Color picture tube electron gun designers were faced with a new challenge when two industry-wide trends started in 1972. They were: (1) the development of the self-convergence precision inline (PI) system to replace the conventional delta gun structure in 90° small-size tubes¹ and (2) the development of the large-size 110° self-convergence PI system.² In both these cases, the neck diameter was reduced from 36 mm to 29 mm and the diameter of the main lens was reduced from 8.9 mm to 4.1 mm initially and 5.4 mm later, to a final 39 percent reduction (Fig. 1).

With the recent introduction of the 29-mm self-convergence PI system in 25-V tubes with 100° deflection, the longer throw distance has required development of guns with improved resolution capability. This improved capability is, of course, also valuable for all sizes and deflection angles as a general improvement in picture tube performance.

A novel high-voltage bipotential gun has been designed and then optimized through computer modeling. Its performance is significantly improved over the conventional bipotential gun and is approximately equivalent to the tripotential gun without the problems caused by the excessively high second focus voltage required through the stem. In addition, the high-focus-voltage bipotential precision inline (HiPI) gun has improved focus tracking characteristics and off-axis deflected spot size.

Abstract: *A unique high-resolution bipotential inline gun design, developed by RCA, is described. It uses a newly developed prefocusing lens to reduce the electron beam divergence angle before the first crossover. Furthermore, with the aid of computer modeling, the prefocusing lens was matched with a G3 length and diameter to provide focus ratio of 28 percent. The performance of this computer optimized design is significantly improved over the conventional 20 percent*

focus ratio large S bipotential gun and is equivalent to the current tripotential gun without the need for the excessively high second focus voltage through the stem. In addition, the new gun design has improved tracking characteristics and off-axis beam size. It has well-balanced performance at both high and low video drive conditions. At low drive condition it has minimum moiré greatly reduced blooming. The small edge spot makes the gun suitable for both 100° and 110° large-screen display.

Theory

In a CRT electron gun design, three factors contribute to the final electron beam spot size: the magnification factor, the spherical aberration; and the space charge effect. The combined effect of the magnification and the spherical aberration is our subject for optimization.

The generally accepted theory is that the thermionic electrons are emitted from the cathode with a Maxwellian velocity distribution. The imaged electron beam spot has no sharp cutoff edge and has a current density approximating the gaussian distribution along its radial cross section.

$$J(r) = Ae^{-Br^2} \quad (1)$$

This implies that the resultant effect of the magnification and spherical aberration should add up quadratically.³⁻⁹

$$D = [D_m^2 + D_{sa}^2]^{1/2} \quad (2)$$

The definitions of the terms and the derivation of the optimization condition are given in Appendix 1.

The optimization condition can be shown as the plotted curves (Fig. 2). From these curves, it is clear that if it is the intention to reduce the optimized electron spot, new lower D_m and D_{sa} curves must be obtained, and most important of all, the new gun must be operated with a reduced beam angle. A thick G2 (four times of the conventional G2 thickness) beam-forming region (BFR) helps to meet all the re-

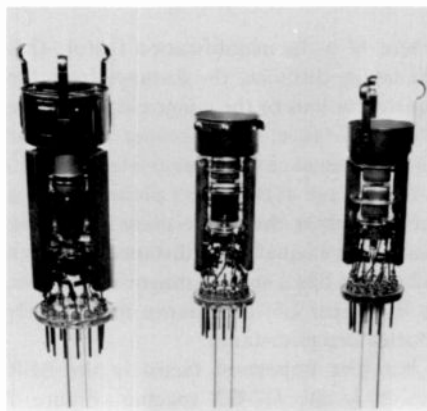


Fig. 1. Main lens size of electron guns used in color picture tubes has changed in recent years.

Reprint RE-25-2-4
Final manuscript received July 20, 1979.

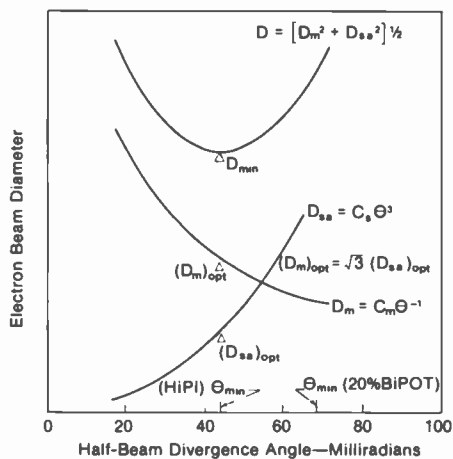


Fig. 2. Optimization curves for the HIPI gun.

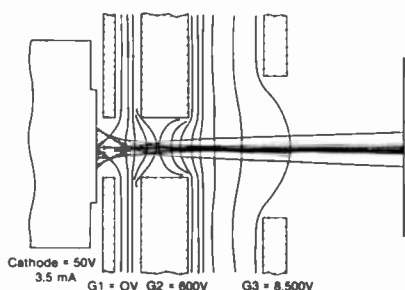


Fig. 3. The equipotential lines outline two distinctive lens regions in the thick G2 BFR.

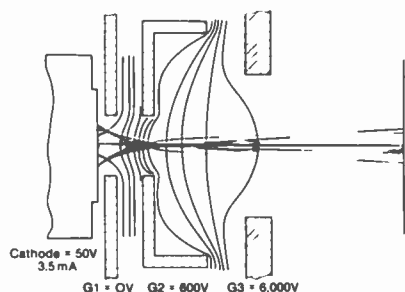


Fig. 5. A cup-shaped G2 beam-forming region gives a smaller divergence angle beam bundle.

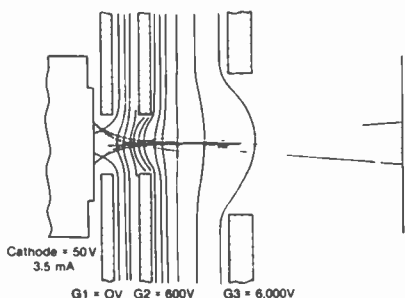


Fig. 4. In a conventional beam-forming region, the equipotential lines form a positive lens only.

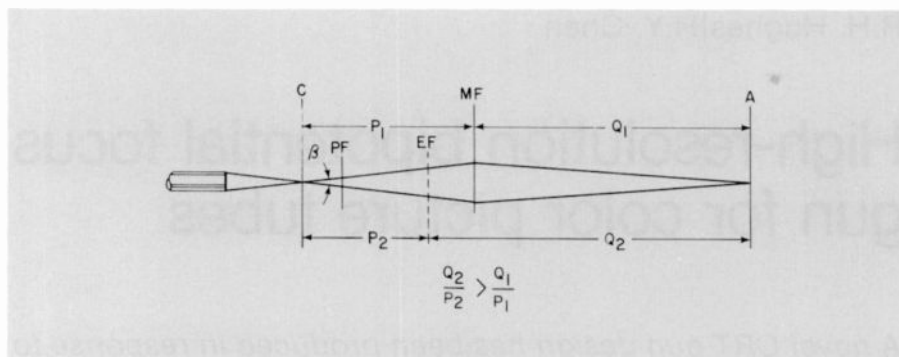


Fig. 6. The effect of adding a prefocusing lens (PF) to a CRT main lens (MF = main focus lens position; EF = equivalent focus lens position).

quirements for an improved bipotential gun design.

Figure 3 shows the plot of equipotential lines in the thick G2 BFR. The equipotential lines outline two distinctive lens regions in the thick G2 aperture. In the bottom of the G2 aperture, close to the G1 side, the equipotential lines are convex in shape, which implies that in this region the lens effect is divergent (or negative). On the top of the G2 aperture, close to the G3 side, the equipotential lines are concave in shape and the lens is convergent (or positive). In a conventional BFR design (such as shown in Fig. 4), the equipotential lines only form a positive lens. On the other hand, a cup-shaped G2 lens field may be used to obtain a smaller divergence angle beam bundle, as in Fig. 5. However, in the cup-shaped G2 lens, only a positive lens field is applied to the beam and the true position of the equivalent lens is pulled back from the main lens as shown in Fig. 6. However, the thick G2 lens, with its negative lens region, offsets some of the G2 positive lens effect. Therefore, the equivalent lens position pullback is greatly reduced as compared to the cup G2 design.

By the formula of lens magnification

$$M = \frac{Q}{P} \sqrt{\frac{V_o}{V_i}} \quad (3)$$

where M is the magnification factor; Q is the image distance, the distance from the equivalent lens to the image plane; P is the object distance, the distance from the virtual crossover to the equivalent lens; V_o is the voltage at the object plane; and V_i is the voltage at the image plane; we know that with an equal $P+Q$ distance, the thick G2 design has a smaller magnification due to its longer object distance and slightly shorter image distance.

Another important factor in the BFR design is the G2-G3 spacing. Figure 7 shows the relationship of the normalized crossover beam spot size to the average G2-G3 electric field strength. The theoretical

minimum beam spot size (S_{th}) at the crossover is determined by the thermal energy of the beam, and the S_{σ} is the actual beam spot size at the crossover. In the HiPI design, an average G2-G3 field strength of 240 V/mil was chosen, which is the trade-off of the minimum crossover spot size to the practical maximum field gradient.

The unique thick G2's back-to-back divergent and convergent lenses, plus an optimized G2-G3 spacing, give a tight electron beam bundle with a reduced beam angle at all current levels. This represents a greatly improved beam forming region design. It was pointed out that the correct course for optimizing the overall gun performance is to match the improved BFR with an improved main lens design.¹³

The bipotential main lens design was maintained for its simplicity. The large "S" main lens diameter is 5.4 mm and the G3 grid length was extended from 14.1 mm (of 20 percent focus ratio) to 23.5 mm for a 28 percent focus ratio design. By doing this, the magnification of the gun was reduced. In the meantime, the reduced divergence angle beam bundle with longer object distance requires a weaker main lens to image the crossover on the screen. Assuming the same lens filling, which is approximately 40 percent of the lens diameter at a beam current of 3.5 mA, the spherical

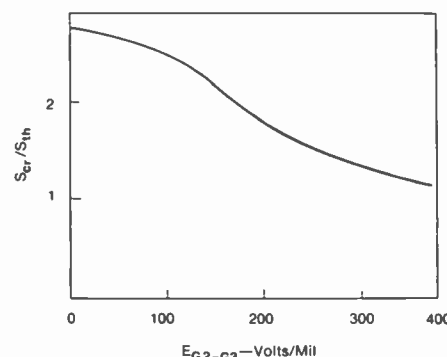


Fig. 7. Normalized crossover beam spot size vs. average G2-G3 field strength.

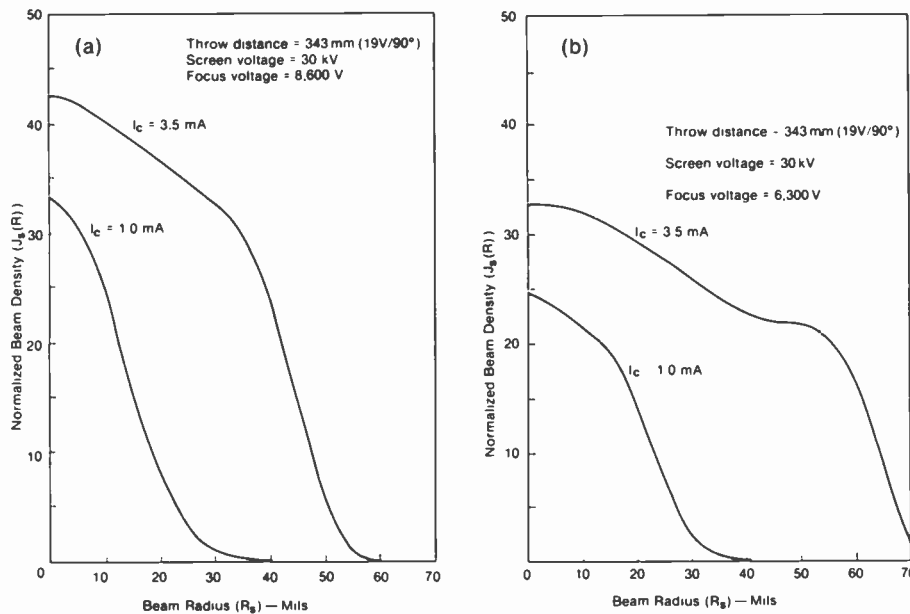


Fig. 8. (a) Computed Gaussian beam profile. 28 percent focus voltage gun. (b) 20 percent focus voltage bipotential gun. The computer gives an integrated Gaussian beam profile at the end of all three computed regions.

aberration is actually smaller at the 28 percent focus ratio gun due to its weaker electric field gradient.

Therefore, with the help of the thick G2 prefocusing lens, an improved bipotential CRT gun design has been achieved, which has both reduced magnification and spherical aberration compared to the conventional 20 percent focus ratio design. On the diagram of the optimization curves, the new design follows both a new D_m and a new D_{sa} curve. The new minimum point gives a smaller final beam spot, and that point is at the left of the original minimum point because ϕ_1 is smaller than ϕ_0 .

Optimization through computer modeling

The computer program used was devised at the RCA Laboratories, Princeton, N.J. The program allows complete design and analysis of electrostatic electron-optical devices in either axial or planar symmetries. Laplace's potential solution of certain arbitrarily shaped electrodes is found on some large number of mesh points by the successive relaxation method. The program initiates the emission determined from the Child-Langmuir equation, and Poisson's equation can then be used to solve the equipotential field lines and the trajectories of the electron rays.

There are a few previously published reports on computer modeling of CRT electron gun design.¹⁰⁻¹⁴ However, to the best of the authors' knowledge, RCA's

ELOP (Electron Optics Program) has a unique advantage. The computer gives an integrated Gaussian beam profile at the end of all three computed regions (BFR, main lens, and drift region) as shown in Fig. 8, the beam profile at the screen. It is like a true focus test only it is performed by computer. In the process, the operator does not have to find out where the virtual crossover is, where the equivalent lens principal planes are, what the spherical aberration of the system is, etc. All the effects of these conventional design parameters are taken care of automatically by the program. This speeds up the optimization process and also minimizes the error introduced by the operator.

Experience has shown that the tube test data may differ slightly from the ELOP computed data but the trend predicted by the ELOP has always been confirmed by test results. By computer modeling, the design feedback time cycle has been greatly shortened. Some parameters, such as the

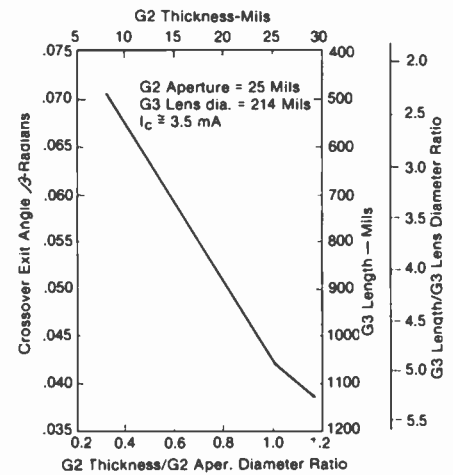


Fig. 9. Normalized G2 thickness and G3 length vs. beam divergence angle.

electron beam divergence angle and the beam size in the deflection region, are essential for the optimization decision, but are impossible to obtain directly from tube testing. In computer modeling, these parameters can be obtained directly from the printout.

The optimization process is started by selecting a group of BFR, each of which has a different G2 thickness. Then each BFR is matched with a number of main lenses, which have different G3 grid lengths. The design is computed at two current levels—3.5 mA and 1.0 mA to check for any focus tracking problems. By adjusting the voltage to bring each design into focus, the final Gaussian beam spot size can be compared in each group. The properly matched BFR and main lens can be spotted quite easily. The best matched group can then be used to generate the beam divergence angle, normalized G2 thickness, and G3 length curve as shown in Fig. 9. All the beam divergence angles are computed at the bottom of the G3 grid, where the field-free region starts, and the beam current was kept at 3.5 mA in all cases. It can be seen that when G2 thickness reaches the G2 aperture diameter size, the

Table I. Comparison of computed and test results of HiPI and bipotential gun.

Tube Type	G2 Thickness (mm)	G3 Length (mm)	Computed Spot Size (mm)		Measured Spot Size (mm)	
			1.0 mA	3.5 mA	1.0 mA	3.5 mA
28% Focus Voltage (HiPI)	0.50	23.50	1.37	2.78	1.65	2.90
20% Focus Voltage (Bipot)	0.13	13.97	1.63	3.65	2.05	3.70

Test Conditions: 19V/90° $E_b = 30$ kV C.O. = 150 V

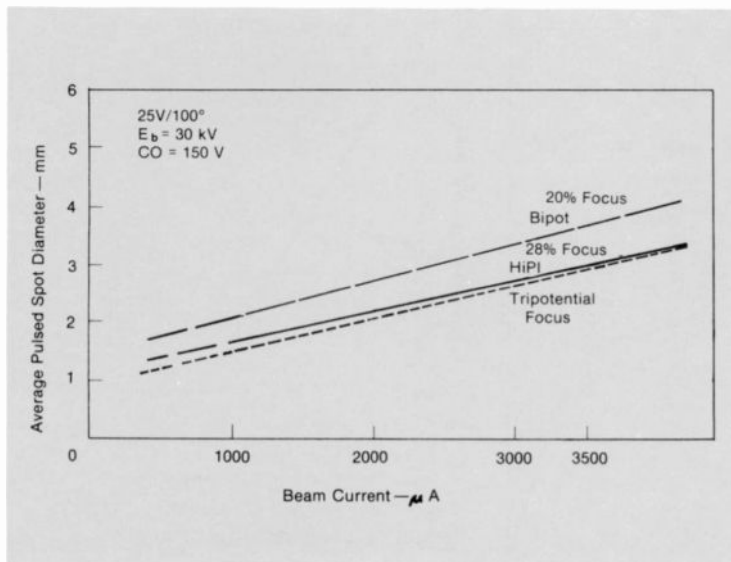


Fig. 10. Comparison of resolution between HiPI, RCA tripotential, and bipotential guns for 25V/100° tubes.



Fig. 11. Comparison of HiPI and bipotential gun size.

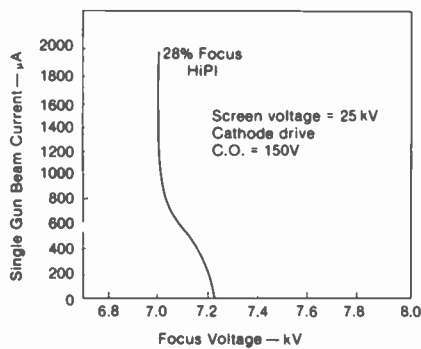


Fig. 12. Focus tracking characteristics of 28 percent focus voltage HiPI gun in 25V/100° tubes.

screen voltage. At 3.5 mA, the electron beam's half divergence angle is approximately 46 mrad, compared to the 68 mrad of the conventional 20 percent bipotential design.

Applications

After the computer modeling, a few versions of the design were selected to be built and the computed results were confirmed by closely matched test data. Two cases are shown in Table I.

The main reason for this HiPI design is to improve the large-screen color picture tube's resolution. The improvement can be readily recognized by comparing the resolution versus current curve of the 28 percent focus ratio HiPI with the 20 percent focus ratio bipotential design (Fig. 10). Also, the curve of an RCA version tripotential gun is plotted for the purpose of comparison. All the data were obtained

at the center of the screen at a 15.2-inch throw distance and without neck component (purity, etc.) correction. Compared to the 20 percent bipotential design at 3.5 mA, the spot size of the HiPI is 20.3 percent smaller and at 1.0 mA it is 19.5 percent smaller. Compared to the tripotential design at 3.5 mA (which represents the high end of the video drive), the HiPI has approximately the same resolution as the tripotential gun, and at 1.0 mA the HiPI beam size is about 10 percent larger. However, this slightly larger low beam current spot size actually serves the purpose of minimizing the moiré problem at the low light level. Also, based on computer study, the beam size of the HiPI gun in the yoke region is about 25 percent smaller than the tripotential gun at 3.5 mA. This gives the HiPI gun a definite advantage on the large-angle deflection display. Figure 11 compares a HiPI gun with a 20 percent bipotential gun.

The HiPI gun has an excellent focus tracking characteristic (Fig. 12) and it helps the picture tube to remain in sharp focus at all current levels. Also, the thick G2 acts as an improved electrostatic shield, which isolates the lower BFR from the changes of the focus voltage. With the specified HiPI tube focus voltage range (± 500 volts), there is hardly any perceivable brightness change on a normal video picture display.

The new gun design has raised the focus voltage from 6 kV to 8.5 kV at a 30-kV screen potential. To ensure proper high-voltage operation, a new single silo base and socket design has been developed. The new design provides an ample safety factor

thick G2 lens starts showing a saturation effect.

In the final design, a 0.5-mm-thick G2 with 0.63-mm-diameter aperture was chosen to match a 23.5-mm-long G3 with the 5.4-mm lens diameter and a nominal focus voltage ratio of 28 percent of the

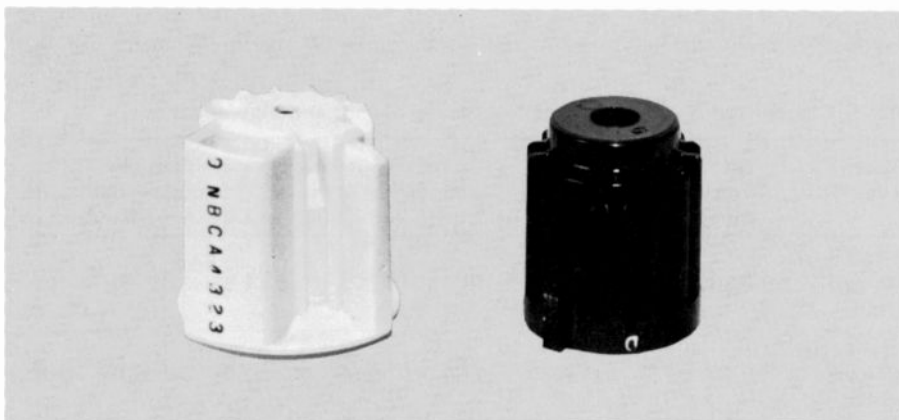


Fig. 13. New single silo base compared to the conventional bipotential base.

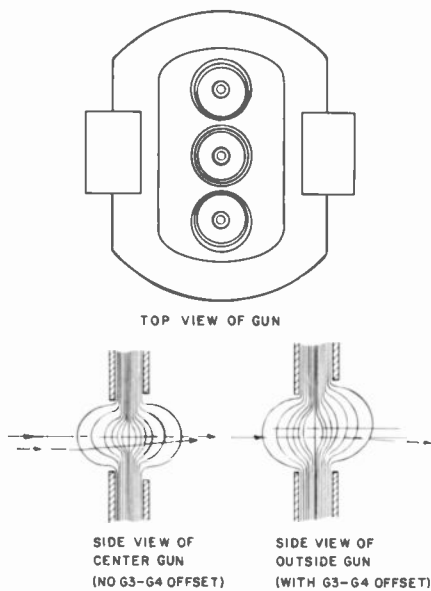


Fig. 14. Schematic drawing of HiPI gun showing G3-G4 offset in outside guns.

for both over-voltage and high-altitude operation, as well as low-cost tube assembly and processing. Consideration has been given to prevention of bent base pins, ease and safety of socket removal without tube damage and high-voltage lead orientation for best receiver lead dress (Fig. 13). The static convergence is obtained by a properly designed G3 and G4 lens offset as it was in the previous 20 percent focus ratio bipotential lens design (Fig. 14).

Conclusion

Through extensive tube design analysis and tests, this optimized RCA thick G2 HiPI electron gun has proven to have a well-balanced performance at both high and low video drive conditions. At low drive condition, it has minimum moire and at high drive condition, the beam remains in sharp focus with greatly reduced blooming.

The small edge spot size makes the gun suitable for both 100° and 110° large-screen displays.

Acknowledgment

The authors wish to thank all persons who have helped in various stages of developing this product at RCA Picture Tube Division (PTD), Lancaster, Pa. Our special thanks go to Dr. F. Campbell and various other people of RCA Laboratories for their valuable assistance with the computer modeling.

Appendix I

The Gaussian distribution approach

$$D = [D_m^2 + D_{sa}^2]^{1/2} \quad (4)$$

$$= [(C_m \phi - 1)^2 + (C_s \phi^3)^2]^{1/2} \quad (4a)$$

where D is the Gaussian beam spot; D_m is the gaussian beam spot distribution due to the magnification of the system; D_{sa} is the gaussian beam spot distribution due to the spherical aberration of the system; C_m is magnification coefficient; C_s is spherical aberration coefficient; and Φ is Half-beam divergence angle.

For the minimum beam spot criterion

$$\frac{dD}{d\phi} = \frac{1/2 [6C_s^2 \phi^5 - 2C_m^2 \phi^{-3}]}{[C_s^2 \phi^6 + C_m^2 \phi^{-2}]^{1/2}} = 0 \quad (5)$$

$$3(C_s \phi^3)^2 = (C_m \phi^{-1})^2 \quad (6)$$

OR

$$3 D_{sa} = D_m \quad (6a)$$

References

1. Barbin, R.L., and Hughes, R.H., "A New Color Picture System for Portable TV Receivers," *IEEE Trans. on Broadcast & TV Receivers*, Vol. B1R-18, No. 3, pp. 193-200 (Aug 1972).
2. Morrell, A.M., "Design Principles of the RCA Large-Screen

110° Precision In-Line Color Picture Tube," *IEEE Spring Conference*, Chicago (June 13, 1973).

3. Klemperer, O., and Barnett, M.E., *Electron Optics*, 3rd ed., University Press, Cambridge, pp. 264-265 (1971).
4. Spangenberg, K., *Vacuum Tubes*, McGraw-Hill, New York, p. 437 (1948).
5. Bakish, R., Ed., *Introduction to Electron Beam Technology*, John Wiley, New York, p. 417 (1962).
6. Grivet, P., *Electron Optics*, 2ed., Pergamon Press, Oxford, p. 390 (1972).
7. Moss, H., *Narrow Angle Electron Guns and Cathode Ray Tubes*, New York, Academic Press, pp. 68 & 129 (1968).
8. Septier, A., Ed., *Focusing of Charged Particles*, Vol. 1, New York, Academic Press, pp. 475-476 (1967).
9. Dorsey, J., "Design Consideration in Magnetic and Electrostatic Electron Optical Systems," Research Report of National Security Agency, Fort George, G. Meado, Maryland, R42 003 1967.
10. Say, D.L., "The High Voltage Bipotential Approach to Enhanced Color Tube Performance," *IEEE, Chicago Fall Conference on CE* (Dec 1977).
11. Carpenter, M.E., Momberger, R.A., and Schultz, T.W., "Application of Computer Modeling to Color Television Picture Tube Systems," *IEEE, Chicago Fall Conference on CE* (Dec 1976).
12. Saito, T., Kubota, S., and Miyaoka, S., "Digital Computer Study of Electron Lenses for Cathode Ray Tubes," *Jour. of App. Physics*, Vol. 44 No. 10 (Oct 1973).
13. Wilson, I.M., "Theoretical and Practical Aspect of Electron-Gun Design for Color Picture Tubes," *IEEE, Chicago Fall Conference on CE* (Dec 1974).
14. Blacker, A.P., Wilson, I.M., and Schwartz, J.W., "A New Form of Extended Field Lens for Use in Color Television Picture Tube Guns," *IEEE, Chicago Spring Conference on CE* (June 1976).

Richard H. Hughes is a senior engineer in color TV tube design. He joined RCA in 1943 and his major work has been in electron gun design for color television picture tubes. He initiated the design of the unitized in-line guns used in self-converging color TV systems introduced in 1972.

Contact him at:
Picture Tube Division
Lancaster, Pa.
Ext. 3356

Hsing-Yao Chen joined RCA Picture Tube Division, Lancaster, in June 1976 as a senior engineer. He currently works on advanced CRT electron gun development.

Contact him at:
Picture Tube Division
Lancaster, Pa.
Ext. 3358



Process requirements for a new generation of precision in-line shadow masks

The production of high-quality in-line shadow masks requires adherence to very tight tolerance levels.

Abstract: Shadow mask processing operations are very similar in principle to the technology employed to make integrated circuits or power transistor devices. However, for masks, the scale of operations is significantly greater, requiring artwork and process equipment capable of handling parts as large as 22 in. by 18 in. A new set of process problems was solved during the 1970s to meet the more exacting demands of masks for use in Precision In-Line Tubes.

Introduction

The first successful public demonstration of a color picture tube, using a shadow mask, was made by RCA in 1950.^{1, 2} Since that time, improvements in overall kinescope design have required significant improvements in the shadow mask's design and construction. This paper deals primarily with the process requirements developed by RCA to meet the challenge of mass producing precision in-line shadow masks.

Color television picture tubes employing shadow masks contain three essential internal components: the electron gun assembly; the phosphor screen; and the shadow mask itself. Two types of shadow-mask color picture tube systems are illustrated in Fig. 1. Three electron guns with either triangular or in-line configurations

emit electron beams which are scanned across a metal shadow mask. Portions of the beam pass through circular holes (Fig. 1a) or elongated slits (Fig. 1b) in the metal mask and impinge on a phosphor screen containing round dots or vertical lines. The phosphor screen is composed of three different types of phosphor, which under electron excitation emit light in the primary colors, red, blue, and green. In ideal operation, the electron beam from

each gun lands only on the parts of the screen associated with that particular gun. For example, the beam from the green gun excites only the light emitted by the green phosphor. With respect to that beam, all other parts of the phosphor screen are in the shadow of the mask.³

In recent years the design and production of color picture tubes have increasingly favored in-line guns employing slit-type masks. As a consequence, RCA manufac-

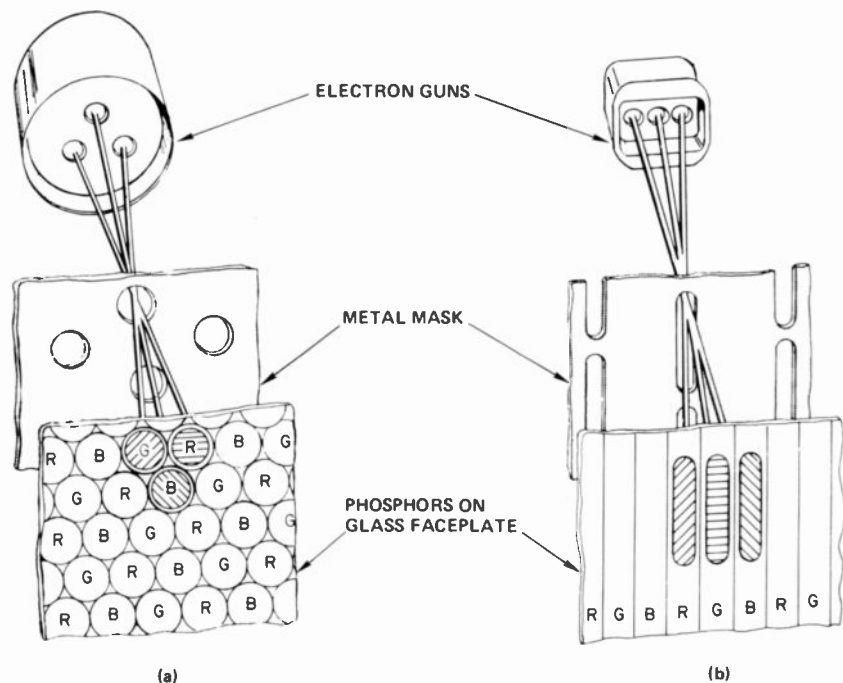


Fig. 1. Two types of shadow-mask color picture tube systems. Three electron guns with either triangular (a), or in-line (b), configurations emit electron beams, which pass through circular holes (a), or elongated slits (b), in a metal mask and impinge on a phosphor screen containing round dots or vertical lines.

Reprint RE-25-2-5
Final manuscript received March 27, 1979.

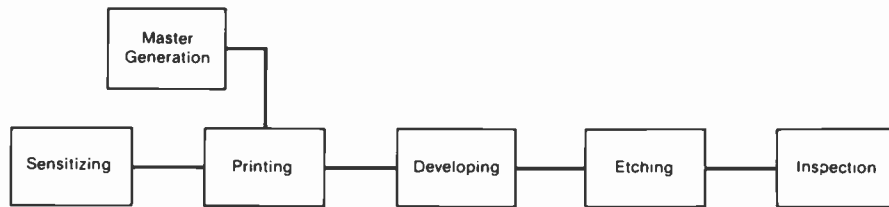


Fig. 2. The general operations of shadow-mask processing.

turing processes have been developed to meet the requirements of producing the higher technology slit-type masks.

The major process steps, outlined in Fig. 2, for making shadow masks consist of photographic master generation, steel strip sensitizing, printing, developing, etching, and inspection. The required tolerances for picture tube masks are much tighter than usually encountered in photochemical machining. For example, slit openings on the gun side of the mask are controlled to within ± 0.3 mil ($\pm 7.6 \mu\text{m}$). To meet this criterion, artwork used to make masks must also adhere to tight tolerances, i.e., no greater range than ± 0.1 mil ($2.5 \mu\text{m}$) on linewidth dimensions in the range of 2 to 20 mils ($51\text{-}510 \mu\text{m}$).

Artwork design is a critical part of the mask-making operation. Artwork is generated using a computer-controlled Gerber plotter and is produced on large-area glass plates (24-inch x 32-inch) having a silver halide photographic emulsion. Kodak Autopositive plates produce a mirror-image copy with the same contrast while Kodak Ortho plates produce a mirror-image copy having reverse contrast. A set of plates, each containing an array of about 250,000 lines, is used to make masks. One plate known as the O (obverse) plate, with relatively narrow lines, and another known as the R (reverse) plate, with relatively wide lines, are brought in close contact with resist-coated steel and then exposed using pulsed xenon lamps.

In general, artwork design is dependent on the nature of the photochemical

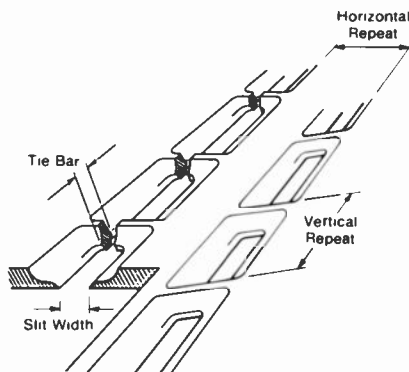


Fig. 3. Schematic cutaway of a slit-type mask.

processing and, in particular, on the prevalent etch conditions and type of etch machine used. Practically, it is desirable to set up an etch machine with constant temperature, density, redox potential, and etch pressure profile. Pressure profile is the actual etchant pressure distribution on both sides of the steel being etched. The goal is to use similar pressure profiles for all types of masks and to vary the mask artwork so that it responds predictably to these similar constant pressure profiles. Using this philosophy, linewidth and tie bar artwork dimensions are specified, which vary depending on the mask design and the actual position of the developed image in the etch tank. These artwork dimensions produce an array of slits and tie bars in the etched mask.

Figure 3 shows a cutaway view of an etched mask looking from the R side. Note the slit width, tie bar, and repeat features.

General operations

Sensitizing

Masks are produced from low carbon steel; that is, steel containing no more than 0.10 percent carbon. The steel is purchased on 1000-lb spools and must have a minimum number of surface and internal defects so as not to interfere with the quality of the finished masks. Foreign oxides and silicates etch at different rates than iron and cause imperfections in the finished mask. In general, mask steel must meet stringent specifications regarding chemical composition, flatness, thickness, width, wrinkling, surface finish, and rust. In order to improve the magnetic properties of steel for use in picture tubes, RCA sometimes further decarburizes the finished mask at the tube-making plant by heating the mask in the presence of moisture, hydrogen, and nitrogen at 850 to 1000°C, which reduces the carbon content to less than 0.01 percent.

Assuming that artwork is available to produce masks, the first processing step in mask making is the sensitizing operation. During this operation, the steel surface is cleaned with a solution containing sodium

hydroxide, rinsed with deionized water, and coated with resist. The resist is then dried in an air-heated oven. The steel cleaning operation is very important and precautions are needed to maintain the alkaline cleaning solution in correct operating condition.

Photoresist formulations developed by RCA are proprietary. They contain sodium caseinate or casein and ammonium dichromate or other photosensitizers that are capable of polymerizing the resist upon exposure to UV light. The preferred material is crystalline-like casein because of the ease of solubility when preparing the resist. A photoresist coating is used in order to provide protection for those portions of the steel that are not to be etched. Important resist parameters during use are viscosity, temperature, and pH.

The resist thickness distribution or resist profile of the strip is also an essential property because excessive slit-width variations in mirror-image positions of the etched masks are encountered when resist profiles are not uniform. Figure 4 shows two possible resist profiles, which depend on the method of application. The profile that most closely resembles a straight line is desirable because the developed image widths, for mirror-image positions on the

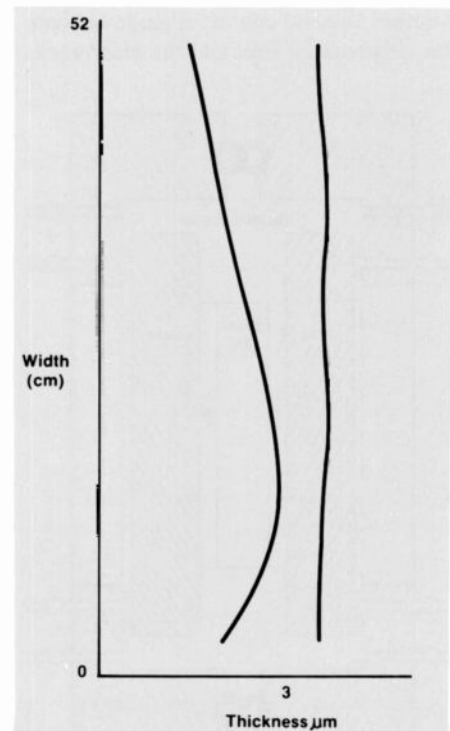


Fig. 4. Two possible resist profiles of the steel strip. The profiles are dependent on the method of resist application. The profile that most closely resembles a straight line is desirable because the developed image widths, for mirror-image positions, will be uniform.

steel, will be uniform. With the bowed profile, mirror-image positions will not etch to the same slit size. After resist application and drying, the strip is wrapped on a spool with interleaving material (plastic or paper) to protect the resist coating.

Printing

Before describing the printing operation, additional information on the photographic glass plates used in printing masks is needed. In general, a primary master is made by the use of computer-controlled plotting, according to specific design inputs. After plotting, additional photographic procedures may be employed until a working master is completed. At the mask manufacturing plant, working masters are used to make the working plates to produce masks. Working masters and working plates are made from Kodak photographic emulsion on glass plates 0.190 in (0.48 cm) thick.

The printing operation is performed using two precisely aligned plates with the resist-coated steel in between the plates. A schematic of the arrangement is shown in Fig. 5. Plates are mounted in a vacuum frame and held in place by vacuum contact.

Another vacuum contact is made between the resist-coated steel and the glass work-

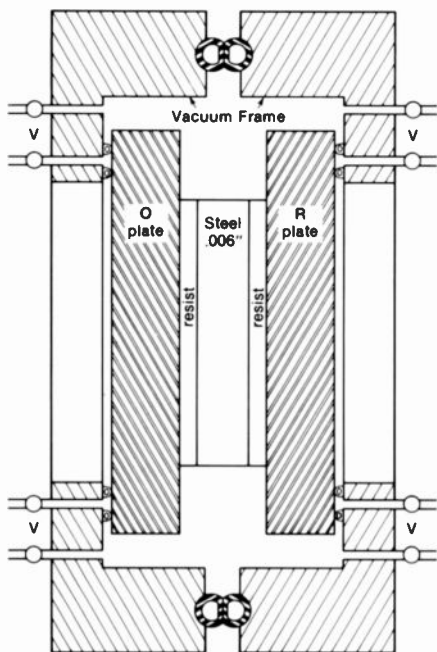


Fig. 5. The printing operation is performed using a set of two precisely aligned plates with the resist-coated steel in between the plates. The plates are mounted in a vacuum frame. Very close alignment between the two plates is extremely important.

ing plates. Very close alignment between the two plates is extremely important. This is accomplished by accurately lining-up registration marks on the plates before the contact printing operation begins.

As mentioned previously, line widths (and also line lengths) must be held to a very close tolerance, that is, variation from design must be less than ± 0.1 mil ($\pm 2.5 \mu\text{m}$). Fig. 6 and Fig. 7 show the relationships between slit width deltas and tie bar deltas respectively. In the case of slit width deltas, the difference between the etched slit width and the image line width on the O plate is known as the slit width delta. A common range of slit width deltas is from 2.8 mils ($71 \mu\text{m}$) to 3.2 mils ($81 \mu\text{m}$). When proper slit widths deltas are not used, distorted slits resulting in visual mask imperfections are obtained.

Tie bar deltas, as illustrated in Fig. 7 are determined by the difference between the clear emulsion between lines on the plate and the etched dimension of the mask tie bar. Tie bar deltas of 2 mils ($51 \mu\text{m}$) to 3 mils ($76 \mu\text{m}$) are frequently used. The extreme tie bar at any position on the mask is an important property and it is determined by a complex interaction among plate tie bars, plate images and slit width deltas.

In the actual printing operation, the resist-coated steel is exposed on both sides, using pulsed xenon lamps. The two plates are drawn close to the resist-coated steel and a vacuum is applied. Careful attention must be directed towards the detection and elimination of dirt on the plates, since dirt results in extra holes in the finished mask. After exposure, the vacuum is released and the strip is advanced for the next printing cycle. This exposure sequence is continued until a spool of several hundred prints is completed. Interleaving material again is used to protect the resist coating.

Developing

In the developing operation, the exposed, resist-coated steel passes through a chamber in which both sides are developed with warm, deionized water. The polymerized resist that was exposed to light at printing is insoluble but the un-polymerized resist washes off, exposing bare metal. After developing with water, a solution of Kodak Photo-Flo is applied to the developed strip so as to prevent spotting of the strip due to uneven evaporation of developing water.

The coated, developed strip is then baked to harden the remaining coating. This enables the resist to withstand the

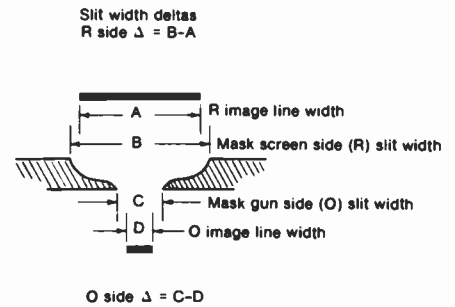


Fig. 6. The difference between the etched slit width and the image line width on the O plate is known as the slit width delta. Generally, the R image line width is much larger than the O image line width, thus enabling clearance for the electron beam to excite the phosphor screen.

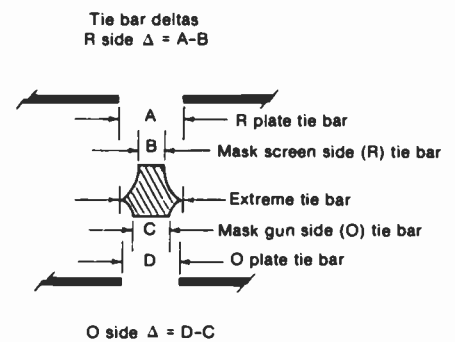


Fig. 7. Tie bar deltas are determined by the difference between the clear emulsion between lines on the plate and the etched dimension of the mask tie bar. The extreme tie bar is a complex function of plate tie bars, plate images and tie bar deltas.

action of the subsequent hot ferric chloride etch solution. Next the strip with the baked coating is wound on a spool with an interleaving material to protect the coating.

Etching

After developing, the resist-coated steel is etched using an acidic solution of hot ferric chloride. The orientation of the strip may be perpendicular to the floor (vertical etching) or parallel (horizontal etching).

Horizontal etching produces masks that are superior to those produced by vertical etching. This is because, in vertical etching, the etch solution which runs down the steel is trapped in the resist overhang on the bottom portion of the slit and results in distorted slits. Where the solution is trapped, less etching occurs, giving an undesirable step height, which is illustrated in Fig. 8. When an undesirable step height is present, clipping of the electron beam in the picture tube occurs, which causes stray emission and loss of color purity. Also,

when slit-type masks are etched vertically with the slits perpendicular to the floor, severe retardation of the etch rate on the bottom portion of the slits results in tear-dropped rather than rectangular slits. Although it is possible to etch masks vertically with slits parallel to the floor, they are, in general, inferior to horizontally etched masks because of the presence of a step height.

As the strip unwinds at the etch station, it passes through drive and guidance mechanisms and then directly into the etch tank. Inside the etch tank, the strip is immediately exposed to an acidic ferric chloride solution. The solution is sprayed on the strip from titanium manifolds, which contain spray nozzles oscillating at an optimized angle to avoid banding in the etched mask. The ferric chloride solution reacts with and dissolves the metal where the developing water removed the unpolymerized resist coating.

Key parameters in the etching operation are the solution density or Baumé, temperature, chlorination rate, steel thickness, strip speed, and mask transmission. These parameters are automatically controlled to produce the desired aperture size in the steel.

As noted above, an important variable in etching masks is the thickness of the steel, which is nominally 6 mils (152 μm). The ordinary thickness range of the metal strip as received from the supplier can produce variations in aperture sizes that are greater than can be tolerated in the manufacturing process. For example, a 0.1 mil (2.5 μm) change in the thickness of a 6-mil-thick steel strip can cause a change of 0.3 percent in the light transmission of the etched mask, or about one-third of the allowable etching tolerance. The steel strip, as received from the supplier, may have a thickness variation of as much as ± 0.5 mil (12.5 μm), which if uncompensated for, will produce masks with a greater than allowable variation in transmission. To overcome this problem, the thickness of the

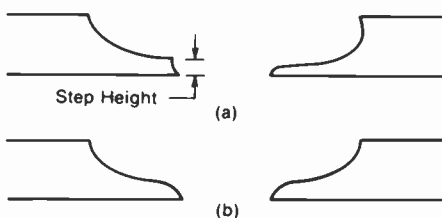


Fig. 8. Masks produced by vertical etching (a) are superior to those produced using horizontal etching (b). In vertical slits, the solution is trapped in the resist overhang, which gives an undesirable step height, resulting in distorted slits.

metal strip along the direction of movement is monitored just prior to etching with control information fed forward to adjust the speed of the strip in the etch tank. The steel thickness is monitored by means of an X-ray source and suitable detection equipment. Running average signals are compared to generate a feed-forward command signal, which changes the strip speed in the etch tank as required. Using this method, variations in light transmission (aperture size) due to variations in thickness of the metal strip can be substantially reduced.

At the exit end of the etch tank, the mask transmission is monitored by an on-line densitometer and a feed-backward command signal is generated, which adjusts the line speed based on the measured transmission.

The operating temperature of the bath is about 160°F (71°C), which is maintained to $\pm 0.1^\circ\text{F}$ ($\pm 0.06^\circ\text{C}$). Larger temperature variations cause fluctuations in the etch rate. Also, changes in the solution Baumé or density must be controlled within narrow limits. As an example, Table I compares solution density and line speed. It can be seen that a 1 percent increase in density corresponds to an 18 percent decrease in line speed.

Additional key parameters in etching are break-through point, etch pressure profile, acid content, and reduction potential.

The break-through point, which is particularly useful for experimental mask types, is the first place along the length of the etch tank where light can be observed through the steel. Lamps illuminate the bottom side of the strip and enable the operator to determine when he first can see light through the strip. The break-through point can be used as a guide in controlling aperture size. In practice, an operator may move the break-through point forward or backward by changing the strip speed. This action produces smaller or larger apertures. By measuring the aperture size and the percent light transmission at various positions on the finished mask, the operator determines if the correct change was made.

In addition to being able to vary strip speed, the operator also has the option of changing ferric chloride pressures at various positions on the etch machine so as to affect slit width and percent transmission. Normally, pressures on the bottom (R) side of the strip are higher than pressures on the top (O) side by a factor of two to three.

Acid content refers to the concentration of hydrochloric acid in the ferric chloride bath. The operator at regular intervals

Table I. Etch solution density (160°F) and etch line speed.

Density (g/ml)	Speed (in/min.)
1.471	62.2
1.481	56.4
1.486	51.0

determines the concentration of acid by a titration with a sodium hydroxide solution.

The degree of bath chlorination is controlled automatically by controlling what is called the reduction or redox potential of the solution. The redox potential is related to the logarithm of the ferrous ion, Fe(II), to ferric ion, Fe(III), concentration ratio. When the log of the ratio falls below a given value, chlorination occurs. When the log of the ratio rises above another given value, chlorination stops. The ferrous ion concentration may also be determined by using a titration solution of potassium permanganate.

After the etching operation is completed, the resist-coated steel strip is rinsed with water to remove any residual ferric chloride from the strip. Then the strip passes into a chamber where it is exposed to a hot sodium hydroxide solution, which removes the resist coating. The strip is then rinsed with deionized water, and dried in an oven to prevent the steel from rusting. There is no windup operation. The steel moves through a photosensor unit, which actuates a cutting blade that shears the strip between etched masks. Then the rectangular steel blanks containing a mask or masks (in the case of multiple arrays) slide into a holding tray.

Inspection

Masks coming off the etch line are checked at regular intervals for visual uniformity using a light box with an inclined mirror. The mask is also checked for slit width, normal transmission, and beam angle transmission. The operator making these checks, feeds information about rejects and trends to the etch line operator, who can then make corrections.

Good mask uniformity requires the absence of streaks, spots, and areas which show nonuniform patterns. Mask uniformity is essentially a subjective judgement, which, however, is aided by placing the mask on top of a light box below a mirror, inclined at 45°.

Slit-width measurements are made using a Vicker's image shearing microscope,

equipped with a direct dimensional readout system. When using this microscope, double images of the same slit are sheared until the images are just touching. The amount of shear can be directly related to the slit width.

Normal transmission refers to the amount of light that is transmitted through the mask from a given perpendicular light source. This measurement is made using a standard densitometer. A more important mask property is beam angle transmission. Beam angle transmission (Fig. 9) is measured at fixed diagonal, major and minor axis positions from the center of the mask. Two other types of beam angle transmission may be distinguished: namely, the ratio of angular transmission at a position other than the center-to-normal transmission at the center of the mask and the ratio of angular transmission at, for example, a diagonal position to normal transmission at the same position. The angle selected for transmission measurements corresponds closely to the angle of the electron beam in the tube.

Beam angle transmission properties are important in tube performance and hence also in performing screening operations in the tube factory. The diagonal-to-center ratio should be maintained to a spread of no more than 10 percent for proper factory screening control. The beam angle diagonal-to-normal transmission ratio should not, in general, be lower than 88

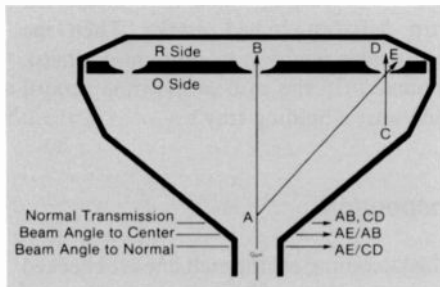


Fig. 9. Normal and beam-angle transmission ratios.

percent so as to avoid beam scattering and clipping in the picture tube.

After etching, the masks are removed from the rectangular steel blank and each one is individually inspected. At the inspection station, masks are accepted or rejected according to prescribed specifications.

In general, slit-type masks are more difficult to produce, from a quality standpoint than masks having round holes (delta type) since certain types of defects on slit masks are not objectionable on delta masks. For example, when small amounts of metal are removed (perhaps because of dirt at printing) from the R side between two vertically adjacent slits, the mask must be repaired or scrapped. This is because the adjacent slits will stretch abnormally at mask forming and result in a visually objectionable section on the screen of a tube. Such defects are not usually a problem in the manufacture of delta-type masks.

Correlation of slit width and transmission is more difficult for slit-type masks compared to the correlation of hole size and transmission with delta-type masks. This is due to the variability in the tie bar. If registration error in the chase is such that slit widths are etched large to compensate for a large tie bar, then poor correlation of slit width and transmission occurs. This is not as likely to happen with delta-type masks.

Summary

As can be recognized from the information presented, mask processing operations for slit-type masks are quite involved. The importance of cleanliness in all phases of the manufacturing steps and especially in the plate making and printing operations cannot be overemphasized.

The mask is an essential part of a color picture tube. Close tolerances must be maintained in order to ensure good picture

tube performance. From the processing point of view, large slit mask types are easier to produce compared to masks with small slits but slits may not be so large that unsatisfactory tube performance results.

References

1. Kennedy, Jr., T.R., "RCA Shows All-Electronic Tube as Key to Color Television," *The New York Times*, p. 1 (Mar 29, 1950).
2. Law, H.B., "A Three Gun Shadow-Mask Color Kinescope," *IRE*, Vol. 39, pp. 1186-1194 (1951).
3. Morrell, A.M., et al. *Color Television Picture Tubes*. New York, Academic Press, pp. 12-14 (1974).



Jack Moscony joined RCA in 1957 and has been active in the areas of materials and process development related to thermoelectric and thermionic energy converters. In 1965 he joined the C & P Lab in Lancaster where he has worked on materials and process developments for color picture tubes. Jack has helped in the solution of a broad range of problems including cathode emission, getters, high voltage stability, metallurgy, phosphor synthesis and shadow mask processing. He is currently Leader Technical Staff, Mask Process and Materials Development Engineering.

Contact him at:
**Process and Materials
 Development Engineering
 Picture Tube Division
 Lancaster, Pa.
 Ext. 2235**

Contoured-line screens for new in-line color picture tubes

Improvements in picture-tube performance and enhanced manufacturing yields are made possible with the contoured-line screen.

Abstract: *The RCA Contoured-Line Screen changes the shadow mask contour and bows the phosphor lines at the edges of the screen. These changes reduce the screen misregister caused by thermal expansion of the mask and also give a more pleasing appearance to the screen. To achieve these advantages, the lines of apertures in the shadow mask have a*

variable pitch and these lines are curved to match the screen outline. Improvements in screen printing and in mask fabrication have also been achieved by these design changes. These new features are incorporated in the color tube types being introduced in this country and have been used extensively in the RCA-designed types for the international market.

The RCA Contoured-Line Screen is a refinement in line screen design. It employs two basic innovations in tube construction. The first involves a change in mask contour and the second curves or bows the phosphor lines at the screen boundaries. The mask contour change reduces the thermal expansion of the mask and its effect on beam register with tube warm-up. The bowed phosphor lines eliminate the previous step appearance at the side edges of the screen caused by terminating the straight phosphor lines to form the curved boundary of the screen. This is accomplished by curving the lines of mask apertures. It also minimizes a geometric distortion that has been a limiting factor in printing well-defined lines near the corners of the screen since the advent of line screens.

The improvement in the handling of the mask thermal expansion will be described first. The nomenclature for this innovation is the Super Arch Mask. This new system helps overcome the problem of mask expansion during tube operation, which

causes changes in screen purity and white uniformity. The new system is applicable to 90°, 100°, and 110° tubes and minimizes a fundamental design liability of in-line tubes.

Shadow-mask thermal expansion effects

To understand this innovation, it is helpful to review the history of the mask expansion problem as related to all shadow-mask picture tubes. From the beginning of color tube production, it was recognized that because the shadow mask absorbed 75 to 85 percent of the electron beam energy, its temperature rose with tube operation. The resulting expansion of the mask and frame assembly moved the apertures radially outward and caused misregister between the beams and the phosphor dots of the tube screen (Fig. 1). This misregister resulted in color field impurity and degraded white uniformity. In 1966, RCA introduced Perma-Chrome¹ as a solution to this problem. This system moves the mask assembly slightly towards the screen as it expands, in such a way that the mask apertures follow the beam path and thus

maintain good register between the beams and phosphor dots (Fig. 2). Movement of the mask towards the screen is achieved by using bimetal elements in the frame's support system which expand in response to an increase in frame temperature. Since the introduction of Perma-Chrome, it has become an industry standard for shadow-mask tubes throughout the world. Minor design variations have been incorporated by some manufacturers, but all of them employ the basic system of using bimetal elements to move the mask and frame assembly in accordance with changes in mask-frame temperature.

With the introduction of 110° deflection as well as the use of higher anode voltages, an additional problem of mask expansion was recognized that was not corrected by Perma-Chrome. This is a transient problem in which the mask temperature increases more rapidly than the frame temperature during the initial few minutes of tube operation at high input power to the screen. Since the mask is restrained at the edges by the slower heating frame, it tends to dome or increase its curvature and thus reduce the mask-to-screen spacing as shown in Fig. 3. To relieve this particular problem, two concepts were employed for partial compensation. The first was an attempt to keep the temperature of the mask as low as possible. While it has been customary for many years to blacken the mask to increase its thermal emissivity, a further step was taken by blackening the back of the phosphor screen to make it a more effective heat sink. This blackening allowed the face assembly to absorb more of the heat from the mask and thus maintain a lower mask temperature.

Reprint RE-25-2-6
Final manuscript received July 24, 1979.

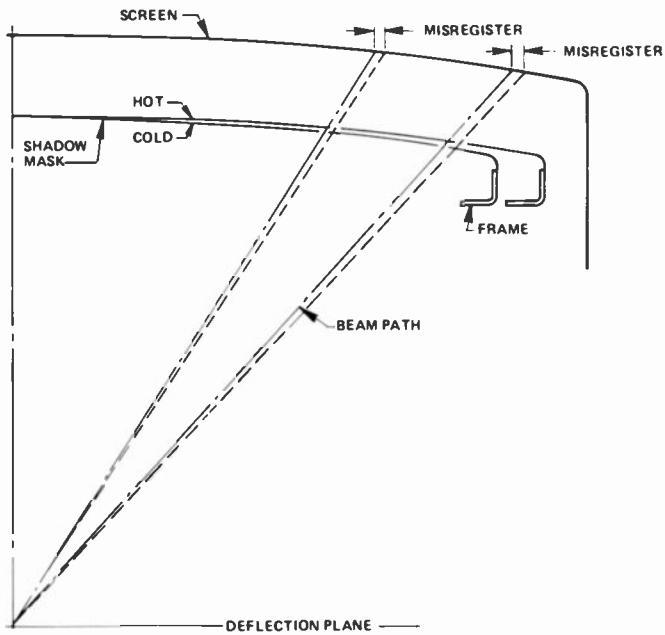


Fig. 1. Thermal expansion of the mask-frame assembly caused misregister between the beam and phosphor dots of the tube screen.

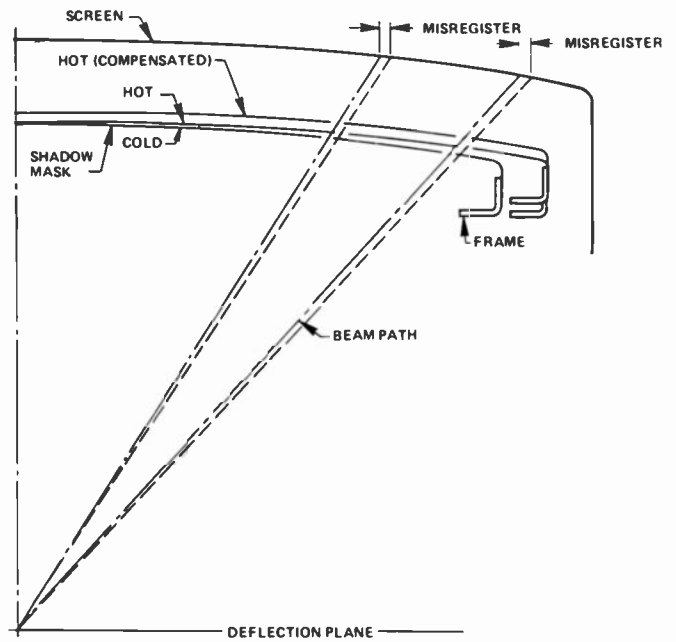


Fig. 2. The Perma-Chrome system compensates for mask-frame assembly expansion using bimetal elements to move the mask-frame assembly in accordance with temperature changes.

A second partial solution was the development of a specific register pattern imposed by the screen printing lens. It was recognized that because of the low deflection angle, register near the center of the tube screen is insensitive to mask doming. Also, the mask movement at the extreme edge of the mask is very limited because of its attachment to the cold frame. Thus, the misregister problem is maximized in the region between the center and the edge of the mask (Fig. 4). A screen printing lens was developed to adjust the beam landing in these specific areas to have the maximum possible tolerance for this mask expansion. Specifically, the position of the phosphor line was adjusted to be displaced slightly in the direction of beam movement due to mask doming. Other systems such as those involving a minimum mechanical coupling between the mask and the frame have been partially successful, but due to

the requirement of maintaining the mechanical integrity of the assembly, they can only be a partial solution.

With the in-line screen tube, the mask expansion problem has become somewhat more pronounced because of the reduced horizontal spacing between screen elements (phosphor lines). As shown in Fig. 5(a), a typical width of a phosphor line is 0.28 mm in an in-line tube as compared to a typical dot diameter of 0.39 mm in a dot-screen tube. A given misregister will result in a larger percent of the beam missing the correct phosphor in an in-line tube than in a phosphor-dot tube. As illustrated in Fig. 5(b), a misregister of 100 μm causes 30 percent of the beam to miss the correct phosphor in the in-line tube compared to 14 percent in the dot-screen tube. To increase the tolerance for mask expansion, a greater spacing between elements could be employed. Since this

would increase the visibility of the screen structure, such a simple approach has been rejected.

Super Arch mask

It can be seen that the basic problem is to minimize the change in spacing between the curved mask and the phosphor screen as the mask expands. The degree of the curvature of the mask structure determines its rise for a given linear expansion. As an example, if the mask were substantially flat, with a given expansion it would rise or dome appreciably more than the same mask with a greater curvature. The Super Arch mask has a greater curvature than the *standard mask*, which minimizes the change in spacing between the mask and the screen as the mask expands as illustrated in Fig. 6.

A more quantitative evaluation of the differences in the expansion characteristics of the Super Arch mask has been made by means of computer modeling of the mask

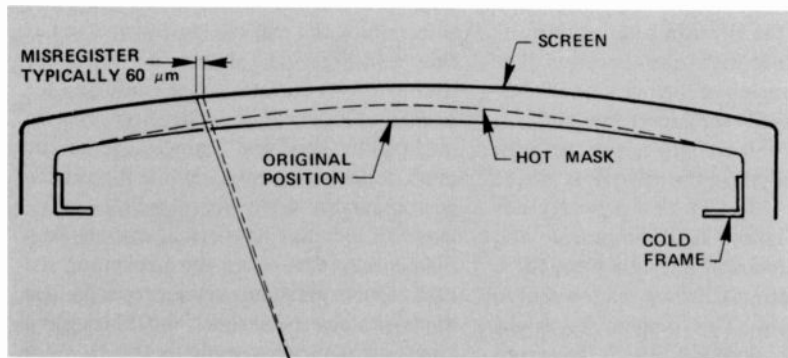


Fig. 3. The mask temperature increases more rapidly than the frame temperature during the initial minutes of tube operation, causing doming.

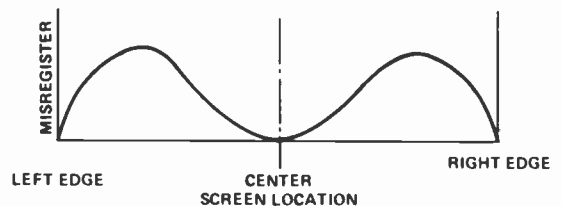


Fig. 4. The doming-induced misregister problem is maximized in the region between the center and the edge of the mask.

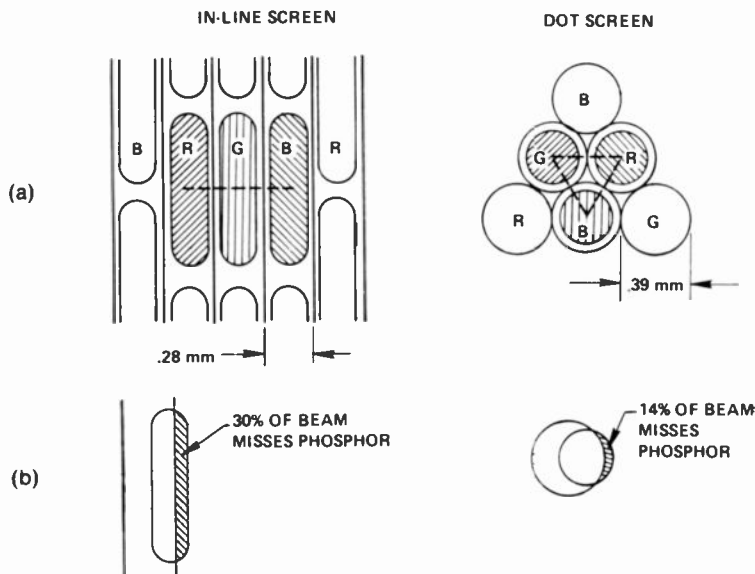


Fig. 5. Misregister caused by mask expansion is more pronounced in in-line tubes than in dot-screen tubes.

using finite element analysis. In this analysis the conventional mask used in a 25-V tube was compared to the Super Arch mask with its increased curvature. As is shown in Fig. 7, the benefit obtained from the Super Arch contour along the major axis has been computed and shown as a percentage reduction in doming. The Super Arch mask shows about a 20 percent reduction at the center decreasing to zero at the end of the major axis. This substantially lower doming results in reduced misregister.

The mask curvature cannot be arbitrarily changed since the curvature of the mask is established by the curvature of the faceplate and the proper tube geometry to insure the correct nesting of the phosphor trios as shown in Fig. 8. Specifically, the mask curvature varies from that of the faceplate such that the spacing q obeys the equation (Fig. 8):

$$q = \frac{La}{3s}$$

where q is the space between the mask and the faceplate; L is the distance from the screen to the deflection plane; a is the spacing between slits in the mask; and s is the beam spacing at the deflection plane. Or, by letting $k = L/3s$ (constants for a given tube)

$$q = ka$$

Therefore, under normal conditions, q is established by the given tube parameters and it is not obvious that the curvature of the shadow mask can be modified. However, if the parameter a is allowed to vary between the center and the edge of the screen with a larger value at the edge than

at the center, the q would also change in a similar manner. Thus, if a increases from center to edge, q will increase proportionally, resulting in a mask with a greater curvature. This greater mask curvature will change less for a given temperature change of the mask.

In addition to the advantage gained by the greater curvature, the Super Arch mask has a secondary benefit in that the larger a value toward the edge of the screen provides a greater tolerance for mask expansion in that critical area.

In the Super Arch mask, the a value gradually increases from center to edge by about 30 percent. A larger a value for the entire screen was previously rejected as undesirable because of increased visibility of the screen structure. In the Super Arch mask, the objection is avoided by having no change in screen structure in the center where the maximum picture detail is desirable, and by increasing the a value only as we approach the edge of the mask. The visual appearance is therefore pleasing to the eye and does not detract from the picture resolution since the line spacing at the edge is still small enough to resolve the maximum video bandwidth.

Bowed phosphor lines

The second feature of the contoured-line screen, which is used in conjunction with the Super Arch mask, is the bowing of the lines of apertures in the shadow mask and hence bowing of the phosphor lines. The comparison of a conventional line screen with the new one is shown in Fig. 9.

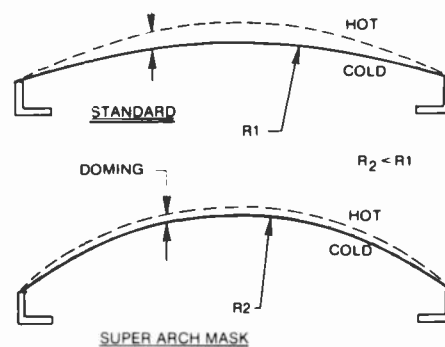


Fig. 6. The Super Arch mask has a greater curvature than the standard mask, which reduces doming.

In this figure, which is not to scale, it can be seen that the phosphor lines of the contoured-line screen follow the curvature of the screen boundary. This allows the edge lines to be continuous as contrasted to the conventional line screen wherein the curvature of the screen boundary must be approximated by segments of straight phosphor lines. The radii of curvature of the phosphor lines increase from the edge to the center of the screen in a gradual fashion until the lines become completely straight at the center of the screen. Because of this very gradual change in curvature, the effect of the contoured-line screen is pleasing to the eye.

In addition to the appearance of the screen, the bowing of the lines has an important geometrical advantage in tube manufacture. It is common in the printing of line screens to print continuous phosphor or matrix lines. The shadow mask does not have continuous slits but rather they are bridged periodically by webs to provide mechanical strength. Figure 10(a) illustrates a portion of a shadow mask showing typical dimensions. The corresponding line screen, shown in Fig. 10(b), does not contain periodic sections to correspond with the webs in the

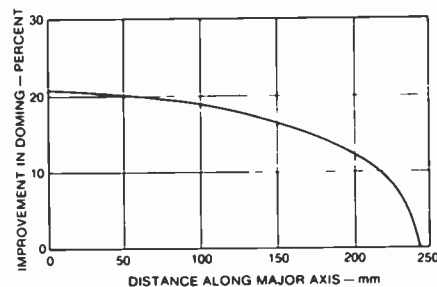


Fig. 7. Computations using finite element analysis compared a Super Arch mask with a conventional mask. The Super Arch mask showed about a 20 percent reduction at the center decreasing to zero at the end of the major axis.

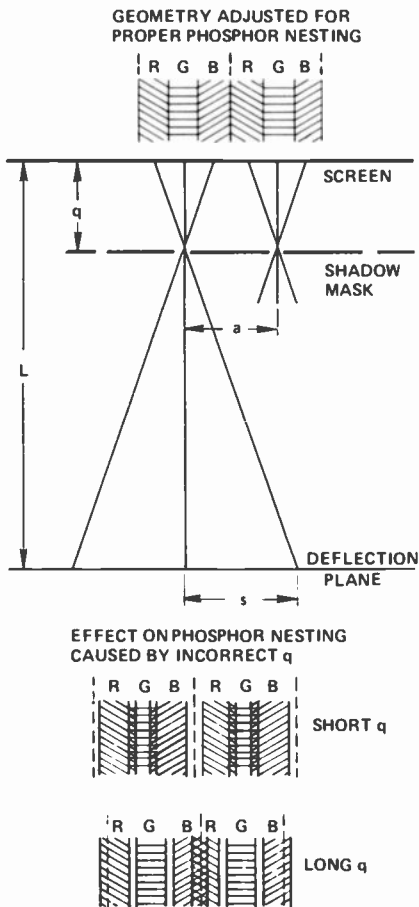


Fig. 8. Mask curvature cannot be changed arbitrarily, since correct nesting of the phosphors is dependent upon screen geometry ($q = \text{spacing}$).

mask. This is because a line source is used in the printing of the screen as shown in Fig. 11. The length of the line source is such that the entire region on the screen is substantially evenly illuminated during screen printing and therefore a continuous line is produced.

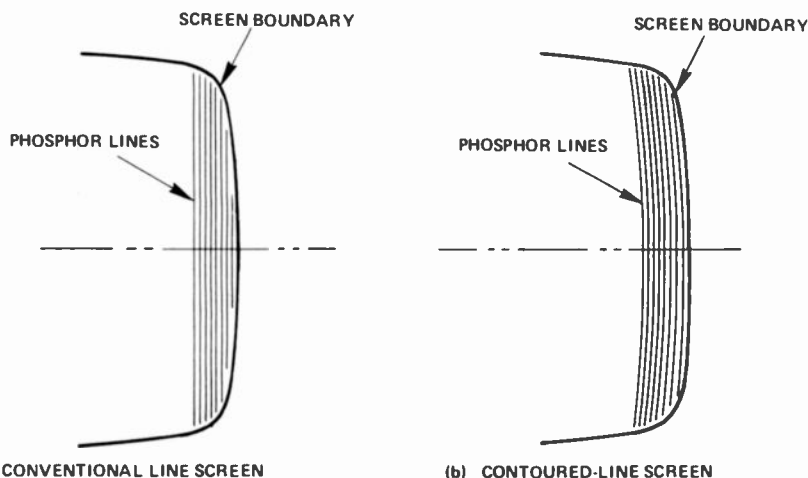


Fig. 9. The phosphor lines of the contoured-line screen follow the curvature of the screen boundary, allowing edge lines to be continuous.

Skew effect

The situation described above assumes that the line light source is located in a plane parallel to the plane of the mask. This is only true in the center of the screen. Due to the curvature of the mask there is a foreshortening of the apparent length of the light source as viewed from the screen at the end of the screen's vertical axis. This effect is of no concern at this location; however, towards the screen corners this same geometric distortion causes a rotation or skew of the light image through each of the mask apertures as it is projected onto the screen. Figure 12(a) shows this skewed pattern. Since in tube operation the phosphor line is bombarded by an electron beam that is substantially from a round point source, there is no skew pattern of electrons through the mask. Therefore a condition exists wherein the printed pattern does not completely correspond to the electron beam pattern. In practice, the phosphor line does not follow the skew pattern completely since light scattering in the phosphor during exposure and the chemical development of the pattern tend to somewhat blend the edges of the lines. However, this difference in patterns represents a significant problem in higher deflection angle tubes, especially if the attempt is being made to print a narrow line pattern as required in exposing a matrix screen.

The skew pattern can be corrected by changing the angle of the light source. This solution, however, requires a zonal exposure system since the tilt angle of the light source for the top half of the screen is opposite to that required for the bottom half of the screen. A second solution is to adjust the line of the shadow-mask aper-

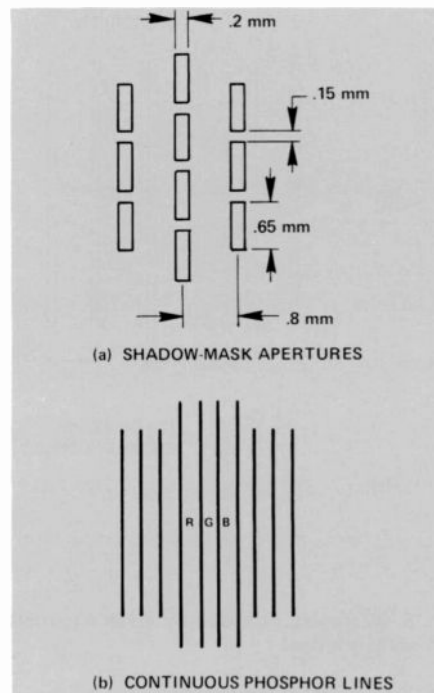


Fig. 10. Although continuous phosphor lines are common in line screens, the shadow mask does not have continuous slits.

tures to curve in accordance with the skew pattern. By doing this the effect is also eliminated. This is the approach used in the Contoured-Line Screen as shown in Fig. 12(b). The curvature of the lines, which has been made to exactly match the screen boundary curvature, is also approximately the correct value to eliminate the skew distortion.

Contoured-line mask designs

The execution of the design of the contoured-line mask is appreciably more complex than that of a conventional mask. Starting with the desired position on the screen for the outermost line, the position of the corresponding line of apertures is computed for the mask contour that would be used for straight lines. Secondly, a decision on the central and edge mask aperture spacing and the function relating these parameters must be established. Now, since the mask-to-panel spacing is a function of this horizontal aperture spacing, an adjustment in the mask-to-panel spacing via a mask contour change must be made to assure line-trio meshing on the screen.

This change in mask contour alters the desired positions of the outermost slit lines on the formed mask, which are then

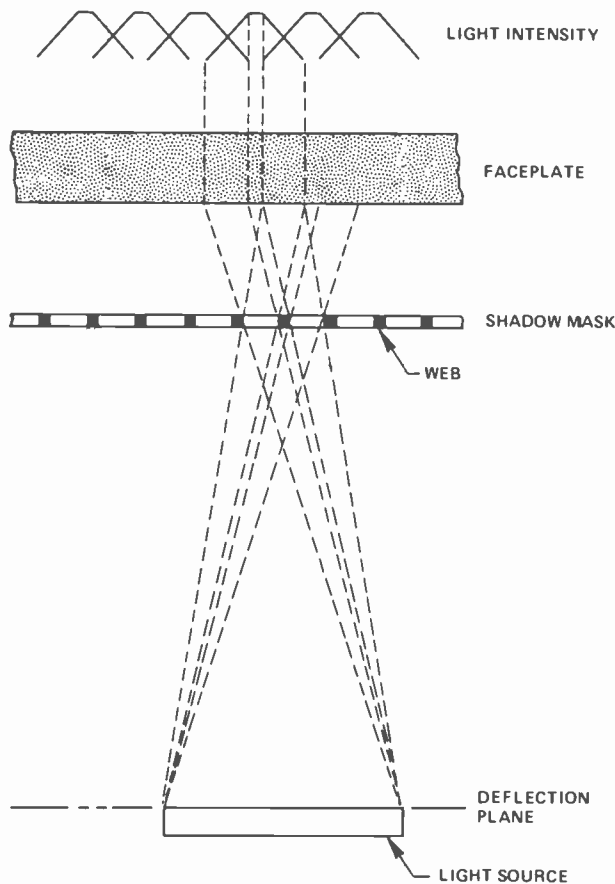


Fig. 11. A line source is used in the printing of the screen.

recomputed. This procedure is repeated until the necessary corrections are negligible.

The flat mask design must be computed from the established slit positions in the mask in its formed-contour position. Since the stretch of the mask from flat to formed generally introduces some nonuniform stretch factors, these must be known and accounted for in the flat mask design.

The generation of the master pattern for photoetching of the flat mask must be done by a numerically controlled plotting machine. Unlike conventional masks wherein the pitch is constant and the lines are straight, a simple line ruling master is no longer adequate for this new mask. The coordinates of each line must be specified and since the curvature of the lines is not a simple radius of a circle, this involves over 60,000 commands for a typical line master plus an additional 320,000 for the web pattern. In addition to describing the line placement, great care must be taken to ensure that minor relative displacements between the lines are small since the human eye can easily detect very small irregularities in a pattern.

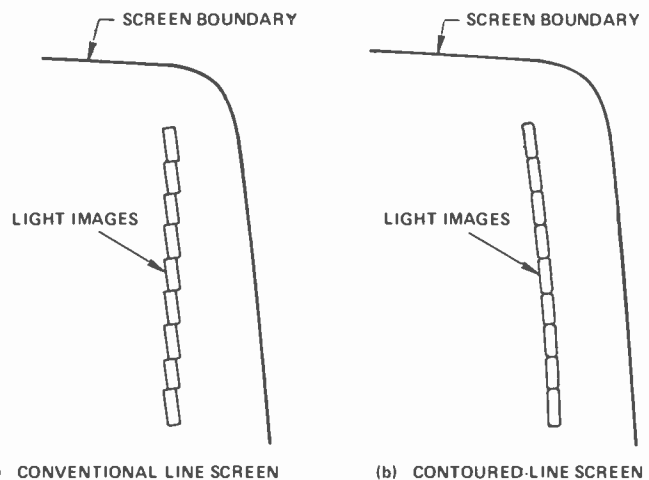
Originally presented at the 1977 IEEE Chicago Fall Conference on Consumer Electronics.

Although the mask master design is complex, the etching of the mask presents no problems over that of a conventional mask. In fact, the mask is somewhat easier to etch since, in general, the slit width is somewhat larger than in a conventional mask. This is due to the larger α value or distance between slits near the edge of the mask. Normally these slits are the smallest since it is conventional to reduce the mask transmission near the edge for greater screen tolerance. With the Super Arch Mask, the slit size can be about constant over the entire mask.

Summary

The features of the contoured-line screen combine to give an optimum design that results in improved performance and at the same time improved processability in tube manufacture, thereby giving a higher quality product. The Super Arch feature improves the thermal characteristic of the mask and also provides a design that is easier to etch. The contoured lines provide a more pleasing finished appearance to the screen and allow the printing of a better controlled-quality line structure.

The Super Arch feature has been in 110° tube types RCA has sold in the inter-



(a) CONVENTIONAL LINE SCREEN (b) CONTOURED-LINE SCREEN
 Fig. 12. With the contoured-line screen, the curvature of the lines approximates the correct value to eliminate skew distortion.

national market for almost three years. This feature has already been copied by tube manufacturers in Europe and Japan. The contoured-line feature was introduced in several new tube types by RCA beginning in 1978.

Acknowledgment

The author wishes to acknowledge the work of many of the personnel of the Tube Development Laboratory in Lancaster and the Artwork Generation Laboratory in Camden in this development.

Reference

1. Godfrey, R.H., Shrader, I.M., and Demmy, R.C., *IEEE Trans. Broadcast and TV Receivers* (Sep 1968)



A.M. Morrell is Manager, Tube Development, RCA Picture Tube Division, Lancaster. He joined the Electron Tube Division of RCA in 1950 and has specialized in color picture tube design and has been associated with most phases of their development.

Contact him at:
Tube Development
Picture Tube Division
Lancaster, Pa.
Ext. 2194

Measurement of cathode temperatures using the retarding potential method

The use of the retarding potential method and an axial magnetic field introduces nearly error-free measurement of cathode temperature.

Abstract: A method is described for the accurate measurement of true cathode temperature using the Boltzmann, or retarding potential, method. The successful measurement of these temperatures is dependent not only upon the use of circuitry which has been carefully constructed to minimize noise and leakage,

but also upon the use of tube conditioning techniques which provide for uniformity of the work function of the electron collector, and the introduction of an axial magnetic field. A discussion of the reliability of the measurements and methods for determining the reliability forms the conclusion.

Introduction

Accurate determination of cathode temperature is a very important factor in the study of emission levels and expected operating life of the cathode. The methods described here have been specifically directed toward the measurement of the true temperature of the oxide cathode as used in a color picture tube, but with little or no modification they can be applied to the measurement of cathode temperatures in many other tube types.

Often referred to as the "retarding potential" method, the Boltzmann method provides an accurate and precise means for measuring cathode temperature. Temperatures that have been accurately determined by this method are equivalent to the true temperature of the emitter, with values expressed in an absolute temperature scale normally in degrees Kelvin. These true temperatures are not to be confused with the often-used brightness temperatures that are determined by optical pyrometers. Brightness

temperatures are always less than the true temperatures unless the object viewed by the pyrometer is a true black body with an emissivity of unity. In many cases the Boltzmann method is the easiest method to use, since the cathode may be neither visible for pyrometric measurement nor easily accessible for measurement with thermocouples. In addition, pyrometric and thermocouple measurements often are made on materials that are substrates for the electron emitters and these measurements cannot describe the cathode temperature because the differential between the two is not known.

In order to determine the best technique for measuring cathode temperature, various sources of error had to be evaluated and provisions made, when required, for eliminating or minimizing these interfering effects. In addition, it was determined that the tube had to be properly conditioned before a satisfactory measurement could be made. It is believed that optimum tube conditioning is attained by methods that promote uniformity of the work function of the collecting grid(s), which acts as the electron collector, or anode, during these measurements.

Computation of cathode temperatures

To accurately compute the temperature of the cathode temperature, a series of equations has been derived which also determines the degree of accuracy of the measurements.

The Richardson-Dushman equation, equation (1), describes the current flow, I_o , in a planar diode for zero field conditions as a function of the true cathode temperature, T , and the work function of the cathode, ϕ_c .

$$I_o = A_o S T^2 \exp - \left(\frac{q\phi_c}{kT} \right) \quad (1)$$

A_o is an emission constant whose value is $120 \text{ A/cm}^2\text{-deg}^2$, S is the area of the emitter, q is the charge of an electron, and k is Boltzmann's constant.

When the diode is connected across an external load without an externally applied potential, the flow of current is in opposition to a retarding potential barrier, V_r , which is

$$V_r = V_a + \phi_a - \phi_c \quad (2)$$

where V_a is the potential developed across the external load.^{1,2} Figure 1 is one schematic representation of the potential barrier under the stated conditions, assuming that if there is a potential minimum caused by space charge it is at the collector. For the very low current levels used in the measurements described here, the space charge is negligible, and the potential follows the dashed line shown in Fig. 1.

The flow of electrons in this retarding field is described by Boltzmann's equation

$$I = I_0 \exp - \left(\frac{qV_r}{kT} \right) = I_0 \exp - \left[\frac{q}{kT} (V_a + \phi_a - \phi_c) \right] \quad (3)$$

Combining equations (1) and (3) gives the following equation for computing the net current:^{1,2,3}

$$I = A_0 S T^2 \exp - \left[\frac{q}{kT} (V_a + \phi_a) \right] \quad (4)$$

Note that equation (4) indicates that the net current flow is independent of the cathode work function, and this independence has been found to exist whenever the potential barrier, V_r , is much greater than kT/q or $T/11,600$.⁴ In practically all cases considered here, it can be shown that the above condition is satisfied and the current flow is indeed independent of the cathode work function. Equation (4) is valid only when the potential minimum is at the anode; current values cannot be sufficiently high to permit distortion of the field by space charge. Ferris⁵ has shown that this type of field distortion can be avoided if the diode current does not exceed a critical value, I_c , which is given by

$$I_c = 7.7 \times 10^{-12} \left(\frac{S T^{3/2}}{d^2} \right) \quad (5)$$

where S is the area of the emitter and d is the spacing between electrodes. For a typical color picture tube cathode with a diameter of 0.084 inch, operating at 1140°K with an interelectrode spacing of approximately 0.003 inch, the value of I_c is calculated to be 182 μ A. In practice, values exceeding 10 μ A are seldom used.

For a conditioned tube operating at a stable temperature, the anode work function should remain relatively constant over a reasonable period of time. Under these conditions, equation (4) can be rewritten without V_r (equation (2)) as follows:

$$I = I' \exp - \left(\frac{qV_a}{kT} \right) \quad (6)$$

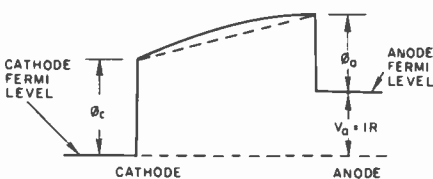


Fig. 1. Potential energy diagram with minimum at collector.

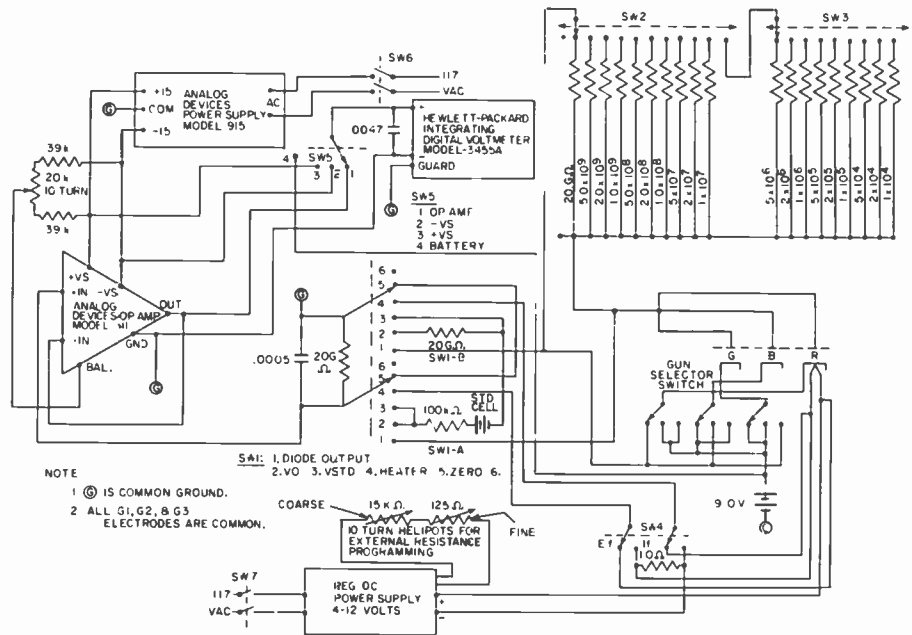


Fig. 2. Retarding potential method for measurement of cathode temperature.

where, according to equation (1):

$$I' = A_0 S T^2 \exp - \left(\frac{q\phi_a}{kT} \right)$$

When successive measurements of the retarding potential have been made, using different values of resistors to shunt the diode, the cathode temperature can be computed from equation (7), which is derived from the use of equation (6) under two sets of conditions.

$$T = \frac{q}{k} \left[\frac{(V_n - V_{n+1})}{\ln(I_{n+1}/I_n)} \right] \quad (7)$$

The subscripts indicate the particular values for the potential developed across the known resistance values and the diode current flowing through them.

By solving equation (4) for ϕ_a , the following equation can be used to determine the anode work function:

$$\phi_a = \frac{kT}{q} \ln \left(\frac{A_0 S T^2}{I} \right) + V_a \quad (8)$$

where $V_a < 0$.

Equation (8) is quite useful in determining the degree of accuracy and self-consistency with which T can be measured for various levels of load resistor and heater voltage and for gaining insight as to the changes occurring within the tube during processing.

Method of measurement

Figure 2 is a circuit diagram of the apparatus used to measure the retarding potential. Most of the circuit very closely follows that used by Corson,⁶ who made major contributions in the development of the method for accurate measurements of cathode temperature. The major departure from Corson's circuit is the provision for measurement of the cathode temperatures in each gun of a multigun tube; more recently, a modification was made which permits these measurements to be made on tubes having common grids.

The basic circuit provides for selecting one of nineteen resistors connected across the diode. With a hot cathode, the diode acts as a thermionic energy converter to drive an electron current through the resistance. The voltage, V_a , developed across the resistor is then sensed by the operational amplifier which is used as a high impedance, noninverting voltage follower. The output of the amplifier is monitored by a Hewlett Packard Model 3455A Digital Voltmeter with a $6\frac{1}{2}$ -digit readout. With the voltmeter set for "high resolution," a minimum of a 6-digit readout is assured for all resistance values. The 24-hour accuracy of the voltmeter at the 1-V range is specified to be ± 0.003 percent of reading + 4 digits (± 0.000034 volt at the 1-V level).

All resistors used for the measurements are high precision types that have been calibrated by the Victoreen Instrument Division to four significant figures. These

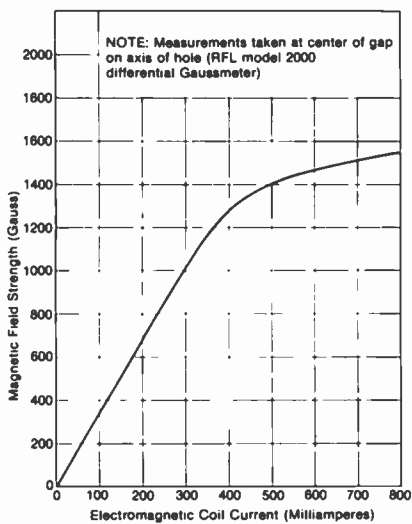


Fig. 3. Field strength of electromagnet versus coil current. (Note: Measurements taken at center of gap on axis of hole (RFL model 2000 differential Gaussmeter).

resistors have been mounted in a plastic enclosure that is believed to be relatively dust free.

Other precautions have been taken (many of which have been found to be necessary) to ensure stable and trouble-free operation.

Error reduction with an axial magnetic field

For the gun constructions considered here, primarily the three-gun type used for color picture tubes, the use of an axial magnetic field is an absolute must, if any reasonable degree of accuracy is expected. For the electromagnet used in the equipment described, the field strength in the magnet gap is shown as a function of coil current in Fig. 3. The actual change in tube characteristics is shown in Fig. 4 as a function of the coil current and the resultant magnetic field. Plots of $\log I$ versus V were formerly used to determine the cathode temperature which can be seen from equation (7) which indicates the temperature is inversely proportional to the slope of the line. The plot for zero field is not even a straight line.

The influence of the axial magnetic field can be even more readily appreciated by reference to Table I. These data show that an error of over 200 K can be obtained when the magnetic field is not used, and that a field of only 350 gauss leads to a reasonable value. The data indicate that the temperature values obtained are relatively constant for all field strengths in excess of

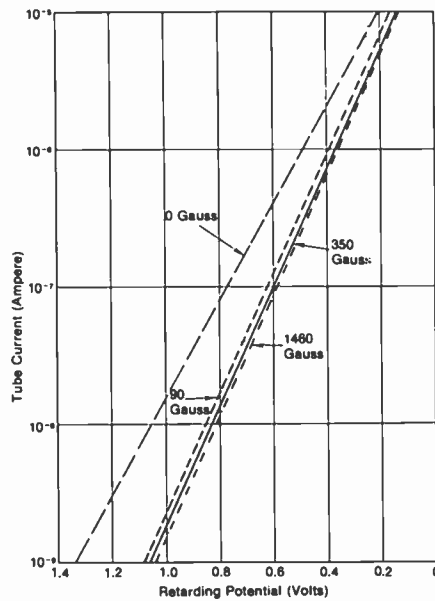


Fig. 4. Tube characteristics versus axial magnetic field strength 25V - 90° bipotential tube (LEKA6105), red gun date of 9/7/76.

400 gauss. A current of 600 milliamperes is used for the coil in routine measurements which provides a field strength of approximately 1450 gauss.

By referring to Fig. 4 and Table I, it can be seen that the most meaningful measurements correspond to the lowest voltages and the lowest temperature plateaus.

Figure 5 illustrates the magnitude of the voltage change that can occur with changes in the magnetic field. With a fixed resistance of 50 megohms, the field across the gap was varied to determine the corresponding voltage change. As long as the coil current is maintained above 500 milliamperes, variations in the potential across the resistors will not exceed 0.1 millivolt.

By changing the value of one of the two voltage values in equation (7), calculations have shown that an error in V_a of only 0.1 millivolt will lead to errors greater than two degrees when computing the temperature. These errors are maintained at a minimum when the magnet coils are operated at a current of 600 milliamperes.

Methods of stabilizing tubes

For too long a period, the initial attempts to measure cathode temperature by the retarding potential method were remarkably consistent in their lack of success. Although the poor results were partly due to lack of sophistication in the measuring circuit, the lack of stability in

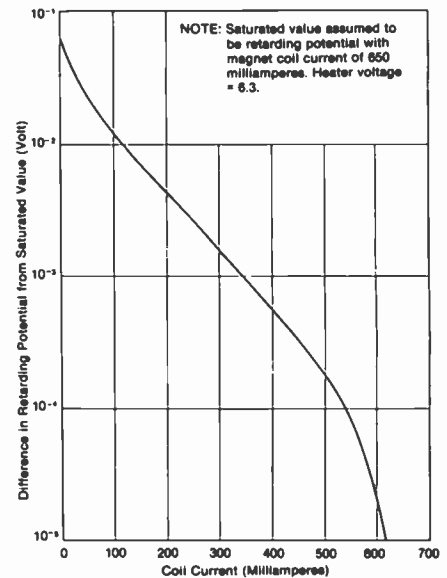


Fig. 5. Effect of magnetic field on retarding potential generated across 50 megohm resistor - 25V, 90° bipotential delta tube.

the tubes contributed significantly to the inability to make good measurements. Equation (4) indicates that the flow of electrons in a retarding field is dependent on the anode work function and independent of the cathode work function. From the results of measurements over the last several years, it has been determined that the most stable tubes — those yielding the desired temperature plateaus — are those in which the anode work function has been made relatively uniform by one of two methods.

The first method involves relatively high temperature operation of the tube for long periods of time during which moderate currents are drawn to electrode G1. The heaters are operated at 9.5 V for one to several hours while the voltage on G1 is regulated to provide a constant current flow of 8 mA. Some tubes respond well with only one hour of this treatment while others require additional time. This method has been found to stabilize approximately half of the tubes processed and permit meaningful determinations of the cathode temperature. Using the data representative of the average temperature, the anode work function is calculated from equation (8). For this method of stabilization, the anode work function usually approaches a limiting value of approximately 2.55 eV. The work function of pure barium is 2.52 eV.^{7,8} This result suggests that the uniformity of the anode, and the resultant successful measurement of cathode temperature, was achieved by depositing a relatively pure layer of barium

Table I. Effect of axial magnetic field on measurement of cathode temperature by retarding potential method.

Resistor number	0 milliamp. 0 Gauss	25 milliamp. 90 Gauss	50 milliamp. 175 Gauss	100 milliamp. 350 Gauss	200 milliamp. 690 Gauss	400 milliamp. 1275 Gauss	600 milliamp. 1460 Gauss
5	none	none	none	none	none	none	none
6	1287.69	1134.05	1128.53	1124.54	1113.05	1117.90	1121.74
7	1333.48	1152.02	1146.65	1141.16	1127.48	1133.26	1132.27
8	1357.15	1153.73	1150.47	1144.50	1140.61	1138.32	1137.18
9	1357.12	1159.23	1158.20	1151.26	1155.44	1145.28	1145.81
10	1331.65	1163.52	1161.83	1154.41	1150.96	1148.81	1150.58
11	1315.90	1160.86	1160.85	1152.45	1138.18	1151.63	1151.83
12	1331.96	1157.81	1159.31	1148.94	1160.19	1152.48	1149.49
13	1398.56	1156.00	1154.98	1144.25	1149.22	1147.96	1148.20
14	1481.33	1156.62	1155.32	1145.78	1152.58	1150.98	1151.54
15	1538.98	1160.80	1157.18	1149.02	1152.23	1151.44	1150.55
16	1576.65	1168.28	1164.18	1153.14	1153.02	1151.60	1150.22
17	1587.16	1173.34	1172.46	1158.92	1155.09	1151.56	1151.60
18	1561.00	1184.41	1181.64	1166.72	1161.32	1160.00	1158.20
19	1523.93	1196.39	1184.61	1171.16	1166.17	1165.00	1164.73
20	1478.94	1198.16	1187.94	1175.25	1167.34	1170.96	1169.89
Indicated temperature	1357.1	1159.3	1160.1	1149.9	1152.6	1150.2	1150.5

Data from 25 V, 90° bipotential tube, red gun (LEKA6105) — heater potential = 6.300 volts.

on the grid surface as a result of excessive evaporation of this element from the hot cathode.

The second method of stabilization involves bombardment of electrode G1 with relatively energetic electrons from a moderately hot cathode. With the heaters at voltages from 8.5 to 9.0 V, a potential of approximately 30 V is applied to G1. Although an initial poisoning of the cathode takes place due to the liberation of gas from the hot grid, the cathode current stabilizes relatively quickly and, for most tubes, asymptotically approaches a limiting value of approximately 120 mA. This treatment will result in the stabilization of slightly more than half of the tubes, and an additional hour of the same treatment will stabilize another 10 to 15 percent of those processed. Tubes subjected to this treatment exhibit temperature plateaus at least as good as the first method, but anode functions calculated from these data tend to show a definite decrease with processing time and approach a lower limiting value of approximately 2.07 eV. This lower value of work function is not well understood, but it is believed to represent a condition where part of the barium film has been stripped away as a result of the electron bombardment and/or it has been partially oxidized.

Although the second method is the one presently preferred for preparing a tube for the retarding potential measurement of temperature, a large number of tubes still fail to respond to this treatment or to any other processing yet tried. Conversely, there have been a limited number of cases where tubes have been successfully measured, either as received from the factory or as aged in the laboratory. Generally, the most successful aging schedule for preparing these tubes adequately includes a liberal amount of electron bombardment of all grids. Work will be continued to determine the best method for adequately preparing these tubes.

Reliability of measurements

In order to assess the retarding potential method and determine whether reliable results can be obtained from its use, two evaluation approaches have been tried. For the first, refer to Fig. 6. The graphs indicate that between 6 and 9 volts, the average difference between the true temperature, T , and the brightness temperature, T_{Br} , is 68 K. According to Wien's radiation law, the relation between these two temperatures and the emissivity of the cathode (at the

point at which it is viewed with the optical pyrometer) is

$$\ln E_\lambda = C_2/\lambda (1/T - 1/T_{Br}) \quad (9)$$

where E_λ is the spectral emissivity, $C_2 = 1.43879$ cm.-deg., and λ is the effective wavelength of the red filter in the optical pyrometer (0.65 micron). With 7.5 V applied to the heater, the true and brightness temperatures (from Fig. 6) are 1224 and 1156 K, respectively. Substituting these values in equation (9) produces a value of 0.345 for the spectral emissivity. Since the spectral emissivity of nickel which is the substrate of the cathode coating and which is viewed by the optical pyrometer during measurement of the brightness temperature is generally quoted at 0.36, it would appear that the temperature values shown are quite reasonable.

The second approach taken to evaluate the accuracy of the retarding potential method involves the use of equation (8) for calculating the anode work function. It would be reasonable to assume that the computed temperatures would be accurate if: (1) temperatures are measured for the same guns at different heater voltages, and (2) the data used to determine the temperature values were also used to compute the anode work function (which should be constant for each gun, regardless

Table II. Calculations of anode work functions from retarding potential measurements of cathode temperature.

Gun	V_f Heater voltage	I Diode current (ampere)	V_a Retarding potential (volt)	T_c Cathode temp. (° K)	Φ_a Anode work function (eV)	Average work function	Maximum difference
Red	5.7	2.6934×10^{-8}	0.53599	1080.9	2.5536	2.5560	0.0118
	6.3	6.1954×10^{-8}	0.61842	1134.1	2.5513		
	6.9	3.5795×10^{-6}	0.35974	1191.1	2.5631		
Blue	5.7	1.5558×10^{-6}	0.15636	1076.4	2.5434	2.5475	0.0143
	6.3	1.5359×10^{-6}	0.30657	1131.5	2.5424		
	6.9	9.9176×10^{-7}	0.49537	1190.2	2.5567		
Green	5.7	3.0884×10^{-7}	0.30759	1099.3	2.6068	2.6048	0.0042
	6.3	1.1279×10^{-7}	0.56642	1154.8	2.6051		
	6.9	1.1868×10^{-5}	0.23736	1207.0	2.6026		

Values of anode work function calculated from

$$\phi_a = \frac{kT}{q} \ln \frac{A_0 S T^2}{I} + V_a \quad \text{where } V_a < 0$$

of temperature). This assumption must also provide that no additional processing was given to the tube to change this anode work function while the measurements were being made. Table II shows the results of the measurements of one tube at heater voltages of 5.7, 6.3, and 6.9V. While the anode work functions were different among the three guns of the tube, the maximum difference in the work function for any one gun for the three heater voltages measured is only of the order of

0.5 percent of the measured value. These results indicate the reliability of the retarding potential of measurement.

Acknowledgments

The writer is indebted to J.D. Levine of RCA Laboratories, Princeton, and R.H. Hughes of Lancaster for their helpful discussions of various physical phenomena related to this method of temperature measurement, and to G.M. Ehemann of Lancaster for assistance with computer programming.

- Jamison, N.C., and Cashman, R.J., *Phys. Rev.*, Vol. 50, 624 (1936)
- Anderson, P.A., *Phys. Rev.*, Vol. 115, 553 (1959)

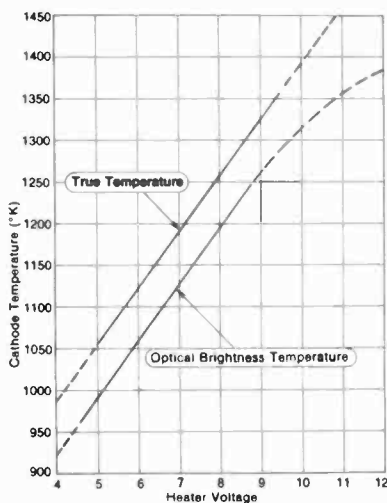


Fig. 6. Cathode temperature as function of heater voltage 25V, 110° PIE tubes (CR8134).

References

- Hatsopoulos G., and Kaye, J., "Analysis and Experimental Results of a Diode Configuration of a Novel Thermoelectron Engine," *Proc. IRE*, Vol. 46, 1574 (1958)
- Moss, H., "Thermionic Diodes as Energy Converters," *Journ. Electronics*, Vol. 2, 305 (1957)
- Beck, A., and Maloney, C., "A New Method for the Measurement of Temperature Changes in Thermionic Cathodes During Pulsed Emission," *Brit. J. Appl. Phys.*, Vol. 18, 848 (1967)
- Nottingham, W., "Thermionic Diode as a Heat-to-Electrical-Power Transducer," *J. Appl. Phys.*, Vol. 30, 413 (1959)
- Ferris, W., "Some Characteristics of Diodes With Oxide Coated Cathodes," *RCA Review*, Vol. 10, 134 (1949)
- Corson, B., "Apparatus and Methods for the Precise Determination of Boltzmann Temperature," *Rev. Sci. Instr.*, Vol. 41, 163 (1970)



Paul R. Liller, Member of Technical Staff, Picture Tube Division, Lancaster, Pa., joined RCA in 1957. After working several years on power tubes, he was transferred to his present location in the Materials and Process Laboratory of the Picture Tube Division. His primary responsibilities include high voltage processing and cathode emission; he has been granted a patent for cathode processing.

Contact him at:
Picture Tube Division
Lancaster, Pa.
Ext. 3636

Rapid scan determination of optical spectra

Monochromators using Vidicon detectors have eliminated the tedious aspects of CIE chromaticity calculations.

Abstract An interpolation procedure for mapping the instrument dispersion of a spectrometer into true wavelength is presented. This procedure is used to generate the true spectrum of a light source from the spectrometer's recorded response to that source. The procedure, using LaGrange interpolation, has found convenient application in the software of a computer-interfaced spectrometer used in the Lancaster Process and Materials Development Laboratory.

Phosphor emission spectra must be accurately determined in order to produce color TV primaries with uniform chromaticity from lot to lot, as well as for studying the effects of material and processing variables. The spectral characteristics of all phosphors tested in the Lancaster Spectroradiometer Laboratory, as well as engineering data derived from those spectra are acquired, stored, and processed by a rapid scan spectrometer. This instrument, purchased from Tektronix, includes a spectrometer unit plugged into a digital processing oscilloscope which in turn is linked to a DEC PDP-11 computer. Tektronix has provided extensive software for generating number arrays from the vidicon signal in the spectrometer plug-in. When the system is properly calibrated, these number arrays represent accurate spectral characteristics of the tested materials. This paper describes a procedure developed by RCA for calibrating the instrument. The

procedure generates proper matching between spectral wavelength and array index, and proper correction of each array number according to the spectral sensitivity of the instrument.

Advantages of the rapid scan approach

The rapid scan system has the computational power to derive CIE chromaticity coordinates x and y from the acquired waveforms. Herein lie two advantages of the rapid scan system: first, all waveform computations are performed by the system rather than by tedious hand calculations. The waveform acquisition provides digitally stored data at 512 wavelengths, virtually unachievable from analog instruments, and hours of human labor. Second, a short waveform acquisition time of 20 milliseconds eliminates data scatter caused by drift in the anode beam

current exciting the phosphor sample. These advantages are utilized in measuring cathodoluminescence of demountable phosphor powders as well as phosphors in finished tubes. (Finished tube chromaticity is also obtained from a three-channel filter colorimeter, except in cases where the phosphors are non-standard. In the latter case, a spectrometer, rather than a filter colorimeter, is required.)

A Tektronix digital processing oscilloscope (DPO) with a spectrometer plug-in unit (containing an RCA silicon target for the vidicon) is being used for routine spectral emission studies of color TV phosphors made at RCA in Lancaster. This rapid scan spectrometer (RSS) system is also used for measuring spectral reflectivity of pigmented phosphors. These are usually blue and red emitters coated with yellow-absorbing and blue-absorbing pigments, respectively. Figure 1 shows spectral emission curves of blue, green, and red phosphors taken with the RSS video

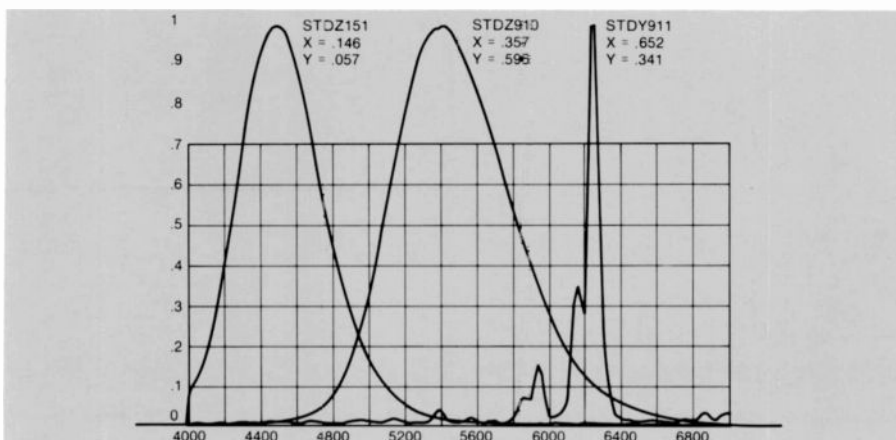


Fig. 1. Spectral energy distributions of blue, green, red color TV phosphors taken with RSS.

Reprint RE-25-2-8
Final manuscript received July 13, 1979.

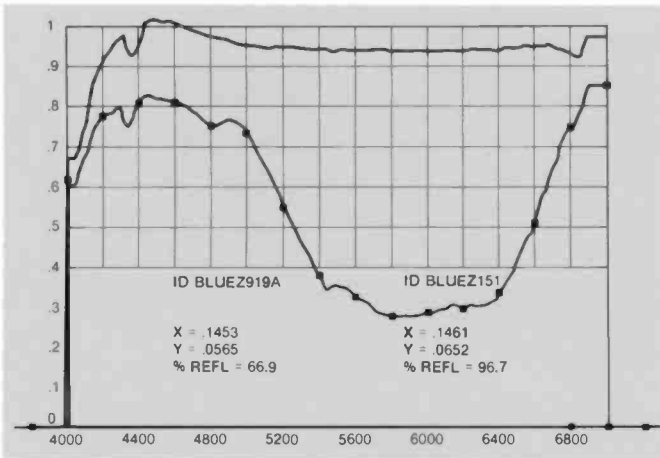


Fig. 2. Spectral reflectivity of pigmented (lower curve) and non-pigmented blue phosphor. Fluorescence is evident in the blue region.

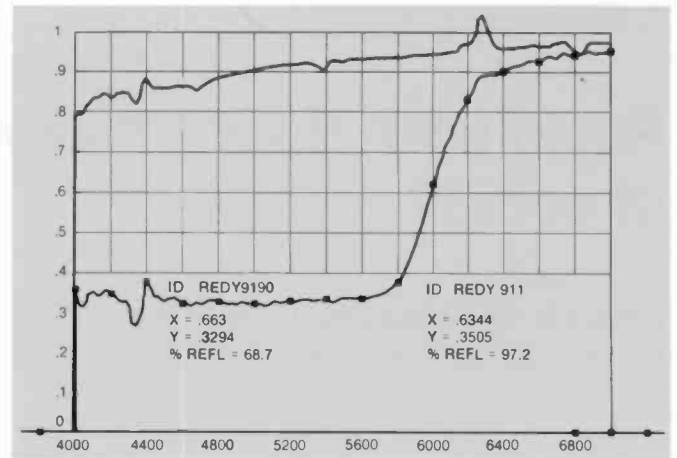


Fig. 3. Spectral reflectivity of pigmented (lower curve) and non-pigmented red phosphor. Fluorescence is evident in the red region.

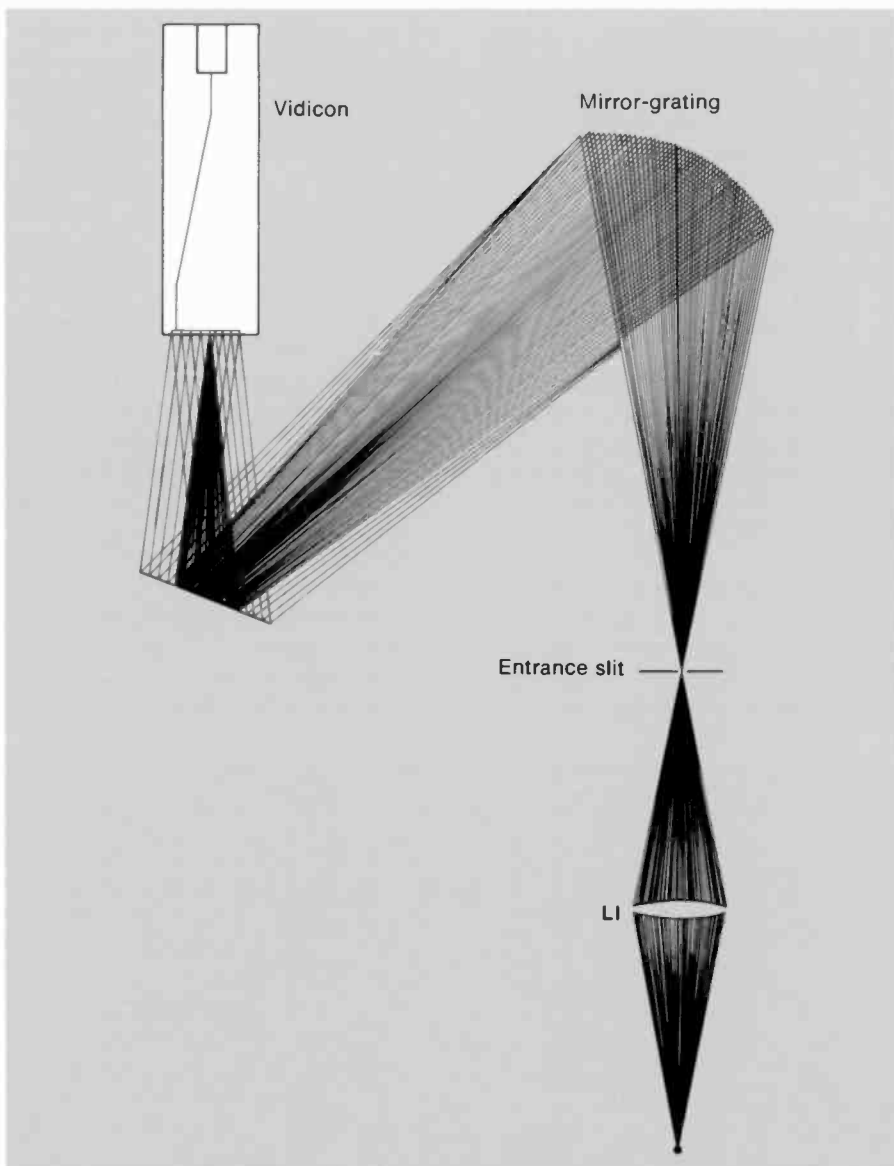


Fig. 4. Light path of RSS monochromator with external lens. Planar grating and spherical mirror in actual instrument are represented here as one "mirror-grating" element.

display terminal and hard copy unit. Figures 2 and 3 show spectral reflectivity curves of both pigmented and non-pigmented phosphors.

In addition to sampling spectra at the rapid rate of the silicon target vidicon (3000Å to 7000Å in 20 ms), the RSS provides complete colorimetric specification in terms of CIE x , y coordinates and curve shape parameters within a period of several seconds. A DEC PDP 11 minicomputer interfaces with the DPO and receives the digitized and stored waveforms generated by the vidicon. A hard disk memory stores instrument calibration data as well as the tabulated tristimulus values (spectral waveforms x , y , z) of the standard CIE observer. The sampled waveform stored in the DPO, call it A , has 512 elements each corresponding to a sampling of the vidicon signal. The instantaneous vidicon beam deflection voltage corresponding to each stored value of waveform A , is also stored as a memory address I . This set of memory addresses are the instrument wavelength indices, ranging from 0 to 511. Into each is written a 10 bit number of waveform A sampling, $A(I)$.

The diffraction grating dispersion knob is normally put in the 3000 - 7000Å position so that the 512 samples of waveform A cover this spectral range. See Fig. 4 for a schematic picture of the light path beginning at the phosphor, striking the diffraction grating, and terminating at the silicon target.

The CIE chromaticity coordinates corresponding to spectral waveform A are mathematically obtained by multiplying A by \bar{x} and integrating the product from $\lambda = 4000$ to 7000Å . The integration is also performed on the products $A\bar{y}$ and $A\bar{z}$.

Denoting the respective product integrals by X , Y , and Z , one finally has CIE $x = X/(X + Y + Z)$ and CIE $y = Y/(X + Y + Z)$. This mathematical procedure is compactly expressed in the Tektronix BASIC waveform processing language, known as TEK SPS BASIC. Here is an example where one computes the CIE x coordinate:

$$F = A * XB$$

$$F = \text{INT}(F)$$

$$X = F(IU) - F(IL)$$

In this example XB is the \bar{x} tristimulus function represented as an array $XB(I)$. Arrays A and XB must have the same number of elements and must be defined over the same wavelength domain. The upper and lower indices IU and IL represent 7000 and 4000Å, respectively, and would to a first approximation be given by $IU = 511$, $IL = (4000 - 3000) \cdot 511 \div (7000 - 3000) = 128$. INT is the waveform integration operator.

Calibrating the wavelength indices

The positioning of the diffraction grating spectrum over the silicon target must be accurately known to ensure meaningful CIE x and y values. It is both convenient and necessary to establish the position of a single line in the visible spectrum as a calibration point every time a group of test spectra are recorded. A white plaque placed in front of the lens L1 will reflect fluorescent ambient lighting into the system, with the Hg 5461 Å serving as a convenient spectral marker. The wavelength index assigned to this line by the RSS is evaluated and stored in disk memory, and subsequently used in a routine which corrects each recorded waveform and generates a spectrum with accurate wavelength indices.

To understand the details of such

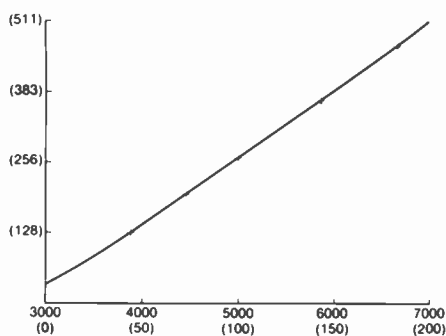


Fig. 5. DPO waveform index (I) vs. true wavelength and true wavelength index (N).

wavelength corrections we begin with the basic data of Fig. 5. Here are shown the DPO waveform indices of a set of five He lines vs. the actual values which are 3889, 4471, 5015, 5875, and 6678 Å. From the information in this figure, one can write the wavelength correction formula, relating each of 201 actual wavelengths, $300 + 20N$, for $N = 0$ to 200, to the DPO waveform indices I , for $I = 0$ to 511:

$$I(N) = \sum_{L=1}^5 R(L) \cdot P(L) \quad (1)$$

where

$$P(L) = \sum_{J \neq L}^5 \frac{N - Z(J)}{Z(L) - Z(J)}$$

and $R(L)$ are the interpolated DPO waveform indices, ranging between 0 and 511, for the actual wavelengths

$$\lambda(L) = 3000 + 20 \cdot Z(L)$$

The result of the correction Eq. 1, which is a LaGrange interpolation procedure, is the capability to generate a true spectrum $S(N)$ from the DPO stored waveform $A(I)$. Expressed in the BASIC language statements, the implementation of the wavelength corrections is straightforward:

```
FOR N = 0 TO 200
  S(N) = A(I(N))
NEXT N
```

$I(N)$ is computed from Eq. 1, where non-integer values result in general for I . This presents no problem for the SPS BASIC language interpreter, which performs an interpolation on the $A(I)$ array to obtain $S(N)$ when $I(N)$ is not an integer.

The entire wavelength correction procedure—beginning with the RSS acquisition of the waveform from the He discharge tube, and ending with the 512 element array $I(N)$ which is later used for correcting all test waveforms $A(I)$ into true spectra $S(N)$ —is performed in a few minutes under control of a BASIC program called from the disk memory. Repetitions of this set-up procedure with the He lamp are seldom required. Instead of recalculating the correction array $I(N)$ each time spectra are to be measured, a much simpler method using the single Hg line at 5461Å is used in conjunction with the initially stored $I(N)$ array based on the He run. This results in the addition of a constant term E to the right side of Eq. 1. The value E is rapidly obtained by storing a waveform representation of fluorescent room lighting reflected from a plaque:

$$E = R - I((5461 - 3000)/20)$$

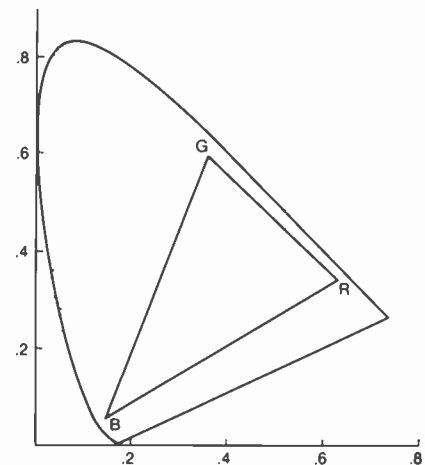


Fig. 6. CIE x,y diagram and R,G,B points. Horseshoe-shaped curve represents locus of spectra from $\lambda = 4000$ -7000 angstroms.

where R is the interpolated DPO index of the waveform peak in the region near 5461Å,

$$R = R_0 + \frac{A(R_0 + 1) - A(R_0 - 1)}{2[-A(R_0 + 1) + 2A(R_0) - A(R_0 - 1)]}$$

and R_0 is the integer waveform index of the largest number, $A(R_0)$, in the waveform A at the 5461Å peak. This completes the discussion of procedures for correcting the DPC waveform indices. The next task is to provide numerical correction for the non-uniform spectral sensitivity of the instrument.

Correcting for spectral sensitivity

The silicon target vidicon approaches unity quantum yield across the visible spectrum; that is one electron per photon, or $e/h\nu$ amperes per watt at the silicon target. This factor contributes to spectral non-uniformity of the over-all system, as ν is inversely proportional to photon wavelength. The spectral sensitivity correction procedure consists of obtaining the waveform $A(I)$ of a standard tungsten lamp and comparing the derived spectrum $S(N)$ with the known spectral emissivity $E(N)$ of the standard lamp. The required spectral correction of the instrument is equal to $C(N) = E(N)/S(N)$, which is a 201-element array stored in the disk memory and recalled each time a waveform array $A(I)$ is stored. This correction array operates upon the derived spectral signal $S(N)$ by direct multiplication.

The long-term reproducibility of the instrument is $\pm .002$ CIE chromaticity units (Δx and Δy coordinates). The average x and y values for the standard phosphors

are listed below. Figure 6 shows the CIE x, y diagram with the R, G, B points at the corners of the picture tube triangular color gamut. The horseshoe-shaped curve is the locus of pure spectra from $\lambda = 4000$ to 7000 angstroms.

Phosphor	CIE x	CIE y
Red — $Y_2O_2S:Eu$.651	.345
Green — $ZnCdS:Cu,Al$.357	.596
Blue — $ZnS:Ag$.146	.057

Color picture tube chromaticity and light output

An important application of the rapid scan spectrometer is the measurement of x, y chromaticity coordinates of the r, g, b primary fields in color picture tubes. The individual fields are excited separately beginning with the red, and the spectrometer, with entrance slit aimed at the raster, records the spectrum. The x, y coordinates are automatically calculated, and the process is repeated for the green and blue fields.

The gathering of the three x, y chromaticity pairs in this manner using the RSS is comparable to the three-channel colorimeter method from the viewpoint of the test set operator who in either case performs measurements on the r, g, b fields sequentially. The colorimeter method requires only three photocells, r, g, b color separation filters, and three digital voltmeters. Nine pieces of data are recorded, which are the r, g, b channel readings for each field.

The x, y chromaticities and the luminous excitation, in foot-lamberts, from each field can be calculated from these nine numbers. The r, g, b gun currents required for any specified white point can also be computed.

The six chromaticity numbers obtained using the RSS on the individual fields are alone not sufficient to calculate r, g, b gun currents for a white point. Three additional numbers, bringing the total to nine, are required. Two of these are the x, y chromaticities of a "white" mixture color obtained by turning on the r, g, b guns simultaneously, and measuring the color with the RSS. The component r, g, b gun currents in the mixed raster must be recorded.

The third and final additional datum needed in the RSS method is the luminance of the "white" mixture. This is normally measured with a calibrated photocell.

The r, g, b gun currents required to

produce a standard white color in the tested tube are given by $C(1), C(2),$ and $C(3)$, the components of the column matrix C .

$$C = D^{-1} \cdot W \quad (3)$$

Column matrix W is the X, Y, Z tristimulus values of the standard white color. Y is the flux in lumens, standardized to produce 8 foot-lamberts at full raster:

$$\begin{aligned} W(2) &= Y = 8x \text{ area in sq. ft.} \\ W(1) &= X = x/y \cdot Y \\ W(3) &= Z = (1-x-y)/y \cdot Y \end{aligned} \quad (4)$$

Matrix D is a three-column matrix, containing in each column the X, Y, Z per unit current (microampere) of the corresponding r, g, b field. Red X, Y, Z per μA comprises column 1 of matrix D , green X, Y, Z per μA comprises column 2, and blue column 3. Matrix D is obtained by scaling each column of the field chromaticity matrix E by the corresponding field luminous efficiency:

$$D = E x \begin{pmatrix} Y_r/I_r & 0 & 0 \\ 0 & Y_g/I_g & 0 \\ 0 & 0 & Y_b/I_b \end{pmatrix} \quad (5)$$

Where E , the field chromaticity matrix, is derived from the x, y chromaticities given by the RSS:

$$E = \begin{pmatrix} x_r/y_r & x_g/y_g & x_b/y_b \\ 1 & 1 & 1 \\ z_r/y_r & z_g/y_g & z_b/y_b \end{pmatrix} \quad (6)$$

$$z_i = 1 - x_i - y_i$$

$$\begin{pmatrix} Y_r \\ Y_g \\ Y_b \end{pmatrix} = E^{-1} \cdot Q \quad (7)$$

and I_r, I_g, I_b are the test currents which produced the "white" mixture color Q in the unknown tube. $Q(2)$ is the emitted flux in lumens from the mixture color measured by the photometer.

$$\begin{aligned} Q(1) &= x/y \cdot Q(2) \\ Q(3) &= z/y \cdot Q(2) \end{aligned} \quad (8)$$

where x, y are the chromaticities of the "white" mixture color.

Tube light output, in foot-lamberts per milliamp, is:

$$fL/mA = 10^3 x W(2) / [C(1) + C(2) + C(3)] / \text{AREA}$$

where AREA is the full picture raster area in square feet.

The advantage of the RSS over a three-channel colorimeter in measuring color

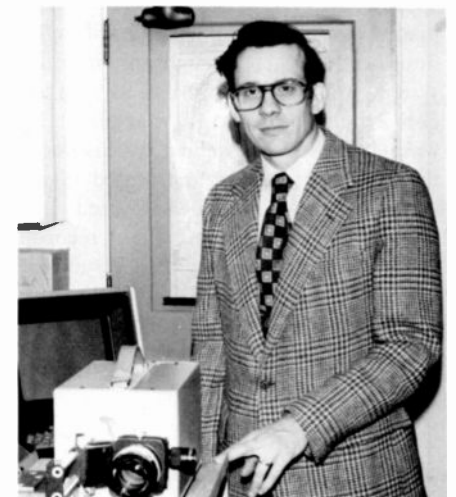
picture tubes is its versatility. The RSS can be used to analyze tubes with various P22 phosphor primaries, while the colorimeter method requires calibration with a known tube having phosphor primaries similar to those in the unknown tube.

Summary

The rapid scan approach to color measurement usually allows automatic computation of color coordinates x and y . Systems with beam-scan readout (Vidicons) can be conveniently calibrated to produce the true spectrum of the source from the stored waveform. This calibration procedure corrects scanning non-linearities as well as non-uniform spectral sensitivities of the photo-detector.

Reference

1. Neuhauser, R.G., "The Silicon Target Vidicon," *RCA Engineer*, p. 40 (Dec 1976/Jan 1977).
2. Ehemann, G.M., Jr., "Three-Filter Colorimetry of Color-Television Picture Tubes," *RCA Review*, Vol. 36, p. 254.



George Ehemann, Jr. joined the Lancaster Chemical and Physical Laboratory in 1964 where he developed colorimetry procedures used kinescope testing. He works in the Spectroradiometry group which tests developmental phosphors.

Contact him at:
Process and Materials Development
Picture Tube Division
Lancaster, Pa.
Ext. 2592

Statistical techniques for evaluation of test results from small groups of data

The science of statistics generally provides for the interpretation of relatively large masses of data. When the sample size is necessarily small, however, here are some straightforward methods of analysis.

Abstract: *Statistical techniques for the determination of significant differences between small 5 to 20 item sample sizes are given. These techniques include both parametric and non-parametric procedures. Their relative advantages are discussed and illustrated.*

Experimenters are often confronted with the problem of determining the significance of data between two seemingly small test runs. Because of the smallness of the samples (about 5-20 per group), it is tempting to check visually, rather than by use of statistical techniques. This may lead to erroneous conclusions because there are so many aspects of the data which may unduly influence the observer. Also, a fairly large difference is required to obtain a meaningful confidence level (90% or greater) and this is difficult to recognize without statistics.

Actually, small sample sizes are easily analyzed statistically by the relatively simple and straightforward methods presented here. Formulas, examples and tables are all included and there is no need for reference to other publications. Perhaps this simple introduction to statistical comparison will lead to additional study and better understanding by the reader.

Statistical techniques

Generally, two statistical approaches may be used — parametric and nonparametric. A parameter is defined as any characteristic object or item of the population which can be measured, such as the mean and the standard deviation. In parametric statistics, estimates of such parameters are compared to determine if any two groups are significantly different. The estimates are obtained from samples which are selected from the population. In this paper, \bar{X} and σ are used to represent the sample mean and standard deviation.

Nonparametric statistics are not involved with the population

or sample characteristics but compare various aspects of the individual values themselves.

Parametric statistics are normally more efficient (same level of confidence, but with a smaller sample size) and actual numbers such as the mean describe and thus better identify the data. However, the tables used for the confidence levels are based on normal distributions and, theoretically, the population should not deviate far from normality. In practice, the distribution of the means closely follows a normal curve if the sample sizes are ≥ 5 , regardless of the distribution of the population (Central Limit Theorem). Therefore, parametric statistics may be used to compare the means for nearly all sets of data.

Nonparametric statistics offer three possible advantages: they can be used with nonquantitative data; they have no requirement for normality of the distribution and are quickly calculated. The latter advantage may not be so important with the advent of the pocket calculator.

Parametric statistics

When comparing two sets of data, there are usually two questions to be answered. Do the two groups have the same standard deviation? Do they have the same mean? The answers will determine just how similar the two sets really are.

Mathematically, these two statistics are defined:

$$\bar{X} \text{ (mean)} = \sum x / n$$

where n is the sample size and x is the individual values; and

$$\sigma \text{ (standard deviation)} = \sqrt{\frac{n(\sum x^2) - (\sum x)^2}{n(n-1)}}$$

They are easily calculated with any one of the small calculators now available.

The first comparison to be made involves the standard deviation squared, called the variance, to determine if the variation is the same for both groups. The smaller variance is divided into the larger and the ratio obtained is called an F value.

Table I. F values. (95% Confidence level).

DF ₁ \ DF ₂	4	6	8	10	12	15	20	50	100	∞
4	6.39	6.16	6.04	5.96	5.91	5.86	5.80	5.70	5.66	5.63
5	5.19	4.96	4.82	4.74	4.68	4.62	4.56	4.44	4.40	4.36
6	4.53	4.28	4.15	4.06	4.00	3.94	3.87	3.75	3.71	3.67
7	4.12	3.87	3.73	3.64	3.57	3.51	3.44	3.32	3.28	3.23
8	3.84	3.58	3.44	3.34	3.28	3.22	3.15	3.03	2.98	2.93
9	3.63	3.37	3.23	3.14	3.07	3.01	2.94	2.80	2.76	2.71
10	3.48	3.22	3.07	2.97	2.91	2.85	2.77	2.64	2.59	2.54
11	3.36	3.09	2.95	2.85	2.79	2.72	2.65	2.50	2.45	2.40
12	3.26	3.00	2.85	2.76	2.69	2.62	2.54	2.40	2.35	2.30
13	3.18	2.92	2.77	2.67	2.60	2.53	2.46	2.32	2.26	2.21
14	3.11	2.85	2.70	2.60	2.53	2.46	2.39	2.24	2.19	2.13
15	3.06	2.79	2.64	2.54	2.48	2.40	2.33	2.18	2.12	2.07
16	3.01	2.74	2.59	2.49	2.42	2.35	2.28	2.13	2.07	2.01
17	2.96	2.70	2.55	2.45	2.38	2.31	2.23	2.08	2.02	1.96
18	2.93	2.66	2.51	2.41	2.34	2.27	2.19	2.04	1.98	1.92
19	2.90	2.63	2.48	2.38	2.31	2.23	2.16	2.00	1.94	1.88
20	2.87	2.60	2.45	2.35	2.28	2.20	2.12	1.96	1.90	1.84
50	2.56	2.29	2.13	2.02	1.95	1.87	1.78	1.60	1.52	1.44
100	2.46	2.19	2.03	1.92	1.85	1.77	1.68	1.48	1.39	1.28
∞	2.37	2.09	1.94	1.83	1.75	1.67	1.57	1.35	1.24	1.00

DF = degrees of freedom (n_1-1 and n_2-1)
 DF₁ = degrees of freedom in denominator (smaller variance)
 DF₂ = degrees of freedom in numerator (larger variance)

This ratio is checked for significance by comparing it with values from Table I. These are referred to as critical values since the calculated value must exceed them to show significance for the given level of confidence.

If there is no significant difference between the variances (the calculated *F* value does not exceed the *F* value from the table), one can proceed to a comparison of the means, which is done by a "t" test. This test compares the actual difference between the two means with the range of mean differences which could be expected to occur normally, based on the pooled standard deviation of the two samples. Pooling is done to use all the data and obtain a better estimate of the standard deviation.

Table II. t values.

Degrees of freedom	Confidence levels			
	80%	90%	95%	99%
1	3.08	6.31	12.71	63.66
2	1.89	2.92	4.30	9.92
3	1.64	2.35	3.18	5.84
4	1.53	2.13	2.78	4.60
5	1.48	2.02	2.57	4.03
6	1.44	1.94	2.45	3.71
7	1.42	1.90	2.36	3.50
8	1.40	1.86	2.31	3.36
9	1.38	1.83	2.26	3.25
10	1.37	1.81	2.23	3.17
12	1.36	1.78	2.18	3.06
15	1.34	1.75	2.13	2.95
20	1.32	1.72	2.09	2.84
50	1.30	1.68	2.01	2.68
100	1.29	1.66	1.99	2.63
∞	1.28	1.64	1.96	2.58

The *t* value is calculated by the following formula, which is not as complex as it looks and can be simplified greatly if $n_1 = n_2$.

$$t = \frac{\bar{X}_1 - \bar{X}_2}{\left\{ \left[\frac{(n_1-1)\sigma_1^2 + (n_2-1)\sigma_2^2}{n_1 + n_2 - 2} \right] \left[\frac{1}{n_1} + \frac{1}{n_2} \right] \right\}^{1/2}}$$

where n_1 and n_2 are the sample sizes; \bar{X}_1 and \bar{X}_2 are the sample means; and σ_1 and σ_2 are the sample standard deviations. These symbols have the same meaning throughout this paper.

The calculated *t* value is compared with those from Table II at the desired level of confidence. If the calculated value exceeds the table (critical) value, the means are considered significantly different at whatever confidence level is chosen.

If the *F* test is significant, showing the samples are from populations with different variances, a correction must be made before proceeding to the *t* test. This is done by reducing the number of degrees of freedom associated with the two groups. Degrees of freedom are defined as the number of independent measurements available to estimate a statistical parameter. For example, if there are six results in a set of data, the degrees of freedom associated with the calculation of the mean is five. The logic is that if the mean and five results are known, the sixth result must be a certain value and cannot vary.

$$\text{Corrected degrees of freedom} = \frac{1}{\frac{C^2}{n_1-1} + \frac{(1-C)^2}{n_2-1}}$$

where

$$C = \frac{\sigma_1^2/n_1}{\frac{\sigma_1^2}{n_1} + \frac{\sigma_2^2}{n_2}}$$

and $\sigma_1 > \sigma_2$

This corrected value for the degrees of freedom is used to find the critical value of *t* from the *t* table with which to compare the calculated *t*.

Example:

Emission is measured on two different groups of cathodes with these results:

Group 1	Group 2
1030 μA	920 μA
1110	1080
1090	980
1060	1070
1090	900
1010	920

$$\bar{X}_1 = 1065.0 \quad \bar{X}_2 = 978.33$$

$$\sigma_1 = 38.86 \quad \sigma_2 = 79.60$$

First, the variances are compared via the *F* test.

$$F = \sigma_2^2/\sigma_1^2 = 79.60^2 / 38.86^2 = 4.20$$

(The highest σ^2 value is put in the numerator.) This value must now be compared with those in Table I. To do so, it is necessary to know the degrees of freedom for both numerator and denominator. These are simply one less than the pieces of data in

each group. The critical value from the table at 95% confidence is 5.07 (interpolated) and, since this is greater than 4.20, the variances are not significantly different at a 95% confidence level.

The *t* test for the means is done next:

$$t = \frac{1065.0 - 978.33}{\left\{ \frac{[(6-1)(38.86)^2 + (6-1)(79.60)^2]}{12-2} \right\}^{1/2} \left[\frac{1}{6} + \frac{1}{6} \right]^{1/2}}$$

$$t = \frac{86.67}{[(3923.1)(1/3)]^{1/2}} = \frac{86.67}{36.16} = 2.40$$

Since the two sets of data are pooled to calculate the standard deviation, the degrees of freedom are 12-2 = 10. The critical *t* values from Table II are 2.23 at 95% and 3.17 at 99%. Since 2.40 is lower than 3.17 and higher than 2.23, the means are significantly different at 95% but not at a 99% confidence level.

To show the effect of an increase in the variation, as expressed by the standard deviation, the first value in Group 2 is decreased by 60 and the second increased by 60.

Example:

Group 1	Group 2
1030 μA	860 μA
1110	1140
1090	980
1060	1070
1090	900
1010	920

$$\bar{X}_1 = 1065.0 \quad \bar{X}_2 = 978.33$$

$$\sigma_1 = 38.86 \quad \sigma_2 = 107.78$$

$$F = \sigma_2^2 / \sigma_1^2 = (107.78)^2 / (38.86)^2 = 7.69$$

This is a significant difference so corrected degrees of freedom must be calculated before the *t* test is used to compare means.

$$C = \frac{(107.78)^2 / 6}{\frac{(107.78)^2}{6} + \frac{(38.86)^2}{6}} = 0.885$$

$$\text{New D.F.} = \frac{1}{\frac{(0.885)^2}{5} + \frac{(1-0.885)^2}{5}} = 6.28$$

A new *t* must also be calculated since one of the standard deviations has changed.

$$t = \frac{1065.0 - 978.33}{\left\{ \frac{[(6-1)(38.86)^2 + (6-1)(107.78)^2]}{12-2} \right\}^{1/2} \left[\frac{1}{6} + \frac{1}{6} \right]^{1/2}}$$

$$= \frac{86.67}{[(6563.3)(1/3)]^{1/2}} = \frac{86.67}{46.77} = 1.85$$

For 6.28 degrees of freedom and 90% confidence, the critical *t* value from Table II is 1.93 (interpolated). Since 1.85 is less than 1.93, the two means are not significantly different at the 90% level.

Nonparametric statistics

Since nonparametric statistics do not include any numbers or values which estimate the population parameters, one must use the individual values themselves in comparing one group of results versus another. There are several methods available.

One technique is ranking, in which the values from both groups are put together and ranked from lowest to highest (or vice versa). The lowest value is given the first rank, or 1, and the highest value is given a rank equal to the total number of items ($n_1 + n_2$).

If the two groups are really not different, the ranking of the items will tend to intermingle the groups and the rank sums of each will be about equal. If the two groups are different, the items from one group will tend toward the lower ranking while the other group will tend towards the higher ranking. Probabilities may be assigned to the occurrence of all ranking combinations by chance alone and the actual results compared with them to determine significance.

Example: After 24 hours of arc counting, two groups of color kinescopes have these results, 6 tubes per group.

Group A	Group B
0 arcs	3 arcs
1	4
1	4
3	10
15	22
17	29

There are 12 tubes so there are 12 ranks.

Rank No.	Arc Count	Group A or B
1	0	A
2	1	A
3	1	A
4	3	A
5	3	B
6	4	B
7	4	B
8	10	B
9	15	A
10	17	A
11	22	B
12	29	B

Tied, Use $(4+5)/2 = 4.5$

Rank Sums

$$A = 1+2+3+4.5+9+10 = 29.5$$

$$B = 4.5+6+7+8+11+12 = 48.5$$

To be significant at the 95% level, the smaller rank sum must be 26 or less (Table III). Since 29.5 > 26, the two groups are not significantly different at 95% confidence.

Paired observations

If the data from the two groups can be paired on some routine basis, two simple comparison tests which may be made are the sign test and the paired replicate rank test.

In the sign test, the data are paired and the number of positive and negative differences counted and compared against the values

Table III. Minimum rank sum value for groups which do not differ at 0.05 and 0.01 significance.

Larger group size, N_2	Smaller group size N_1									
	1	2	3	4	5	6	7	8	9	10
<i>At 0.05 significance</i>										
1	-									
2	-	-								
3	-	-	6							
4	-	-	6	11						
5	-	3	7	12	19					
6	-	3	8	13	20	28				
7	-	3	8	14	21	29	39			
8	-	4	9	15	23	31	41	51		
9	-	4	10	16	24	33	43	54	66	
10	-	4	10	17	26	35	45	56	69	82
<i>At 0.01 significance</i>										
1	-									
2	-	-								
3	-	-	-							
4	-	-	-	-						
5	-	-	-	10	16					
6	-	-	-	11	17	24				
7	-	-	6	11	18	25	34			
8	-	-	6	12	19	27	36	46		
9	-	-	7	13	20	28	37	48	59	
10	-	-	7	13	21	29	39	50	61	74

Table IV. Maximum significant number of less frequent signs in n observations when $P(+)$ = 0.50.

n	90%	95%	99%
8	1	0	0
9	1	1	0
10	1	1	0
12	2	2	1
14	3	2	1
16	4	3	2
18	5	4	3
20	5	5	3
25	7	7	5

Table V. Maximum value of smaller sums of rank of either sign at indicated probability levels for replicates which differ.

n	95%	99%
6	0	0
7	2	0
8	4	0
9	6	2
10	8	3
12	14	7
14	21	13
16	30	20
18	40	28
20	52	38
25	89	68

in Table IV. In the paired replicate rank test, the absolute differences are ranked and the rank sums for the negative and

positive differences are calculated. The smaller of these two sums is compared with the values in Table V.

Example: Emission from the red and blue cathodes from 10 different color picture tubes was read after three weeks of life. It is reasonable to pair the red and blue cathodes from the individual tubes to make the comparison.

<u>Red</u>	<u>Blue</u>	<u>Sign of Red-Blue</u>
1140 μ A	1020 μ A	+
1080	970	+
1090	1010	+
1070	1090	-
980	920	+
1110	1100	+
1070	1010	+
990	980	+
1100	1110	-
1040	1070	-

There are 7 plus and 3 minus signs. Table IV, sample of 10, requires a maximum of one in the less frequent sign group at 90%. Therefore, the two groups are not significantly different at 90% confidence.

In the paired replicate rank test, for the same data, the differences are as shown below:

<u>Red</u>	<u>Blue</u>	<u>Red-Blue</u>	<u>Rank</u> <i>(Absolute Value)</i>
1140 μ A	1020 μ A	120	10
1080	970	110	9
1090	1010	80	8
1070	1090	-20	-4
980	920	60	6.5
1110	1100	10	2
1070	1010	60	6.5
990	980	10	2
1100	1110	-10	-2
1040	1070	-30	-5

The sum of ranks for the positive differences is 44, for the negative differences it is 11. Table V, $n = 10$, 95% level, requires a maximum value of 8 to show significance and so the two groups are not significantly different at 95% confidence.



Frank Hinnenkamp is presently Manager of Reliability, Warranty and Life Test for the Picture Tube Division. His previous experience at RCA includes cathodes, heaters, life test and statistical work in the areas of design of experiments and data analysis.

Contact him at:
Picture Tube Division
Lancaster, Pa.
Ext. 2583

Picture tube x-radiation measurement and control

RCA takes a leadership position in the development of industry standards for the control and measurement of TV picture-tube x-radiation.

Abstract: *X-radiation from television picture tubes has always been controlled by the inherent shielding provided by the absorption characteristics of the special glass from which the picture tube bulbs are made. This absorption has been increased from time to time as operating voltages have increased and as more stringent requirements have been placed upon TV set manufacturers by Federal regulations. To accurately measure the low-level x-radiation from television picture tubes, special test facilities are required. The*

equipment which constitutes the RCA Picture Tube Division's X-Radiation Measurements Laboratory in Marion, Ind. is described along with how the calibrations of the various measuring instruments is traceable to the National Bureau of Standards. The test method used for the measurement of x-radiation from picture tubes is described. How these test data are used to establish the limit x-radiation curves which are the voluntary standards for the industry is also discussed.

The recognition of the need to control x-radiation from cathode-ray tubes because of a possible health hazard can be traced back to the turn of the century when radioactivity and x-radiation were first discovered. Serious injuries, some fatal, from permanent skin burns on the hands of demonstrators and early experimenters with x-ray machines led to the recognition that protective shielding was required.¹ This shielding is provided in television picture tubes by the glass bulb from which it is made.

This paper discusses the television picture tube (cathode ray tube) and its unwanted by-product, x-rays; how attenuation and shielding are achieved to protect the public, and how measurements of x-rays from the tube are made.

X-rays are generated within the picture tube in a manner similar to that of an x-ray tube. Electrons, which gain very high velocity within a high-voltage field, gain kinetic energy which changes to other forms of energy when the electron strikes a target. In a picture tube, light (a desirable quality), heat and x-rays (both undesirable) are the types of energy obtained.

As the voltage increases, the intensity of the x-rays increases and the wavelength of the x-rays decreases and becomes more penetrating.

The intensity of the generated x-rays is also proportional to the atomic number of the element or elements which comprise the target (any material the electron beams strikes). The target in a color TV picture tube includes the phosphor screen, the aperture mask and its frame, and the glass face plate shown in Fig. 1. The amount and distribution of the getter material (barium), which is deposited upon these tube parts, is, therefore, critical because of the relatively high atomic number of barium.

Integral shielding protects the public

X-rays generated within a picture tube are attenuated by the materials used in the glass envelope. The glass is made up of many different materials, each of which has absorbing qualities; the total mass absorption of the glass is the sum of the individual

mass absorptions of each component. Highly absorbing elements, such as lead, barium and strontium, are commonly used today in the glass for TV picture tubes.

The early cathode ray tubes for the most part were relatively low-voltage devices as compared to that of an x-ray tube and, therefore, the x-rays were less penetrating and the potential biological effect, if any, was minimal. The biological effect, if any, received from x-rays from these early cathode ray tubes, would become apparent only in later generations as a result of the damaged genes of the irradiated victim. To date there is no known injuries or evidence of mutations which could be attributed to irradiation from these early cathode ray tubes.^{2,7} In any event, where an x-ray generating device was involved, shielding was required for the protection of the individuals working with the devices. The bulb glass composition and thicknesses of television picture tubes have been modified from time to time to maintain adequate shielding as TV voltages have increased and maximum x-ray limits have been reduced.^{4,5}

Maximum permissible x-radiation limits

Researchers have learned much about the biological damages that could occur from different levels of radiation, particularly, since the arrival of the atomic age during World War II. It was obvious that dose-rate limits of radiation to the body were needed. Two groups recommended that limits of exposure for industrial workers be

Reprint RE-25-2-10

Final manuscript received Aug. 14, 1979.

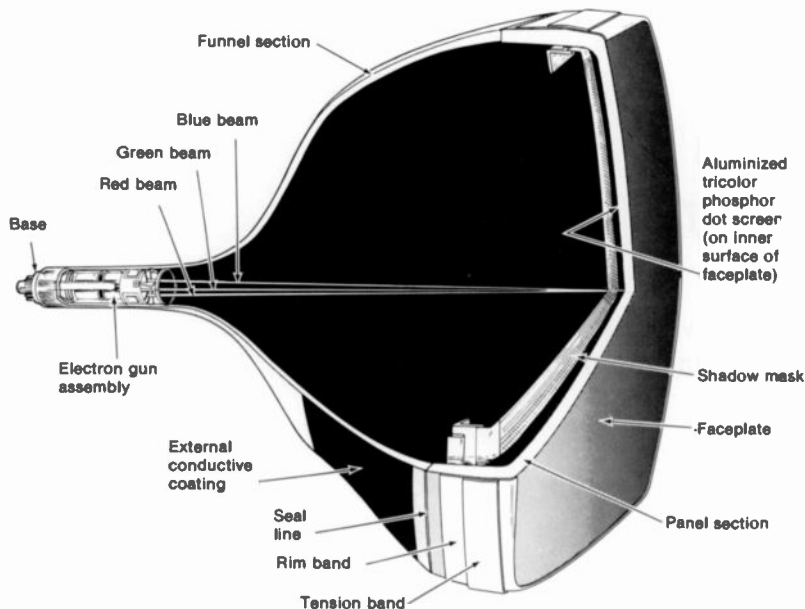


Fig. 1. Cross-sectional view of color tube showing targets.

established — The International Commission on Radiological Protection (ICRP) and the National Council on Radiation Protection (NCRP). These groups recommended that the maximum permissible exposure-rate for radiation workers be 6.25 milliroentgens per hour (mR/h).

With the advent of the commercial television boom, beginning in the late 1940s, scientists, and television and tube designers were concerned and aware of the hazards of x-rays especially when the picture tube operation exceeded 16 kilovolts. Labels warning of the x-radiation hazards when the anode voltage exceeded 16 kilovolts were placed on all commercial tubes. The tubes presented no problem in meeting the industrial limit of 6.25 mR/h.

Since the industrial standard was directed toward protecting the industrial and medical workers and these were few in numbers as compared to the total population, genetic factors were not the main consideration. With the arrival of television, a larger proportion of the population would have access to a device that was capable of generating x-rays. This eventuality brought about the realization that genetic effects must be taken into consideration. In 1957, both the ICRP and NCRP recommended that the industrial limit be changed to 2.5 mR/h, and were considering a limit of 0.5 mR/h measured at 5 cm from the surface of television receivers under normal operating conditions.

The television industry made design changes particularly in the glass composition of the bulbs to accommodate the new

limits under consideration. A chronological listing of glass design changes was highlighted in a report given by Dr. John L. Sheldon in 1970.⁵

Studies were undertaken in the late 1940s and '50s by an x-ray task force formed by the Joint Electron Tube Engineering Council (JETEC)* with regard to x-ray emission from electron tubes. The studies and measurements indicated that the picture tube complied with recommended standards of the day. In the late 1960s, more public and political concern was generated within the nation. Consequently, the 1968 Congress passed a law which resulted in the establishment of Federal Performance Standards for Television Receivers.⁶ Cathode-ray tubes also became a controlled product under government surveillance but no performance standards were established.

The JEDEC* X-Radiation Task Force took upon itself to develop its own voluntary x-radiation standards for television picture tubes. Out of these efforts evolved JEDEC Publication 64D, which provided a recommended test procedure for the measurement of x-radiation from TV picture tubes with the precision needed for limits at low levels.⁷ This very important

* Joint Electron Tube Engineering Council (JETEC) is a group within the Electronic Industries Association (EIA). This later became Joint Electron Devices Engineering Council (JEDEC). The X-Radiation Task Force was a working group within JT-6, the committee on cathode-ray tubes under JETEC or JEDEC. The tube group within JEDEC recently was separated to become the Tube Engineering Panel Advisory Council (TEPAC). The X-Radiation Task Force was expanded to be a committee under TEPAC covering all aspects of electron tube safety. This committee is JT-32.

document provided the technique by which the television picture tube industry could measure x-ray emission from picture tubes in a standard fashion and resulted in the development of industry x-radiation limit curves and 0.5 mR/h isoexposure-rate limit curves for all existing picture tube types.

The voluntary standards for TV picture tubes and how they were derived were then published by the task force as JEDEC Publication 94. Although these standards were initially developed for tubes manufactured utilizing domestic glass bulb parts, the information paved the way for off-shore picture tube manufacturers to measure and publish x-ray characteristics in the same manner. This publication also described the method used to establish values for the x-ray absorption characteristics of glass used for TV picture tubes. This enables off-shore manufacturers to describe their glass characteristics in a similar manner assuring compliance with the voluntary U.S. standards.⁸

X-Radiation Measurements Laboratory

RCA, taking a leadership position in developing these voluntary industry standards, established the X-Radiation Measurements Laboratory at the Marion, Ind. picture tube plant. Its goal was to achieve a measurement capability having an accuracy second to none. The criteria being developed were much beyond that previously used for the testing of picture tubes for other characteristics.

Very accurate equipment, instruments and reading techniques are required to obtain reliable x-ray measurements. Up-to-date calibration of equipment, meters, and survey meters are required. Measurement techniques to provide accurate measurements are very time-consuming and are not adaptable for mass production testing. Extreme patience is required of the technician to thoroughly survey and measure a complete tube.

Instrumentation and equipment used

X-radiation transmitted through the bulb of a picture tube is proportional to approximately the twentieth power of the anode voltage. Consequently, for accuracy, the high-voltage supply must be very stable and have essentially no ripple.

The accuracy of voltage measurement and control must be commensurate with this requirement. To accomplish this, not one but two Spellman 0-40k Vdc, 3 mA power supplies in parallel supply the high voltage to the tube. The required accuracy of high voltage measurements is achieved by utilizing a high voltage divider rated for 100 kV. (The high voltage divider is an Electrical Instrument Service, Inc., Model PHVD resistive type divider. Unique features of the divider are the one hundred one-megohm resistors individually shielded and arranged in a vertical helix, selected and matched to provide cancellation of individual negative and positive temperature coefficients; and a specially designed large "hat" or high voltage electrode to prevent corona formation at the high potential end of the resistor and to provide uniform gradients to ground.) The voltage measurement is made by utilizing the 1-volt tap and applying this voltage to a digital voltmeter. The anode current measurement is accomplished utilizing a digital voltmeter modified to read anode current. This equipment can supply a stable anode condition of 40k V at 3 mA, which is required for measuring x-rays from a face of a 25-inch tube such as the 25VEHP22.

Another important and vital piece of equipment is a prototype Ball Engineering Co. Scanning Generator. This unit can be adapted by board changes to overscan at 40kV any tube size, either color or black and white. Scanning can be obtained for any deflection angle from 70 degrees to 114 degrees with any of the various deflection yokes which RCA or its customers may utilize and with good linearity.

The low voltage supplies and controls for the electron gun are not as critical and were obtained from an obsolete factory color picture tube test set. Switching circuits and video amplifiers were similarly obtained.

A unique fixture was constructed of aluminum which holds the picture tube either in the normal horizontal position or in a face down position (the screen then being observed in a mirror). This makes the tube surface totally accessible for search and measurement of x-radiation. This fixture also supports the x-ray measuring instrument (Victoreen 440RF/C survey meter) in any horizontal plane and adjustable in distance from the tube. The meter can be rotated about the tube at a fixed axial distance. The meter is kept horizontal at all times to avoid needle drag, which could result in unreliable readings.

The high voltage divider was calibrated

by the manufacturer and a certificate of calibration by the National Bureau of Standards has been provided. Periodic checks of the high voltage measuring device is made using a Ross Engineering high voltage divider and a Hewlett Packard DC Standard/Differential Voltmeter. A certificate of calibration by the National Bureau of Standards is provided for the Ross Engineering divider. The calibration of the various current and volt meters are also made using the Ross Engineering divider and the Hewlett Packard Differential Voltmeter.

The Victoreen 440RF/C survey meter is periodically calibrated by the manufacturer and a certificate of calibration furnished. For calibrating instruments, Victoreen uses an x-ray machine. For comparison with the National Bureau of Standards they have ion chamber transfer standards. A radiation check source within the instrument can supply a day-by-day check of the instrument's calibration.

Picture tube x-radiation testing

A color tube normally consists of three different glasses in its fabrication. These include the panel on which the phosphor screen is placed, the funnel, and the neck. Each of these utilize a different type of glass, of different composition and different x-ray absorption qualities. All three of these glass components are taken into consideration in the picture tube testing.

JEDEC Publication 64D gives the measurements of a hypothetical cabinet from which testing is done.

Picture tube anode contact shielding

In a television receiver, the anode contact must have a connector that will provide adequate attenuation to reduce the x-radiation level so that the 0.5 mR/h limit is not exceeded. JEDEC Publication 94 gives a very clear procedure for determining the minimum anode connector attenuation required from the registered x-ray curves for each tube type. JEDEC Publication 64D gives a procedure whereby television receiver designers can determine the attenuation factors of the connectors being considered for their designs.

Determination of x-radiation limit curves

Since accurate x-radiation measurements require a laboratory test and only limited numbers can be measured within a specified time period, analysis of the data against the design criteria of the glass becomes all important. Earlier in the report the glass absorption qualities were discussed. Design limits are established for glass thickness, and for the linear absorption coefficient for each glass component of the tubes. The glass vendors, after chemical analysis of the glass for composition, calculate the linear absorption coefficient. The result obtained for each glass melting tank is supplied to RCA each week. The panel and funnel glass parts are vendor and date coded. It is, therefore, possible to know with accuracy the linear absorption coefficients for the glass of any finished tube.

Glass thickness is measured on finished tubes utilizing an ultrasonic gauge which provides an accurate nondestructive method. These measurements are usually limited to those areas where the x-radiation is most intense. Knowing both the linear absorption coefficient and the thickness of the glass in the tube which has been measured for x-radiation makes it possible to correct the x-ray data to represent a tube containing glass of minimum limit absorption and thickness. Thus, by measuring a few tubes randomly selected, the x-radiation expected from the worst-case tube is known.

The worst-case data is utilized by the industry in establishing the x-radiation limit curves which comprise the voluntary standard. A moderate safety factor of about 1 kV is added to the worst-case data to allow for future modifications which might be made in tube design, materials or processes. A safety factor of at least 1 kV is also used in establishing the limit curves for x-radiation through the anode contact. This is to allow for any cleaning process which might be used by the tube manufacturer in salvage operations or by a tube rebuilder which might erode away some of the nominally 0.012-in thick, basically iron, anode contact.

The test facility at the Marion X-Radiation Measurements Laboratory has been demonstrated to the Bureau of Radiological Health (part of the U.S. Food and Drug Administration) and to the picture tube industry. In the interest of standardization, RCA has released detailed drawings of the special fixture for holding the picture tube and survey meter.

How RCA sets the pace in x-radiation measurement

The procedure at RCA for the measurements of picture tubes is to search, measure and record the radiation from the (1) tube neck, (2)

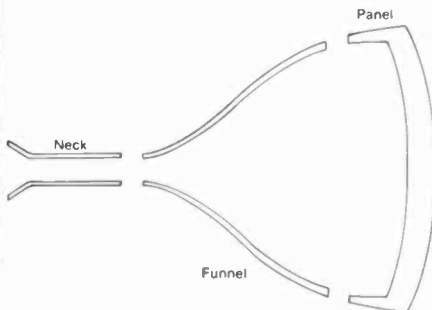


Fig. 2. Component parts of a picture tube showing glass parts.

tube face, (3) panel skirt (the side-wall of the panel), (4) the funnel and (5) bare anode contact. These are shown in Fig. 2. The neck measurement is made with the tube in a face down position. This allows the measuring instrument to be rotated freely about the tube. Figure 3a shows the set-up as well as the shielding of the other tube parts so that radiation from these parts will not add to the neck readings. The operating conditions for making neck x-ray measurements are based upon the published or anticipated maximum rating for the difference between anode and focus voltages. X-radiation emanating through the tube

neck is not the result of the main electron beam but results from stray electrons between the electron gun elements or between the electron gun and the glass wall of the neck. Measurable x-radiation is rarely found.

The tube is next prepared for face measurements. The tube is placed in a normal horizontal position (Fig. 3b) and operating conditions are adjusted to the desired value. The raster is adjusted to be overscanned both horizontally and vertically by 10 percent. When the anode voltage is the same as the published registration reference point, an anode current of 0.3 mA represents a point on the 0.5

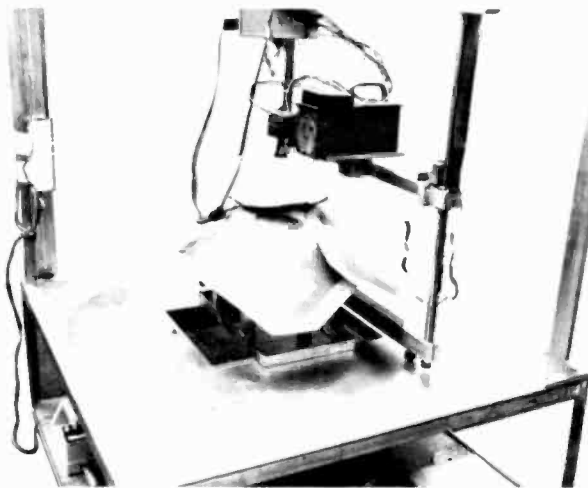


Fig. 3a. Neck radiation measurements.

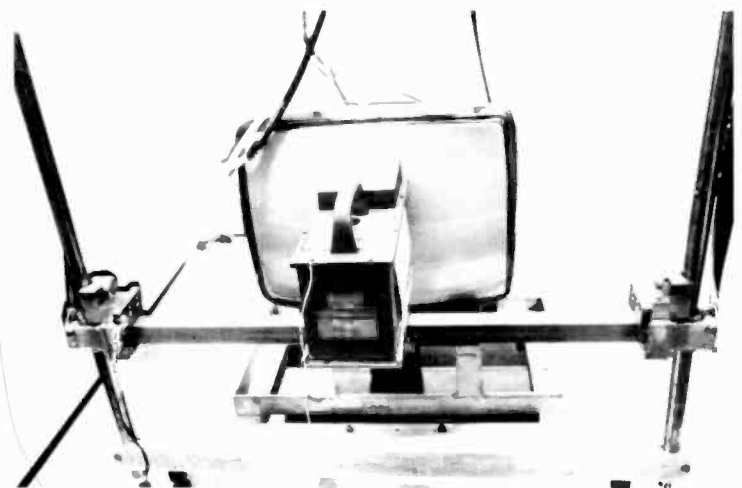


Fig. 3b. Face plate radiation measurement.

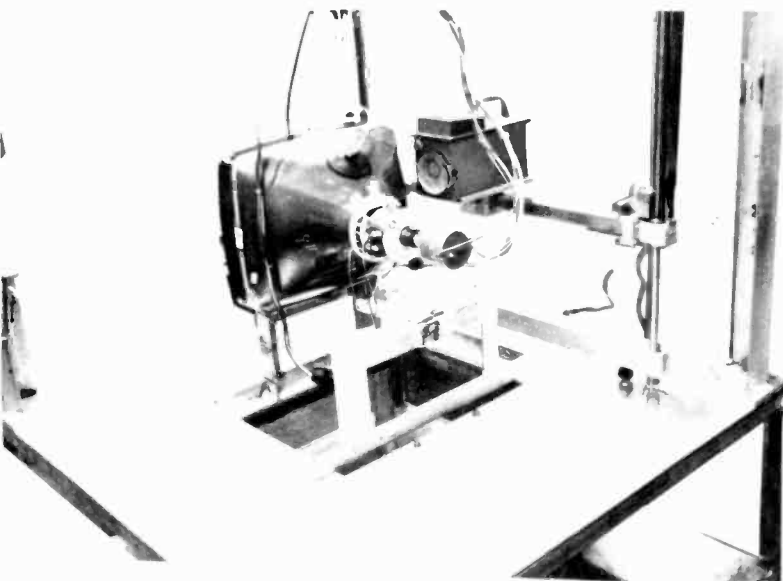


Fig. 3c. Funnel radiation measurement.

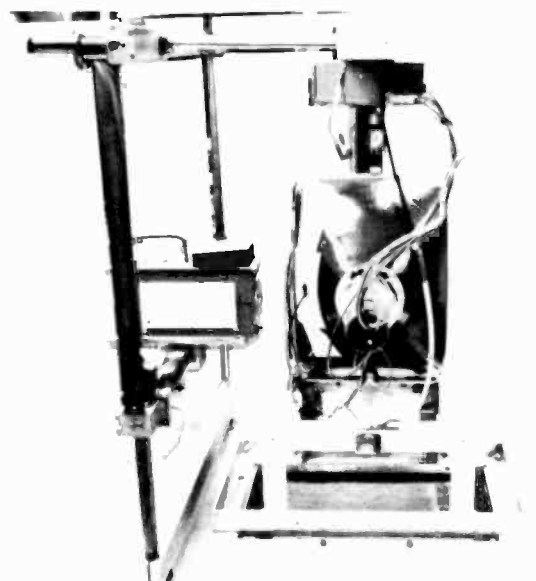


Fig. 3d. Anode contact radiation measurement.

mR/h isoexposure-rate limit curve. By setting the current at 0.3 mA, a direct comparison of the measured value can be made with the 0.5 mR/h limit value. At RCA, in actual practice, the current is increased to a much higher level to take advantage of a more accurate scale of the Victoreen 440RF/C survey meter and to obtain readings significantly larger than natural background radiation. Normally the current is increased to 3 mA for most of these measurements. The measured values are then corrected based on the linear function of x-radiation with respect to current to a value equivalent to 0.3 mA. The corrected values can then be compared to a point on the 0.5 mR/h isoexposure-rate limit curve.

While the tube is set up for face measurement, the face, the panel skirt, and funnel are searched over the entire tube surface with the Texas Nuclear 2650 search meter for the highest meter indication for each of the parts to be tested. The "hot spot" locations are marked. The Victoreen 440RF/C survey meter is placed directly against the face at the "hot spot" and the measurement recorded.

Measurement of the panel skirt and funnel requires the survey meter to be placed in a position against the hypothetical television cabinet. The location of the panel skirt and funnel hot spots will determine the plane or planes against which the survey meter will be placed. The meter is then moved both vertically and horizontally along the plane until the maximum meter reading is found. The maximum reading is recorded and corrected as described previously. A typical location is shown in Fig. 3c.

Occasionally, the panel skirt and/or funnel hot spots may be found on the top or the bottom portion of the tube. To avoid the necessity of tilting the survey meter, the tube is turned 90 degrees so that the normal width of the tube is now in a vertical position. In this position, the meter can be adjusted as described in the previous paragraph for the maximum reading.

The final measurement made on a picture tube is the x-radiation that comes through the bare anode contact. Depending upon the location of

the anode contact, the tube is turned to a position so that the survey meter can pick up the anode contact radiation without being tilted. An x-radiation absorbing shield having a 2.5 cm diameter aperture is placed against the tube with the aperture centered over the anode contact to eliminate x-rays from the funnel from being picked up during the anode contact reading. This is shown in Fig. 3d. X-ray emission coming through the unshielded anode contact is considerably higher than from any other part of the tube. RCA, for this measurement, normally uses an anode current level of 0.6 mA. The x-radiation of the tube face, panel skirt and funnel are judged against the registration reference point on the appropriate 0.5 mR/h isoexposure-rate limit curve. All survey meter readings must be corrected by subtracting any background readings of the meter. The background reading (which includes meter circuitry leakages) is taken with the survey meter in its measuring position but with no voltages applied to the tube. The calibration factor supplied by the manufacturer is applied to the resultant value. The x-radiation from the bare anode contact is judged against its design limit x-radiation curve which is usually greater than 0.5 mR/h. Examples of the x-radiation measurement of the various tube components are shown Table I.

Table I. X-radiation measurements of the tube components of tube type 19VHYP22.

Note: All x-radiation measurements have been adjusted for meter calibration, background reading and to a value that would be equivalent to a 0.3 mA beam current x-radiation level.

<i>Tube portion measured</i>	<i>Anode voltage (KV)</i>	<i>X-radiation (mR/h)</i>
Face	37	0.12
Skirt	35.5	0.10
Funnel	35.5	0.06
Anode contact	35.5	0.55
Neck	*	0.00

* Neck Measurements are made with a potential difference of 32 kV between anode and the focus electrode. Beam current is set at 1.5 mA.

B.Z. Littlefield joined the Cathode Ray Tube Lab as a Design Engineer in 1951 at RCA Lancaster. In 1954, he was transferred along with the Black and White Picture Tube Engineering organization to Marion, Ind. His involvement in x-radiation measurements of picture tubes began in 1967 with the responsibility of developing measurement techniques and establishing picture tube x-radiation specification for black and white picture tubes. He later assumed the same responsibility for color picture tubes. He developed and improved the x-radiation testing facilities at the Marion laboratory which has gained the recognition of the industry and the Bureau of Radiological Health. He presently has the responsibility for the product control of x-radiation for all of the RCA picture tube plants.



Contact him at:
X-Radiation Measurements Laboratory
Marion, Ind.
Ext. 5579

References

- "Atomic Radiation." Prepared by RCA Service Company, Inc. Reprinted by permission of Wright Air Development Center (1957).
- Mills, W.A., Wolff, A.H., and Shore, M.L., "Biological Considerations in Measuring and Evaluating X-Ray Exposures from Color Television Receivers." NCRH, presented at the Conference on Detection and Measurement of X-radiation from Color Television Receivers, Washington, D.C. (Mar 28-29, 1968).
- Moseley, R.D., Jr., M.D., "Biological Considerations: Radiation from Color Television Receivers." The University of Chicago, Chicago, Ill., presented at the Conference on Detection and Measurement of X-radiation from Color Television Receivers, Washington, D.C. (Mar 28-29, 1968).
- Braestrup, C.B., and Mooney, R.T., "X-ray Emission from Television Sets." *Science*, Vol. 130 (Oct 23, 1959).
- Sheldon, J.L., Phd., "Progress in the Development of X-ray Absorbing Glasses for Television Picture Tubes," Corning Glass Works, presented at the International Symposium on Radiological Protection Problems Associated with Parasitic X-ray Emission from Electronic Products, Toulouse, 3-6 XI (1970).
- Public Law 90-602, Radiation Control for Health and Safety Act of 1968.
- JEDEC Publication 64, September, 1967, and 64A, September, 1970, entitled, "Recommended Practice for Measurement of X-radiation from Display Cathode Ray Tubes," Publications 64B, August, 1972, 64C, August 1973, and 64D, November 1974, had the title changed to "Recommended Practice for Measurement of X-radiation from Direct-View Television Picture Tubes.
- JEDEC Publication 94, June 1975, "Considerations Used in Establishing the X-radiation Ratings of Monochrome and Color Picture Tubes;" JEDEC Publication 94-1, November 1977, is a supplement to Publication 94. TEPAC Publication 94-2, another supplement is due for publication late in 1979.

A cure for FM modulation overshoot

The DOC processor uses the time-proven technique of peak clipping to solve the problem of overmodulation in FM broadcasting.

Abstract: *The use of input low-pass filters (LPFs) in FM broadcasting produces two overmodulation effects: peak overshoot caused by transposition of the harmonics (the Gibb's phenomenon) and nonlinear phase shift. RCA's digital overshoot compensation processor uses bilevel clipping to eliminate overshoot caused by the Gibb's phenomenon and a 7-pole elliptic function LPF with known phase characteristics to correct for non-linear phase response. The problem of dc restoration, which is encountered in clipping-type controllers, is resolved using predictive peak restorations.*

FM stations have, in the past, taken pride in their unprocessed audio. High-quality full dynamic programming was the rule, and the extremely low noise generated within the system made audio limiting or processing unnecessary. When limiters were used, they were for preventing sudden overmodulation by loud passages in the music or for reducing the burden of continuously "riding gain" at the broadcast studio.

As interest by the general public in high fidelity increased, FM became more popular. Stations changed their formatted programming to sharpen this interest with diversified music other than concert type, which had been their stock-in-trade. In addressing their market, country-western, hard and soft rock, and other upbeat musical formats crept into FM programming. FM stations were now competing

directly with AM stations for a larger share of the audience both at home and in the commuter's automobile.

Loudness considerations

In spite of the differences in system considerations, many FM stations adopted an "AM syndrome" with respect to the need for maximum loudness. The need for loudness in FM, however, does not arise from the same consideration as loudness in an AM operation. If the RF signal input to the FM receiver is strong enough to saturate the noise limiting circuitry, FM is a "noise-free" service, and loudness is

largely a matter of the volume control setting on the receiver. In AM, clarity depends on the signal strength and a average level of modulation to override both natural and man-made noise.

There is another difference between AM and FM signal processing. An AM processed signal need only be acoustically dense and amplitude limited to the modulation capability of the transmitter (within FCC regulations) in order to provide the maximum loudness. An FM broadcaster, on the other hand, must deal with modulation that is not only amplitude sensitive but frequency dependent as well. The standard 75- μ sec pre-emphasis presents a frequency-dependent limit im-

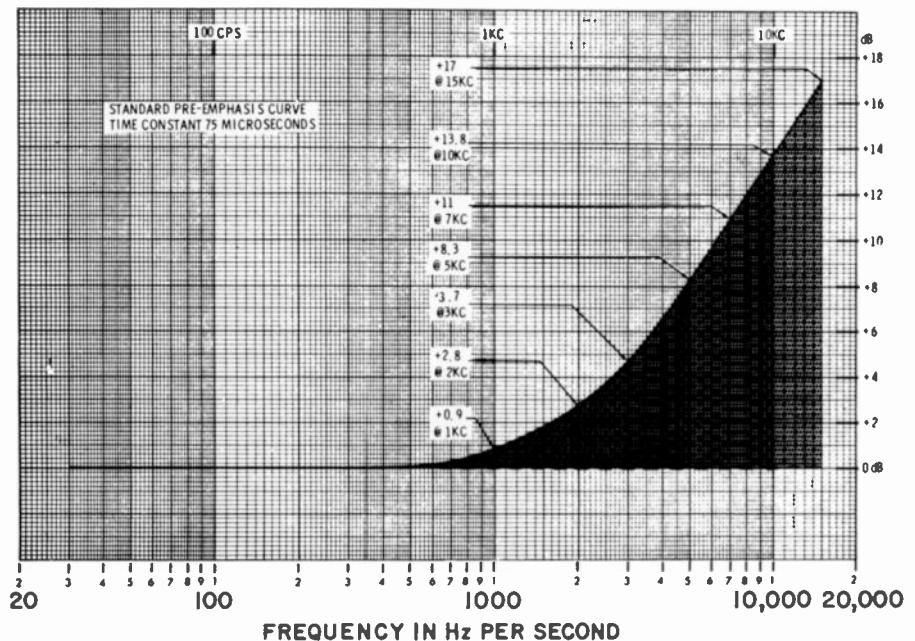


Fig. 1. The standard 75- μ sec pre-emphasis presents a frequency-dependent limit in FM broadcasting.

Reprint RE-25-2-11
Final manuscript received June 14, 1979.

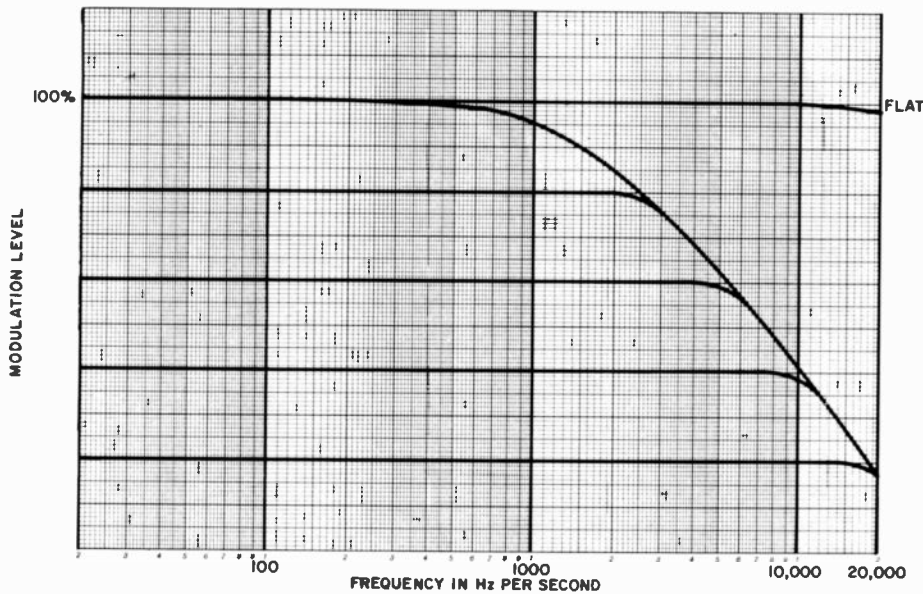


Fig. 2. One approach to eliminating overmodulation is the selective attenuation of the high-frequency program content based upon the amount of energy present.

posed by the severe high-frequency boost given the audio signal. Figure 1 illustrates the pre-emphasized amplitude boost of 17 dB at 15 kHz. If the distribution of the audio spectrum produced equal energy on a per-octave basis, the resultant overmodulation to even a tightly amplitude-controlled signal would result in modulation levels of up to 700 percent. Apparently, a different audio processor is needed for FM.

The age of the FM limiter

Every combination and permutation of limiting before pre-emphasis and after pre-emphasis, including clipping, clipping and filtering, single-band variable frequency roll-offs, double-band, triple-band, etc., has been heralded as the solution to FM modulation without overmodulation. Two basic approaches were finally adopted to eliminate the overmodulation caused by the 75- μ sec pre-emphasis. One approach was the selective attenuation of the high-frequency program content based upon the amount of energy present in these higher frequencies. In other words, the bandwidth of the audio was dynamically rolled off in direct proportion to the high-frequency signal level (see Fig. 2). For low-level signals, the audio bandwidth was essentially flat. As the high-frequency energy content increased, high-frequency roll-off began until, at levels corresponding to 100 percent modulation, the frequency response was the inverse of the 75- μ sec pre-

emphasis curve. This was an effective way to control overmodulation, but at the detriment of response quality.

The second approach that met with greater acceptance from a viewpoint of signal fidelity was peak clipping. Implementing this concept required only pre-emphasizing the audio and hard clipping of all peaks at 100 percent modulation. Harmonic distortion generated by this process was attenuated by the subsequent de-emphasis in the receiver. Based on subjective listening tests in 1970, RCA

determined that a full-response limiter with clipping of the high frequencies along the FM pre-emphasis curve to prevent overmodulation gave the most pleasing sound. RCA audio processors followed these findings, resulting in audio quality being maintained with full response. For years, this method of processing was preferred by many FM broadcasters because of its basically "cleaner, brighter sound," and simplicity.

Peak clippers became companions to fast peak limiters and the heavy dense sound sought after by the broadcaster was now thought to be available in FM. However, strange discrepancies began to appear. Peak flashers would suddenly bloom for no apparent reason at unexpected times. System problems were most often blamed for these overmodulations with explanations that "clipping diodes had a soft knee;" "the pre-emphasis curves don't match the one in the exciter;" or "I don't know what it is but let's back off a dB or two on modulation." In most cases, the last explanation satisfied the condition.

The real problem redefined

Basically, all stereo generators are designed to use input low-pass filters (LPF) in the audio path to do the following:

- Prevent interference with the 19-kHz pilot
- Limit aliasing distortion caused by the

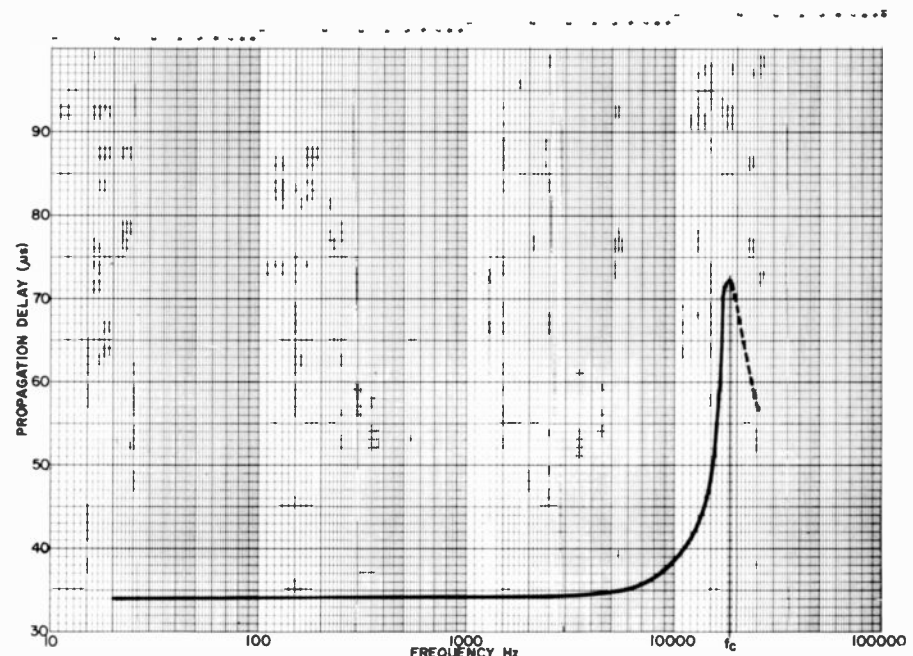


Fig. 3. The increase of the propagation-delay of signals through a filter at higher frequencies contributes to the problem of FM overmodulation.

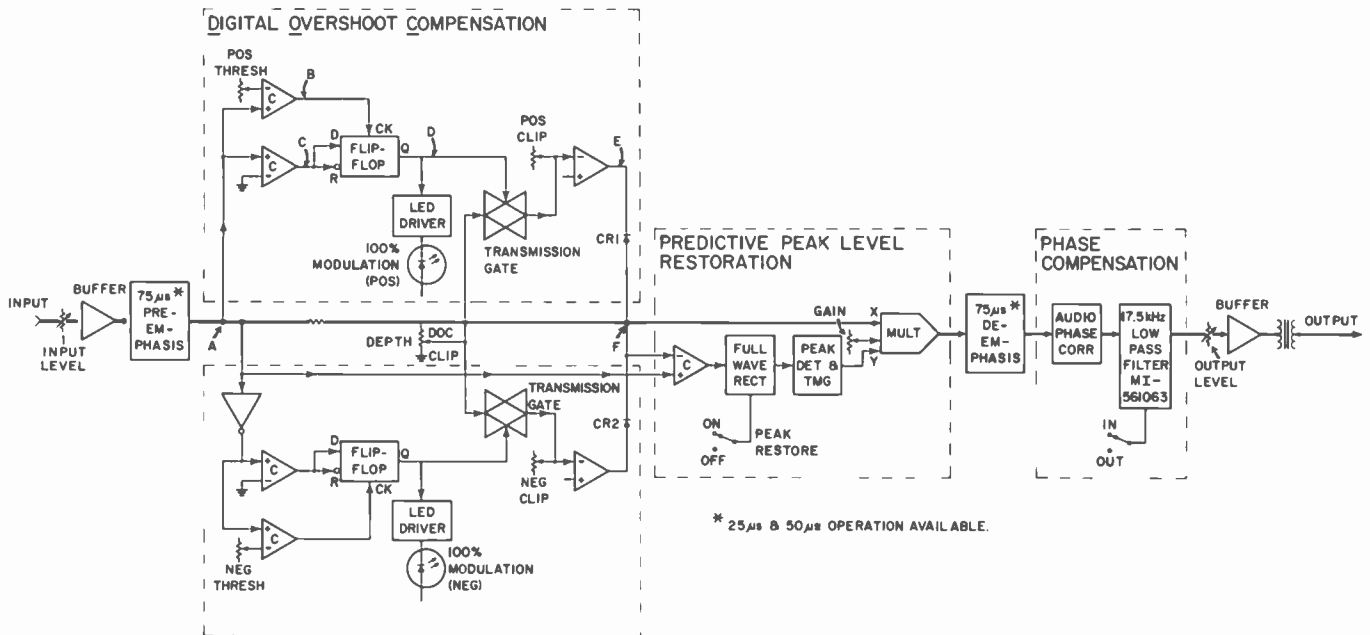


Fig. 4. The digital overshoot compensation processor addresses both the Gibbs and phase-shift problems.

high-frequency $L + R$ channel leaking into the upper or lower $L - R$ subchannel

- Minimize spurious emission
- Reduce cross-talk in the stereo and SCA subcarriers.

To accomplish these tasks, while maintaining a flat audio bandwidth to 15 kHz, rather sophisticated filters are employed. Some filters utilize transition rates in the area of 100 dB/octave or more and are typically 45 dB down at 19 kHz.

These filters produce two overmodulation effects: the Gibb's phenomenon and nonlinear phase shift.

The Gibb's phenomenon: Consider the low-pass filter to have an extremely fast cutoff rate (as required to prevent 15-kHz audio from interfering with a stereo pilot at 19 kHz). A square-wave excitation of the filter will produce output components only within the audio passband of the filter.

Fourier expansion of a square-wave excitation is shown in equation (1):

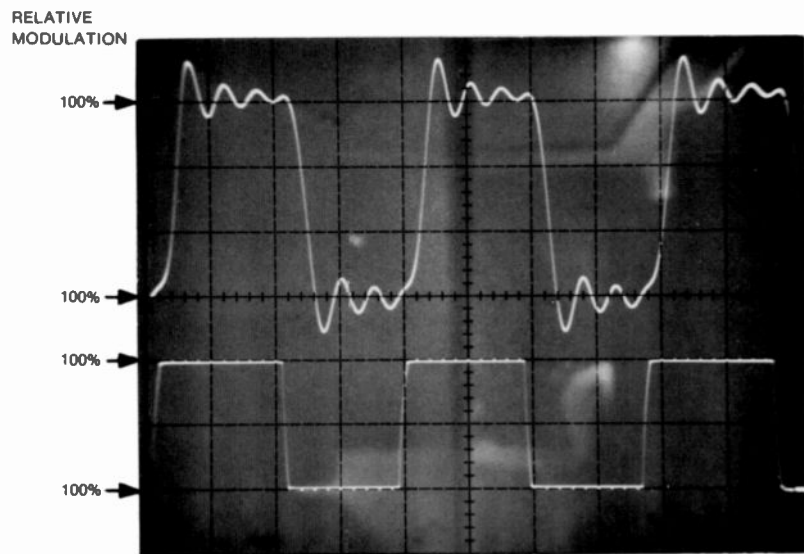
$$V(t) = A \frac{4}{\pi} \sum_{n=1,3,5,\dots}^{\infty} \frac{1}{n} \sin(2\pi fnt) \quad (1)$$

with f being the fundamental square-wave frequency. For example, if f is 10 kHz and the filter cutoff is 15 kHz, only the fundamental of the excitation will be recovered. Thus, the peak amplitude of the output will be $[A(4/\pi)]$. The result is that a square wave with a 1-V peak amplitude going into the LPF will emerge from the filter with only the fundamental at a peak

amplitude of $4/\pi$ or 1.273 V peak and a peak overshoot of 27 percent. This effect caused by the truncation of the harmonics in the LPF is commonly referred to as the Gibb's phenomenon.

Nonlinear phase shift: The propagation time of signals through a filter varies with the signal frequency. This fact, although not often recognized as a source of filter overshoot, contributes greatly to the overall problem of FM overmodulation. Figure 3 illustrates the propagation delay

of a typical elliptic function low-pass filter. Low frequencies exhibit minimum delay through the filter, while at higher frequencies, the delay increases with a maximum occurring at the cutoff frequency. It can readily be appreciated that an audio signal, consisting of many frequencies (the amplitudes of which are not time coincident), upon entering the filter may become coincident at the filter's output. This process of random amplitude addition is a major cause of filter overshoot.



UPPER TRACE -LOW PASS FILTER RESPONSE
LOWER TRACE -SQUARE WAVE INPUT TO LOW PASS FILTER

Fig. 5. Conventional low-pass filter response to square-wave input may be the result of the input LPF and a series of distributed LP filters within the FM exciter with a different cutoff frequency.

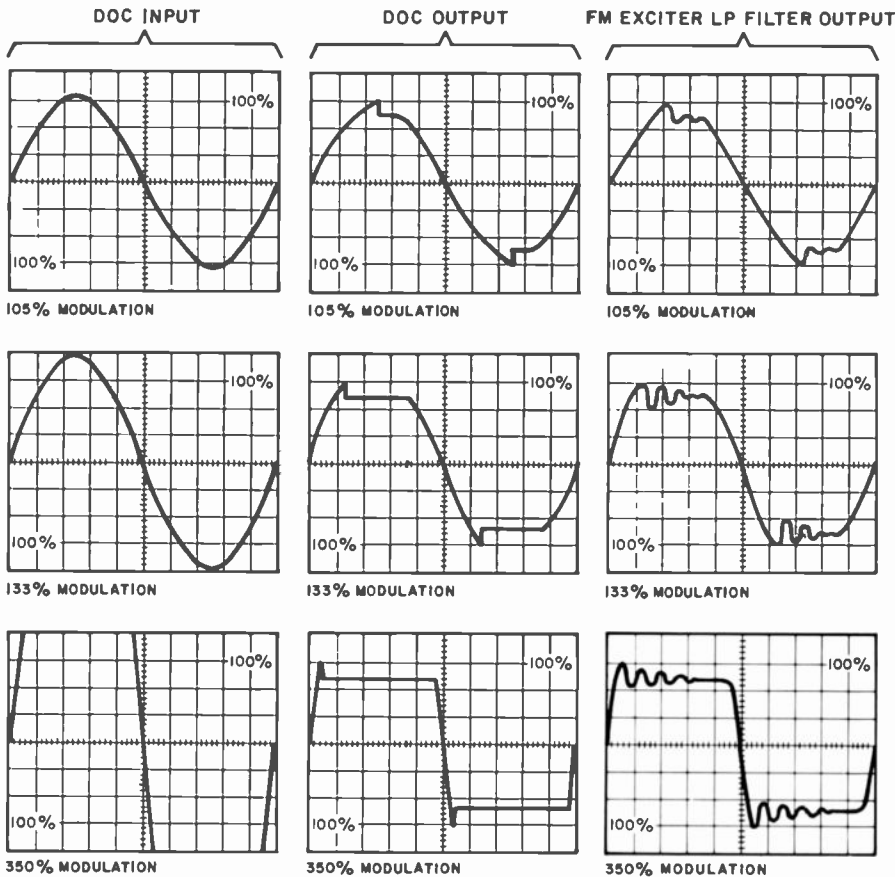


Fig. 6. The bilevel clipping action of the DOC constrains ringing amplitude to 100 percent modulation.

The solution — digital overshoot compensation

In an effort to deal realistically with FM overshoot, both the Gibb's and phase-shift problems must be corrected. Each of these problems is addressed by the digital overshoot (DOC) processor, which consists of the following (see Fig. 4):

- Pre-emphasis
- Digital overshoot compensator
- Predictive peak level restorer
- De-emphasis
- Phase compensator low-pass filter
- Output amplifier

The limitation of the audio bandwidth created by the LPF and the problems created by this limitation are discussed below.

It must be recognized that amplitude overshoot does not occur only in the input audio low-pass filter circuit, but rather as an anomaly that is distributed throughout the FM exciter system. A universal solution to the problem requires that the cure

be made external to the FM exciter and stereo generator. This should interest any cost-conscious FM station manager since it does not involve scrapping a currently working and reliable exciter and stereo generator for one that is unproven or of questionable operation because it reduces the occurrences of peak overmodulation.

Figure 5 illustrates the ringing output of a conventional 15-kHz LPF with a 3-kHz square-wave excitation. In an FM exciter, this response may be the result of the input LPF and a series of distributed LP filters within the exciter each with a different cutoff frequency (as is the case of band-limited operational amplifiers). If this is the case, it is then necessary to modify the type of processing circuitry that produces these square-top audio waveforms (i.e., the peak clipper) to one that retains the beneficial nature of peak clipping (i.e., clean audio with full frequency response) while not producing overshoot above 100 percent modulation. Also, the processor must not affect the signal with modulation levels of less than 100 percent. A further requirement is that the device must be able to operate with any signal conditioning ahead of it (AGC, peak limiting, etc.) and any

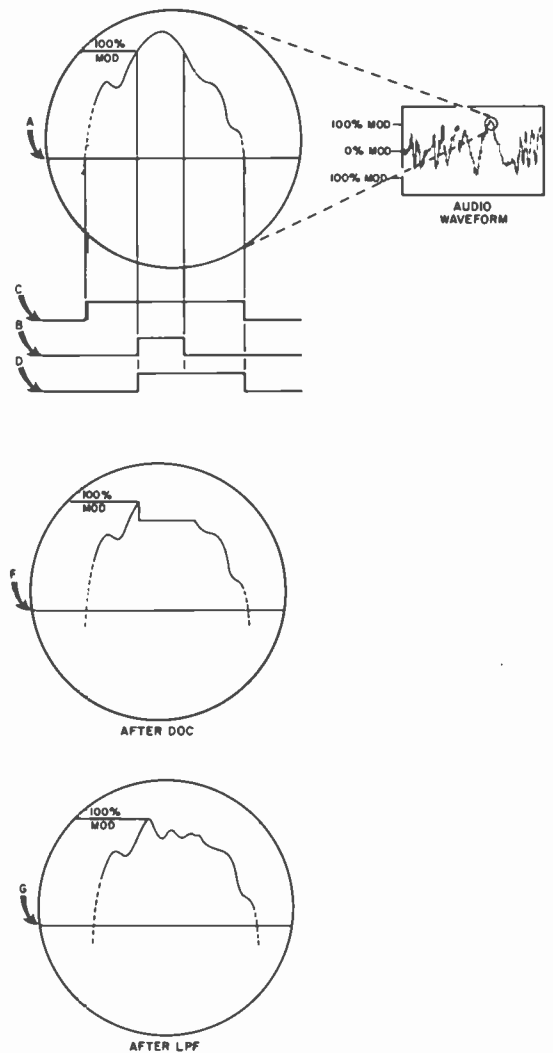


Fig. 7. DOC processor audio peak.

type of FM exciter system behind it. The RCA DOC processor is such a device.

As illustrated in Fig. 6, the shaped peaks generated by the DOC will produce a low-pass filter response that exhibits ringing (due to the loss of harmonics in the LPF). However, the ringing amplitude will be constrained to 100 percent modulation and will decay to a value always less than 100 percent for the duration of the peak overdrive. Figure 4 illustrates the operation of the DOC bilevel clipper. The audio signal, after a 75- μ sec pre-emphasis at point A, initiates the sequence of timing pulses B through D by virtue of exceeding an established peak level corresponding to 100 percent peak modulation in the FM transmitter (only positive peaks are shown for simplicity; negative peaks are handled in a like manner). The signal at point D is a digitally generated aperture lasting for the duration of the peak overload and is used to strobe a transmission gate, which subtracts a precise amount of dc voltage from

point *E*. The dc voltage is the "depth" or the amount of amplitude overshoot any given filter or system of distributed filters would exhibit because of the Gibb's phenomenon. (Bilevel clipping eliminates only overshoot caused by the Gibb's phenomenon.) The voltage at point *E* reverse bias diode CR1, which will clamp the audio signal to this depth voltage for the duration of the overload aperture (see Fig. 7f). The signal shown in Fig. 7g is the DOC processed peak after low-pass filtering. Observe that the peak amplitude is maintained at 100 percent modulation and that the filter ringing excursion is negative and damps out to an amplitude of less than 100 percent. Of equal importance is that the FM exciter system is presented with an audio waveform that achieves 100 percent modulation during the initial wavefront rise time. This preserves the percussive attack of the music and eliminates transient intermodulation distortion. Figure 6 illustrates this bilevel clipping action at various overmodulation drive levels for sine-wave excitation and the resultant signal after the FM exciter LPF network for comparison.

The waveforms at the extreme right in Fig. 6 illustrate the output of a typical 15-kHz LPF or series of LPF's making up the stereo generator/exciter audio chain fed by the DOC modified waveform. As the percentage of peak overdrive increases (as illustrated by the second series of waveforms), the aperture time is increased to accommodate the longer overload duration. The third set of waveforms illustrates the input overload forcing the audio into an almost perfect square wave. With this excitation, the DOC produces an aperture width of almost 180 electrical degrees. It is a simple matter to adjust the front panel depth control for the proper voltage corresponding to the filter ring produced by the truncation of the harmonics whether caused in one LPF or a combination of LP networks. This type of bilevel clipping eliminates peak overmodulation effects caused by the Gibb's phenomenon. However, the problem of filter phase linearity must be contended with for a complete cure of FM modulation overshoot problems.

Phase compensation

To totally eliminate peak amplitude overshoot caused by the audio LP filters in FM stereo generator/exciter systems, the nonlinear phase response of the filters must be corrected. Since every stereo generator

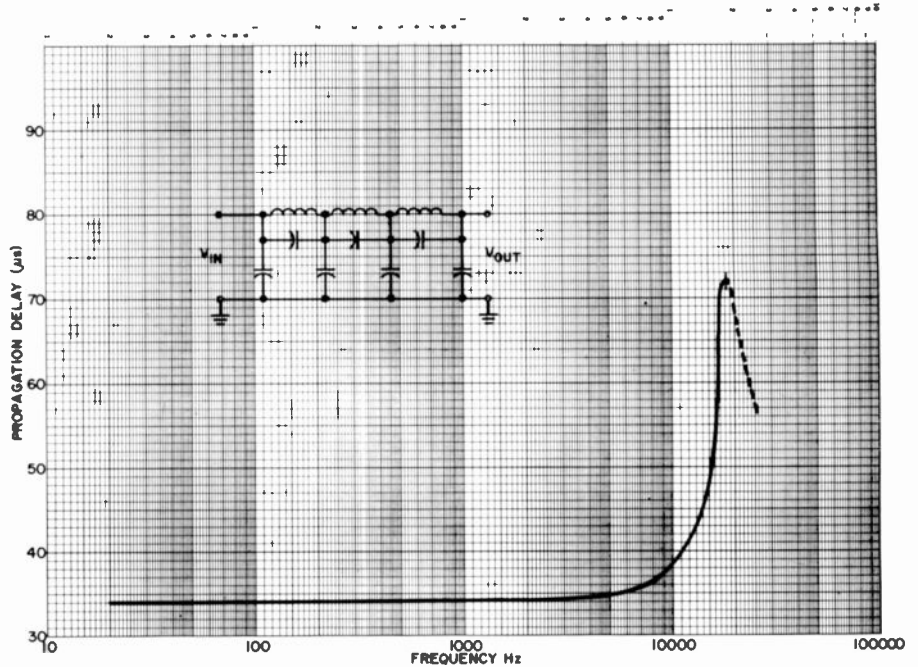


Fig. 8. A 7-pole elliptic function LPF is supplied with new RCA stereo generators or may be plugged into the BA-150 DOC processor to correct the nonlinear phase response.

from every manufacturer is different, the job of designing a phase corrector to compensate every LPF is impossible. Since the DOC processor must stand alone and work not only with RCA FM exciter systems but with any manufacturer or combination of manufacturers (i.e., stereo generator, exciter, transmitter combinations), the audio LPF must be a known quantity. Therefore, the solution decided upon uses a 7-pole elliptic function LPF with known phase response characteristics.

This filter is a plug-in printed wiring board that is supplied in the new RCA stereo generators or may be plugged into the BA-150 DOC processor when stereo generators of a different manufacture are used. The internal LPF in the stereo generator is bypassed and the filter resident in the BA-150 DOC processor is utilized.

Figure 8 illustrates the elliptic filter form and its phase response plot. Perfect phase compensation is a theoretical possibility. However, a circuit with the biquadratic all-

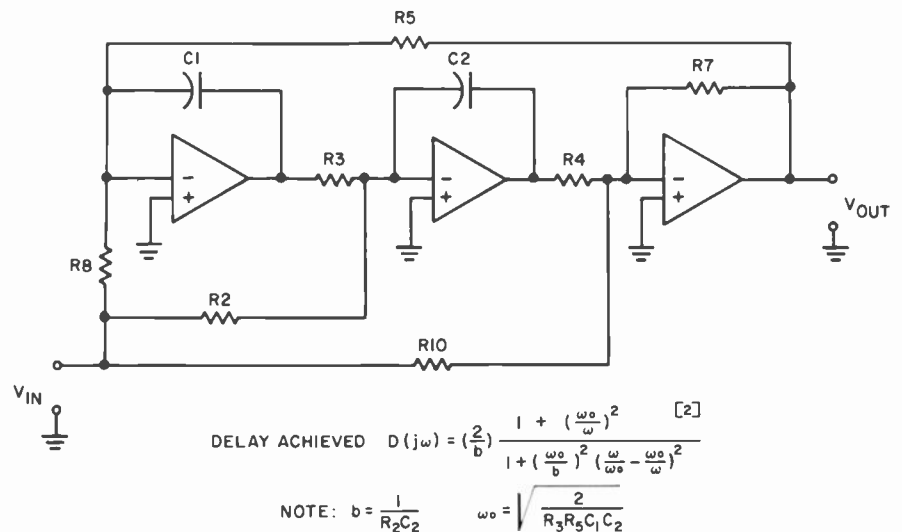


Fig. 9. Delay equalizer — single section.

pass function shown in equation (2):

$$T(s) = \frac{S^2 - bs + \omega^2}{S^2 + bs + \omega^2} \quad (2)$$

was used to minimize complexity. Figure 9 illustrates a typical section of the active delay equalizer.¹ By varying the resonant frequency ($\omega = 2f_0$) and the Q or bandwidth (b), various phase response curves are possible. A decision was made to use two sections of delay equalization to obtain an inverse delay response of the elliptic filter shown in Fig. 8. The phase response of each section along with the sum of both equalizers were optimized to produce the desired results shown in Fig. 10.

Figure 10d illustrates the resultant equalized phase response. An almost 5:1 reduction in phase response peak excursion was achieved. This results in a linearity of $\pm 3 \mu\text{sec}$ throughout the audio bandwidth. Tolerances in component values for both LPF and phase equalizer restrict further optimization since no circuit adjustments, as far as tuning, were permitted to minimize field alignment.

The final hurdle

Now that the LP filter ringing problem is under control and the audio peak amplitude can be tightly held to 100 percent modulation, consider one last problem—dc restoration. This is a problem that has existed with all clipping-type controllers and one that has been universally ignored. Somewhere in the stereo generator/exciter, the audio signal, which has been controlled by the DOC processor (or a similar-type peak clipper), must be ac coupled. Whether it is a simple audio input buffer, pre-emphasis amplifier, or the 15-kHz LP filters, the audio signal will eventually encounter a dc blocking capacitor.

Figure 11a illustrates the bilevel clipping of a symmetrical (equal positive and negative energy) waveform. After ac coupling, the positive and negative peak amplitudes are unchanged (relative to a fixed 100 percent modulation level). Figure 11b illustrates a more realistic signal. A slightly asymmetrical audio signal is bilevel clipped. (Old-fashioned peak clipping produces the same effect.) When this signal is capacitively coupled, the capacitor tries to redistribute the energy above and below zero volts equally. In this example, some positive energy was clipped off. The capacitor responds by shifting the entire

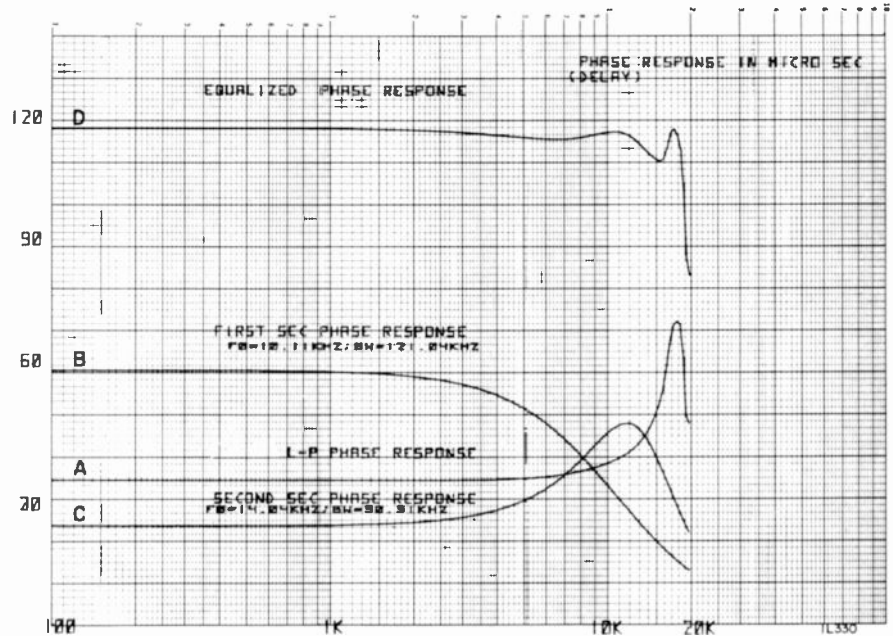


Fig. 10. The phase response of two sections of delay equalization, along with the sum of both equalizers, were optimized.

waveform slightly positive to re-establish equal area energy. The tightly held 100 percent peak is now overmodulating. This condition was largely left unanswered by previous peak clipping circuits since dc restoration usually involves a feed-forward signal to inject the proper polarity dc

correction at the last ac coupled stage; but, who wants to redesign the inside of an FM exciter. This last bit of possible overmodulation is usually not significant in terms of percentage. However, a modulation monitor usually does not split hairs and in the end, the peak flasher has the last

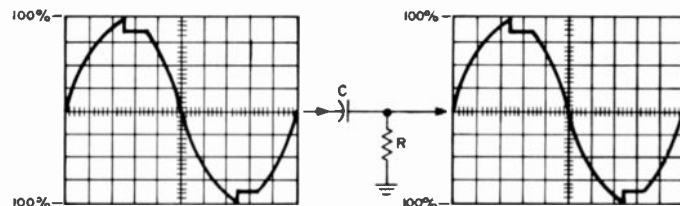


Fig. 11a Symmetrical Input

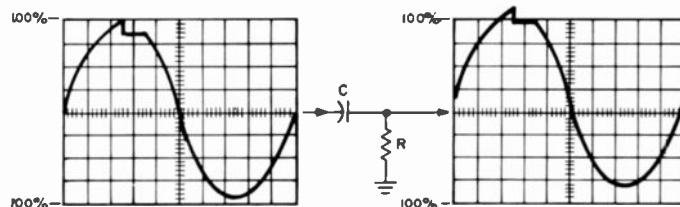


Fig. 11b Asymmetrical Input

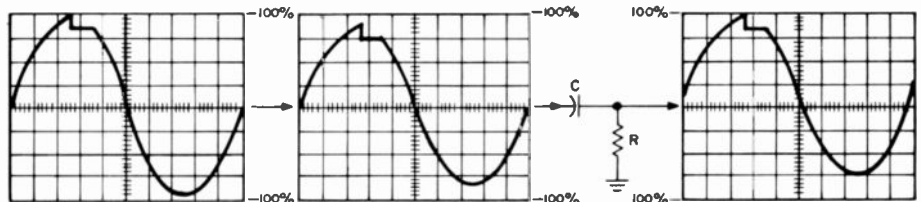


Fig. 11c Asymmetrical Input

Fig. 11. In order to correct for dc restoration, the DOC uses predictive peak restoration.

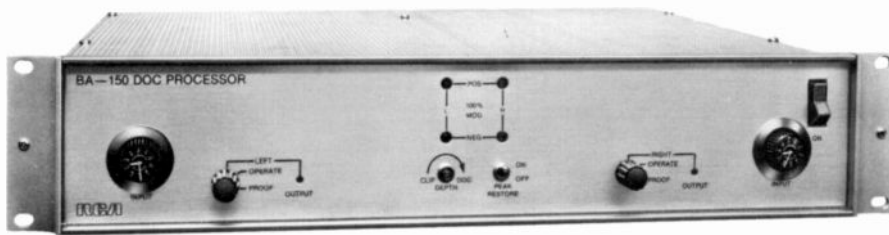


Fig. 12. The DOC processor is a universal black box that is inserted ahead of any FM stereo generator/exciter, and will operate with any type of signal processor preceding it.

word. To eliminate this source of trouble and still have a Black Box that will work with any FM exciter without modifying the exciter or injecting strange dc correction signals, the DOC has its own cure for dc restoration—predictive peak restoration.

Referring to the block diagram of the DOC processor (Fig. 4), shows that the path of the audio (the heavy dark line) encounters an XY multiplier after being bilevel clipped. This multiplier is capable of causing a gain reduction to the audio signal between 0 to 1.5 dB. The control signal (the Y input) is generated by measuring the amount of peak asymmetry at the time of bilevel clipping. This is done by comparing the audio signal before and after processing. The amount of peak energy imbalance caused by the peak clipping is stored in a peak detector and used to control the attenuation of the audio signal. This control averages 0.5 dB and the release time is approximately 15 ms so that total average modulation of the program is not affected. In addition, harmonic distortion is not increased since the release of the attenuation is extremely fast when compared to the total harmonic distortion produced by the original clipping, which is removed later by the 75- μ sec de-emphasis. Figure 11c illustrates the action taken on a slightly asymmetrical signal. The second trace shows a slight gain reduction (exaggerated for clarity) predicting a subsequent dc shift

due to ac coupling external to the DOC processor. The third trace shows the effect of the ac coupling in the FM exciter raising the peak amplitude again to 100 percent modulation.

The amount of peak restoration necessary to prevent overmodulation is a function only of the signal excitation since it depends on the nature of the peak symmetry.

The final analysis

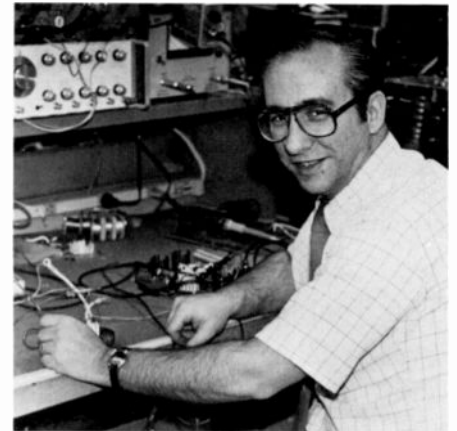
The DOC processor (shown in Fig. 12) is a universal black box that is inserted ahead of any FM stereo generator/exciter and will operate with any type of signal processor preceding it.

Installation is simple and set up is as easy as adjusting a 400-Hz sine wave to 100 percent modulation as displayed by LED indicators on the front panel. This is accomplished with dual input-level attenuators to preserve left and right channel balance. A front-panel depth control is adjusted with program material until no peaks trigger the peak flasher. The DOC processor is now tuned to the FM exciter. It is a simple task to increase the audio drive to the DOC, which boosts the modulation level of any program format to individual requirements or preference without worry about overmodulation.

The DOC processor is the state-of-the-art cure for overmodulation in FM broadcasting. It utilizes the time-proven technique of peak clipping most preferred by the majority of listeners. The DOC solves the problems of overshoot caused by LP filter ringing, nonlinear phase response, and dc restoration of peak values.

References

1. Fleisher, P.E., "Active Adjustable Loss and Delay Equalizers," *IEEE Trans. on Circuits and Systems*, Vol. CAS-21, No. 4 (July 1974).
2. Fleisher, P.E., and Tow, J., "Formulas for Biquad Active Filters Using Three Operational Amplifiers," *Proc. IEEE(Lett.)*, Vol. 61, pp. 662-663 (May 1973).



Dick Abt is a Design Engineer for the Broadcast Systems Division in Meadow Lands, Pa. He joined RCA in 1966 and became involved in the Design and Development of Broadcast Audio Equipment. He is presently a member of the technical staff in the Aural Broadcast Group where he is engaged in the design of the 5-kW AM Solid-State Transmitter.

Contact him at:
Broadcast Systems
Meadow Lands, Pa.
Ext. 6253

RCA Americom spacecraft reliability

Built-in reliability characteristics, plus extensive quality assurance, and qualification acceptance testing have produced the high degree of reliability evidenced by Satcom I and II. New technology will make Satcom III even more reliable.

Abstract: Assurance of spacecraft reliability is not by chance. It is accomplished through a dedicated program of design evaluation, controlled production, and test verification. The efforts that went into achieving a reliable, long-life segment for the RCA Satcom system, as ultimately demonstrated in orbit, are described. The future of reliable spacecraft communications at RCA, starting with the F3 satellite and looking beyond, is also discussed.

Introduction

At the heart of the RCA Americom Domestic Satellite Communications system are the two synchronous, orbiting Satcom spacecraft, F1 and F2. Not unlike the human heart, they are called upon to perform reliably day after day, year in and year out. Yet the users, caught up in their everyday activities do not fully understand how they function or the intricacies that are involved in achieving a high degree of reliability.

Spacecraft reliability is simply a measure of how well a combination of events are performed — design, qualification, manufacture, and acceptance test. High reliability was achieved only through the support of a comprehensive, well-managed reliability and quality assurance (R&QA) program.

Spacecraft equipment was designed for reliability from the beginning. Attention to the surrounding environment; suitability

of the parts, materials, and equipments used; optimization of the system redundancy configuration; as well as the use of proven designs and hardware were required.

New design concepts and non-space-proven hardware underwent special performance and environmental qualification testing to prove their acceptability for use on the Satcom spacecraft. Qualification was performed at all levels — piece part, component, subsystem, and spacecraft — selected to minimize program risks and cost.

Manufacturing was closely controlled both internally and at the vendors, as was close surveillance of all phases of production and test. Special process controls, inspections, and nonconforming material disposition were the responsibilities of the quality assurance organization. Additionally, strict procedures for trouble reporting and corrective action implementation were maintained.

Design verification tests; piece part testing and screening; and component, subsystem, and spacecraft level tests were performed under various environmental conditions to assure compliance with specified requirements.

During the first three years, the availability performance of the two "birds" has been outstanding and better than predicted. All projections indicate that each spacecraft will meet its design life of eight years.

The immediate future sees the launch of Satcom F3, containing several reliability improvements. Beyond this, system studies reveal some fantastic, seemingly "blue sky" ideas that will definitely benefit the in-

dustry through enhanced reliability and performance.

System overview

Designed for insertion into a 22,300-mile circular-equatorial, geostationary orbit (Fig. 1), the Satcom communications spacecraft are active repeaters operating within the 6/4-GHz band. The spacecraft provide network quality TV transmissions at the specific effective isotropic radiated power (EIRP), independent of the satellite's actual longitudinal station.



Fig. 1. Launch of the RCA Satcom I, December 12, 1978 — Thor-Delta 3914 launch vehicle.

Three RCA unique developments have been utilized to achieve 24 transponder service within the weight and volume capacity of an improved Delta launch vehicle:

1. Frequency spectrum reuse, employing four, cross-linear polarized, interleaved antennas with 12 channels at each polarization;
2. Lightweight, input and output multiplex microwave filters, antenna feed tower, waveguides and feed horns, all made of graphite-fiber epoxy-composite (GFEC) material; and
3. Development of a three-axis-stabilized attitude control system, with earth-oriented antenna and sensors.

Several functionally separate but interfacing subsystems comprise the RCA Satcom satellite: communications (antenna, TWTA's, receiver/drivers, filters), command, propulsion (reaction control and apogee kick motor), electrical power, thermal, and structural.

Reliability through design

Just like any performance characteristic, reliability is designed into the equipment, from piece part through overall system level. A good designer wears the "white" reliability hat in selecting components and configuring them into the optimal, most effective system. The reliability engineer is, of course, an integral part of the design effort, providing assistance through a well-established reliability program. The successful combination of the efforts of these two disciplines is the ultimate achievement of a highly reliable spacecraft design.

A number of unique features have been designed into the Satcom spacecraft that enhance system reliability. These features are briefly summarized in Table I.

The earth-facing antenna and feed subsystem, is rigidly mounted to a fixed, stabilized platform. There are no deployment mechanisms or complex gimbal bearing schemes that would reduce spacecraft reliability. Fine grids of parallel wires are embedded in each antenna, with the grids of the two polarizations orthogonal. The antenna itself is made of an RF transparent material. This simplifies antenna alignment, with true orthogonality achieved to better than 0.4 percent. Linear polarization also provides maximum isolation between the vertical and horizontal signals, improving system performance.

Another place where the Satcom design departs from the conventional is the use of a transistorized amplifier in lieu of a TWTA driver, and a 4-GHz tunnel diode amplifier in the common, preamplifier section of the transponder receiver, as shown in Fig. 2. The benefits derived from the use of solid state are apparent: increased reliability; lower weight; and equal or better performance. Transponder configuration was also designed to minimize switching complexity and its associated high failure rate. Only the receiver selection and TWTA ON/OFF functions are switched in the final design.^{1,2}

Perhaps the most important spacecraft housekeeping subsystem is the electrical power, shown functionally in Fig. 3. Next to propellant depletion, it is the primary spacecraft life limiting factor. Proportionally, much effort was expended during the design phases to maximize electrical power reliability.

The solar arrays, driven by a clocked motor, continuously track the sun. Full

illumination made it possible to reduce the complexity of the array by 30 percent compared to fixed-array systems. Direct transfer of the array power to a shunt-regulated bus not only improves efficiency, but eliminates the need for unreliable series regulation and complex battery boosters.

On-orbit energy storage is available to supply all loads during the two, 44-day eclipse periods each year. The Satcom design objective was to push the five-year, conventionally accepted life for NiCd batteries out to eight or ten years. To achieve this, operating temperatures were maintained between 0°C and 10°C, the negative electrodes were treated with Teflon to minimize cadmium migration failure modes, and regulators continuously fed the cells a trickle charge of electrons. However, perhaps the most significant life-prolonging feature of the design is the on-board reconditioning networks that effectively recover lost capacity by improving the end of discharge voltage characteristics.

Table I. Satcom spacecraft reliability enhancement design features.

<i>Component</i>	<i>Reliability Enhancement via Design</i>
Antenna	<ul style="list-style-type: none"> • Fixed, nondeploying platform • Orthogonal linear polarization
Transponder	<ul style="list-style-type: none"> • Solid-state transistor amplifier driver • Common 4-GHz tunnel diode preamplifier • Switching limited to receiver selection and TWTA on/off
Solar array	<ul style="list-style-type: none"> • Sun oriented — one-third less cells required than for a spinner spacecraft • Direct connection to load bus eliminates need for buck/boost regulation • Ultraviolet cell coatings to reduce degradation
Batteries	<ul style="list-style-type: none"> • On-board reconditioning • Teflonated negative plates • Continuous use of trickle charging • 0°C to 10°C operating temperature range
Propellant tanks	<ul style="list-style-type: none"> • Passive surface-tension web expulsion system versus bladder design • Half system isolation via valve system
Beacon transmitter	<ul style="list-style-type: none"> • Thermally aged ferrite divides to insure frequency stability
Structure	<ul style="list-style-type: none"> • Modularized construction • Segregation of RF and housekeeping components • Rigid base for antenna platform

The propellant system, shown in Fig. 4, was designed to minimize the effects of in-orbit failures. Twelve valve-controlled thrusters are supplied from isolated half systems to provide system redundancy. Equalization between the two fuel segments is achieved through the use of isolation valves. The propellant expulsion system utilizes a unique RCA design that eliminates the unreliable tank bladder used in many earlier hydrazine systems.

Caution was taken to ensure that all parts utilized were thermally aged before

the components were integrated in the spacecraft. This provided for stable operation after launch. A good example of this aging was the 60°C temperature bake of the ferrite devices within the telemetry beacon transmitter.

When thinking of design reliability, often overlooked, is the spacecraft structure. Design attention was given to assure rapid and complete spacecraft venting after launch; to prevent corona discharge and potential damage; to ensure mechanical integrity of the lightweight, multiplexer

and tower components; and to maintain alignment of all attitude sensors, momentum wheels, and thruster engines. Equally as important is the modularity of the design, allowing maximum space utilization but facilitating on the ground testing and access for maintenance.

Proper thermal control is paramount in achieving long life. Just as important as maintaining correct battery temperature is keeping the reaction control system (RCS) lines and propellant from freezing, cooling the transponders and electronics, and dissipating the shunted excess solar array power. Thermal designers account for thermal control surface degradation, load profile variations, and seasonal variation in solar heating. Thermal models and nodal analyses of component-to-spacecraft interfaces were developed and verified in test.

Radiation affects several areas: solid-state device life, static charging and degradation of spacecraft surfaces, and solar pressure attitude disturbances. Radiation-hardened IC's and transistors were selected for use in the design whenever possible. When radiation-sensitive devices were used, lead strips were placed over the devices for shielding. Protective coatings, used in the solar cell design, block out ultraviolet light.

Solar pressure disturbances on the spacecraft are compensated for by the use of magnetic bias coils. Incremental dipole settings are varied seasonally. Rare disturbances could interfere with spacecraft magnetic attitude control, but the design is fully redundant through the use of the back-up RCS-thruster system.

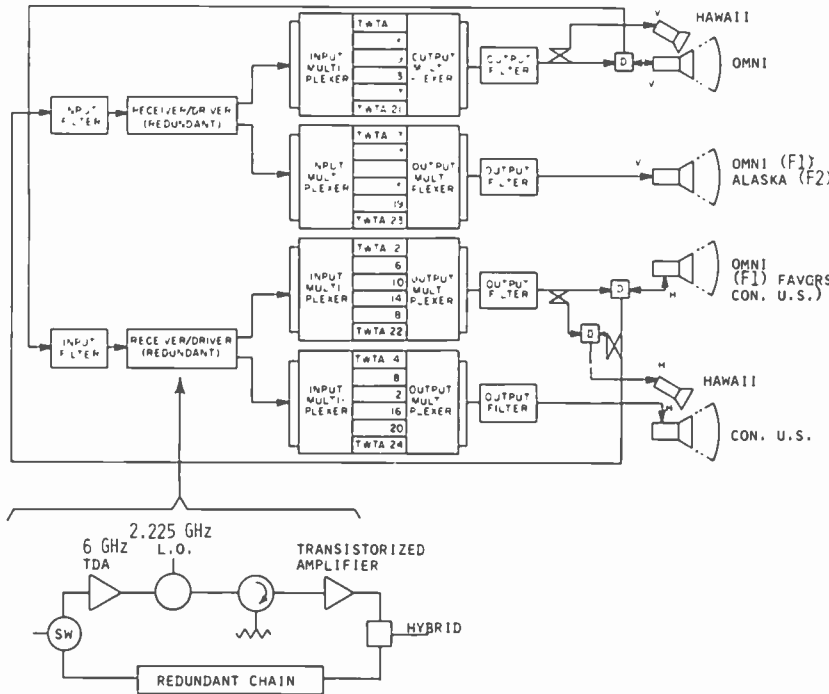


Fig. 2. Satcom communications subsystem.

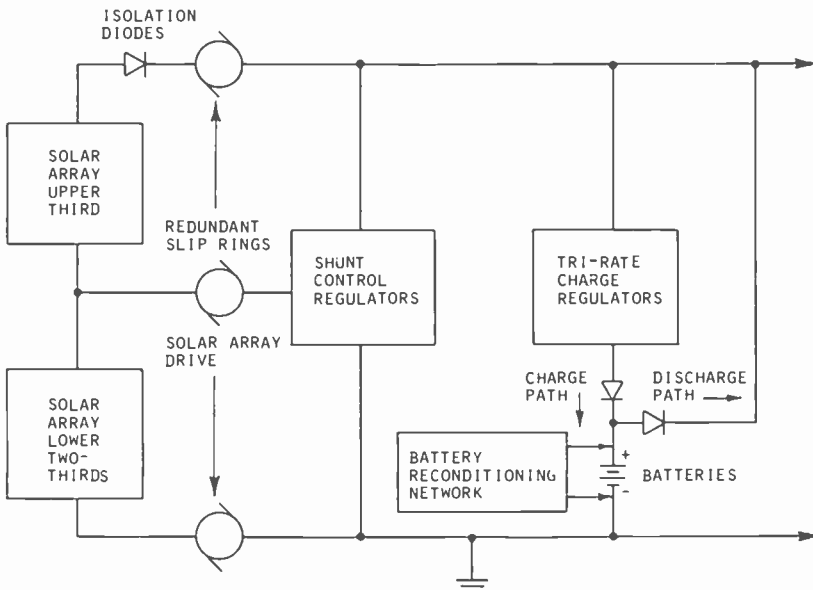


Fig. 3. The electrical power subsystem includes several features to maximize reliability.

Reliability engineering — design, evaluation, and demonstration

A comprehensive and controlled reliability program, highlighted in Table II, was established and implemented on the Satcom program as part of the total product assurance effort. Its objectives were:³

- To define and carry out reliability tasks necessary for all program phases, including design, procurement (vendor and subcontractor control), fabrication, and hardware test;
- To ensure that all hardware met the specified storage, orbital life, and reliability goals via a program of specification and control, apportionment and prediction, analysis, evaluation, and feedback for corrective action; and

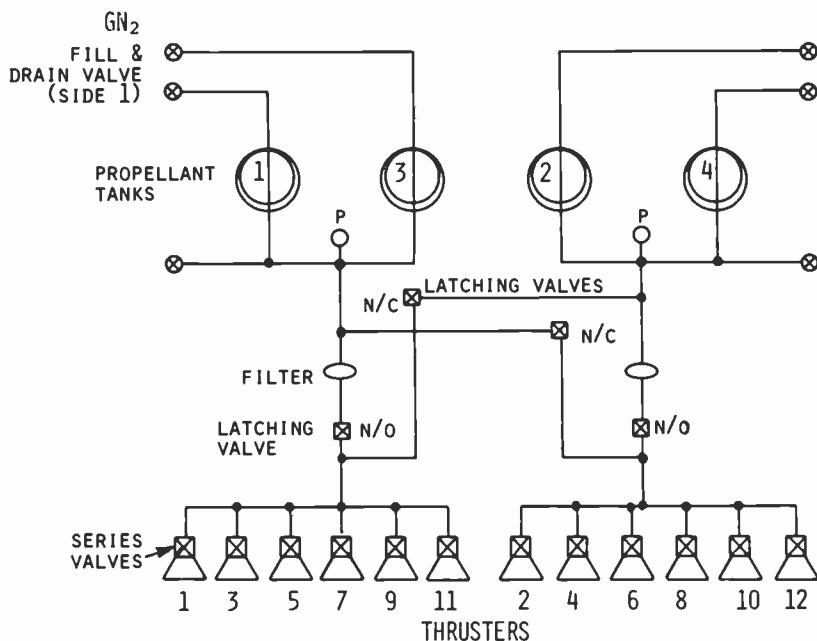


Fig. 4. The propellant system was designed to minimize the effects of in-orbit features.

To ensure that the inherent design reliability was not compromised during the fabrication, integration, and test processes.

Quantitative reliability requirements were established and incorporated into the performance specifications for the overall system, and each major subsystem and/or equipment. The performance specifications, in addition to the functional requirements, defined the environmental, safety, life, storage, and reliability goals. Responsible for assuring compliance with these requirements, the reliability engineers exercised controls over the various processes through technical assistance and support of the design and procurement activities. They provided design review, analysis, and evaluation, and maintained approval authority.

Reliability analyses of the Satcom system and equipment were performed in order to optimize the balance between cost, schedule, and reliability, and demonstrate compliance with reliability objectives. Mathematical models, based on mission analyses, were developed to functionally define the spacecraft system. Top-level reliability requirements were apportioned to the component levels, and appropriate failure rates were established based on equipment duty cycles and environmental stress. Redundancy was incorporated into the models to compensate for the effects of hardware failures and to eliminate critical, single-point failures or reduce their probability of occurrence to acceptable levels.

Through iterative prediction processes, an optimal system configuration was developed to meet the reliability requirements for the spacecraft.

As an integral part of the design effort, a worst case analysis of all electrical circuits was performed. Parameter variations which affect performance were considered, including the following: part tolerances, time induced degradation, temperature variation, variations in supply voltages (including transients), input signals and loads, radiation degradation, maximum performance demand, fail-safe provisions, and redundancy. Computer-aided analysis allowed for investigation of parameter variations that would cause maximum deviation of output from the norm. Sensitivity analyses allowed the designer to locate parameters having large effects on the output variations and replace components with low-tolerance devices. Monte Carlo parameter variation analyses were also used to simulate real-world drift conditions.

A failure mode, effects, and criticality analysis (FMECA) was performed to the component level in order to systematically evaluate the most probable modes of failure, their effects on the system, and their probability of occurrence. Critical, single-point failures were analyzed down to the piece part level to determine means for their elimination or to minimize their probability of occurrence. Results of the FMECA were fed back to design for appropriate design changes.

Several reliability critical items were identified, such as the batteries, TWTA's,

solar array drive, and momentum wheels. Lists of these items were maintained by reliability, which established procurement constraints, special testing and/or handling procedures, and compensating design requirements (e.g., redundancy). Additional items were identified as being reliability-sensitive, including AKM, RCS thrusters and valves, and the passive hybrids and circulators in the communications subsystem. All of these items were closely specified during procurement to include process controls, testing, screening, and special handling.

The design engineer was and is subjected to the scrutiny of his peers as well as top management through the vehicle called the design review. RCA Americom's own spacecraft management engineering team, RCA corporate consultants, and the NASA Goddard design review organization were employed to review the preliminary and final Satcom designs, at component and spacecraft levels. Data packages containing drawings, specifications, analyses, and plans presented the details of the Satcom design. Critical review of the equipment and systems by formal presentations and dialogue resulted in the establishment of action items, all resolved prior to the launch. Representatives of each major engineering discipline were in attendance.

Table II. Key product assurance program elements.

Reliability

- Quantitative requirements
- Apportionment/prediction
- Worst case statistical analysis
- Parts and materials control
- Failure mode, effects, and criticality analysis
- Reliability critical items
- Design review

Quality assurance

- Vendor/subcontractor control
- Material control
- Process control
- Incoming, in-process, final, and shipping inspections
- Test/measurement equipment control
- Trouble reporting/corrective action system
- Test monitoring and control

Quality assurance

After the system was designed and all equipments had been specified, it became the role of quality assurance (QA) to control the translation of the design into hardware, and to assure that the specifications were met.

A procurement system was established to assure maximum likelihood of success while maintaining the total system schedule and cost controls. Careful selection of all suppliers, and particularly of subcontractors and part/material vendors of critical items, was extremely important. A vendor rating system, utilizing previous quality and reliability records, was employed in addition to pre-award contract reviews and quality surveys. After program award, progress monitoring by the field quality organization and/or permanent QA residents assured that all specified requirements were achieved.

Parts and materials for use on Satcom were segregated from nonflight items in a controlled storage area. Part numbers, quantity, lot traceability information, etc., were placed into a computerized inventory control system for ease of identification, control, and retrieval. Test data and records were separately identified and filed. Nonconforming materials, marked and secured in a separate area, were subjected to disposition by a Material Review Board, chaired by Quality Assurance. Records allowed for determining recurring defects and providing follow-up on corrective actions.

Space hardware development requires the use of many special processes to achieve a high degree of reliability at minimum weight, volume, and cost. Special processes were involved during the welding of RCS propellant line connections; solar array fabrication; high-density, welded wire board assembly; manufacturing of the magnetic bias coils; and in many other areas. Quality assurance, in conjunction with manufacturing and design, developed specialized controls for these processes, and required sample certifications periodically to ensure repeatability and accuracy.

The root of any QA program is the controlled inspection of all parts, materials, and equipments received; of items as they are being manufactured; and of those ready for delivery. Incoming items were both mechanically and electrically inspected either on a 100 percent or on a sample basis, depending on lot size, to verify compliance with drawings and/or specifications. Manufacturing inspection

points were designed by QA engineering to minimize program risks and costs. Special attention was given to inspection of critical items and those requiring special processes. For example, every weld joint in the RCS thruster system was x-rayed in multiple axes to ensure proper material flow and joint integrity. Inspections were performed after all environmental tests and after spacecraft shipment to the Kennedy Space Center. All manufacturing, testing, and inspection procedures were fully documented, in log book folders, showing positive evidence of all actions taken, discrepancy resolutions, and the overall item configuration.

During the equipment test phase, a carefully monitored, closed-loop trouble reporting and corrective action system was maintained for prompt reporting of each test discrepancy and material review board (MRB) action. Thorough analyses were performed to define causes of malfunctions, identify any secondary effects, and record corrective actions taken to ensure that the problem was resolved and would not recur. All problems were formally reviewed and resolved by a test review board, chaired by QA.

QA personnel witnessed all test phases of the Satcom program, from component through launch, assuring that all necessary actions, including lower level tests, trouble report closeouts, and inspections had been completed. Surveillance and control over the test activity minimized damage to flight hardware, assured that all test data were recorded and were acceptable, and provided visibility to program management on problems uncovered and their resolution.

Qualification/acceptance testing

A test verification program was designed for Satcom, providing a high level of confidence that all spacecraft mission objectives would be met. The hardware levels at which tests were performed were carefully selected to ensure that all key parameters were measured and component/subsystem interfaces verified. Test sequences and types were established that would give the earliest problem indications, minimizing schedule delays and costs. Electrical performance tests were conducted to demonstrate the ability of each component, and the overall system, to meet the performance requirements when exposed to environments simulating ground, launch, and orbital conditions.

A proto-flight concept was used for component, subsystem, and spacecraft level testing. Essentially what this meant was that the first completed flight item was exposed to higher qualification level environmental stresses for flight acceptance durations. In this manner, the capability of the component/subsystem/spacecraft to comply with its specification requirements was demonstrated, yet its usefulness for flight purposes was not degraded. Some additional, one-time tests, such as electromagnetic interference (EMI), were performed only on the proto-flight configurations to verify the design integrity.

A special grouping of qualification tests were performed early in the program for verification of new designs, qualifying non-space-proven hardware, and testing new manufacturing techniques. Some of the more important of these are listed in Table III.

Special attention was paid to the mechanical integrity and temperature stability of the input and output multiplexer assemblies containing GFEC components. The narrow-band filters are perhaps the most frequency sensitive parts of the transponder. Thus, thorough analyses were made considering even the small, but significant, difference in dielectric constants between air and vacuum. Qualification level vibration and thermal vacuum tests were successfully performed. Radiation degradation was also simulated, with exposure rates equivalent to ten years in orbit. Highly stable electrical performance characteristics, at temperature ex-

Table III. Design qualification.

<i>Mechanical/thermal model</i>
Structural static load test
Sinusoidal vibration
Acoustics
Thermal vacuum/thermal balance
<i>Input/output multiplexer</i>
Thermal/structural/dielectric analyses
Sinusoidal vibration
Thermal vacuum
Cobalt radiation — 10 year dosage
<i>Solar array — Q board</i>
Thermal cycling life test (+60°C to -160°C)
<i>Propellant tank</i>
Burst test (>3:1 margin of safety)

Table IV. Qualification/acceptance tests.

Component

- Electrical performance
- Sinusoidal vibration
- Random vibration*
- Thermal cycling**
- Thermal vacuum*
- EMI*
- Weight

Housekeeping

- Electrical performance
- Temperature cycle*
- Power subsystem outdoor*
- Solar panel illumination

Spacecraft

- Electrical performance
- RF range
- RFI
- Alignment/boresite
- Thermal balance*
- Thermal vacuum
- Solar array deployment
- Mass properties/spin balance
- Sine vibration
- Acoustics
- Separation/pyrotechnic shock*
- RCS leak
- Magnetic dipole
- Power system end-to-end test

* Proto-flight only

** Flight only

tremes of -5°C to $+45^{\circ}\text{C}$, were demonstrated. Worst case group delay and gain slope have been presented in a previous paper.²

Synchronous orbit spacecraft see two periods of solar eclipse each year. These vary as a cosine function, lasting from a few moments to a maximum of 72 minutes each day. During this time, the normally sun-warmed solar array cools rapidly to as low as -160°C . To verify the solar array's ability to survive a lifetime of extreme temperature cycling, a group of solar cells, isolation diodes, and temperature sensors was affixed to a piece of solar array honeycomb panel and temperature cycled in a regime simulating nine years of orbital conditions. The results of the test showed only minimal degradation, verifying the design.

The four hydrazine propellant storage tanks, spherical in shape and gold plated to enhance their thermal properties, have a nominal launch tank pressure of about 350

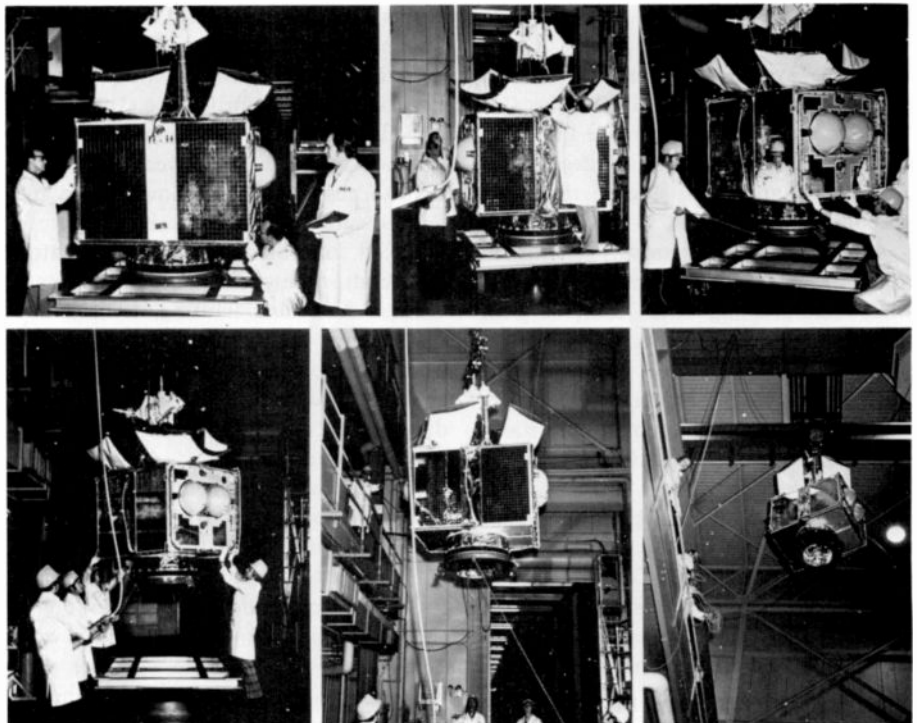


Fig. 5. Satcom I is transferred into a 24-foot thermal/vacuum chamber for testing.

psi. A proof load test to failure was conducted to qualify the tank design and determine the actual safety margins. Rupture occurred at nearly four times the nominal stress.

Extensive testing of the first flight components (or boxes) was performed to prove out the functional design and its performance in worst case launch/space environments. In accordance with the proto-flight concept, environmental exposure levels were higher than those for subsequent flight units. A summary of the qualification/acceptance testing, at all hardware levels, is provided in Table IV.

Electrical performance tests were performed before, during, and after environmental exposure, simulating the conditions of actual operational modes. These tests included more detailed measurements than could be performed at subsystem or spacecraft levels, and verified compliance with all component specifications and their stability when exposed to external stresses.

Proto-flight units received three axes of random vibration in addition to a sinusoidal sweep, to obtain an early indication of the units' responses to the launch acoustics. Thermal cycling tests were performed on all units; proto-flight items that were determined to be vacuum-sensitive, such as the batteries, TWTA's, and momentum wheels, were thermal cycled in a bell jar, under vacuum. EMI tests were performed only on proto-flight units to

look at the effects of turn ON-OFF and inrush currents (conducted susceptibility), power line noise (conducted emissions), radiated interference (E-field radiated emissions), and external presence of radiated electromagnetic energy (radiated susceptibility).

Spacecraft Testing of the integrated system was the ultimate proof of design performance. Complex interfaces and interactions had to be characterized and within-specification operation verified. Computer-aided electrical performance testing of the spacecraft system was basically a composite of the individual subsystem performance tests plus those tests, such as RF range, that could only be performed at the system level.

The F1 proto-flight spacecraft received three special tests as part of the system level qualification: thermal balance, separation/pyrotechnic shock, and power subsystem end-to-end testing. As part of a thermal vacuum test, a thermal balance situation, similar to the tests run on the mechanical/thermal model, was conducted, this time with actual spacecraft equipment and finalized thermal subsystem design (Fig. 5). Complete electrical performance tests were run at ambient and at each temperature extreme.

To demonstrate the launch vehicle third-stage-to-spacecraft marmon clamp separation system and the solar array cable cutter release mechanism, a one-time, live squib test was conducted. The pyrotechnic

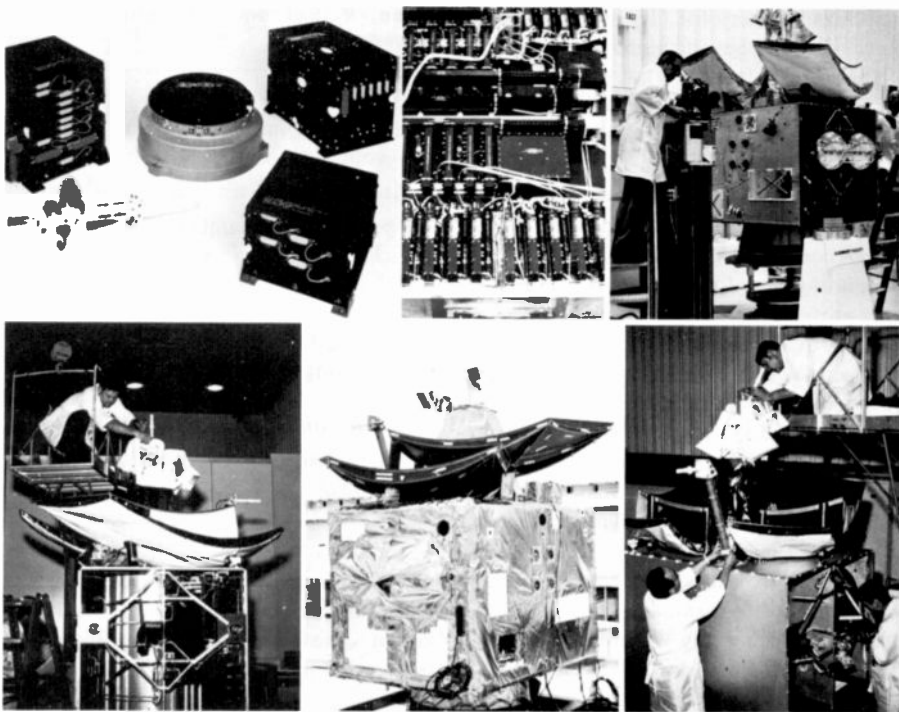


Fig. 6. Top (left to right): flight components; transponder panel; optical alignment. Bottom (left to right): F1 mechanical assembly; thermal model; omni antenna installation.

devices and release mechanisms worked perfectly and no adverse, shock aftereffects were recorded.

While the North panel contained the basic power subsystem components and was separately tested, a special power test with the entire spacecraft, including solar arrays, was conducted. The solar array-to-bus interface, via slip rings, was checked and the effects of load switching, solar eclipse (battery mode), and load regulation were measured.

In addition to direct coupled, electrical transponder testing, a complete set of antenna range measurements was made. A group of horn antennas, mounted on a 200-foot tower, was used to transmit/receive RF from/to the spacecraft. The satellite was mounted on a three-axis positioner within a fully calibrated anechoic chamber for these measurements. Complete antenna profiles were recorded and pointing alignment (boresite) verified. While still in the chamber, RFI measurements were made to ensure that the spacecraft's own field would not interfere with command functions or performance.

Alignment of the attitude control subsystem sensors, momentum wheels, RCS thrusters, solar array drive, and antenna subsystem was performed optically (Fig. 6). Checks were made before and after environmental exposure to verify alignment stability.

At the completion of thermal vacuum testing, and again after acoustic testing, the

two solar arrays were installed on the spacecraft and tested for proper deployment. The deployment mechanism consisted of three spring-loaded hinges and viscous dampers on each side. Air bearings were attached to the arrays to simulate zero gravitational forces.

The fully integrated spacecraft, configured in the launch mode, was subjected to a three-axis, sinusoidal vibration environment, at programmed g levels, over the frequency band of 5 to 200 Hz (Fig. 7). Immediately following, worst case launch acoustic levels were simulated. Both tests verified the ability of the spacecraft and components to operate during and survive the Delta launch environment.

The final, pre-shipment test performed on the spacecraft measured the satellite's magnetic dipole for proper attitude control performance. The dipoles were adjusted, using bar magnetics, to less than ± 1.0 ATM³ in each of the three axes.

Spacecraft reliability — predicted versus demonstrated

Reliability predictions for the Satcom spacecraft were performed during the design phase to estimate the system probability of survival due to random failure causes, and to establish the optimal redundancy configuration, within the weight constraints of the Delta 3914 launch

vehicle. System specifications required at least a 50 percent chance that 20 out of 24 transponders would survive a life expectancy of eight years. Single-point failures that might cause a loss of half or more of the payload capacity were required to have better than a 99 percent chance of surviving seven years.

After three years in orbit, both spacecraft are operating normally and are expected to meet their reliability objectives. Three out of the 48 transponders, two on F1 and one on F2, experienced failures, all during the first several months of operation. One has since recovered and is back in service. Using the chi-square distribution at 60 percent confidence, a transponder failure rate estimate, based on actual in-orbit experience, was calculated. Demonstrated versus predicted reliability curves for 22 of 24 transponders (Fig. 8), show better than predicted performance. Note that the demonstrated curve reflects a 100 percent spacecraft less the two transponder failures. One must be cautioned not to use the demonstrated curve to predict transponder life, since the number of operational hours is small and the confidence level is low. Prediction failure rates are better substantiated, and give a truer, more accurate estimate of reliability performance. Transponder failures can be expected over the spacecraft life and must be compensated for through restoration.

While reliability predictions look at catastrophic hardware failures, they do not encompass operational problems that can affect service availability. Several short duration anomalies have occurred that

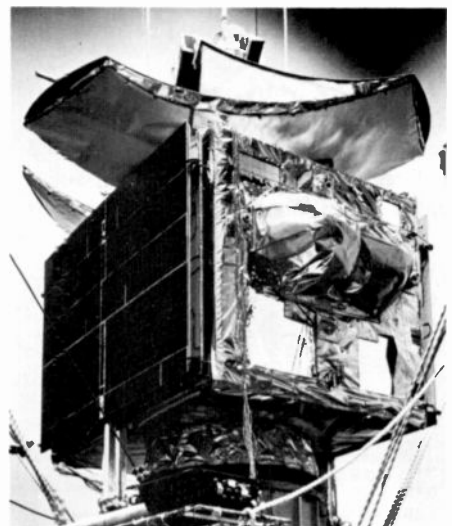


Fig. 7. Satcom I proto-flight vibration tests verified the ability of the spacecraft and its components to operate during and survive the launch environment.

were caused by operational errors, other carrier interferences, or unexplained phenomena. Each of these occurrences is documented and was addressed by our spacecraft engineering personnel. They represent, however, less than 0.01 percent of the total spacecraft operational time, and have only a small impact on customer services.

Satcom III and beyond

RCA is aggressively pursuing new technology and design improvements that will make the F3 and subsequent spacecraft even more reliable than the exceptional F1 and F2 spacecraft—improvements that will serve the total communications community. The upcoming F3 launch will open up new horizons for on-orbit reliability. Planned design changes that will improve reliability, but are capable of implementation within the established production/-test schedule, are listed in Table V.

Increased launch payload capacity, available due to the proven Delta 3914 design, allows for the addition of four in-orbit spare TWTA's, one for each bank of six transponders. Redundancy compensates for potential random or infant mortality failures. Two early TWTA failures experienced on F1 and F2 appeared to be related to the dedicated high-voltage power supplies. Special thermal vacuum life-cycling tests were conducted, utilizing spare on-ground TWTA's, but they failed to precipitate any failures. Each F3 TWTA was recently subjected to an intensive visual quality-control inspection to detect potential workmanship-related failure modes. Suspect and marginal areas were reworked to reduce the risks of further in-orbit problems.

After three years in-orbit, spacecraft battery performance has been as expected. Weight limitations on the F1 and F2 satellites, however, required higher battery depths of discharge than are desirable for

maximized battery life. To extend the life expectations to beyond eight years, the F3 will use higher capacity batteries, proven on the Telsat ANIK-B program, while maintaining essentially the same bus load.

An improved concept for interactive magnetic yaw/roll control was developed by RCA Astro-Electronics and also flight proven on the ANIK-B spacecraft. By eliminating tandem magnetic attitude error correction, faster yaw error damping can be achieved, and tighter pointing accuracies can be maintained. Additionally, the maximum available yaw dipole was doubled on F3 to eliminate any dependency upon the RCS thrusters for large roll error correction, and to compensate for the higher expected sun spot activity, predicted to peak in 1982.

RCA's improved Satcom spacecraft are being designed to maximize user flexibility and system reliability. Ongoing development programs in digitized TV transmissions, video noise reduction equipment, program audio distribution, and teleconferencing have been described previously.⁴ Multiplexed digital voice, facsimile, time-share computer terminals, and teletype, in addition to TV, can provide industry with a total communications system.

Conclusions

The advent of a highly reliable spacecraft communications system at RCA has permitted a full range of communication services to be available as a cost/systems effective alternative to the old, less reliable terrestrial microwave networks.

Through a comprehensive program of design analysis, manufacturing and procurement controls, and test verification, a high degree of spacecraft reliability has been achieved. Ongoing efforts are being directed at making the F3 and all subsequent spacecraft even better, with longer life expectancies and payloads that are responsive to the needs of the communications community.

Acknowledgments

The R&QA program described was developed and implemented by RCA Astro-Electronics (RCA-AE). Success of the F1 and F2 spacecraft program is thus largely attributable to the efforts of their fine spacecraft team.

Special thanks are extended to RCA-AE for the use of the photographs presented

Table V. Satcom F3 reliability improvements.

Communications

TWTA redundancy—for 6 configuration

Antenna panel tilt—0.6° southward

Special quality control inspection—TWTA's

Power

Increased battery capacity for prolonged life

Attitude control

Interactive magnetic yaw/yoll control

Doubled yaw magnetic dipole

within this paper; to M. Rosenthal of RCA-Americom for his editorial and layout assistance, and to E. Blount for typing this manuscript.

References

1. Keigler, J.E., "RCA Satcom—Maximum Communications Capacity Per Unit Cost," *RCA Engineer*, Vol. 22, No. 1, pp. 50-55 (Jun/Jul 1976).
2. Napoli, J., and Greenspan, J., "RCA Satcom, The Next Generation Domestic Communications Satellite System," Wescon Communication Satellite Systems (Sep 16-19, 1975).
3. RCA Astro-Electronics, "Reliability Program Plan," Revision B, Company Private (Dec 1973).
4. Langhans, R., and Lansey, R.M., "RCA Americom Communications System," *RCA Engineer*, Vol. 24, No. 2, pp. 62-67 (Aug/Sep 1978).



Paul DeBaylo is Manager, Reliability and Quality Assurance at RCA Americom. As part of the Technical Operations department, he is currently responsible for the reliability of the spacecraft and ground segments of RCA's domestic satellite communications system and the overall service quality.

Contact him at:
RCA Americom
Piscataway, N.J.
Ext. 4187

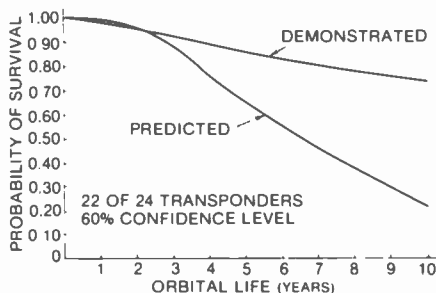


Fig. 8. Spacecraft demonstrated versus predicted reliability curves show better than predicted performance.

NTSC color television performance measurements in communication systems

Video-parameter and time-base measurement charts aid in the monitoring of the transmission performance of video programming.

Abstract: *As color television systems increase in complexity, the techniques for performance evaluation must become equally sophisticated to ensure high-quality video. Signal processing techniques are described for evaluating linear and nonlinear distortions in the received picture and signal channel performance.*

At RCA Americom, research into video networking control methods demonstrated a need for a method for locating system or component failures in television communication circuits when a particular video parameter is in question. Three large charts were researched and constructed based on the Marconi 2900 series automatic video measuring instrumentation for the NTSC 525-line color television system. This equipment is capable of monitoring both video parameters and time base measurements during normal programming using vertical interval test signals (VITS). Two of the charts include 16 video parameters, definitions, limits, and probable area of failure. The third chart contains 14 time-base parameters, standard definitions, and limits. However, only the video passband distortions will be discussed.

The parameters outlined in the main matrix include the more pertinent linear and non-linear distortions which affect NTSC color television performance. The limits displayed on the charts are referenced to the EIA RS-250B standards for analogue microwave and satellite relay

facilities, and the NTC-7 Network Transmission Committee of Television Network Broadcasters and the Bell System.

In television systems, there are two general categories of signal degradation: linear and nonlinear. Linear distortions are changes in signal parameters that do not vary with changes in signal amplitude; nonlinear distortions are changes in signal parameters that do vary with changes in signal amplitude.

Two specialized oscilloscopes have been developed for examining the two classifications of signal degradation and noise phenomena. These are the video waveform monitor and the vectorscope.

The video waveform monitor

The video waveform monitor is a rectangular-coordinate display instrument, with special triggering time base circuits and vertical filter characteristics for accurate measurement of the composite video signal. Waveform monitors easily synchronize with composite video using field and line information. This allows the examination of either field, selected lines, or part of a selected line. Electronic information which may not be relevant to a particular test may be extracted out with a range of vertical passband filters contained in the instrument.

The amplitude scale of the waveform monitor is calibrated in IRE divisions. One volt of video peak-to-peak, including sync pulses, equals 140 IRE units.

1 IRE unit = 1/140 volts = 7.14 mV

The IRE unit was originally defined by the

Institute of Radio Engineers, now the IEEE.

The vectorscope

The vectorscope displays the chrominance information directly as a function of the modulation encoding process. The modulation scheme used for the chrominance information in the NTSC color system is known as double sideband suppressed carrier AM in quadrature. The saturation of the color information is transmitted as amplitude modulation, and is resolved as the vector sum of the two color signals, I and Q .

$$\text{Chrominance amplitude} = \sqrt{I^2 + Q^2}$$

The hue or color is a function of phase difference between the chrominance signal and the color burst, as shown in Fig. 1. The hue is transmitted as phase modulation, and can be determined graphically with the aid of the following equations:

for $I \geq 0, Q < 0$,

$$\text{Hue} = \Phi = \tan^{-1} I/Q + 33^\circ;$$

for $I \geq 0, I \leq 0, Q \geq 0$,

$$\text{Hue} = \Phi = \tan^{-1} I/Q - 147^\circ; \quad \text{Ref.}$$

for $I \leq 0, Q \leq 0$,

$$\text{Hue} = \Phi = \tan^{-1} I/Q - 327^\circ. \quad \text{Burst}$$

The I component is a vestigial sideband signal with the lower sideband equal to 1.5 MHz and an upper sideband equal to 0.5 MHz, about the 3.58-MHz subcarrier. The Q component is modulated with a 90-degree phase delay with respect to the I signal, and it is a symmetrical sideband signal, with 0.5-MHz sidebands. The I and Q designations refer to "in phase" and "quadrature" with respect to the 3.58-MHz

subcarrier. However, the *I* and *Q* signals maintain their orthogonal relationship; they are offset by 57 degrees with respect to the reference burst. This 57-degree phase displacement increases the color fidelity of flesh tones since they now lie directly on the *I* axis (orange-cyan). The *I* component is 1.5-MHz wide, while the *Q* signal is only 0.5 MHz. This increased bandwidth is a consequence of the enhanced resolution that the human eye sustains in the visual spectrum, for orange and cyan energies.

Linear distortions

Although frequency content is normally used to describe the passband limits of a video channel, it is not a good indicator of system performance. Since video waveforms are usually non-sinusoidal and, in general, are very complex, the amplitude and phase relationships of their harmonic content must be translated or passed through a system with little or no modification.

As a result, time measurements are used to investigate the performance of a video signal with high precision.

Linear distortions are usually examined in four major time domains which are relevant to the fundamentals of the television system: short time distortion, line time distortion, field time distortion, and long time distortion.

Short time distortion

Short time distortions ($0.125 \mu\text{s}$ to $1 \mu\text{s}$) are deviations that occur at some fractional part of a horizontal line. This phenomenon usually affects horizontal resolution, sometimes referred to as definition.

This particular distortion is examined using the sine-squared $2T$ pulse to bar ratio. The bar portion of this test signal is the integral of the $2T$ sine-squared pulse, where the risetime of the bar is 0.96 h.a.d. (half amplitude duration) of the integrated pulse. T is the Nyquist rate, and is referenced at $0.125 \mu\text{s}$ for the 525-line 60-Hz NTSC color television system, where $f_c = 4.2 \text{ MHz}$ is the cutoff frequency of the video baseband.

$$T = 1/[2(f_c)] = 0.125 \mu\text{s}.$$

Note that f_c for this definition is taken at 4.0 MHz as the upper cutoff frequency of the video baseband.

The $2T$ pulse to bar waveform is normally contained in the composite test signal (Fig. 2). The particular pulse is peaked with respect to the bar which should be

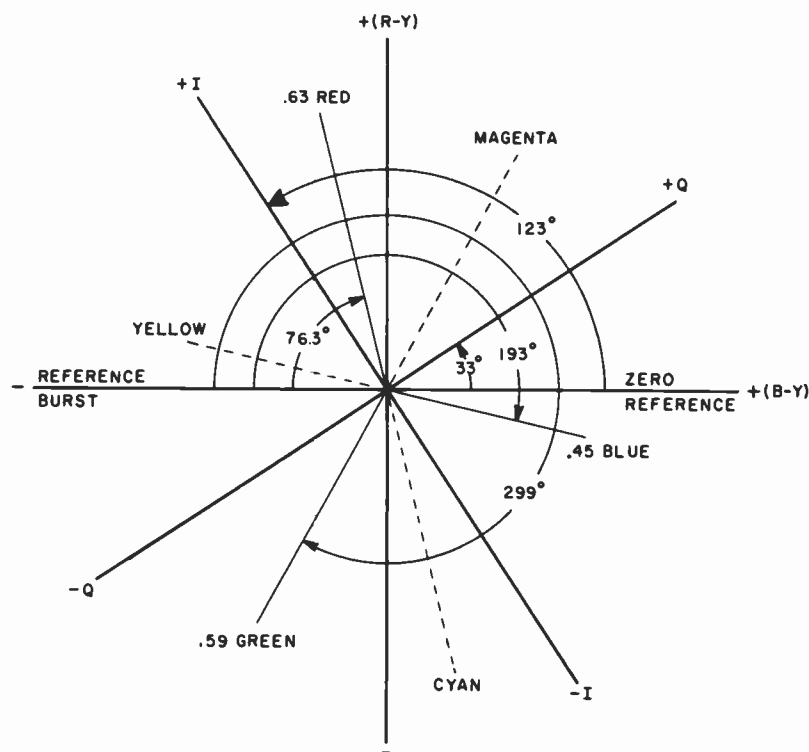


Fig. 1. Note: Θ is the angle that moves clockwise with respect to the burst.

referenced at the 100 IRE line. The $2T$ pulse has a spectral distribution which extends up to 3 MHz.

If this $2T$ pulse falls below the bar, there is a high-frequency rolloff condition existing in the channel. Insufficient high-frequency response has a tendency to reduce the resolution of the received picture, thus, the images will appear to be soft.

If the $2T$ pulse is projected above the bar, the result is known as an overshoot characteristic and is a very important aspect of the $2T$ pulse. This unique quality indicates that the frequency response of the video passband is probably peak between 1-3 MHz, and that any aberration noted in the symmetry of the $2T$ sine-squared pulse indicates group envelope delay distortion. This particular aspect of the $2T$ sine-squared pulse demonstrates a superiority to the well known multiburst signal, since the multiburst signal is not a good indication of delay distortion.

The $2T$ sine-squared pulse is also useful in identifying group envelope delay or multipath distortion. When this pulse is symmetrical, there is no delay distortion in the passband region. However, if the pulse is asymmetrical, there is delay distortion.

Line time distortion

Line time distortions ($1 \mu\text{s}$ to $50 \mu\text{s}$) are mid-frequency errors which occur at line

frequency and cause horizontal smearing or streaking in the received picture. Line time distortion is examined with the 18 μs bar which is also a component of the composite test signal (Fig. 2).

In terms of frequency, the bar checks passband performance occurring below 1 MHz to about the horizontal line rate which is 15,734.264 Hz for NTSC color television. The phenomenon is generally of long duration and portrayed by the tilt noticed at the top of the bar. The bar can also be a reference pulse for insertion gain measurements.

Field time distortion

Field time distortions ($50 \mu\text{s}$ to 16 ms) are problems in the low-frequency regions of the video passband. Obvious field time errors display objectional vertical shading in the received picture.

This particular distortion is common with ac-coupled video amplifiers, and microwave and satellite circuits where the video signal would not be clamped to permit a more symmetrical FM spectral distribution. Also, power supply, power line hum, or any other unwanted low-frequency signal in this range would be considered as a field time distortion.

The techniques used to measure field time distortion are somewhat different than for the other time distortions. To

accurately determine field time distortion, a low-frequency 60-Hz squarewave signal should be inserted into the circuit. However, since some television communication channels require sync pulses, the 60-Hz signal must be integrated with composite sync.

Long time distortion

Long time distortions (>16 ms) are aberrations noted as dc or very low-frequency errors which cause intermittent and slow variation in picture brightness. These distortions are usually viewed over long periods of time. Flicker is an example of a long time distortion.

There are many factors which can cause a long time distortion, most of which are power line and power supply related.

The procedure to measure this type of distortion requires the bouncing flat-field test signal supplied by the Textronix 147A signal generator. The system under test is terminated with a waveform monitor, in direct coupled mode.

If a vertical shift is observed in the horizontal blanking interval, this would indicate the potential for long time distortion.

Chrominance to luminance gain

In the NTSC color format, one of the generic problems is to transmit the signal through a channel without altering the relative amplitudes of the chrominance or luminance components. If one component is changed with respect to the other, a chroma error occurs. This aberration will affect the saturation levels in the received picture.

To measure chrominance to luminance gain inequality the 12.5T modulated sine-squared pulse provides a very sensitive indication of amplitude-frequency response errors. These errors are present in the region where the 2T pulse is less sensitive, the 3-4 MHz region of the chrominance/luminance gain and delay which causes saturation errors and color registration problems.

Chrominance to luminance delay

Chrominance to luminance delay inequality is the time displacement between

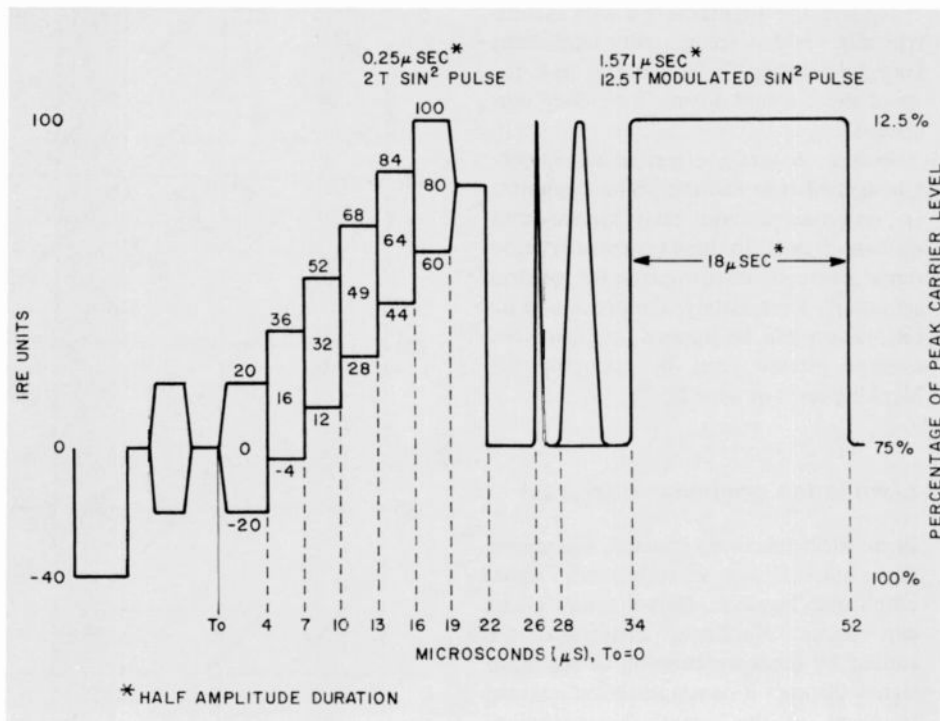


Fig. 2. Composite test signal.

chrominance and luminance information. This phenomenon is most noticeable with red lettering smearing into a white or gray background. In more severe examples of this distortion, the effect is color ghosting on the received picture.

Group delay is the formal category for this particular distortion found in communication systems. It is defined as the slope of the phase characteristic, specifically,

$$\text{Group Delay} = \frac{d\Phi}{d(\omega)}$$

the derivative of the phase.

This type of distortion can occur almost anywhere in a communication channel; however, it is usually found in frequency translation devices such as transmitters and receivers. Also, IF amplifiers and envelope detectors can contribute significant amounts of chrominance to luminance delay, if improperly adjusted.

To measure chrominance to luminance delay, the modulated 12.5T pulse is used again. Note: chrominance-to-luminance gain and delay inequality usually appear together.

A sinusoidal type base line on the 12.5T modulated pulse indicates chrominance to luminance gain and/or delay inequality. This information can be decoded using the modulated 12.5T, 1.57 μs h.a.d. for the 525/60-Hz standard. This graph is shown in Fig. 3 where gain inequality is given in decibels and delay in nanoseconds.

Nonlinear distortions

The more involved distortions associated with the television signals are of the nonlinear classification. As mentioned before, these errors are a function of signal amplitude, and can display distortion with the chrominance relative to luminance and the reverse order. This particular type of distortion is very important, since it represents the dynamic performance of a video signal. Typical causes of these phenomena are: frequency translation devices, overdeviation in FM systems, misalignment of discrimination in FM systems, pre-emphasis and de-emphasis networks, group delay in IF amplifiers, quadrature distortion in vestigial sideband modulation, and envelope detectors. In general, nonlinear distortion measurements are made at average picture levels of 10 percent, 50 percent, and 90 percent of signal amplitudes.

Average picture level

The average picture level or dc component of picture signals is determined by the brightness of a scene. It can be defined as the luminance level relative to blanking level for active picture lines, averaged over a period of one field. It can be numerically expressed in percent as changes between blanking and white amplitudes. (The origin of this definition is the IRE, now IEEE.)

The average brightness of a dark scene is typically 10-15 percent; a very light scene may be between 75-90 percent; and the mean value would normally be 40-50 percent.

Average picture level is especially important in FM type communication systems, i.e., microwave radio relay systems and satellite circuits. In these systems the video signal is ac-coupled to improve RF spectral symmetry. Fortunately, the process of dc restoration can be applied to regain the average picture level by clamping the blanking level or sync tip.

Luminance nonlinear distortion

In an ideal television channel, the system gain should not change with signal amplitude, however, in real systems, this can occur. Nonlinear distortions are caused by misrepresentation of the input signal through a communication channel in terms of the signal's Fourier components, both amplitude and phase, becoming a function signal level. This criteria is sometimes examined with respect to the transfer characteristics of discrete black box type components used to construct a communication circuit. The transfer contours may expand or compress the mean video information as a function of amplitude, frequency, or phase of the input signal and become compounded by the addition of other spurious signals.

The usual procedure for measuring luminance nonlinear distortion is to use the staircase signal and terminate the system with a waveform monitor. The signal is then processed by a differentiator and the resulting spikes give an indication of the amplitudes of each riser. The tallest spike is referenced at 100 IRE and the measurement is taken with respect to the shortest spike.

The modulated staircase signal displayed as part of the composite test signal (Fig. 2) can also be used for this measurement by filtering out the 3.58 MHz burst on each riser before application to the differentiator. Then the same procedure described above can be applied.

Luminance to chrominance distortions

Differential gain: Differential chroma gain is the change in chroma amplitude with respect to a change in luminance level. The chroma amplitude changes with average picture level or brightness

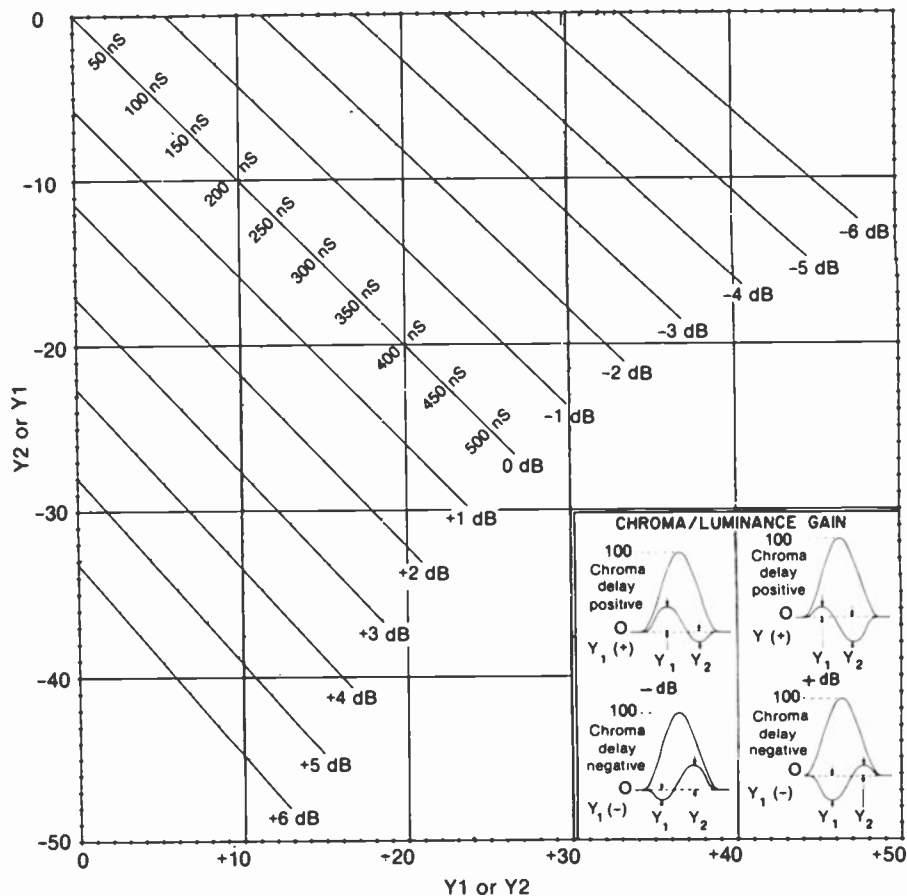


Fig. 3. Modulated sine-squared pulse application nomograph. 12.57 1.57 μ s half-amplitude difference for 525-line, 60 Hz standards.

variations. The visual observation, noted as a result of this degradation, is saturation errors in received picture information.

To examine this particular distortion, the modulated staircase signal is used. This signal is part of the composite test signal (Fig. 2), and can be obtained as a single test signal from a Textronics 147A video signal generator.

Normally, for this measurement, the modulated staircase signal would consist of five risers with a peak amplitude limited to 80 IRE. The subcarrier levels on each riser are set to 40 IRE to reduce noise interference which can introduce errors in differential gain or differential phase measurements. Each of the subcarrier envelopes, displayed on the five risers, are phase-locked to the 3.58-MHz reference burst.

The modulated staircase signal is applied to the input of a system and terminated with a waveform monitor, typically the Tektronics 1480 series instruments. The vertical input filter selector is switched to the 3.58-MHz chrominance bandpass filter. This mode will pass the subcarrier frequency and associated sidebands; however, it will reject the staircase signal.

The waveform monitor is then adjusted so the largest frequency envelope is peaked at 100 IRE. The difference in amplitude between the largest and smallest envelope is the differential chroma gain.

Differential phase: If amplitude variations in luminance signal phase modulate the color subcarrier, the condition is referred to as differential phase. The color subcarrier phase changes with variation in luminance levels.

The visual observations displayed on the received picture are changes or errors in hue as a function of luminance amplitude variations. Typically a differential phase error of as small as 4 degrees can be identified by a trained observer with normal color perception.

The same test used for differential gain, the modulated staircase, is used for differential phase measurements; however, this distortion can only be measured using a vectorscope.

Instead of examining the amplitudes of each of the 3.58-MHz envelopes located on each riser, the phase relationships relative to the reference 3.58-MHz burst located on the back porch of the horizontal sync porch are examined.

The differential phase measurement can be examined directly on a vectorscope. Deviation in the vector alignments may easily be observed for medium and large errors. For very small errors, or a very accurate analysis of this distortion, the Tektronics 520A vectorscope, with special circuitry and calibrated phase control, can provide accuracies approaching 0.2 degrees.

Chrominance to luminance distortion

Chrominance to luminance distortion, also referred to as chrominance to luminance crosstalk or intermodulation, incorrectly reproduces the increased saturated colored areas of the received picture. Through experimental visual observation of this signal impairment, it appears that the human eye is tolerant to some degree of its effects.

This nonlinear type of distortion is typically contingent upon misalignment of discriminators in FM systems, pre-emphasis/de-emphasis circuits, and group delay in IF amplifiers.

In AM systems, quadrature distortion in vestigial sideband transmissions seems to always support this type of distortion.

To measure chrominance to luminance crosstalk, the modulated pedestal test signal (Fig. 4) is used. It consists of a luminance pedestal normally referenced at 50 IRE, although it can be varied with some test signal generators, and a three level chrominance bar signal superimposed on the pedestal. The color bar amplitudes are typically 20, 40, and 80 IRE units respectively. The subcarrier phase of these three color envelopes is 90 degrees with respect to the reference burst. The vectorial position of this signal displayed on a vectorscope is coincident with the *R-Y* axis.

This test signal is also used for chrominance nonlinear gain and chrominance nonlinear phase measurements. To examine chrominance to luminance crosstalk, the modulated pedestal test signal must be inserted at the input of the system and terminated at the output with a waveform monitor. The vertical input selector is positioned to filter out the chrominance information, low-pass mode.

The measurement is taken as the maximum amplitude variation of the filtered region of the luminance pedestal, with respect to the region which did not contain any chrominance information. The

luminance bar is first referenced to 50 IRE units, and the results of the test recorded in IRE units.

Chrominance nonlinear gain distortion

This distortion is specified for fixed levels of luminance components and average picture levels and analyzed for amplitude variations in chrominance signal at the output of a system. The changes measured are with respect to set minimum and maximum chrominance amplitude at the input of the system in question.

The visual effect for this video impairment could also be the incorrect reproduction of increased saturated areas. However, this may not be apparent by just observing the received picture without knowing or comparing it to the transmitted information.

The modulated pedestal test signal used for chrominance to luminance crosstalk is also used for this distortion measurement.

The test signal is inserted at the input of the system and terminated with a waveform monitor. The vertical input filter selector is switched to the 3.58-MHz chrominance passband mode. The measurement is taken as the largest change in amplitude of the three chrominance envelopes with respect to their original reference levels. The middle color envelope is first referenced to its original value of 40 IRE units. This measurement can be recorded in either percent or IRE units.

Chrominance nonlinear phase distortion

Chrominance nonlinear phase distortion is defined as the deviations in phase of the chrominance subcarrier at the output of a system, as a function of variations in subcarrier amplitude, with respect to specified minimum and maximum values. The measurement is taken with respect to a fixed luminance level and average picture level.

The visual observation noted at the received end would be hue shifting in highly saturated areas. This parameter is also measured using the modulated pedestal test signal. To examine the parameter, the modulated pedestal test signal is applied to the input of the system, and the output is terminated with a vectorscope.

The phase of the three envelopes is usually measured with respect to the reference 3.58-MHz burst, and recorded. The chrominance nonlinear phase is the peak-to-peak phase deviation of three level chrominance envelopes relative to minimum and maximum displacement.

Vertical interval test signals

In order to ascertain that the television signal parameters are within tolerance during an actual broadcast transmission, three test signals are sent with the active video information. These test signals are

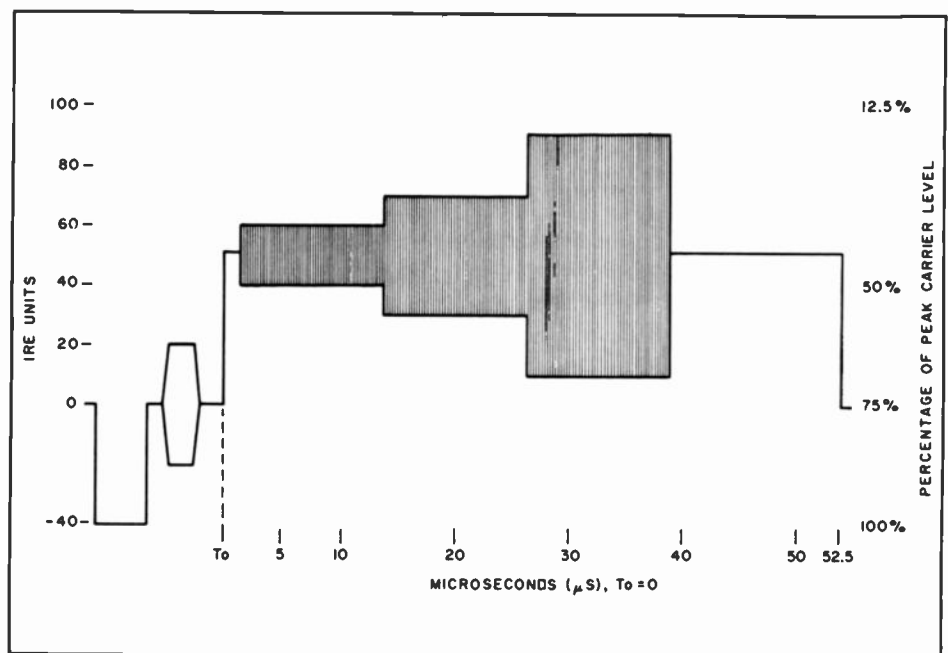


Fig. 4. Modulated pedestal test signal.

inserted during the vertical blanking period, hence, they are referred to as vertical interval test signals (VITS).

The multiburst signal

In examining video system performance, the multiburst signal is useful for checking the middle to upper frequency response characteristics of the video signal. The signal is composed of envelopes of discrete frequencies within the television passband. The highest-frequency burst is equal to the upper limit of the system being tested which is about 4.2 MHz in the United States. The next lowest frequency is 3.58 MHz to examine color subcarrier transfer characteristics, and the lower frequency bursts are distributed down to 500 kHz. Also included at the start of the multiburst signal is a flat luminance level or white flag. This component serves as a reference to which the frequency envelopes contained in the multiburst can be compared. The multiburst signal is shown in Fig. 5.

NTSC color bars

The NTSC color bar signal was designed in accordance with EIA color bar signal specification RS-189. The EIA requires the color bars to have a 75 percent amplitude, 100 IRE white reference, and 7.5 percent setup. The luminance signal accuracy should be within 2 percent. Chrominance signal absolute amplitudes should be within 3 percent of all subcarrier frequency components. The color bar signal is shown in Fig. 6.

The 100 percent white bar amplitude level permits a convenient check of relative chrominance/luminance gain by comparing the peak amplitudes of yellow and cyan to white bar. An additional feature is the black reference following the bar. Checking timing errors in different locations within the facility is an important use of the color bar signal displayed on a vectorscope.

Conclusion

Recently the video-parameter and time-base measurement charts were used in a proposal to the management at RCA Americom for a video networking control system. This exhibit displayed the significance and need for a quality control arrangement to monitor the transmission performance of video programming. The

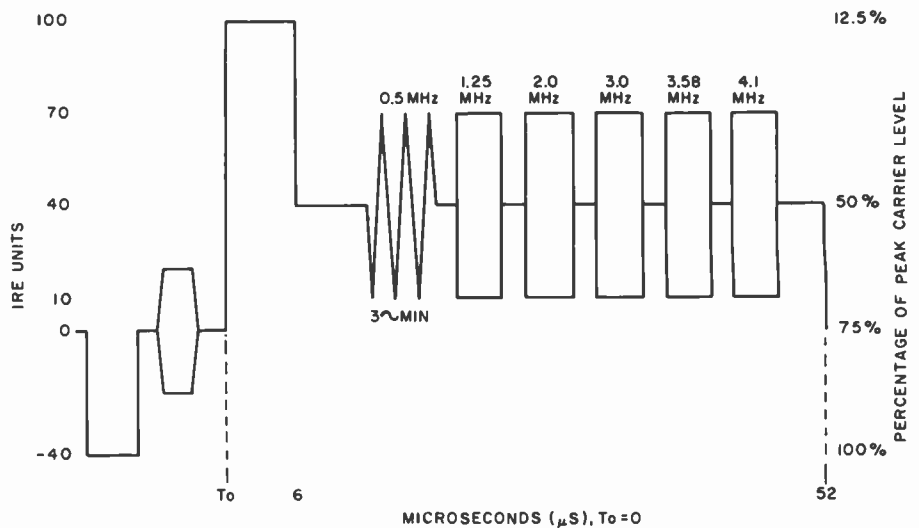


Fig. 5. Multiburst signal is used to check the middle to upper frequency response characteristics of the video signal.

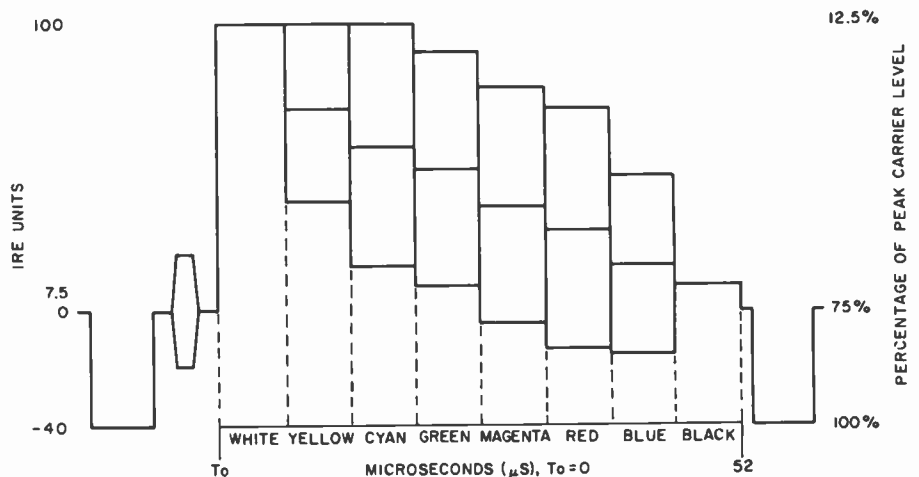


Fig. 6. Color bar signal is used as a video-tape step signal.

network monitoring system was based on a completely automated system which could continuously scan several video circuits, or be manually controlled. In the event of a failure or performance error, the engineer could confirm the malfunction with standard video test instruments, and a quality color television monitor. He could then

cross reference the distortion on the charts to a possible system or component failure.

The video-parameter and time-base measurement charts will be reproduced and distributed to earth station personnel for use as a parameter limit guide and failure reference. Copies of these charts are also available on request.



Mike Shumila is a Senior Member of the Engineering Staff at RCA Americom, and is a member of the Advanced Technology Group. He is currently involved in research concerning the measurement techniques of video parameters, and their origin in FM and AM communication systems.

Contact him at:
RCA Americom
Piscataway, N.J.
Ext. 4132

C-band FET power amplifier for TWTA replacement

Advances in GaAs FET power amplifiers in terms of reliability, efficiency, and power output have made these devices suitable for space applications as a replacement for TWTAs.

Abstract: A 6-W GaAs FET power amplifier (FETA) is being designed, fabricated, and tested. The FETA covers the down-link communication satellite band of 3.7 to 4.2 GHz. The specifications call for better than 20 percent dc-to-RF efficiency at the 6-W level and better than 10 percent efficiency at a backed-off 1.5-W output level. The amplifier is formed by six cascaded stages. A 5-W solid-state power amplifier laboratory model shows that GaAs FETs can replace traveling-wave-tube amplifiers in spaceborne transponders.

Introduction

The technology of gallium-arsenide field-effect power transistors has by now advanced to the point where these relatively new devices can offer serious competition to traveling-wave-tube amplifiers (TWTAs) in spaceborne communication applications. A number of programs, at RCA and elsewhere,^{1,2,3} have amply demonstrated their capabilities.

Although the TWTA is one of the most efficient and reliable devices yet developed for wide-band microwave power amplification, the size, weight, and cost of dc power generation equipment on the satellite impose severe limits on the amount of RF power that can be generated on-board, and necessitate operation of the TWTA at or near the saturation point where the device is most efficient. Unfortunately, operation at or near saturation also causes undesirable properties including amplitude

and phase nonlinearities causing cross-talk among the signals sharing the transponder. This is the area where power GaAs field-effect transistors (FETs) are challenging the domination of the TWTA since, in addition to yielding good power output and efficiency characteristics, they also offer superior linear performance.

At RCA, present GaAs FET work is centered around the design, fabrication, and testing of a 6-W nominal GaAs FET power amplifier (FETA) covering the down-link communication satellite band of 3.7 to 4.2 GHz.* In addition, before starting work on this amplifier and in order to prove the capabilities of a solid-state power amplifier (SSPA), a 5-W laboratory model was built and tested at RCA. These two programs will be covered in some detail in this paper.

6-watt FET amplifier design

The most salient specifications of the 6-W FETA call for better than 28 percent dc-to-RF efficiency (excluding the power supply) at the 6-W level and a two-tone carrier to third-order intermodulation ratio better than 15 dB at full operating two carrier power output.

The specifications of the FETA are shown in Table I and a block diagram is shown in Fig. 1. As can be seen in the figure, the amplifier is formed by six cascaded stages, all designed with input and output at 50 ohms. The circulators are of the drop-in microstrip type and are helpful in reducing intrastage ripple in the

passband considering the strict 0.01 dB/MHz gain slope specification. The input and output circulators help in meeting the FETA voltage standing-wave ratio (VSWR) specifications of 1.25:1 maximum, and in protecting against excessive reflections that could easily damage the input and output GaAs FETs. The first four stages of the SSPA operate in class A and were designed from the device S-parameters with an RCA generated analysis and optimization computer program (COSMIC) used in the calculations of the matching circuit parameters. The last two stages consist of a single-ended amplifier, which drives the three final amplifiers by means of a three-way serial divider; the outputs are summed, again by means of a three-way serial combiner. Since these output stages operate at the beginning of saturation, all assumptions of linearity become invalid and the measured small-signal S-parameters (especially the output S_{22} parameters) become questionable. The output impedance of these power FETs must, therefore, be matched using an automatic load-pull system, a unique, computer-controlled instrument developed by RCA⁴ which allows the determination of the optimal load impedance as a function of output power.

Selection of the FETs for the power stages was made principally on the basis of their efficiency: the output power levels per device specified in the diagram of Fig. 1 can be obtained using devices by a number of manufacturers, but the efficiency requirements of the program practically imposed the selection of the Fujitsu FLC-30 devices. The first four stages, on the other hand, were selected principally on the basis

Reprint RE-25-2-14
Final manuscript received July 13, 1979.

*This work is sponsored by Intelsat under Contract No. IS-1000.

Table 1. Specifications for the 6-W FET power amplifier.

Item	Specification	Item	Specification
Frequency band	3.7-4.2 GHz	Third-order carrier to intermodulation ratio	15 dB at high power operating point
Instantaneous bandwidth	300 MHz	Spurious and noise (dc to 12 GHz)	-24 dBm/MHz
Output power	6.0 W at the operating point	Harmonics 2nd	-12 dBc
Amplifier gain	High power gain >55 dB; Small-signal gain ≥57 dB	3rd	-21 dBc
Small signal gain slope (any channel)	0.01 dB/MHz	Efficiency	28 percent at 6 W (excluding EPC)
Group delay variation (any channel)	0.5 ns	Dc power supply	+22 to +37 V
AM-to-PM conversion (K_p)	2.5°/dB	Turn-on, turn-off	No damage
Input VSWR	1.25:1	Gain stability	±0.1 dB over a 24-hour period at constant T
Output VSWR	1.25:1	Operating temperature	-5°C to +50°C
		Weight	2.0 lbs (including EPC)

of their gain so that the number of stages in the power FETA could be kept to a minimum: attention was paid also to the devices' output characteristics, which had to provide the required output power (500 mW at the output of the FLC-08 stage) without significant gain compression.

Serial divider/combiner

As Fig. 1 shows, the output stage of the power FETA is formed by three single-ended, identical amplifiers whose outputs are summed to yield the required output power and whose inputs are obtained from the outputs of a three-to-one power divider. By using this technique, it is possible to multiply the output power obtainable from one device by the number of devices in the stage, although the stage gain remains unchanged and equal to the gain of a single device. Usually the number of transistors in the last stage is a binary number, which allows a very simple power combination (or division) using 90° hybrids. In our case, because of the required output power level and the characteristics of the FLC-30 devices, the number of transistors in the power stage is not binary, and serial combination techniques must be used. These techniques are well known and are shown in Fig. 2a in a generalized form for an n -way divider, and in Fig. 2b for the particular case of a three-way divider. The

interdigitated Lange coupler was chosen for this application because of its low insertion loss, excellent wide-band coupling, and its suitability for microstrip technology. Typical performance characteristics of a Lange three-way divider are shown in Fig. 3.

Breadboard results

The practical realization of the design described above is underway and a breadboard model is being built. The first four cascaded stages shown in Fig. 1 (two

HFET 2201, one FLC-02, and one FLC-08) have been built, integrated, and tested. The room temperature frequency response over the band 3.7 to 4.2 GHz is shown in Fig. 4.

The flatness is approximately 0.5 dB peak to peak out of a total gain of the four stages totaling 47 dB: the nominal design value is 45 dB, but it should be kept in mind that the extra two dB will be used up during the development of the amplifier temperature compensation.

The next module developed was the power module using the FLC-30 FET. This module is used in the power driver stage

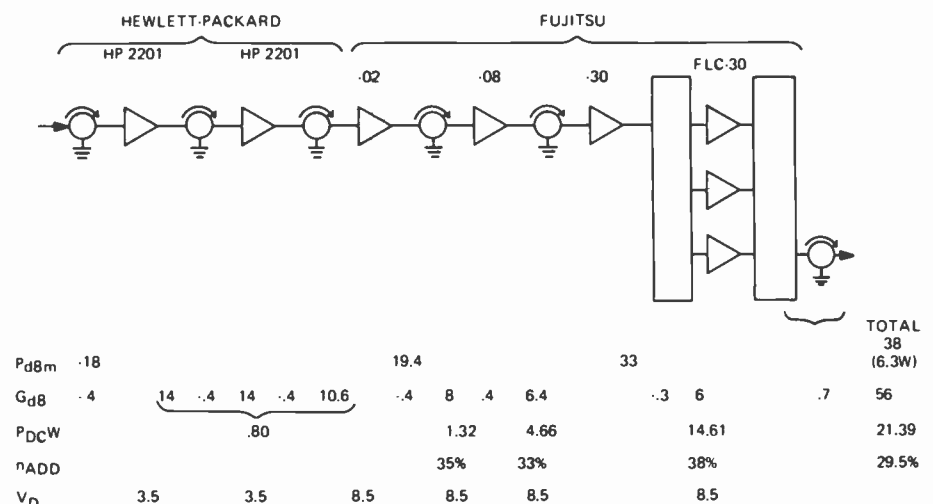


Fig. 1. The FET amplifier is formed by six cascaded stages.

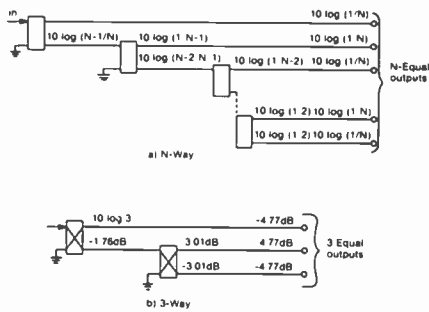


Fig. 2. Since the number of transistors in the power stage is not binary, serial combination techniques must be used. (a) n -way divider. (b) Three-way divider.

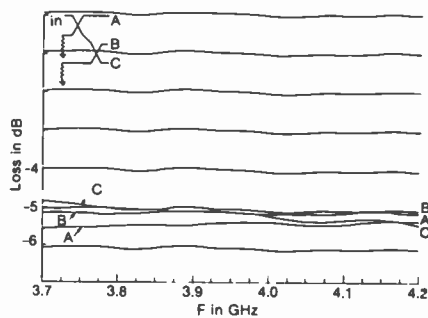


Fig. 3. Typical performance characteristics of a Lange three-way divider.

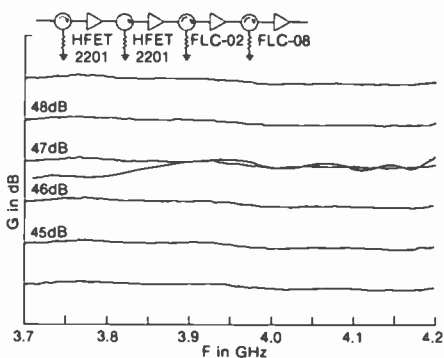


Fig. 4. The room temperature frequency response of the first four stages.

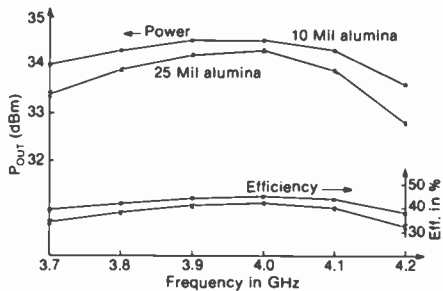


Fig. 5. Frequency response and power added efficiency of the power module using the FLC-30 FET for two different matching circuits with 25- and 10-mil substrate thicknesses.



Fig. 6. The 5-W solid-state power amplifier laboratory model was designed and built to prove that GaAs FETs could replace TWTA's in spaceborne transponders.

and in the last power stage. The module frequency response and power added efficiency over the frequency range of interest are shown in Fig. 5 for two different matching circuits realized using two different substrate thicknesses, 25 mils and 10 mils. The improvement in performance obtained with the 10-mil-thick alumina substrate is due to the fact that lower impedance circuits become realizable without having to print impractically wide linewidths. Therefore, a better match over a wider bandwidth can be offered to the very low input impedance of the FLC-30 FETs. After completing optimization of the module design, the full 6-W FETA will be integrated and tested.

5-watt laboratory model

The 5-W solid solid-state power amplifier laboratory model was designed and built to prove that GaAs FETs were indeed good candidates to replace TWTA's in spaceborne transponders. The amplifier, whose photograph is shown in Fig. 6, consisted of seven stages (six single-ended and one balanced) as can be seen in the block diagram of Fig. 7. The individual amplifier assemblies were constructed in ceramic microstrip using a modular approach that enabled testing and tuning of the modules prior to integration. After assembly, the amplifier was extensively tested; the more salient results are shown in Fig. 8 through 10. Figure 8 shows the SSPA frequency response and a 1-dB bandwidth of better than 250 MHz with a dc-to-RF efficiency between 30 and 28 percent.

Figure 9 shows the two-tone intermodulation performance measured using two equal-amplitude carriers 1 MHz apart. It can be seen from the figure that the SSPA yields a carrier-to-intermodulation

ratio of better than 16 dB at the 5-W operating level. In addition, the SSPA can be operated in a linear mode (carrier-to-intermodulation ratios larger than 25 dB) for an output back-off from two carriers' saturation of only 2.5 dB, at an output level (two carriers) of 2.25 W. It should be noted that at that power level the efficiency of the SSPA is better than 10 percent while if a typical 5-W TWTA is operated backed off to achieve the same linearity, its efficiency would be no greater than 5 percent and the output level would be about 1 W.

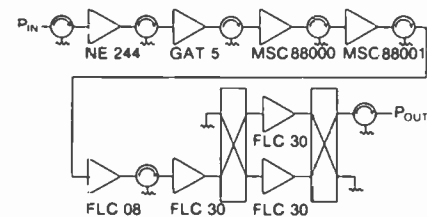


Fig. 7. The 5-W SSPA consisted of six single-ended stages and one balanced stage.

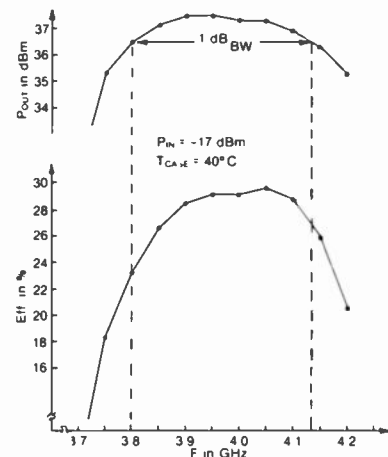


Fig. 8. The SSPA frequency response showed a 1-dB bandwidth of better than 250 MHz with a dc-to-RF efficiency between 30 and 28 percent.

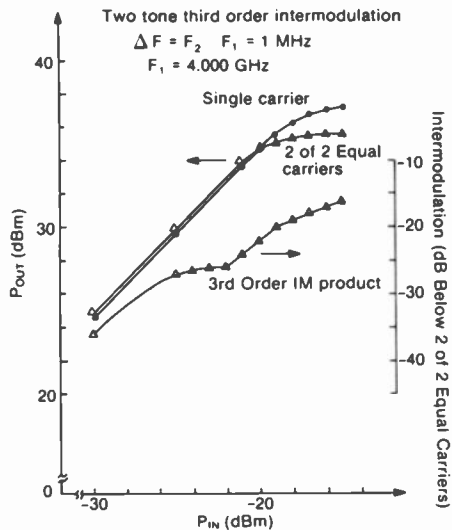


Fig. 9. Two-tone third-order intermodulation.

Figure 10 shows the amplifier total phase shift (defined as the phase shift of an unmodulated carrier measured at the amplifier output for different input power levels), the AM-to-PM conversion coefficient K_p , and the AM-to-PM transfer coefficient K_T . All these measurements confirm that the GaAs FET SSPA exhibits improved linear performance over the TWTA: as an example the AM-to-PM conversion coefficient for a TWTA is of the order of 4 degree/dB compared to less than 1.5 degree/dB for the SSPA. Added to the good amplitude linearity performance already reported, these phase linearity characteristics hold very good promise for satellite systems operating with multiple carriers in one RF channel.

Conclusions

The test results of the 5-W laboratory model and the preliminary results from the

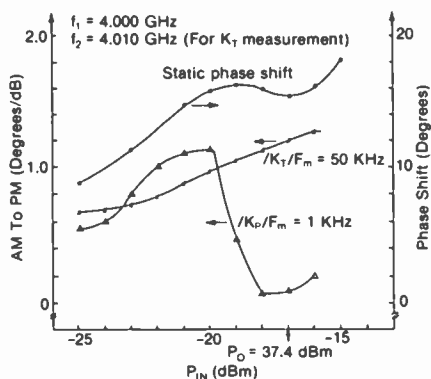


Fig. 10. The amplifier total phase shift, the AM-to-PM conversion coefficient, and the AM-to-PM transfer coefficient confirm that the GaAs FET SSPA exhibits improved performance over the TWTA.

work being carried out on the 6-W, 56-dB gain FET amplifier clearly demonstrate the feasibility of using FETs for power amplification in spaceborne communication transponders. The advances in reliability, efficiency, and power output levels of GaAs field effect power transistors have very rapidly brought these devices forward from the laboratory into the very demanding world of space applications where, both at the full power operating point and backed off, they offer a very powerful challenge to TWTAs.

Acknowledgment

The authors wish to thank Dr. W.S. Wu of the RCA Laboratories and J.N. LaPrade of RCA Astro-Electronics for their technical contributions to this work. They

are also grateful to R.J. Manna and M.T. Cummings of the RCA Laboratories and R.S. Wondowski of RCA Astro-Electronics for their technical assistance.

References

1. Fukuta, M., Suyama, K., Suzuki, H., Nakayama, Y., and Ishikawa, H., "Power GaAs MESFETs With A High Drain-Source Breakdown Voltage," *IEEE Trans. on Microwave Theory and Tech.*, Vol. 24, No. 6 (June 1976).
2. Drago, F., and Goel, J., "GaAs FET Power Amplifiers for Communication Transponders," *Conf. Record, EASCON '78* (Sep 1978).
3. Sechi, F.N., and Huang, H.C., "4 GHz Solid State, Medium-Power Amplifier," RCA Labs. Final Rept., Communication Satellite Corp., Contract No. IS-764 (Apr 1978).
4. Cusack, J.M., Perlow, S.M., and Perlman, B.S., "Automatic Load Contour Mapping for Microwave Power Transistors," *IEEE Trans. on Microwave Theory and Tech., Part II*, Vol. 12, pp. 1146-1152 (1974).



Authors (left to right) F. Drago, B. Dornan, J. Hawley and H. Huang.

Frank Drago joined RCA, Missile and Surface Radar, in 1970. In 1974, he transferred to Astro-Electronics where he has been responsible for the design of a number of microwave solid-state components and is presently involved in the development of high-power GaAs FET microwave amplifiers.

Contact him at:
Astro-Electronics, Princeton, N.J.
Ext. 2423

Ho-Chung Huang joined RCA in 1969 and has been heavily engaged in microwave fabrication technology, device physics, and circuit interaction since 1970. He initiated the GaAs Impatt program at RCA and proposed a high-low junction Impatt structure, now widely adopted, for the improvement of dc-to-rf conversion efficiency. He also directs the fabrication of GaAs MESFETs for high-power applications.

Contact him at:
Microwave Technology Center
RCA Laboratories, Princeton, N.J.
Ext. 3349

Jim Hawley, Systems Engineering, RCA Astro-Electronics, joined Astro-Electronics in 1960. Since joining RCA, Mr. Hawley has worked on television camera design and the development of the TIROS-N and DMSP Transmitters, and translator equipment for the APL Transat Satellite and its ground station. Most recently Mr. Hawley has been working on satellite communication studies for commercial and classified programs.

Contact him at:
Astro-Electronics, Princeton, N.J.
Ext. 2722

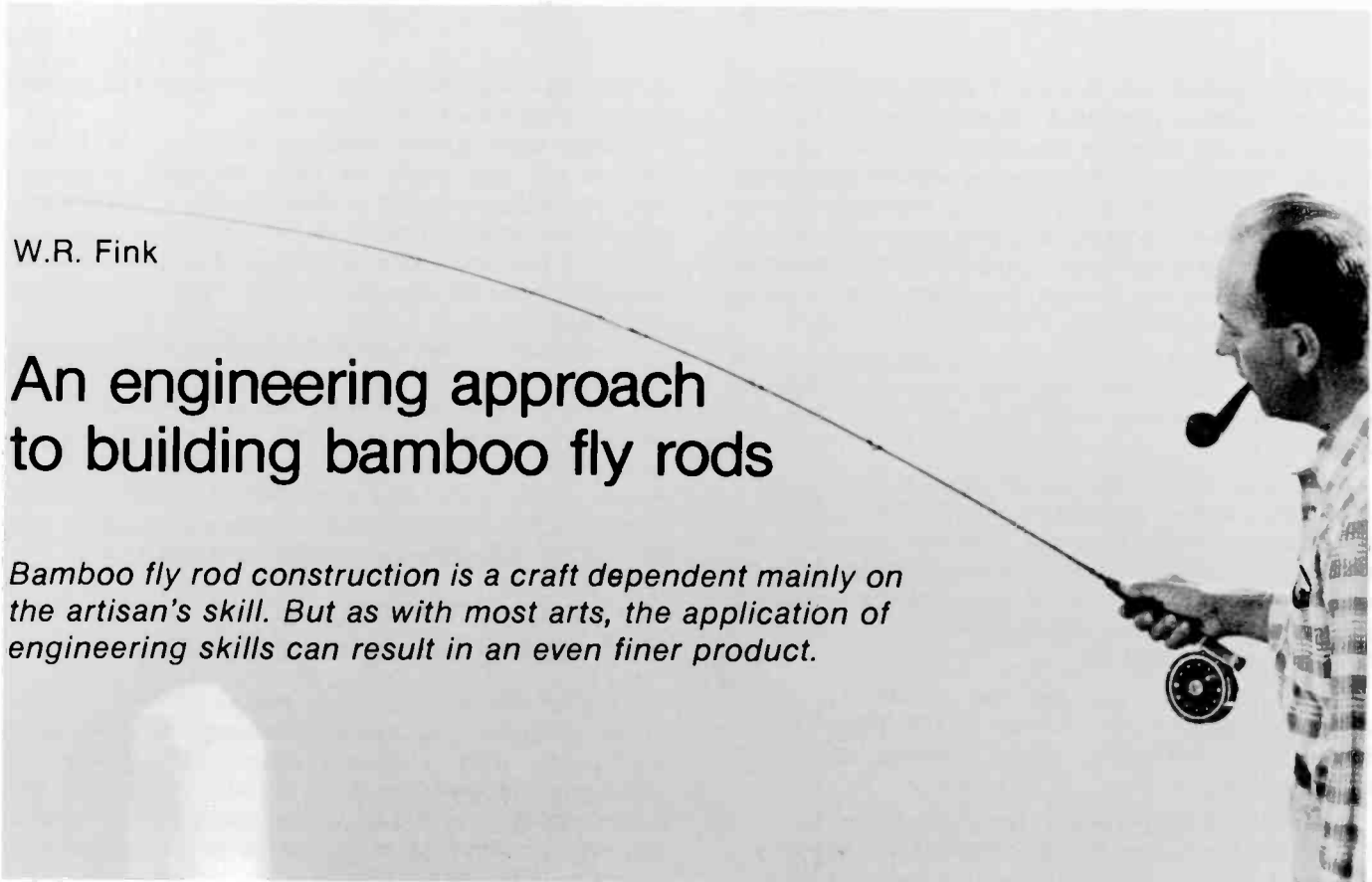
Brian R. Dornan joined RCA, Microwave Technology Center, in 1968. He has worked on microwave tubes and active solid-state microwave devices. This includes extensive work on voltage-controlled oscillators, linearizers, laser modulators, and amplifiers. Mr. Dornan is currently working on microwave FET amplifiers for use on the SATCOM satellite program.

Contact him at:
Microwave Technology Center
RCA Laboratories, Princeton, N.J.
Ext. 3166

W.R. Fink

An engineering approach to building bamboo fly rods

Bamboo fly rod construction is a craft dependent mainly on the artisan's skill. But as with most arts, the application of engineering skills can result in an even finer product.



I greatly enjoy fly fishing and tinkering with fly fishing tackle. When it comes to the choice of fly rod material, I am a bamboo traditionalist. I have followed the romantic evolution of bamboo as the natural successor of the greenheart and lancewood rods used by our angling ancestors. As an amateur rod builder, I attach great importance to what I perceive as the subtle bamboo feel—the special balance and flowing power often mentioned in the rich literature of fly fishing.

Despite this preference for bamboo, I have no real quarrel with the efficient laminated fiberglass rods which dominate the fishing scene today. They are competent wonders of mass production, attractively priced, and practical casting tools. Fiberglass rods, together with the new graphite and even newer boron compounds, are in the forefront of modern technology. Rod design has been enhanced with the introduction of nonmetallic ferrules, computerized taper designs, and constant improvements in materials and processing. For the rod-building hobbyist, however, these materials are inappropriate because of the major investment in capital equipment needed to process them into practical rods.

Bamboo, on the other hand, is ideal for the home craftsman. In fact by its nonuniform, organic nature, bamboo resists mass production techniques, which accounts for the astronomical prices for commercially available bamboo rods today. But isn't it reasonable to expect that some of our rapidly expanding scientific knowledge could be profitably applied to improve bamboo rod construction? This article is a report of my investigations in this area.

Bamboo bondings— which one?

To understand the importance of adhesives in bamboo rod building, a knowledge of rod design and construction is helpful. A bamboo rod section is composed of six individual tapered strips, each of which is an equilateral triangle in cross section, as shown in Fig. 1. These strips are formed by hand planing, using methods which have not changed in a hundred years. Rod builders take pride in holding those crucial sixty-degree strip angles to very tight tolerances; the strip dimension (vertex to opposite flat) is routinely held to within a thousandth of an inch of the design value. The technique involved in handcrafting these precision bamboo strips is really another story in itself and won't be pursued further in this article.

After planing, the six strips are glued together to form a rod section which is hexagonal in cross section. The performance of the bonding used in this construction is, therefore, highly critical. The requirements for a good rod adhesive are: high strength, good flexibility, relatively long cure time, resistance to moisture and temperature extremes, and a color that is cosmetically compatible with spar varnish. While hot animal glue—the traditional choice—gets poor marks for moisture and temperature resistance, it has one outstanding property. Being thermoplastic, it can be softened after curing which permits the rod builder to correct misalignments and bends and produce absolutely straight finished products. But the performance of a hot-animal-glued rod degrades in hot weather, and rods so constructed can delaminate under high-humidity conditions.

The modern thermosetting adhesives have excellent specifications on most counts, except that they deny the rod builder the opportunity to straighten that pesky little

Reprint RE-25-2-15
Final manuscript received July 24, 1979.

jiggle by judicious use of a steam kettle. Thermosetting bonding, therefore, presents a major challenge to bamboo rod builders. My review of developments in the adhesive field identified three bonding types as possible candidates: phenol-formaldehyde resins, used in plywood; phenol-resorcinols, used in boat building; and polyamide-epoxies. Although for the latter family I could find no substantiating data covering its use in high flex stress, high-humidity wood-adhesive applications, it seemed worth a try.

I quickly dismissed the phenol-formaldehyde resins because the formidable heat and pressure processing requirements removed them from the home-hobbyist realm.

The phenol-resorcinols can be cured at room ambient conditions and their parameters meet all the rod-builder's requirements, except for color. The dark reddish-brown hue would be clearly visible in the glue joints under the varnish; even worse, it would highlight the occasional uneven gap that animal glue hides so neatly. My craftsman's vanity ruled out resorcinol.

Epoxy adhesives were my next choice. The epoxy formulation used widely at RCA, EPON 828 with VER-SAMID V40 (E828-V40), has excellent color and specifications.

My next rod, a lightweight eight-foot model for trout fishing, was made using the E828-V40 epoxy. The adhesive mix was proportioned for maximum stiffness. The gluing process took nearly an entire day as I used extreme care in the manual straightening operation. Finally, the glued sections seemed satisfactorily straight. After the prescribed curing period was completed the new rod was unveiled. It felt just great, with worlds of flowing power, yet retaining the desirable bamboo flex characteristic. This rod, a copy of

an existing design, was to be the qualification test sample for epoxy-laminated rod construction.

Fittings were quickly installed, and the first epoxy-bonded rod was ready for tests. Its static deflection characteristics, measured as shown in Fig. 2, were highly satisfactory, showing a definitely better modulus of elasticity than I had been able to achieve with thermoplastic adhesives. The next step was to test it under actual fishing conditions.

Probably no rod was ever worked as hard as that original epoxy-bonded sample. From the frosty cold of early-spring Pocono streams to the blazing heat of mid-summer bass ponds, this rod met all requirements. Even when challenged by the power of Canadian Atlantic salmon, a load far in excess of its trout-rated capability, it performed well. Repeating the deflection measurements at season's end showed no degradation in modulus of elasticity.

Rod taper — the key to performance

Convinced that epoxy bonding was successful, my next area of study examined optimum rod taper design. My early rod-making work consisted simply of copying the dimensions of pleasing rods, thereby duplicating the original designer's performance as closely as possible. But this was far from a satisfying answer to the challenge of achieving improved performance.

A fly rod is basically a cantilever beam. The static deflection of cantilevers is defined by Castigliano's equations for linear moments of inertia. The best performing rods, however, have nonlinear tapers, and it appears that the dynamic characteristic, rather than the static deflection, establish their performance. This suggests

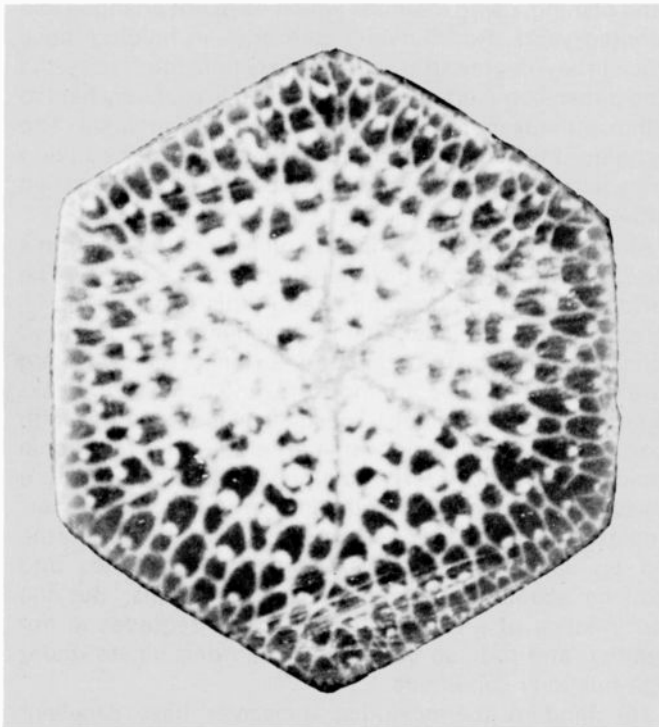


Fig. 1a. Photograph of a typical cross section of a bamboo fly rod showing the glued joints and cellular structure of the material.

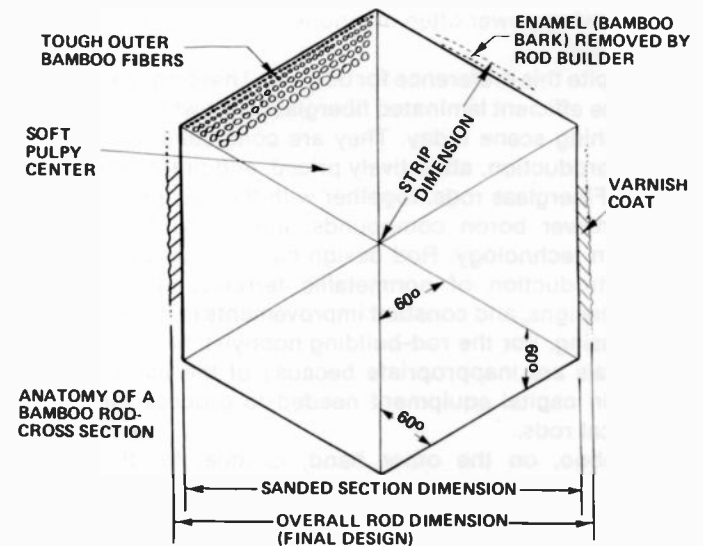


Fig. 1b. Anatomy of a bamboo rod. This cross section shows the geometric configuration and physical characteristics of the six strips that comprise a typical bamboo fly rod. The two fly rods encountered in bamboo rod building. The range of dimensions of the sides of the individual equilateral strips of bamboo for these two rods is 0.122 to 0.190 inch at the butt ends, and 0.041 to 0.047 inch at the tip ends. To put these dimensions in perspective, the 0.041-inch strip dimension at the tip of the 6-foot-8-inch fly rod is *half* the diameter of the cathode in a color TV set (typically 0.084 inch).

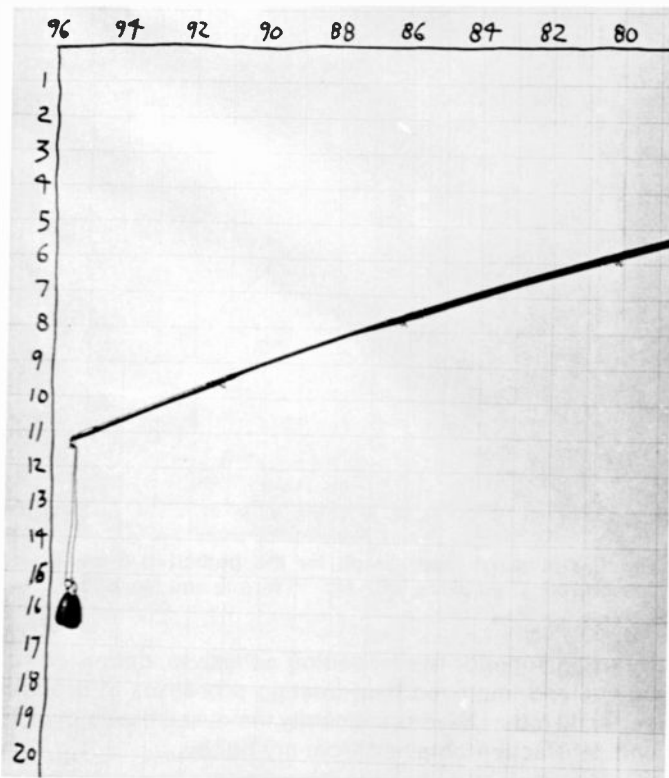


Fig. 2. Measurement of static deflection of an eight-foot fly rod. The weight shown is not critical in value; just enough to flex the rod sufficiently to permit comparative (not absolute) measurement of deflection. In this instance, a 1-ounce Dipsey sinker worked just fine.

that wave motion analysis and energy storage properties would need to be considered in writing a fly rod design algorithm. Human factors such as physical strength, personal preferences, casting skill, and individual style are also considerations. Expert casters and fishermen cannot always agree among themselves as to what constitutes superior fly rod performance. The bottom line seems to be that fly rod design is a matter of trial and error in the evolution of improved designs.

Rod design through analysis

Even if the name of the game is trial and error, I thought that perhaps there still was an engineering approach to improve the process of rod design. Consequently, for the next few months, I bugged my fishing buddies with requests to borrow their collections of bamboo rods. For each rod, I made micrometer measurements at six-inch stations along its length and plotted a graph of length versus diameter on transparent paper, along with detailed notes on that rod's performance. It was then a simple matter to make optical comparisons, using a light table, to identify the common design profiles that characterize the good performers and the dullards.

After measuring and analyzing about thirty rods, a pattern became recognizable. Furthermore, as my data bank grew, the results were reinforced. I found that I was able to measure a rod, and then predict its casting efficiency from its taper curve. My optical comparisons showed that as a

Table I. Design specification for two optimized fly rod types. Rod 1 is an 80-inch, two-piece fly rod with a No. 11 ferrule and No. 5 top. Rod 2 is a 105-inch, two-piece salmon rod with a No. 16 ferrule and a No. 6 top. Refer to Fig. 1b for a definition of the *final*, *strip*, and *sanded* dimensions described in the table.

Butt Section						
Rod Dimensions (in thousandths)						
	Final Design		Strip		Sanded Section	
Station (inches)	Rod #1	Rod #2	Rod #1	Rod #2	Rod #1	Rod #2
0	255	380	122	190	250	375
6	255	380	122	190	250	375
12	239	380	119	190	234	375
18	228	362	114	181	223	357
24	215	344	107	172	210	339
30	200	326	100	163	195	321
36	182	308	91	154	177	303
(40)	173	---	86	---	168	---
42		286		143		281
48		258		129		253
52		255		122		250
Tip Section						
40	173	---	86	---	168	---
42	169	---	84	---	164	---
48	157	---	78	---	152	---
52	---	255	---	122	---	250
54	146	---	73	---	141	---
60	133	230	66	115	128	225
66	118	214	59	107	113	209
72	101	198	50	99	96	193
78	84	184	42	92	79	179
80	83	166	41	83	78	161
84		148		74		143
96		128		64		123
102		104		52		99
105		94		47		89

general characteristic, all superior-performing fly rods are built using a basic compound taper. That is, they carry their thickness well up into the tip section before breaking into a sharper taper. The secondary characteristic or "personality" of the rod is determined by the relative diameter of the lower or butt section. A proportionally thick butt section results in a quick, responsive casting action, and conversely a thin lower section yields a slow, soft, deliberately paced performer. This rod data was readily quantized.

The final step was to tabulate the optimum tapers for rods

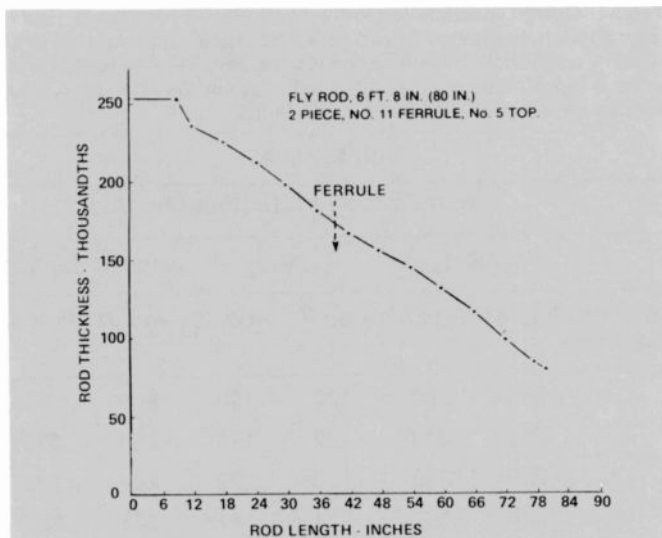


Fig. 3. Optimized taper graph for the optimized 6-foot-8-inch fly rod of Table I. (Two piece, with No. 11 ferrule and No. 5 top.)

of various lengths in terms of dimensions at each six-inch station. The dozen-plus rods that I have built with this optimized data are varied in length and purpose, but all have been very pleasing performers indeed. Specifications for two of these rod designs are shown in Table I, and the optimized taper graphs are shown in Figs. 3 and 4.

Future improvements

The rod-building operation I am studying currently is the heat-treating of the bamboo. The controlled application of heat accomplishes two things: first, the excess moisture is driven off from the bulk bamboo (drying); second, a series of subtle chemical changes occurs in the cellular structure (hardening). I am performing modulus of elasticity experiments with both fast, high heat (>185°C) and slow, low heat (<170°C) heat-treating cycles in conjunction with chemical dehydrating reagents such as ammonium carbonate.

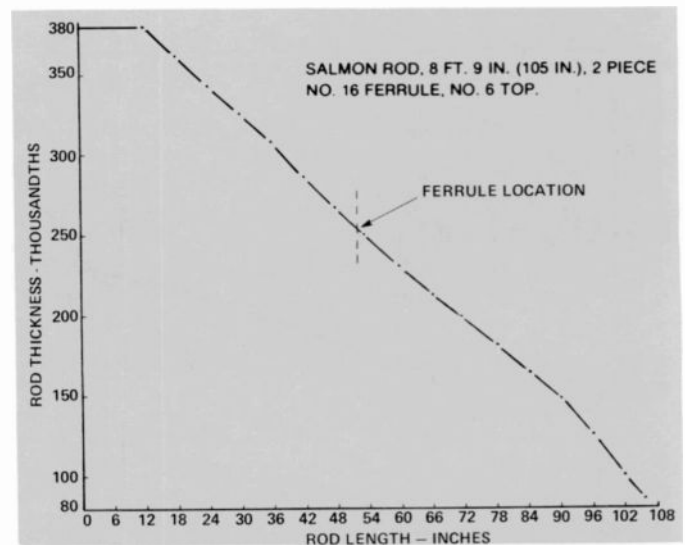


Fig. 4. Optimized taper graph for the optimized 8-foot-9-inch salmon rod. (Two piece, with No. 16 ferrule and No. 6 top.)

By using superior thermosetting adhesives, optimized rod tapers, and improved heat-treating processes to produce better fly rods, I have significantly increased the enjoyment and satisfaction obtained from my hobby.

Bill Fink joined the Central Standards Engineering Activity in 1956. He transferred to the MSR Technical Assurance Group to work on the BMEWS Program in 1957. He is currently a senior member of the MSR Engineering Department responsible for electronic component parts and devices standardization and application engineering on the AEGIS Program.

Contact him at:
Technical Assurance Group
Missile and Surface Radar
Ext. 2338



Dates and Deadlines

Upcoming meetings

Ed. Note: Meetings are listed chronologically. Listed after the meeting title (in bold type) are the sponsor(s), the location, and the person to contact for more information.

OCT 21-25, 1979—**Electrical Insulation & Dielectric Phenomena** (NRC/NAS & EI) Pocono Hershey Resort, White Haven, PA **Prog Info:** Dr. P.K. Watson, Xerox Corporation, Webster Research Center, 800 Phillips Rd., Webster, NY 14580

OCT 22-23, 1979—**4th Conf. on Local Computer Networking** (C. Local Chapter, TCCC) Marquette Inn, Minneapolis, MN **Prog Info:** Kenneth Thurber, Sperry Univac, P.O. Box 3525, St. Paul, MN 55165 (612-456-3806)

OCT 22-24, 1979—**Second Computers in Aerospace Conf.** (C, AIAA, ACM, & NASA) Hyatt House Hotel, Los Angeles, CA **Prog Info:** Richard Erkeneff, McDonnell Douglas Astronautics Co., Dept. 236, Bldg. 13-3, 5301 Bolsa Ave., Huntington Beach, CA 92644 (714-896-4975)

OCT 23-25, 1979—**1979 Test Conf. on Semiconductors** (C, IEEE Phila. Section) Hyatt House, Cherry Hill, NJ **Prog Info:** Raymon Oberly, Prog. Chairman, IBM Corp., P.O. Box 100-53X 057, Kingston, NY 12401

OCT 29-NOV 2, 1979—**Automotive Electronics** (VT, IEEE) Institute of Elec. Engr., Savoy Place, London WC2 **Prog Info:** Conference Dept., IEE, Savoy Place, London WC2R OBL, England

NOV 5-7, 1979—**Engineering Management** (EM, Washington Section, Northern Virginia Section) Stouffers Nat'l Center Inn, Arlington, VA **Prog Info:** Dr. Edward A. Wolff, 1021 Cresthaven Drive, Silver Spring, MD 20903 (301-344-7496 Ofc., 301-439-1152 Home)

NOV 6-8, 1979—**Midcon '79** (Regions 4 & 5, Chicago & Dallas Sections) O'Hare Convention Center, Hyatt Regency - O'Hare, Chicago, IL **Prog Info:** Dale Litherland, Electronic Conventions, Inc., 999 N. Sepulveda Blvd., El Segundo, CA 90245 (213-772-2965)

NOV 6-8, 1979—**Digital Avionics Conference** (AES, AIAA) Sheraton Hotel, Fort Worth, TX **Prog Info:** L.R. Wagner (Vice Chairman), c/o Third Digital Avionics Systems Conference, P.O. Box 12628, Ft. Worth, TX 76116 (817-732-4811, Ext. 4562, 3741, 2344, or 4398)

NOV 12-13, 1979—**1979 9th Annual Chicago Fall Conference on Consumer Electronics** (BCCE) Ramada O'Hare Inn, Rosemont, IL **Prog Info:** Robert Rockwell, Zenith Radio Corp., 1000 Milwaukee Ave., Glenview, IL 60025

NOV 12-13, 1979—**Computing Systems 8th Texas Conference** (C) Southern Methodist University, Dallas, TX **Prog Info:** T.N. Rao, Computer Science Dept., Southern Methodist Univ., Dallas, TX 75275

NOV 14-16, 1979—**Intl Micro and Mini Computer Conference** (C, Oklahoma City & Houston Sec. & Reg. 5) Astro Village, Houston, TX **Prog Info:** Dr. Sam Lee, School of Elec. Engr. & Computer Science, Univ. of Oklahoma, 202 W. Boyd, Norman, OK 73019 (405-325-4721)

NOV 18-21, 1979—**Micro 12** (C, ACM, SIGMICRO) Hershey, PA **Prog Info:** Harry Hayman, Micro 12, P.O. Box 639, Silver Spring, MD 20901 (301-439-7007)

NOV 27-29, 1979—**Data Communications Symposium** (COM, GE, AES, C) Asilomar State Beach, Pacific Grove, CA **Prog Info:** Jack Salz, Bell Laboratories, Holmdel, NJ 07733 (201-949-3000)

NOV 27-29, 1979—**National Telecommunications Conference** (COM, Washington Section) Shoreham Americana, Washington, DC **Prog Info:** John N. Birch, Dept. of Defense, 3311 Marlborough Way, College Park, MD 20740 (301-935-0684)

DEC 3-5, 1979—**Electron Devices Meeting** (ED) Washington Hilton, Washington, DC **Prog Info:** Ms. Sarah Cooper, Courtesy Associates, 1629-K Street, N.W., Washington, DC (202-296-8100)

DEC 3-5, 1979—**Winter Simulation Conference** (SMC, C) Holiday Inn—Embarcadero, San Diego, CA **Prog Info:** Mr. Mitchell G. Spiegel, FedSim/Na, Washington, DC 20330 (202-274-7910)

DEC 3-6, 1979—**9th International Symposium on Acoustic Imaging** (SU) The Houston Grand Hotel, Houston, TX **Prog Info:** Keith Wang, Dept. of Elec. Engr., Univ. of Houston, Houston, TX 77004 (713-749-4419)

DEC 10-15, 1979—**Infrared and Near Millimeter Waves** (MTT) Americana of Bal Harbour, Miami Beach, FL **Prog Info:** K.J. Button, MIT National Magnet Lab., Cambridge, MA 02139 (617-253-5561)

DEC 12, 1979—**Computer Networking Sym-**

posium (C, NBS) Gaithersburg, MD **Prog Info:** Harry Hayman, P.O. Box 639, Silver Spring, MD 20901 (301-439-7007)

DEC 12-14, 1979—**18th Conference on Decision and Control** (CS) Galt Ocean Mile Hotel, Fort Lauderdale, FL **Prog Info:** Prof. Stephen Kahne, Dept. of Systems Engineering, Case Institute of Technology Case Western Reserve Univ., Cleveland, OH 44106 (216-368-4076)

JAN 7-9, 1980—**Pacific Telecommunications Conference** (COM) Ilikai Hotel, Honolulu, HI **Prog Info:** Richard J. Barber, 2424 Maile Way, #704, Honolulu, HI 96822 (808-948-7879)

JAN 7-10, 1980—**Photovoltaic Specialists Conference** (ED) Town & Country Hotel, San Diego, CA **Prog Info:** Prof. C. Backus, Arizona State Univ., Coll. of Engr. & Applied Science, Tempe, AZ 85281 (602-965-3857)

JAN 22-24, 1980—**Reliability & Maintainability Symposium** (R) San Francisco Hilton and Tower, San Francisco, CA **Prog Info:** A.M. Smith, General Electric Co., Fast Breeder Reactor Dept., 310 De Guigne Dr., M/C/S-65, Sunnyvale, CA 94086 (408-297-3000, Ext. 627)

JAN 23-30, 1980—**Integrated & Guided Wave Optics** (QEA, OSA) Hyatt Lake Tahoe, NV **Prog Info:** Joan Connor, Optical Society of America, 2000 L St., NW, Suite 620, Washington DC 20036 (202-293-1420)

JAN 29-31, 1980—**Aerospace and Electronic Systems Winter Convention (WINCON)** (AES, Los Angeles Council) Sheraton Universal Hotel, N. Hollywood, CA **Prog Info:** Phillip G. Halamandaris, Gould Inc., —NAVCOM Systems Div., 4323 Arden Drive, El Monte, CA 91731 (213-442-0123, Ext. 602)

FEB 13-15, 1980—**Intl. Solid State Circuits Conference** (SSC, San Francisco Sec.) Hilton Hotel, San Francisco, CA **Prog Info:** Lewis Winner, 301 Almeria Ave., Coral Gables, FL 33134 (305-446-8193)

FEB 25-28, 1980—**COMPCON Spring '80** (C) Jack Tar Hotel, San Francisco, CA **Prog Info:** Harry Hayman, P.O. Box 639, Silver Spring, MD 20901 (301-439-7007)

FEB 26-28, 1980—**Laser and Electro-Optical Systems/Inertial Confinement Fusion** (QEA, OSA) Town & Country Hotel, San Diego, CA **Prog Info:** Joan Connor, Optical Society of America, 2000 L Street N.W. (Suite 620), Washington, DC 20036 (202-293-1420)

MAR 3-5, 1980—**NCC Office Automation Congress (C) Prog Info:** Harry Hayman, P.O. Box 639, Silver Spring, MD 20901 (301-439-7007)

MAR 4-6, 1980—**International Zurich Seminar on Digital Communications** (Switzerland Sec. COM (Cooperating)) Swiss Federal Institute of Tech. on Digital Communications, Zurich, Switzerland **Prog Info:** Prof. P.E. Leuthold, Eidgenossische Technische Hochschule Zurich Institut Fur Hochfrequenztechnik, Sternwartstrasse 7, Zurich, Switzerland (Tele.: T41-1-326211)

MAR 11-14, 1980—**Computer Architecture for Non-numeric Processing 5th Workshop (C) Pacific Grove, CA Prog Info:** Harry

Hayman, P.O. Box 639, Silver Spring, MD 20901 (301-439-7007)

MAR 16-18, 1980—**Particle Accelerator Conference (NPS) Prog Info:** Dr. Louis Costrell, NPS Meetings Coordinator, National Bureau of Standards, C333 Radiation Physics, Washington, DC 20234

MAR 24-25, 1980—**Radio Transmitters and Modulation Techniques (IEE, IERE) IEE,** Savoy Place, London, WC2 **Prog Info:** Conference Dept., IEE, Savoy Place, London WC2R OBL, England

MAR 24-27, 1980—**Magnetic Fluids 2nd Intl. Conf. (MAG) Marriott Inn, Orlando, FL Prog Info:** Markus Zahn, Dept of EE, Univ. of Florida, Gainesville, FL 32611, (904-392-4964 Ofc., 904-392-4960 Sect.)

Calls for papers

Ed. Note: Calls are listed chronologically by meeting date. Listed after the meeting (in bold type) are the sponsor(s), the location, and deadline information for submittals.

JAN 7-10, 1980—**14th IEEE Photovoltaic Specialists Conf., San Diego, CA Deadline Info:** 7/15/79 300-word abstract to: Charles E. Backus, College of Engineering and Applied Sciences, Arizona State University, Tempe AZ 85281

FEB 26-28, 1980—**CLEOS/ICF 80 (IEEE) San Diego, CA Deadline Info:** 10/1/79 35 word abstract/2-500 word summary to CLEOS, c/o Optical Society of America, Suite 620, 2000 L Street, N.W., Washington, DC 20036

Pen and Podium

Recent RCA technical papers and presentations

To obtain copies of papers, check your library or contact the author or his divisional Technical Publications Administrator (listed on back cover) for a reprint.

Advanced Technology Laboratories

G.J. Ammon

Wideband optical disc data recorder systems—Proceedings, SPIE 23rd Intl. Tech. Symp., San Diego, CA (8/28-30/79)

K.R. Andersen|Staff

LSI Testing—a tutorial-reliability section—IEEE Computer Society LSI Tutorial, Los Angeles, CA (1/22/79)

D.A. Gandolfo|A. Boornard|L.D. Elliott
D.S. Kent|B.M. McCarthy|J.R. Tower
Charge coupled devices: design, operation and application—Princeton Section of IEEE, Princeton, NJ (4/23/79)

D.A. Gandolfo|J.R. Tower
J.I. Pridgen|S.C. Munroe
Analog-binary CCD correlator: A VLSI signal processor—IEEE Trans. on Electron Devices, Vol. ED-26, No. 4, pp. 596-603 and IEEE J. of Solid State Circuits, Vol. SC-14, No. 2, pp. 518-525 (Joint Special Issue) (4/79)

E.P. Herrmann|D.A. Gandolfo
Programmable CCD tapped delay line—IEEE Trans.-Electron Devices, Vol. ED-26, No. 2, pp. 117-122 (2/79)

R.F. Kenville
The optical disc as a data storage medium—Proceedings, ICCH/4 Data Bases in the Humanities and Social Sciences Con., Hanover, NH (8/19-22/79)

R.F. Kenville

Digital data application of the optical disc—IGC's Fifth Annual Analysis of New Developments in Techniques, Markets and Applications, Carmel, CA (7/22-24/79)

T.D. Michaelis

Laser diode evaluation for optical analog link—IEEE Cable Television Transactions, Vol. CATV-4, No. 1, pp. 30-42 (1/79)

A.B. Sally

Research and development in Advanced Technology Laboratories—AFCEA Exhibit, Washington, DC (6/19-21/79)

D.P. Schnorr|Staff

Chapter 13: assembly repair—Printed Circuits Handbook—Second Edition by C.F. Coombs, McGraw Hill Co. (1979)

W.M. Skiba

Interfacing the pro-log series 90 PROM programmable to the PRIME 400—1979 Nat'l. Prime Users Conf., Denver, CO (6/25-27/79)

W.W. Thomas|Staff

Industry views of Government specifications and standards—Army Logistics Management Center, Ft. Lee, VA (Defense Specifications Management Course) (1/10/79)

W.W. Thomas|Staff

Reliability specification tailoring—Proceedings, '79 Annual Reliability and Maintainability Symposium, Shoreham Americana, Washington, DC (1/23/79)

Automated Systems

M.J. Cantella|J.J. Klein
E. Kohn|W. Kosonocky

A Schottky barrier monolithic IRCCD focal plane array—27th National IRIS, San Diego, CA (5/79)

B.R. Clay

Laser rangefinder optics—Laser Optics Seminar, U. of Lowell, Lowell, MA (5-79)

H.L. Fischer

Non-electronic applications for ATE—Keynote Speaker ATE Seminar/Exhibit, Danvers, MA (6/79)

J.C. Haggis|R.J. Monis

Co-Leaders at the ATE Seminar/Exhibit workshop for hybrid board test techniques, Danvers, MA (6/6/79)

B.E. Hendrickson|L.S. O'Hara

Development of a 2.06 μ m eye safe laser rangefinder—1979 IEEE/OSA Conf. on Laser Eng. & Applications, Washington, DC (5/79)

M.L. Johnson

Moderator, Boston IEEE Reliability Spring Seminar, Waltham, MA (4/79)

J.M. Laskey

Role of ATE in supporting tomorrow's technology—SOLE meeting at Ft. Monmouth, NJ (5/79)

F.R. Shirak

Automated test systems for the YAH-64—American Helicopter Society Annual Meeting, Washington, DC (5/79)

Government Communications Systems

P. Pierson

Design considerations for a flexible high resolution film recording system—SPIE's 23rd Annual Intl. Tech. Symposium & Exhibit, San Diego, CA (8/27-30/79) *Conf. Record*

D. Herzog

Description of a dry film tactical laser beam recorder—SPIE's 23rd Annual Intl. Tech. Symposium & Exhibit, San Diego, CA (8/27-30/79) *Conf. Record*

Laboratories

M. Ettenberg

A statistical study of the reliability of oxide-defined stripe CW lasers of (AlGa)As—*J. of Applied Physics*, Vol. 50, No. 3 (3/79)

M. Ettenberg|H. Kressel|I. Ladany

Long-term lifetimes of C.W. (AlGa)As laser diodes at room temperature—*Electronics Letters*, Vol. 14, No. 25, pp. 815-816 (12/7/78)

M. Ettenberg|C.J. Nuese|H. Kressel

The temperature dependence of threshold current for double-heterojunction lasers—*J. Appl. Physics*, Vol. 50, No. 4 (4/79)

D.G. Fisher|G.H. Olsen

Properties of high sensitivity GaP/In_xGa_{1-x}P/GaAs:(Cs-O) transmission photocathodes—*J. Appl. Physics*, Vol. 50, No. 4 (4/79)

P.J. Flanders|G. Kaganowicz|Y. Takei

Magnetostriction and stress-induced playback loss in magnetic tapes—*IEEE Transactions on Magnetics*, Vol. MAG-15, No. 3 (5/79)

H. Friedrich|W.F. Kosonocky

Editorial College for the April 1979 joint special issue on VLSI—*IEEE J. of Solid-State Circuits*, Vol. SC-14, No. 2 (4/79)

W. Kern|G.L. Schnable

Low-pressure chemical vapor deposition for very large-scale integration processing—a review—*IEEE Transactions on Electron Devices*, Vol. ED-26, No. 4 (4/79)

H. Kiess

On the limits of the electrophotographic process—*RCA Review*, Vol. 40 (3/78)

C.W. Magee

Depth profiling of n-type dopants in Si and GaAs using Cs⁺ bombardment negative secondary ion mass spectrometry in ultrahigh vacuum—*J. of the Electrochemical Society*, Vol. 126, No. 4 (4/79)

V. Mangulis

Criteria for optimum distribution of fire control system radar blockage—*Naval Engineers Journal*, pp. 77-81 (8/79)

V. Mangulis

Taylor-type amplitude distribution for circular arrays—*Antennas and Propagation*, Vol. 1, IEEE Antenna and Propagation Society, (6/18-22/79)

V. Mangulis

Effective sidelobe levels due to scatterers—*IEEE Transactions on Aerospace and Electronic Systems*, Vol. AES-15, No. 3 (5/79)

J.T. McGinn|A.M. Goodman

The effects of oxygen doping and subsequent annealing in nitrogen on the structure of polycrystalline silicon—*Applied Physics Letters*, Vol. 34, No. 9 (5/1/79)

D.A. Peters|C.A. Deckert

Removal of photoresist film residues from wafer surfaces—*J. of the Electrochemical Society*, Vol. 126, No. 5 (5/79)

A. Rosen|R.U. Martinelli

A. Schwarzmann|G.J. Brucker|G.A. Swartz High-power low-loss PIN diodes for phased-array radar—*RCA Review*, Vol. 40, No. 1 (3/79)

W.C. Stewart

Signal delay in Turner's beam-indexing kinescope—*IEEE Transactions on Electron Devices*, Vol. ED-26, No. 6 (6/79)

C.W. Struck|W.H. Fonger

Linear and derivative nuclear operators in single-*h_ν*, multiple-coordinate models of luminescence centers—*Physical Review B*, Vol. 19, No. 9 (5/1/79)

T.M. Wagner

A computer evaluation of colorimetric effects of differential gain and differential phase distortions in color TV receivers having phosphors and demodulation matrices different from NTSC—*RCA Review*, Vol. 40 (3/79)

H.A. Weakliem|D. Redfield

Temperature dependence of the optical properties of silicon—*J. Appl. Phys.*, Vol. 50, No. 3 (3/79)

A.E. Widmer|M.L. Hitchman

Oxygen determination in SIPOS using a differential thickness measurement—*J. of the Electrochemical Society*, Vol. 125, No. 10 (10/78)

R. Williams

Schottky barriers at the interface between amorphous silicon and electrolytes—*J. Appl. Phys.*, Vol. 50, No. 4 (4/79)

C.P. Wu|C.W. Magee

Pulsed laser annealing of ion-implanted polycrystalline silicon films—*Applied Physics Letters*, Vol. 34, No. 11 (6/79)

Missile and Surface Radar

E.M. Allen

Wideband analysis of a rapidly tumbling

rocket body (Object 11030)—Eleventh Annual NORAD Spacecraft Identification Conference, Air Force Academy, Colorado Springs, CO (8/79)

R.D. Bachinsky|S.I. Newburg

LRIR near earth imaging results—Eleventh Annual NORAD Spacecraft Identification Conference, Air Force Academy, Colorado Springs, CO (8/79)

J.A. Bauer

Design automation at RCA MSR—IEEE Computer Packaging Group, New York City (6/79)

B.F. Bogner

Vehicular traffic radar handbook for attorneys—Brehm Corp., Mt. Holly, NJ (6/79)

M.W. Buckley

Project Management—Instructor, IEEE Continuing Education, Cleveland, OH (6/5-6/79; Billings, MT (6/9-10/79)

D. Fennessy

Details of COSMOS 1065 analysis—Eleventh Annual NORAD Spacecraft Identification Conference, Air Force Academy, Colorado Springs, CO (8/79)

D. Fennessy

Further analysis of COSMOS 816, 885, 913, 965, and 1065 associated pieces—Eleventh Annual NORAD Spacecraft Identification Conference, Air Force Academy, Colorado Springs, CO (8/79)

G.R. Field

RCA Minorities in Engineering Program—Multi-Cultural Conference, Washington, DC (6/79) *Conference Proceedings*

B.A. Francis

Motion analysis of SEASAT-A using wide-band imaging—Eleventh Annual NORAD Spacecraft Identification Conference, A8

B.A. Francis

Motion analysis of SEASAT-A using wide-band imaging—Eleventh Annual NORAD Spacecraft Identification Conference, Air Force Academy, Colorado Springs, CO (8/79)

I.E. Goldstein, et al

Summer course: combat systems engineering and ship design—MIT, Cambridge, MA (8/79) (Handout material for course)

J. Golub|J.A. Clancy (NSWC)

Drummer Computer Simulation Conference, Toronto, Canada (7/18/79) *Conf. Proceedings*

M.C. Johnson

AEGIS low voltage power supply system—1979 Power Electronics Specialists Conference (IEEE), San Diego, CA (6/79) *PESC Record*

O.L. Patterson

Inter-Sensor Association and Correlation—USAF Warning and Attack Assessment Symposium-ANSER, Arlington, VA (7/24-26/79)

L.C. Pickus

Conducted Communication and Report Writing Workshop, Sheraton-Boston, Boston, MA (6/79)

R.J. Rader

Advanced software design techniques—Petrocelli Books, Inc. (6/79)

M.I. Rozansky

Doppler servo tracker with frequency synthesizer feedback—*RCA Review*, Vol. 40, No. 2 (6/79)

M.I. Rozansky|F. Haber

Pseudotransfer function to characterize a hard limiter—*AES Transactions*, Vol. AES-15, No. 3, pp. 457-459 (5/79)

A. Schwarzmann

High-power low-loss PIN diodes for phased-array radar—*RCA Review*, Vol. 40, No. 1 (3/79)

D. Staiman

Large aperture solid state antenna for space-radar—National Radio Science Meeting (URSI), University of Washington (6/79)

H. Urkowitz|N.A. Ricciardi

Upgraded BMEWS discrimination experiments—USAF Warning and Attack Assessment Symposium-ANSER, Arlington, VA (7/24-26/79)

National Broadcasting Company

J. Frischette

NBC planning for the 1980 Olympics—1979 National Association of Broadcasters Convention (NAB), Dallas, TX (3/28/79)

M. Negri

Tracking chroma keys with digital video processors—13th SMPTE Television Conference, San Francisco, CA (2/3/79)

Patents

Automated Systems

Sutphin, E.M., Jr.

Ignition spark zone duration circuit—4163192 (assigned to U.S. government)

Commercial Communications Systems

Dischert, R.A.

Automatic setup system for television cameras—4158208

Goldschmidt, A.M.|Hedlund, L.V.

Tracking servo system for video disc player/recorder—4160270

Thomas, R.G.|Sadashige, K.

Dropout compensator with proportional duration dropout detector—4158855 (assigned to U.S. government)

Consumer Electronics

Beyers, B.W., Jr.|Suchko, A.J.

Television system scheduler—4162513

Carter, G.W.

Mixer injection voltage compensation circuit—4160213

Harlan, W.E.

Video signal translating circuit—4158852

Molinari, T.E.

Printed circuit impedance transformation network with an integral spark gap—4160210

Smith, J.L.

Magnetizing apparatus and method for use in correcting color purity in a cathode ray tube and product thereof—4159456

Smith, J.L.

Magnetizing apparatus and method for producing a statically converged cathode ray tube and product thereof—4162470

Torrington, L.A.

Video disk package—4159827

Laboratories

Alphonse, G.A.|Vilkomerson, D.H.R.

Hurley, B.

Random phase diffuser for reflective imaging—4153894 (assigned to U.S. government)

Anderson, C.H.|Marlowe, F.J.

System and method for keying video information to electron beam deflection—4160194

Berkman, S.|Kim, K.|Temple, H.E.

Apparatus for the production of ribbon-shaped crystals—4157373

Curtice, W.R.

Pulse train generator—4158784

Curtice, W.R.

Exclusive-OR circuit—4160919

Desai, N.V.|Himics, R.J.

Method for purifying methyl alkyl siloxane lubricants—4159276

Dingwall, A.G.

Method of making a substrate contact for an integrated circuit—4159561

Firester, A.H.|Heller, M.E.

Apparatus for the determination of focused spot size and structure—4160598

Gale, M.T.|Knop, K.

Technique for recording micropicture-information on a diffractive subtractive filter embossing master—4157220

Goldman, A.

Aqueous photoresist comprising casein and methylol acrylamide—4158566 (assigned to U.S. government)

Hanak, J.J.

Photodeposition of CRT screen structures using cermet IC filter—4157215

Hanak, J.J.

Inverted amorphous silicon solar cell utilizing cermet layers—4162505

Hawrylo, F.Z.

Heterojunction semiconductor device—4158849

Hernqvist, K.G.

Method of reducing absorption losses in fused quartz and fused silica optical fibers—4157253 (assigned to U.S. government)

Hopta, D.F.|Beelitz, H.R.

Switched current regulator—4160943

Hsu, S.T.

Floating gate solid-state storage device—4162504

Keizer, E.O.

Keel-tipped stylus for video disc systems—4162510

Kovac, M.G.

CCD electrode and channel structure for 180 degree turn—4160262

Levine, P.A.

CCD comb filters—4158209

Marinelli, D.P.

Apparatus for depositing epitaxial semiconductor from the liquid phase—4159694

Marlowe, F.J.|Dawson, R.H.

Digital memory addressing system—4160273

Mawhinney, D.D. | Rosen, A.
Turski, Z. | Wolkstein, H.J.

Microwave power limiter comprising a single-gate FET — 4162412

Mezrich, R.S. | Robbins, C.W.

Portable ultrasonic measurement system — 4123944 (assigned to U.S. government)

Toda, M. | Matsumoto, Y. | Osaka, S.

Velocity correction system for video disc player — 4162511

Weitzel, C.E. | Scott, J.H., Jr.

Planar semiconductor devices and method of making the same — 4160260

Williams, R. | Bloom, A.

Process for storing solar energy in the form of an electrochemically generated compound — 4160816 (assigned to U.S. government)

Wine, C.M.

System for reducing the number of binary signals representing channel numbers — 4158815

Wine, C.M.

Memory type tuning system with provisions for skipping nonpreferred tuning positions — 4158816

Missile and Surface Radar

Martinson, L.W.

Correlator/convolver using a second shift register to rotate sample values — 4161033

Perry, R.P.

Parallel transform analyzer for performing the chirp Z transform — 4159528

Stachejko, V.

Precision microwave delay circuit and method — 4160220

Picture Tube Division

Butterwick, G.N.

Electron beam tube — 4160188 (assigned to U.S. government)

Morrell, A.M.

Cathode ray tube having corrugated shadow mask with slits — 4162421 (assigned to U.S. government)

Nolan, R.A.

Implosion protected CRT — 4158419

Wardell, M.H., Jr.

CRT with tension band adapted for pusher-type tensioning and method for producing same — 4160510

Solid State Division

Ahmed, A.A.

Voltage regulators — 4160201

Ahmed, A.A.

Current amplifier capable of selectively providing current gain — 4160944

Dietz, W.F.

Regulator with short circuit protection — 4162434

Hoover, M.V.

Complementary-FET driver circuitry for push-pull class B transistor amplifiers — 4159450

Neilson, J.M.

Semiconductor device — 4158206

Schade, O.H., Jr.

Anti-latch circuit for amplifier stage including bipolar and field-effect transistors — 4158178

Tomasetti, C.M. | McDonie, A.F.

Red sensitive photocathode having an aluminum oxide barrier layer — 4160185

Wittlinger, H.A.

Long-tailed-pair with linearization network — 4159449

Engineering News and Highlights

Staff announcements

Americom

A reorganization of responsibilities has been announced by **Harold W. Rice**, Vice President, RCA American Communications. **Lawrence Driscoll** is Manager, Broadcast Services; **Lou Donato** has responsibility for Network Relations; **Bradley Dusto** is Manager, Video Services; **Jim Grady** is Manager, Audio Services; and **William Kopacka** is Manager, CATV Services.

Astro-Electronics

Paul Wright is appointed Vice President and General Manager. He will report to **John D. Rittenhouse**.

Broadcast Systems

Stanley E. Basara is appointed Division Vice President and General Manager, Broadcast Systems. Mr. Basara will report to **J. Edgar**

Hill, Division Vice President and General Manager, Commercial Communications Systems Division.

Consumer Electronics

Jack K. Sauter is elected Vice President and General Manager, Consumer Electronics Division, by the Board of Directors of RCA Corporation. He will report to **Roy H. Pollack**, Executive Vice President.

Joseph L. Sekula, Jr. is appointed Manager, Quality Assurance Engineering. He will report to **Aldo R. Neyman**, Manager, Plant Quality Control.

Richard E. Molyneux is appointed Manager, Processing Engineering. He will report to **J.B. Thomas**, Manager, Manufacturing Engineering.

Global Communications

Joe T. Swaim was elected Vice President, Engineering, by the Board of Directors of

RCA Global Communications. He will report to **Eugene F. Murphy**, President. Mr Swaim's organization was announced as follows: **Brian J. Mair**, Manager, Systems Engineering; **John F. Scannapieco**, Manager, Project Engineering; **John P. Shields**, Manager, Project and Implementation Engineering; **Louis P. Correard**, Manager, Project Engineering; **Alexander A. Avanesian**, Manager, Project Engineering; **Solomon J. Nahum**, Manager, Engineering Services and Construction; **William Katz**, Administrator, Project Control and Administration.

David Mer, Manager, Operations and Engineering, announces the organization as follows: **Samuel A. Thompson**, Manager, Operations; **James M. MacKenzie**, Administrator, Engineering; **Morris Olcerst**, Administrator, Customer Services.

Government Communications Systems

Joseph B. Howe is appointed Division Vice President and General Manager, Government Communications Systems. Mr. Howe

Roy H. Pollack elected Executive Vice President



Edgar H. Griffiths has announced the election of **Roy H. Pollack** as Executive Vice President. In his new position, Mr. Pollack has overall responsibility for the company's Consumer Electronics Division, the Solid State Division and the "SelectaVision" VideoDisc Operation. He also supervises the company's Government and Commercial Systems. Prior to this appointment, he had been a Group Vice President of the Corporation. He was elected to the RCA Board of Directors on October 5, 1977.

Before becoming Group Vice President, Mr. Pollack was Vice President and General Manager, Consumer Electronics since June 1974. In this capacity, he directed the company's various Consumer Electronics Operations.

Mr. Pollack first joined RCA in 1950, serving in a series of marketing management and engineering positions at RCA's Solid State and Electronic Component Divisions in Somerville, N.J. and Mountaintop and Lancaster, Pa.

Dr. James Vollmer elected Group Vice President



Dr. James Vollmer has been elected an RCA Group Vice President by the company's Board of Directors and assigned responsibility for the Commercial Communications Systems Division and the Government Systems Division. Before his promotion, Dr. Vollmer was Division Vice President and General Manager, Government Systems Division, a position he had held since September, 1976. Dr. Vollmer joined RCA in 1959 as a physicist in the Applied Research activity.

The Commercial Business Operation, based in Camden, N.J., is composed of four units: Avionics Systems, Van Nuys, Calif.; Broadcast Systems, Camden; Cablevision Systems, North Hollywood, Calif.; and Mobile Communications Systems, Meadow Lands, Pa. The Government Organization, with headquarters in Moorestown, N.J., is also made up of four business units: Astro-Electronics, Princeton, N.J.; Automated Systems, Burlington, Mass.; Government Communications Systems, Camden; and Missile and Surface Radar, Moorestown.

John D. Rittenhouse Appointed Division Vice President



The promotion of **John D. Rittenhouse** to Division Vice President and General Manager, RCA Government Systems Division, Moorestown, N.J., was announced recently.

Mr. Rittenhouse had been Division Vice President and General Manager, RCA Government Communications Systems, Camden, N.J., one of the Division's four business units, since September 1975. In his new capacity he reports to Dr. James Vollmer, Group Vice President, and his predecessor as Division chief executive.

Mr. Rittenhouse joined RCA in 1958 as an engineer in the company's Applied Research activity, and earned his master's degree in electrical engineering as a member of the RCA Graduate Study program. He was named leader in the Electro-Mechanics section of Applied Research four years after joining RCA, and has held managerial positions since 1964.

will report to **John D. Rittenhouse**, Division Vice President and General Manager, Government Systems Division.

Laboratories

Appointment of **Herbert J. Wolkstein** as Manager, Space and Countermeasure Programs, has been announced by **Dr. Fred Sterzer**, Director of the Microwave Technology Center.

Appointment of **Samuel Cohen** as Director, Patents — Electronic Systems, and **Birglt E. Morris** as Director, Patents — Electronic Materials and Devices, has been announced by **John V. Regan**, Vice President, Patent Operations.

Picture Tube Division

Joseph H. Colgrove is elected Vice President and General Manager, Picture Tube

Division, by the Board of Directors of RCA Corporation. He will report to **Julius Koppelman**, Executive Vice President.

David N. Herd is appointed Manager, Project Engineering. He will report to **Gene W. Duckworth**, Director, Operations-Soviet Contract.

SelectaVision

James M. Alic is appointed Staff Vice President, SelectaVision, VideoDisc Strategic Planning. He will report to **Roy H. Pollack**, Executive Vice President.

Solid State Division

Robert S. Pepper, Vice President and General Manager, Solid State Division, announced the organization as follows: **Walter J. Glowczynski**, Division Vice President,

Finance; **Ben A. Jacoby**, Division Vice President, Marketing; **Donald Kirchoffer**, Division Vice President, Industrial Relations; **Richard C. Pinto**, Division Vice President, Integrated Circuits; **Ralph E. Simon**, Division Vice President, Electro-Optics and Power Devices; **Carl R. Turner**, Division Vice President, Product Assurance and Planning.

Parker T. Valentine, Manager, Operations Support, announces that the Engineering Publications and Standards organization is transferred to the staff of the Manager, Operations Support. **Anthony J. Bianculli** will continue as Manager, Engineering Publications and Standards.

James T. O'Brien is appointed to the newly created position of Manager, Engineering. He will report to **Frederick R. Hughes**, Manager, Solid State Emitters and Systems.

Stotts is Assistant Editor of the *RCA Engineer*



Betty C. Stotts was recently appointed Assistant Editor of the *RCA Engineer*. She succeeds Bill Lauffer, who took a teaching position at Prince George Community College in Maryland. Ms. Stotts began her career in the Technical Publications Department of the Perkin Elmer Data Communications Systems in 1974 as an editor/technical writer of minicomputer manuals. In 1977, she moved to The Bendix Corporation Electric and Fluid Power Division where she worked as a Technical Writer and Assistant Supervisor of the Publications Department. She joined RCA American Communications in April 1979 where her duties as Technical Administrative Specialist included proposal preparation, report writing and Technical Librarian functions.

Diaconoff Appointed Ed Rep for Automated Systems



Peter Diaconoff is the new Ed Rep for Automated Systems, Government and Commercial Systems Division, Burlington, Massachusetts. He joined RCA in January of this year as Senior Technical Writer.

Mr. Diaconoff holds a doctorate in political science from Indiana University and has taught government and political science courses at Chicago State University. As an editor/writer, he has edited and contributed articles to weekly *Petroleum Report* and *Daily Digest* of the Norwegian Press, written reports on automatic traffic control systems and international computer market trends, and written training materials on heavy diesel-electric vehicle power systems. Contact him at: Automated Systems, Burlington, Mass., ext. 2975.

Devarajan is new Ed Rep for Consumer Electronics



Dave Devarajan is Manager, Industrial and Systems Engineering, RCA Records, Indianapolis. A graduate of Mechanical Engineering from Kerala University in India, he has done graduate work in Operations Research in France and holds an M.S. degree in Industrial Management from Purdue University. An ardent student of mathematical modeling, his publications on "Inventory and Distribution Management," "Manufacturing Capabilities Planning," and "Equipment Evaluation Techniques" have appeared in *RCA Engineer* and other technical journals. Mr. Devarajan is a Professional Engineer and a Certified Public Accountant. Contact him at: Consumer Electronics, Industrial and Systems Engineering, Indianapolis, Ind., ext. 6109.

Promotions

Broadcast Systems

Jack Monahan from Senior Member, Engineering Staff, to Unit Manager.

Consumer Electronics

James B. Waldron from Senior Member, Engineering Staff, to Manager, Chassis—Mechanical.

SelectaVision

T.J. Christopher from Leader, Engineering Staff, to Manager, Player Electronics Design.

Jack J. Drake from Senior Liaison Engineer to Manager, Engineering Player Technology Center.

George A. Kim from Leader, Engineering Staff, to Manager, Manufacturing Engineering, Cartridge Manufacturing Operations.

M.E. Miller from Leader, Engineering Staff, to Manager, Stylus/Cartridge Design.

F.R. Stave from Leader, Engineering Staff, to Manager, Player Mechanical Design.

He was born in Frederick, Md., and received his bachelor's and master's degrees in chemistry from Washington and Lee University. Following his graduation he joined the General Electric Co. and became an RCA employee when RCA acquired the Edison Lamp Works in Harrison, N.J., where radio tubes were being manufactured.

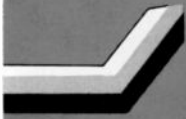
Dr. Shaw first headed the chemical section where pioneer work was carried out on oxide-coated cathodes and tube filaments for ac/dc radios. Early efforts on phosphors for display tubes found utilization in cathode ray tubes for radar during World War II and for television.

Obituary

Dr. George R. Shaw

Dr. George Robert Shaw, a leader in vacuum-tube development during the early years of radio and Chief Engineer of the RCA Tube Division from 1939 to 1961, died July 1 in Charlottesville, Va. He was 83 years old and had lived in Verona, N.J., since 1930 before moving to Charlottesville.

In 1939 Dr. Shaw was appointed chief engineer of the RCA Electron Tube Division, a post he held until his retirement in 1961. During these years he was responsible for development of electron tubes which were the real work horses of the explosively growing electronics industry. Dr. Shaw was a member of the American Chemical Society and a fellow of the IEEE.



Moorestown lists seven first-quarter 1979 Technical Excellence Award Winners



Ammann



Corbett

Seven Technical Excellence Awards were presented to Missile and Surface Radar personnel during the first quarter 1979. AEGIS work continues to be prominent in the selections, and many of the awards are to individuals who led or contributed heavily to AEGIS system-design or system-test efforts. The award winners and brief summaries of the citations are given below.

Printer. It simplifies the manufacture of thick film hybrids and significantly advances the hybrid state of the art. His creativity and enterprise have heightened RCA's technological prestige in this field and have resulted in a Navy contract for further development.



Harmening



Winkelman

R.E. Ammann—for contributions to the system design of communications facilities and terminals to support the AEGIS ship's Combat Information Center (CIC). He developed a way to define clearly the complex interior and exterior communications needs of the several CIC stations under multimission battle conditions. His analysis of needs resulted in a simpler, smaller system for CIC communications.

J.V. Melody—for outstanding performance as Test Director during testing of the AN/SPY-1A Radar Control Program with the Interface Simulator System (simulating the remainder of the AN/SPY-1A). His leadership and technical expertise expedited the isolation, definition, and frequently the solution of problems involving two large complex programs generated by two different engineering activities.



Melody



Perham

J.E. Corbett—for his contribution to the layout, configuration, and design of the AEGIS-ship CIC, the heart of the vessel's air, surface, and undersea warfare operations. His configuration of the crowded, 40-station, CIC achieves easier coordination, simplified communications, and increased battle efficiency.

D.A. Perham—for technical leadership and systems engineering expertise in the integration and test of the AN/SPY-1A Radar Control Computer Program with the Signal Processor and other equipments at the CSED Site. In leading the systems engineering effort, he applied his electronic equipment design background to direct fixes to a number of equipment and programming problems, thus enabling the March 1979 achievement of a fully integrated AN/SPY-1A radar system.



Kolc



Berry

W.A. Harmening—for design, development, and implementation of the Near Field Scanner, an essential part of the Near Field Antenna Test Facility for AN/SPY-1A array antenna testing. Significant design margins have been incorporated so that little or no periodic mechanical alignment or calibration is required. His X-Y scanner traverses the front of the array, exhibiting positional accuracies heretofore achieved only by much smaller devices.

R.J. Winkelman—for outstanding computer program project engineering accomplishments in the integration and test of the AN/SPY-1A Radar Control Computer Program with the Signal Processor and other equipments at the CSED Site. His leadership in the area of program design modifications and program problem solutions was a major element in the successful demonstration of operational status for the AN/SPY-1A radar system in March 1979.

R.F. Kolc—for his concept and initial development of a Computerized Thick Film

Marion presents Technical Excellence Awards



Berry



Davin

The Engineering Excellence Committee at Picture Tube Division, Marion, Ind., has presented two awards for outstanding and innovative accomplishments. The award winners and brief summaries of their citations are given below.

tube operational characteristics on the SATS in Marion and by the TV set manufacturer when installing the tubes in chassis.

M.D. Berry—for his design of a combination yoke-holder and alignment fixture for the SATS carts. The device was designed to improve the setup capabilities for OT types, solving a problem in correlation of picture-

J. Davin—for his work in developing and implementing several new checks for quality control inspection over the past few months and for his knowledge of foreign languages. This knowledge was a significant benefit to RCA both in relationships with OTM customers in Latin America and in providing assistance to the Industrial Relations department.



The First Annual Mountaintop Technical Excellence Committee Recognition Awards Dinner was held on June 9, 1979. The recipients of recognition awards from the previous twelve months were the honored guests.

Seated left to right: B. Czeck, E. Teno, R. Heinrich, S. Blaskowski, R. Kosco. Standing left to right: J. Moran, Chairman, Technicians' TEC; T. Ruskey; J. Neilson; M. Zelinka; F. Stensney; R. Shemanski; V. Osadchy, Chairman, Engineers' TEC. (Absent when picture was taken — A. Baloga)



RCA-Burlington honors authors and patent holders at the twelfth Professional Recognition Dinner on June 10.

Inventor Recognition Dinner at Cherry Hill

A Recognition Dinner was held on July 10 to honor inventors in GCS and CSD. John Regan, Bill Hittinger and Jim Vollmer, in addressing the inventors and guests, expressed the appreciation of the company for the contribution to RCA which a patent represents. The speakers emphasized the importance of patents as a tangible result of creativeness and inventive imagination of RCA's scientists and engineers. Arch Luther, Jr., CSD, and Robert A. Dischert, CSD, were both recognized for the issuance of their thirtieth RCA patent. Ludwig Muhlfelder, AED Hightstown, was recognized for the issuance of his tenth RCA patent. William J. Derenbecher, Jr., CSD; Kazuo Katagi, AVS-Van Nuys; John E. Keigler, AED Hightstown; Lawrence P. Nahay, GCS; and Matti S.O. Siukola, Gibbsboro, were each honored for the issuance of their fifth RCA patent.

Degrees granted

Engineering; University of Pennsylvania, Phila., Pa.

Government Communications Systems

C. Humphries — Masters of Science, Electrical Engineering; University of Pennsylvania, Phila., Pa.

Government Systems Division

R. Metkowski — Masters of Science, Electrical Engineering; University of Pennsylvania, Phila., Pa.

P. Ray — Masters of Science, Electrical

Licensed engineers

When you receive a professional license, send your name, PE number and state in which registered, RCA division, location, and telephone number to *RCA Engineer*, Bldg. 204-2, RCA Cherry Hill, N.J. New listings (and corrections or changes to previous listings) will be published in each issue.

Solid State Division

R.L. Wilson, Dallas; TX-45211



Luther



Dischert



Muhlfelder



Derenbecher



Katagi



Keigler



Nahay



Siukola

Recognition Dinner held, in Cherry Hill, N.J., to honor inventors to whom one or more patents were issued between July 1, 1977 and December 31, 1978. Jim Vollmer is shown on the right, in the photographs, giving the awards.

Automated Systems holds Corporate ATE Symposium

A Corporate symposium on automated test equipment (ATE) was held at Automated Systems in Burlington, Mass. on June 18. A wide range of topics was covered at the symposium, including an overview of ATE technology, ATE manufacturing, ATE cost effectiveness, hybrid circuit testing with ATE, large-scale and microprocessor test systems, three specific test systems, and

advanced research concepts in analog testing.

After a welcome address by Harry Woll, Division Vice President and General Manager, the program began with an overview of Automated Systems' business areas by Gene Stockton, Chief Engineer.

Dick Monis, Manager, Automated Test and Monitoring Systems Design, planned and organized the symposium which was attended by 25 RCA people. The following presentations made up the day's program:

Corporate ATE Symposium

"ATE Technology"	R.J. Monis Automated Systems	"ST 37 Test System"	R. Woodson Government Communications Systems Division
"Non-Electronic Test Technology at Automated Systems"	H.L. Fisher Automated Systems	"Ground Equipment (AGE)"	E. Dusio Astro-Electronics
"ATE, When and Where Is It Cost Effective?"	F. Pfifferling Commercial Communications Systems Division	"Automated Phased Array Antenna Testing"	R. Martin Missile and Surface Radar
"STE/ICE Testing"	J.H. Minteer Automated Systems	"Advanced Concepts in Analog Testing"	S. Freeman RCA Laboratories
"Comercial Electronics — ATE Overview"	B. Borman Consumer Electronics	"Hybrid Testing with ATE"	B. Joyce Automated Systems
"Calculator-Based Test System"	K. Weydemann/ E. Leach Automated Systems		

Professional Activities

Morrell receives IEEE Vladimir K. Zworykin Award

Albert M. Morrell was awarded the Vladimir K. Zworykin Award for his contributions to shadow mask color picture tube development and design.

The award was established in 1950 by Dr. Vladimir K. Zworykin. The award is made by the Board of Directors upon the recommendation of the Field Awards Committee and the Awards Board for outstanding technical contribution to electronic television.

Mr. Morrell joined RCA in 1960 during the inception of Color TV and has been associated with most phases of color picture tube development, first as a design engineer and later as Manager of Tube Development, RCA Picture Tube Division, which position he presently holds. He has 21 issued United States patents which cover the full range of color tube development starting with the basic patent on the internal-pole-piece gun.

Mr. Morrell has published a number of

technical papers and is co-author of the book *Color Television Picture Tubes*, published by Academic Press in 1974. His work at RCA has been recognized by two David Sarnoff awards.

D'Arcy appointed Chairman for EE Honor Society

Jim D'Arcy is appointed Chairman of the Award Organization Committee of Eta Kappa Nu, the Electrical Engineering Honor Society. Jim served as Vice-Chairman last year.

The Committee is responsible for soliciting and processing nominations for the annual Recognition of the Outstanding Young Electrical Engineer of the U.S.

Books by RCA authors

Two scientists at RCA Laboratories in Princeton, **G.W. Cullen** and **C.C. Wang**, are the editors of *Heteroepitaxial Semiconductors for Electronic Devices*, recently

published by Springer-Verlag, New York. This book brings together a description of materials science and device engineering. It introduces a collaborative effort between individuals who represent the disciplines of materials preparation, materials characterization, device design and processing, and the analysis of the device operation to establish relationships between device performance and the materials properties.

Parvin S. Titus of the Picture Tube Division and **Ben S. Graham** are the editors of *The Amazing Oversight*, recently published by AMACOM, New York. The book is a collection of essays on operations improvement through involvement. In the first section, pioneers in the field of Work Simplification describe the origin and theory of this method. The second section expands upon the philosophy and applications of participative improvement. Varied proposals have been made to solve the problems of productivity. All agree that the quality of working life and the degree of involvement people have in their work are critical factors. This great resource is often overlooked. This is the "Amazing Oversight" which this book examines.

Editorial Representatives

Contact your Editorial Representative, at the extensions listed here, to schedule technical papers and announce your professional activities.

Commercial Communications Systems Division

Broadcast Systems

BILL SEPICH* Camden, N.J. Ext. 2156
KRISHNA PRABA Gibbsboro, N.J. Ext. 3605
ANDREW BILLIE Meadow Lands, Pa. Ext. 6231

Mobile Communications Systems

KARL NEUMANN* Meadow Lands, Pa. Ext. 6444

Avionics Systems

STEWART METCHETTE* Van Nuys, Cal. Ext. 3806
JOHN McDONOUGH Van Nuys, Cal. Ext. 3353

Cablevision Systems

JOHN OVNICK* N. Hollywood, Cal. Ext. 241

Government Systems Division

Astro-Electronics

ED GOLDBERG* Princeton, N.J. Ext. 2544

Automated Systems

KEN PALM* Burlington, Mass. Ext. 3797
PETE DIACONOFF Burlington, Mass. Ext. 2975

Government Communications Systems

DAN TANNENBAUM* Camden, N.J. Ext. 3081
HARRY KETCHAM Camden, N.J. Ext. 3913

Government Engineering

MERLE PIETZ* Camden, N.J. Ext. 2161

Missile and Surface Radar

DON HIGGS* Moorestown, N.J. Ext. 2836
JACK FRIEDMAN Moorestown, N.J. Ext. 2112

Solid State Division

JOHN SCHOEN* Somerville, N.J. Ext. 6467

Power Devices

HAROLD RONAN Mountaintop, Pa. Ext. 633 or 827
SY SILVERSTEIN Somerville, N.J. Ext. 6168

Integrated Circuits

FRED FOERSTER Somerville, N.J. Ext. 7452
JOHN YOUNG Findlay, Ohio Ext. 307

Electro-Optics and Devices

RALPH ENGSTROM Lancaster, Pa. Ext. 2503

Consumer Electronics

CLYDE HOYT* Indianapolis, Ind. Ext. 5208
FRANCIS HOLT Indianapolis, Ind. Ext. 5217
PAUL CROOKSHANKS Indianapolis, Ind. Ext. 5080
STEVE RACE Indianapolis, Ind. Ext. 5636
DON WILLIS Indianapolis, Ind. Ext. 5883

SelectaVision VideoDisc Operations

W.M. WORKMAN* Indianapolis, Ind. Ext. 3313

RCA Service Company

JOE STEOGER* Cherry Hill, N.J. Ext. 5547
RAY MacWILLIAMS Cherry Hill, N.J. Ext. 5986
DICK DOMBROSKY Cherry Hill, N.J. Ext. 4414

Distributor and Special Products Division

CHARLES REARICK* Deptford, N.J. Ext. 2299

Picture Tube Division

ED MADENFORD* Lancaster, Pa. Ext. 3657
NICK MEENA Circleville, Ohio Ext. 228
JACK NUBANI Scranton, Pa. Ext. 499
J.R. REECE Marion, Ind. Ext. 5566

Americom

MURRAY ROSENTHAL* Piscataway, N.J. Ext. 4363

Globcom

WALT LEIS* New York, N.Y. Ext. 7711

RCA Records

DAVE DEVARAJAN* Indianapolis, Ind. Ext. 6109

NBC

BOB MAUSLER* New York, N.Y. Ext. 4385

Patent Operations

JOSEPH TRIPOLI Princeton, N.J. Ext. 2992

Research and Engineering

Corporate Engineering

HANS JENNY* Cherry Hill, N.J. Ext. 4251

Laboratories

MAUCIE MILLER Princeton, N.J. Ext. 2322
JUDY YEAST Somerville, N.J. Ext. 7357

*Technical Publications Administrator, responsible for review and approval of papers and presentations.

RCA Engineer

A technical journal published by
Corporate Research and Engineering
"by and for the RCA engineer"

Printed in the U.S.A. Form No. RE-25-2